Microbial Fe(II) oxidation:

cell-mineral interactions

and implications for modern and ancient environments

Dissertation
der Mathematisch-Naturwissenschaftlichen Fakultät
der Eberhard Karls Universität Tübingen
zur Erlangung des Grades eines Doktors der Naturwissenschaften
(Dr. rer. nat.)

vorgelegt von
M.Sc. Florian Hegler
aus Tübingen

Tübingen
2011

Tag der mündlichen Qualifikation: 08.02.2011
Dekan: Prof. Dr. Wolfgang Rosenstiel
1. Berichterstatter: Prof. Dr. Andreas Kappler
2. Berichterstatter: Dr. Karim Benzerara

42

Ultimate answer to the ultimate question of life, the universe, and everything*

*Douglas Adams, The Hitchhiker's Guide to the Galaxy

Contents

List of Figures

List of Tables

Abbreviations

Co	cobalt
DL	detection limit
Ga	giga annum – billion of years
EPS	exopolysaccharide
Ga	giga annum – billion of years
LPS	lipopolysaccharide
M	mol L^{-1}
TE	trace element
Mo	molybdenum
Ni	nickel
XEDS	X-ray energy-dispersive spectrometry
OD	optical density
SEM	scanning electron microscope
STEM	scanning transmission electron microscopy
V	vanadium
XRD	X-ray diffraction
CLSM	Confocal laser scanning microscopy
BIF	banded iron formation
Fe(II)	iron(II) or ferrous iron
Fe(III)	iron(III) or ferric iron
XRD	X-ray diffraction

Glossary

BIF banded iron formations, sedimentary iron-ore deposits of alternating layers of silicates and iron oxides

CCCP carbonyl cyanide 3-chlorophenylhydrazone, a protonophore

chalybeate containing the salts of iron, e.g. water from a spring

chelation formation of a polydentate binding between a metal ion and a ligand, usually an organic compound

DAPI 4',6-diamidino-2-phenylindole; a fluorescent dye that binds strongly to DNA and serves to stain a bacterial cell in fluorescence microscopy

EDTA Ethylenediaminetetraacetic acid, a chelating agent which chelates Ca^{2+}, Fe^{2+}, Fe^{3+} and Cu^{2+}

ferric iron iron compounds with the oxidation state of three

ferrous iron iron compounds with the oxidation state of two

iep isoelectric point: pH at which a surface is not net electrical charged

NTA nitrilotriacetic acid, a chelating agent which chelates Ca^{2+}, Fe^{2+}, Fe^{3+} and Cu^{2+}

pzc point of zero charge – pH at which the charge on a surface is zero

TE trace element, an element that is required only in minute quantities by an organism

1 Summary

Iron is an ubiquitous redox-active element in the environment – today and already in the Precambrian more than two billion years ago. Ferrous (Fe(II)) and ferric iron (Fe(III)) are the dominant redox species. Fe(III) is dominant today while Fe(II) was more abundant on early earth. Biological as well as chemical processes mediate the redox-change between the two species.

While Fe(II) is rather soluble at circumneutral pH, Fe(III) is scarcely soluble and Fe(III) minerals form which precipitate as Fe(III)(hydr)oxides. These Fe(III) minerals may sorb or precipitate on the cell surface of Fe(II)-oxidizing bacteria and ultimately this can lead to encrustation of the cells. Encrustation of cells of chemotrophic Fe(II)-oxidizers – e.g., microaerophilic and nitrate-reducers – as well as photoferrotrophs would ultimately hinder the exchange of the cell with its environment. Furthermore, light required by phototrophic organisms would also be reduced by encrustation.

In order to determine differences in encrustation of phototrophic and nitrate-reducing Fe(II)-oxidizing bacteria, cell-mineral aggregates were visualized and analyzed by scanning electron microscopy. In this thesis we show that most of the known photoferrotrophic bacteria are not encrusted with Fe(III) minerals while one of the nitrate-reducing Fe(II) oxidizers is heavily encrusted with Fe(III) minerals.

Encrustation is likely harmful for the Fe(II)-oxidizers. It is so far not clear how bacteria can avoid encrustation by Fe(III) minerals. In order to determine, how cells can avoid encrustation, the cell surface pH of photoferrotrophs was determined. My work showed that the cell surface pH of a photoferrotroph is lower than the bulk pH. Geochemical calculations showed that the low cell surface pH is sufficient to reduce Fe(III) precipitation at the cell surface. In addition to a low cell surface pH, we found that photoferrotrophs localize Fe(III) mineral precipitation away from the cell onto extra-cellular fibers.

In contrast to the lower cell surface pH, I did not find any evidence, that a difference in the pH of the medium from pH 6.2 to 7.4 leads to a change in encrustation of nitrate-reducing Fe(II)-oxidizing bacteria – although a lower pH leads to a higher solubility of Fe(III). The influence of bulk pH on the identity and crystallinity of the minerals formed was found to be negligible.

The cell surface is in direct contact with the cell's environment and thus also governs the interaction of cells with minerals. In order to determine the cell surface functional groups and their density, acid-base titrations of encrusting and not encrusting bacteria were performed. Modeling of the titration data showed, that the cell surface of not-encrusting bacteria is more

negatively charged than that of encrusting bacteria. In contrast to chemically synthesized Fe(III) minerals, Fe(III) minerals precipitated in mineral medium are negatively charged. The repulsion between cells and Fe(III) minerals is stronger the higher the surface charge. Due to their more negatively charged cell surface photoferrotrophs are therefore expected to encrust less.

In contrast to pure laboratory cultures, iron oxidation in the environment is mediated by complex bacterial communities. I chose a bicarbonate rich chalybeate spring to determine which factors control the composition of iron-metabolizing microbial communities and how the same factors additionally influence mineralogy. The spatial and temporal variability in the microbial community structure was determined with a cluster analysis of DGGE band patterns. Members of the community were identified with a 16S-rRNA based clone library. I showed that seasonal variability and the habitat influence the microbial community strongly while geochemical gradients have less influence. In contrast, I showed that geochemical gradients influence the crystallinity of the minerals while seasonal effects could not be detected.

Fe(II)-oxidizing bacteria are not only ubiquitous in modern environments, these bacteria likely played a vital role in shaping our planet in the Precambrian. The habitats available for Fe(II)-oxidizing bacteria were ubiquitous on an anoxic earth and these bacteria were likely involved in the precipitation of the iron for the oldest banded iron formations. Trace element requirements of bacteria may yield insights into the evolution of a bacterial strain and its metabolism. In order to determine if one of the available photoferrotrophs is a suitable model organism to study the the formation of BIFs, I determined the requirements of *"Rhodobacter ferrooxidans"* strain SW2 for the trace elements nickel, vanadium, cobalt and molybdenum. This strain has preserved the use of trace metals typically abundant on ancient earth. Therefore, it is likely a good model for the past.

Additionally, I determined rates of Fe(II) oxidation for photoferrotrophs under various conditions such as light, temperature and pH. Furthermore, we showed with geochemical modeling that a temperature shift of only 25 °C is sufficient to explain the banding in banded iron formations. An increase in temperature leads to a faster bacterial oxidation rate of Fe(II) and a decrease in silica precipitation while a decrease in temperature has opposite effects.

Fe(II)-oxidizing bacteria are not only exposed to the threat of encrustation, high radical concentration due to the presence of Fe(II) is a constant threat for mutation. Therefore, a lab-protocol was developed to cryo-preserve Fe(II)-oxidizing bacteria anoxically using glycerol and thus avoid loss of function and mutation.

Fe(II)-oxidizing bacteria have shaped our planet since more than 2 Ga and we are only now beginning to understand their role in the environment and how they solve the challenges they face in order to survive.

2 Zusammenfassung

Eisen ist ein allgegenwärtiges redox-aktives Element. Zwei- und dreiwertiges Eisen sind die wichtigsten Oxididationsstufen in der Umwelt. Biologische, aber auch chemische Prozesse können Eisen sowohl reduzieren als auch oxidieren.

Die Löslichkeit von zweiwertigem Eisen in Wasser bei neutralem pH ist recht hoch, dahingegen ist dreiwertiges Eisen unter diesen Bedingungen nur sehr schlecht löslich und Fe(III)(hydr)oxide fallen aus. Diese dreiwertigen Eisenminerale können an den Zelloberflächen von eisenoxidierenden Bakterien ausfallen, die Zellen verkrusten dann mit einer Mineralschicht. Eine Mineralschicht auf den Zelloberflächen von chemotrophen (also mikroaerophilen und nitratreduzierenden Eisenoxidierer) und phototrophen Eisenoxidierer würde die Diffusion von Metaboliten einschränken. Bei phototrophen Organismen kommt hinzu, dass weniger Licht für die Photosynthese zur Verfügung stünde. Um Unterschiede in der Enkrustierung von phototrophen und chemotrophen, nitratreduzierenden Eisenoxidierern zu bestimmen, wurde solche Bakterien und die Minerale mittels Rasterelektronenmikroskopie analysiert. Phototrophe Eisenoxidierer haben normalerweise keine Eisenkrusten auf den Zelloberflächen, nitratreduzierende Eisenoxidierer sind meist stark verkrustet.

Die Minerale an der Zelloberfläche sind vermutlich schädlich für die Zellen. Bisher ist unbekannt, wie die Zellen eine Mineralausfällung an den Zelloberflächen verhindern können. Daher wurden Strategien der Zellen untersucht, wie diese eine Mineralausfällung an den Zelloberflächen vermeiden können. Dazu wurde der pH an den Zelloberflächen von einem phototrophen Eisenoxidierer gemessen. Dieser ist niedriger als der pH in der die Zelle umgebenden Flüssigkeit. Geochemische Berechnungen zeigen, dass der pH Unterschied zwischen Zelloberfläche und Medium ausreichend ist, um die Mineralausfällung an die Zelloberflächen zu verhindern. Zusätzlich zu dem dargestellten Prozess konnte gezeigt werden, dass Zellen Fasern ausscheiden, an denen die Eisenminerale binden.

Im Gegensatz zu dem unterschiedlichen pH an der Zelloberfläche und dem Medium scheint eine Änderung im pH-Wert des Mediums von 6,2 nach 7,4 wenig Einfluss auf die Mineralausfällung an der Zelloberfläche der nitratreduzierenden Eisenoxidierer zu haben – auch wenn die Löslichkeit des Eisens stark mit niedrigerem pH ansteigt. Außerdem scheint der Einfluss des pHs auf die Mineralphase vernachlässigbar.

Die funktionellen Gruppen an der Zelloberfläche der Bakterienzelle bilden den direkten Kontakt mit der Umwelt und auch mit den Mineralien. Daher wurde die Menge und Art der funktionellen Gruppen an der Zelloberflächen von eisenoxidierenden Bakterien mit Hilfe von

Säure-Base Titrationen bestimmt. Modellierung der Daten zeigte, dass die Zelloberflächenladung von Bakterien, die nicht verkrusten, stärker negativ geladen ist als die Zelloberfläche von Bakterien, die stark verkrusten. Außerdem wurde gezeigt, dass chemisch synthetisiere Eisenoxide positiv geladen sind wohingegen die Eisenoxide aus Bakterienkulturen negativ geladen sind. Daher ist die elektrostatische Abstoßung der stärker negativ geladenen Zelloberflächen von den Eisenmineralien stärker als die der Zellen, welche mit Mineralien verkrusten.

Im Gegensatz zu den Reinkulturen im Labor wird die Eisen in der Umwelt von einer Bakteriengemeinschaften oxidiert. Ein Eisensäuerling wurde ausgewählt um die unterschiedliche Faktoren zu bestimmen, die eine Bakteriengemeinschaften, aber auch die Mineralausfällung bestimmen. Dazu wurde eine örtlich und zeitlich aufgelöste Clusteranalyse der Bakteriengemeinschaften mittels denaturierender Gradientengelelektrophorse durchgeführt. Zusätzlich wurden die dort vorhandenen Bakterien mit einer 16S-rRNA basierten Klonbibliothek bestimmt. Ich konnte zeigen, dass die saisonalen Veränderungen und das Habitat die Bakteriengemeinschaft stärker beeinflussen als der geochemischer Gradient. Im Gegensatz dazu verändern sich die Minerale mit dem geochemischen Gradienten.

Eisenoxidierende Bakterien sind nicht nur zu den gegenwärtigen Bedingungen in den Eisenkreislauf der Erde eingebunden, vielmehr waren sie vermutlich schon im Präkambrium an der Entstehung der gebänderten Eisenerzformationen beteiligt. Eine Analyse, welche Spurenelemente Bakterien brauchen, könnte Besonderheiten im Metabolismus aufzeigen aber auch unter welchen Bedingen die Evolution eines Bakterienstamms abgelaufen sein könnte. Dies wurde genutzt um zu bestimmen, ob ein phototrophes Bakterium (*"Rhodobacter ferrooxidans"* sp. SW2) als Modelorganismus für Studien zur Entstehung der gebänderten Eisenerzformationen verwendet werden könnte. Das Bakterium verwendet Molybdän, Cobalt, Vanadium und Nickel ähnlich den Konzentrationen typisch fr die frühe Erde und kann daher als gutes Modelsystem angesehen werden.

Zusätzlich wurde die Eisenoxidationsrate unter verschiedenen physiologischen Bedingungen, wie beispielsweise pH, Temperatur und Licht, bestimmt. Geochemische Modellierung zeigte außerdem, dass eine Temperaturveränderung von 25 °C ausreicht, um die Bänderung der Eisenerzformation zu erklären: ein Temperaturanstieg führt zu schnellerer bakterieller Eisenoxidation, ein Absinken der Temperatur führt zur Ausfällung von Silikaten.

Eisenoxidierende Bakterien sind nicht nur von der Verkrustung durch Eisenminerale betroffen, hohe Radikalkonzentrationen, die durch zweiwertige Eisen entstehen, können leicht zu Mutationen führen. Daher wurde ein Protokoll entwickelt, um die eisenoxidierenden Bakterien einfrieren zu können. Damit kann bei Laborkulturen eine Mutation verhindert werden.

Seit mehr als zwei Milliarden Jahren verändern eisenoxidierende Bakterien unseren Planeten. Erst heute fangen wir an, deren Rolle in der Umwelt zu verstehen und auch, welche Probleme diese Bakterien lösen müssen, um zu überleben.

3 Introduction

3.1 Iron in the environment and iron-metabolizing bacteria

Iron plays an essential role in our everyday live. But we likely owe much more to iron than just the metal we use daily or even the oxygen-transport by hemoglobin in our blood: iron-sulfur minerals have likely played a key role in the advent of life: life might not have evolved without iron-minerals at all (Wächtershäuser, 1990, Gold, 1992, Wächtershäuser, 2000). It is thought, that biotic or abiotic Fe(II) transformation was utilized as energy source right from the beginning of life (Wächtershäuser, 1990, Gold, 1992). Enzymes that evolved very early in life to fulfill this task can be present in all organisms throughout the tree of live. Therefore, it is no surprise that the capability for Fe(II) oxidation is found in all phylogenetic groups of eubacteria (Lane et al., 1992) and in a variety of environments on earth (Kappler & Straub, 2005, Canfield et al., 2005, Konhauser, 2007, Ehrlich & Newman, 2009).

It was recognized early that Fe(II) oxidation by bacteria is widespread in the environment (Ehrenberg, 1836, Winogradsky, 1888, Pringsheim, 1949). However, in contrast to many other environmentally relevant elemental cycles such as carbon, nitrogen and sulfur it took almost 150 years before research focused on iron-metabolizing bacteria. The role of bacteria in iron-cycling, e.g., Fe(II) oxidation and Fe(III) reduction, has been shown clearly (Kappler & Straub, 2005, Weber et al., 2006). Additionally, the reduction and oxidation of iron plays an important role in the fate and transport of contaminants (Klausen et al., 1995, Tufano & Fendorf, 2008, Borch et al., 2010).

In contrast to most other biologically relevant ions, the solubility of iron changes fundamentally depending on the redox-state (Cornell & Schwertmann, 2003). While Fe(II) is rather soluble at circumneutral pH (in the range of mmol L^{-1}), Fe(III) is barely soluble at pH 7 (less than 1×10^{-12} mol L^{-1}) (Cornell & Schwertmann, 2003) and precipitates quickly as Fe(III) minerals under these conditions (Waite et al., 2000, Pham et al., 2006, Rose & Waite, 2007).

Different metabolic pathways involved in the microbially mediated iron-cycle at circumneutral environments became apparent only in the last 30 years (Balashova & Zavarzin, 1979, Lovley, 1991, Hafenbradl et al., 1996, Straub et al., 1996, Emerson & Moyer, 1997, Widdel et al., 1993).

So far, three different metabolic pathways for Fe(II) oxidation at circumneutral pH are known: **Microaerophilic** bacteria which gain energy by oxidizing Fe(II) at µmolar concentrations of

oxygen (Emerson & Moyer, 1997, Emerson et al., 2010) according to the following equation:

$$4\,Fe^{2+} + O_2 + 10\,H_2O \longrightarrow 4\,Fe(OH)_3 + 8\,H^+ \tag{3.1}$$

Microaerophilic chemotrophic Fe(II)-oxidizers are amongst the first bacteria described by scientists (Ehrenberg, 1836, Winogradsky, 1888). Lately, other metabolic pathways for Fe(II) oxidation have been identified: **Photoautotrophic** Fe(II)-oxidizing bacteria gain electrons from oxidizing Fe(II) while using light as energy source (Widdel et al., 1993, Ehrenreich & Widdel, 1994, Heising et al., 1999, Croal et al., 2004) according to the following equation:

$$HCO_3^- + 4\,Fe^{2+} + 10\,H_2O \longrightarrow <CH_2O> + 4\,Fe(OH)_3 + 7\,H^+ \tag{3.2}$$

The third, identified metabolic pathway is **Fe(II) oxidation coupled to nitrate reduction**. These bacteria can either grow autotrophically (Hafenbradl et al., 1996, Straub et al., 1996) or mixotrophically (Kappler et al., 2005). Nitrate-reducing Fe(II)-oxidizers metabolize Fe(II) according to the following equation (Miot et al., 2009a) while some additionally oxidized acetate or use acetate as carbon source (not shown):

$$2\,Fe^{2+} + 5\,H_2O + NO_3^- \longrightarrow 2\,Fe(OH)_3 + 4\,H^+ + NO_2^- \tag{3.3}$$

The iron cycle is completed by dissimilatory Fe(III)-reducing bacteria which use Fe(III) as electron acceptor coupled to various electron donors (Balashova & Zavarzin, 1979, Myers & Nealson, 1988, Lovley, 1991).

3.1.1 Research questions

Iron-oxidizing bacteria have been discovered nearly 200 years ago (Ehrenberg, 1836) and several questions have intrigued researchers since:

- How do Fe(II)-oxidizing bacteria deal with the poorly soluble Fe(III) which can precipitate onto the cell surface?
- Which factors influence microbial communities in Fe(II) rich environments and which bacteria are present in such communities?
- How do Fe(II)-oxidizing bacteria influence mineralogy of Fe(III) precipitates?
- Have Fe(II)-oxidizing bacteria been present in the Precambrian and have they been involved in the precipitation of the banded iron formations?

My thesis focuses on several aspects of the questions outlined above.

3.2 Cell-mineral interaction of Fe(II)-oxidizing bacteria

The association of cells with minerals is a well known phenomenon and has been observed frequently in the environment (Ehrenberg, 1836, Konhauser, 1997, Banfield & Nealson, 1997, Fortin & Langley, 2005, Phoenix & Konhauser, 2008) as well as in laboratory cultures (Ferris et al., 1986, Thompson & Ferris, 1990, Banfield & Nealson, 1997, Fortin et al., 1998, Konhauser et al., 2004, Posth et al., 2010 and chapter 8). Various particles are known to be associated with cells, such as carbonates (Thompson & Ferris, 1990), silicates (Ferris et al., 1986) and iron minerals (Fortin et al., 1998). Different processes can lead to the association of cells with minerals (Konhauser, 1997): either minerals precipitate chemically and cell surfaces work as nucleation templates or the mineral formation is induced by the bacteria directly followed by the association of minerals with the cells. Furthermore, minerals that are not freshly precipitated can associate with cells and finally bacteria can sorb to minerals in order to dissolve these (Banfield & Nealson, 1997).

The precipitation of minerals on the cell surface can be beneficial for bacterial cells, for example as a shield against ultra-violet radiation (Phoenix et al., 2000). Biominerals on the cell surface could also be a source and storage for essential nutrients (Konhauser et al., 1994). Other benefits for cells encrusted with minerals include a protection against predatory microorganisms such as amoebae (Phoenix & Konhauser, 2008) or a protection of the cells from dehydration by storing water (Phoenix & Konhauser, 2008).

Despite all the apparent benefits of mineral precipitation onto the cell surface, major disadvantages persist for all encrusted cells: minerals on the cell surface lead to a decrease in the exchange of nutrients and metabolites between the cell and its environment. Additionally, light required by phototrophic bacteria is reduced by a mineral envelope limiting the energy available for photosynthesis. Therefore, cells that do not benefit directly from encrustation, need strategies for avoiding it. Cells oxidizing Fe(II) to Fe(III) are particularly prone to minerals precipitation onto their surface because of the low solubility of Fe(III) minerals.

In order to determine how Fe(II)-oxidizing bacteria interact with Fe(III) minerals and if these bacteria encrust, cell-mineral interaction was visualized with scanning electron microscopy (chapter 8). Most of the known phototrophic Fe(II)-oxidizing bacteria are not encrusted with Fe(III) minerals (Kappler & Newman, 2004, Schaedler et al., 2009, Miot et al., 2009b). So far, the only exception is *Rhodomicrobium vannielii* (Heising & Schink, 1998) which – in contrast to the other photoferrotrophs – is growing mixotrophically and not autotrophically. In contrast to photoferrotrophs, the nitrate-reducing Fe(II)-oxidizing *Acidovorax* sp. BoFeN1 is known to encrust heavily with Fe(III) minerals (Kappler et al., 2005).

In order to avoid Fe(III) minerals to precipitate onto the cell surfaces, several strategies are plausible for bacteria. Generally, the initial phase of the mineral precipitation onto the cell surface is governed by the electrostatic interaction of cationic metal ions with the anionic functional groups of the the cell surface (Beveridge & Murray, 1976, 1980). Only in the second

step the already adsorbed metals act as a nucleation site for further ions that coprecipitate with the primary ion. This leads to mineral encrustation of the cell (Beveridge & Fyfe, 1985).

Hence, cells can avoid the primary interaction with ions from solution by reducing the cell surface functional charge. Cell surface titrations allow determining the functional groups and their density at the cell surface. Therefore, cells of the non-encrusting photoferrotroph *"Rhodobacter ferrooxidans"* strain SW2 and the encrusting *Acidovorax* strain sp. BoFeN1 were titrated (chapter 5).

Additionally, cells could avoid encrustation by matching the mineral surface charge. If both, cell surface and the mineral properties are the same, they will not interact. Fe(III) minerals, such as ferrihydrite and goethite are positively charged at circumneutral pH when precipitated from pure systems (Dzombak & Morel, 1990, Cornell & Schwertmann, 2003). In contrast, if Fe(III) minerals precipitate in complex solutions containing other ions, the surface charge may become negative at circumneutral pH. Negative surface charges of Fe(III) minerals have been observed in the environment, for example in the presence of humic substances (Tipping, 1981) and carbonates (Evans et al., 1979). In order to determine the interaction of cells and minerals, the surface charge of minerals and cells was measured (chapter 5).

The solubility of Fe(III) is strongly depending on pH (Cornell & Schwertmann, 2003). As a result, the kinetics of Fe(III) mineral precipitation is slower the lower the pH (Waite et al., 2000, Pham et al., 2006, Rose & Waite, 2007). Furthermore, a lower pH reduces the negative surface charge leading to less interaction of the cell surface functional groups with the Fe(III) ions. Johnson et al. (2007) showed a correlation between the adsorption of metals onto the cell surface depending on if cells were alive or not – less Cd^{2+} was adsorbed to living cells. Urrutia Mera et al. (1992) correlated the proton motive force and the adsorption of metal ions. Therefore, cells that need to avoid encrustation, may also reduce their cell surface pH (Kappler & Newman, 2004, Schaedler et al., 2009). In order to determine if photoferrotrophs use this strategy to minimize Fe(III) minerals precipitating on the cell surfaces, the cell surface pH of the photoferrotroph *Thiodyction* sp. strain F4 was measured on a single cell level (chapter 4).

Another strategy for cells to avoid encrustation is to produce extracellular fibers acting as nucleation sites for Fe(III) mineral precipitation (Hallbeck & Pedersen, 1995, Chan et al., 2004). In order to test this hypothesis, scanning electron microscopy (SEM) and synchrotron based scanning x-ray microscopy (STXM) was used to visualize such fibers of *"Rhodobacter ferrooxidans"* strain SW2 and the respective mineral sorption behavior for photoferrotrophic cells (chapter 7).

This strategy is similar to shedding the cell surface including the sorbed minerals and thus remove iron minerals from the cell surfaces after precipitation (Emerson & Revsbech, 1994).

Another potential strategy which was not tested yet is that cells could also produce chelators to avoid encrustation (Croal et al., 2004). Chelators or ligands could complex Fe(III) and thus keep it in solution. An effective recycling of the ligands is a prerequisite because ligands and chelators require many carbon atoms and are therefore "expensive" to synthesize for the cell: autotrophic cells need to be oxidized four Fe(II) to fix one carbon atom (CO_2) (equation 3.2).

Thus, even a small organic acid as ligand, such as citrate, require already four electrons × six carbon atoms = 24 Fe(II) to be oxidized. Furthermore, most Fe(III) complexing molecules are photoreactive and degrade over time in systems containing Fe(III) which are exposed to light (Barbeau et al., 2001). Bacteria use the degradation products of these chelators as organic carbon source rather than fixing CO_2 (Caiazza et al., 2007). Therefore, the production of organic ligands seem unlikely and was out of the scope of this study.

The overall-strategy of the Fe(II)-oxidizing bacteria to avoid encrustation is likely a combination of the mentioned strategies.

3.3 Iron-metabolizing bacteria at a chalybeate spring

Fe(II)-oxidizing bacteria in the environment not only face the challenge of encrustation. Microorganisms live in complex microbial communities which are influenced by several physicochemical factors: geochemistry, e.g., ions, ionic strength, pH; temperature, minerals and the availability of resources, e.g., light, ferrous iron (Madigan et al., 2006, Ehrlich & Newman, 2009).

Which factors influence a microbial community in an Fe(II)-rich habitat? Which factors influence the mineralogy?

A bicarbonate rich chalybeate (e.g., rich in Fe(II)) spring was chosen to identify the interplay of geochemistry, physicochemical factors and the available resources and the microbial community present at the field site. The geochemistry of the spring is defined by the water content, such as the high bicarbonate/CO_2 concentration and pH but also the water-flow, the mineralogy, the elevated concentrations of Fe(II) and the availability of light.

The mentioned factors are not stable over time and they may even influence each other. Furthermore, the individual contribution of the factors on the microbial community of the iron-metabolizing bacteria is unclear.

Therefore, I determined geochemical conditions, the availability of Fe(II) and mineralogy at different sampling times over the course of a year (chapter 9). Minerals were identified using X-ray diffraction and Mössbauer spectroscopy. The microbial community members were identified using a 16S-rRNA based clone library. The shifts in the microbial community depending on the physiochemical factors was determined by a cluster analysis of DGGE-gels.

Overall, we describe a model habitat of Fe(II)-oxidizing and also Fe(III)-reducing microorganisms.

3.4 Fe(II)-oxidizing bacteria on early earth

Fe(II) oxidation is believed to be one of the oldest metabolic pathways on earth (Wächtershäuser, 1990, Gold, 1992) and Fe(II)-oxidizers likely played a role in the deposition of the banded iron formations (BIFs) (Garrels et al., 1973) in the Precambrian between 3.8 and 1.6 Ga ago. BIFs are large deposits of alternating iron-rich layers intermixed with iron-poor chert layers (Beukes et al.,

1992). The atmosphere of the early earth was anoxic and reducing (Kasting, 1993, 2001, Kasting & Siefert, 2002) and the concentrations of Fe(II) in the oceans were high (about 0.5 mmol L^{-1} (Beukes et al., 1992). Before the earth's atmosphere turned more and more oxic about 2.3 Ga ago (Kasting, 1993, 2001, Kasting & Siefert, 2002), iron(II)-oxidizing bacteria were likely abundant and found optimal conditions in the oceans. High Fe(II) concentrations in the water (Canfield, 2005, Planavsky et al., 2009) and any or only little molecular oxygen to compete with for the oxidation of Fe(II) (Kasting, 1993, 2001, Kasting & Siefert, 2002), were advantageous.

It is still heavily debated how banded iron formations formed; in particular the oxidation mechanism of the Fe(II) to Fe(III) in ancient oceans has not been clarified yet. Several hypothesis exist on how the Fe(II) was oxidized: i) cyanobacteria could have produced enough oxygen for the chemical oxidation of Fe(II) to Fe(III) (Cloud, 1968, Beukes et al., 1992); ii) UV-radiation caused direct oxidation of Fe(II) (Cairns-Smith, 1978). Konhauser et al. (2007) though doubted that this process is likely of importance; iii) Finally, Garrels et al. (1973) suggested a direct oxidation of Fe(II) by photoferrotrophs.

It seems likely that photoferrotrophs were involved in the oxidation of Fe(II) prior to the production of the first molecular oxygen (Kasting, 2001, Bekker et al., 2004). Finding evidence that photoferrotrophs were involved in the deposition of the banded iron formations is not straight forward considering the uncertainties of the conditions in the Precambrian. Therefore, we have to rely on indirect evidence and modern photoferrotrophs are used as analogues for photoferrotrophs present on early earth.

In order to determine, if photoferrotrophs could have been involved in the formation of the BIFs, Fe(II) oxidation rates were determined for three phylogenetically different bacteria. pH-, temperature- and light conditions were varied and thus allow a better understanding of the ecophysiological necessities of the photoferrotrophs – in the present and in the past (chapter 10).

The distinct layering in the BIFs of chert and iron-minerals is intriguing. Thus, understanding, how the layering developed is vital for our knowledge of the conditions on early earth. In order to understand, how the layers could have formed, Fe(II) oxidation rates at different temperatures were coupled to the geochemical behavior of silicate at different temperatures (chapter 12).

Trace metals are required by all organisms in the reactive centers of enzymes (Madigan et al., 2006). The use of the trace metals depends on two factors. Firstly, the availability of the trace metal in the respective environment of an organism. Some organisms are able to use other enzymes and enzymatic pathways if certain trace metals are not available (Fraústo da Silva & Williams, 2001, Zhang & Gladyshev, 2010) and replace trace metals by others, e.g., by iron (Ferrer et al., 2007). Secondly: enzymes may require specific trace metals which cannot be replaced and are needed even if the availability in the environment is low. The requirement of these trace metals by enzymes may date back to the time when the enzyme evolved (Fraústo da Silva & Williams, 2001, Zhang & Gladyshev, 2010) and thus may reflect the trace metal availability at that time (Fraústo da Silva & Williams, 2001).

The trace metal availability in the environment has changed fundamentally since the Pre-

cambrian when a lot of the metabolic pathways known today developed (Fraústo da Silva & Williams, 2001, Zerkle et al., 2005, Williams & Fraústo da Silva, 2006, Anbar, 2008). Therefore, even today the conditions on early earth may still be reflected in the utilization of trace elements.

The trace metal content and requirements of the photoferrotroph *"Rhodobacter ferrooxidans"* strain SW2 can be used to determine how well this organism reflects the suggested conditions on early earth in its trace metal content (chapter 11).

3.5 Laboratory techniques – cryopreservation of photoferrotrophs

The high concentration of Fe(II) additionally to the exposure to light causes radicals to form via the Fenton reaction (van der Zee et al., 1993, Touati, 2000). These radicals may damage the DNA and cause mutations ultimately leading to a loss of genes and thus functions in the Fe(II)-oxidizing cultures in the laboratory. In order to overcome this problem, a protocol to cryo-preserve anoxygenic Fe(II)-oxidizing bacteria was developed (chapter 13).

Fe(II)-oxidizing bacteria dominantly shaped the face of our planet in the past and remain doing so on a smaller scale up to today. Such features consisting of cell-mineral aggregates intrigued scientist in the 19^{th} century and laid the path for the questions of cell-mineral interaction.

Bibliography

Anbar, AD: Oceans: Elements and evolution. *Science*, 322:1481–1483, 2008.

Balashova, VV & Zavarzin, GA: Anaerobic reduction of ferric iron by hydrogen bacteria. *Mikrobiologiia*, 48:773–78, 1979.

Banfield, JF & Nealson, KH: *Geomicrobiology: Interactions between microbes and minerals*, vol. 35 of *Reviews in Mineralogy* (Mineralogical Society of America, Washington D.C.), 1st ed., 1997.

Barbeau, K; Rue, EL; Bruland, KW; & Butler, A: Photochemical cycling of iron in the surface ocean mediated by microbial iron(III)-binding ligands. *Nature*, 413:409–13, 2001.

Bekker, A; Holland, HD; Wang, PL; Rumble III, D; Stein, HJ; Hannah, JL; Coetzee, LL; & Beukes, NJ: Dating the rise of atmospheric oxygen. *Nature*, 427:117–120, 2004.

Beukes, NJ; Klein, C; Holland, HD; Kasting, JF; Kump, LR; & Lowe, DR: *Proterozoic Atmosphere and Ocean*. The Proterozoic Biosphere: a multidisciplenary study (Press Syndicate of the University of Camebridge, New York), 1992.

Beveridge, TJ & Fyfe, WS: Metal fixation by bacterial-cell walls. *Canadian Journal of Earth Sciences*, 22:1893–1898, 1985.

Beveridge, TJ & Murray, RG: Uptake and retention of metals by cell walls of *Bacillus subtilis*. *Journal of Bacteriology*, 127:1502–1518, 1976.

Beveridge, TJ & Murray, RG: Sites of metal deposition in the cell wall of *Bacillus subtilis*. *Journal of Bacteriology*, 141:876–887, 1980.

Borch, T; Kretzschmar, R; Kappler, A; Cappellen, PV; Ginder-Vogel, M; Voegelin, A; & Campbell, K: Biogeochemical redox processes and their impact on contaminant dynamics. *Environmental Science and Technology*, 44:15–23, 2010.

Caiazza, NC; Lies, DP; & Newman, DK: Phototrophic Fe(II) oxidation promotes organic carbon acquisition by *Rhodobacter capsulatus* SB1003. *Applied Environmental Microbiology*, 73:6150–6158, 2007.

Cairns-Smith, AG: Precambrian solution photochemistry, inverse segregation, and banded iron formation. *Nature*, 276:808–808, 1978.

Canfield, DE: The early history of atmospheric oxygen: Homage to robert a. garrels. *Annual Review of Earth and Planetary Sciences*, 33:1–36, 2005.

Canfield, DE; Thamdrup, B; & Kristensen, E: *Aquatic Geomicrobiology*, vol. 48 of *Advances in Marine Biology* (Elsevier Academic Press, San Diego, California), 1st ed., 2005.

Chan, CS; de Stasio, G; Welch, SA; Girasole, M; Frazer, BH; Nesterova, MV; Fakra, S; & Banfield, JF: Microbial polysaccharides template assembly of nanocrystal fibers. *Science*, 303:1656–1658, 2004.

Cloud, PE: Atmospheric and hydrospheric evolution on primitive earth. *Science*, 160:729–737, 1968.

Cornell, RM & Schwertmann, U: *The iron oxides: structure, properties, reactions, occurrences and uses* (VCH, Weinheim, Cambridge), 2nd ed., 2003.

Croal, LR; Johnson, CM; Beard, BL; & Newman, DK: Iron isotope fractionation by Fe(II)-oxidizing photoautotrophic bacteria. *Geochimica et Cosmochimica Acta*, 68:1227–1242, 2004.

Dzombak, DA & Morel, F: *Surface complexation modeling: hydrous ferric oxide* (Wiley, New York), 1990.

Ehrenberg, CG: Vorläufige Mitteilungen über das wirkliche Vorkommen fossiler Infusorien und ihre grosse Verbreitung. *Poggendorfs Annalen der Physik und Chemie*, 38:213–227, 1836.

Ehrenreich, A & Widdel, F: Anaerobic oxidation of ferrous iron by purple bacteria, a new type of phototrophic metabolism. *Applied and Environmental Microbiology*, 60:4517–4526, 1994.

Ehrlich, HL & Newman, DK: *Geomicrobiology* (CRC Press, New York), 5th ed., 2009.

Emerson, D; Fleming, EJ; & McBeth, JM: Iron-oxidizing bacteria: an environmental and genomic perspective. *Annual Review of Microbiology*, 64:561–83, 2010.

Emerson, D & Moyer, C: Isolation and characterization of novel iron-oxidizing bacteria that grow at circumneutral pH. *Applied and Environmental Microbiology*, 63:4784–4792, 1997.

Emerson, D & Revsbech, NP: Investigation of an iron-oxidizing microbial mat community located near Aarhus, Denmark: Field studies. *Applied and Environmental Microbiology*, 60:4022–4031, 1994.

Evans, U; Leal, J; & Arnold, P: The interfacial electrochemistry of goethite (α-FeOOH) especially the effect of CO_2 contamination. *Journal of Electroanalytical Chemistry*, 105:161–167, 1979.

Ferrer, M; Golyshina, OV; Beloqui, A; Golyshin, PN; & Timmis, KN: The cellular machinery of ferroplasma acidiphilum is iron-protein-dominated. *Nature*, 445:91–94, 2007.

Ferris, FG; Beveridge, TJ; & Fyfe, WS: Iron-silica crystallite nucleation by bacteria in a geothermal sediment. *Nature*, 320:609–611, 1986.

Fortin, D; Ferris, FG; & Scott, SD: Formation of Fe-silicates and Fe-oxides on bacterial surfaces in samples collected near hydrothermal vents on the Southern Explorer Ridge in the northeast Pacific Ocean. *American Mineralogist*, 83:1399–1408, 1998.

Fortin, D & Langley, S: Formation and occurrence of biogenic iron-rich minerals. *Earth-Science Reviews*, 72:1–19, 2005.

Fraústo da Silva, JJR & Williams, RJP: *The biological chemistry of the elements: the inorganic chemistry of life* (Oxford University Press, Oxford), 2nd ed., 2001.

Garrels, RM; Perry, EA, JR; & Mackenzie, FT: Genesis of precambrian iron-formations and the development of atmospheric oxygen. *Economic Geology*, 68:1173–1179, 1973.

Gold, T: The deep, hot biosphere. *Proceedings of the National Academy of Sciences of the United States of America*, 89:6045–9, 1992.

Hafenbradl, D; Keller, M; Dirmeier, R; Rachel, R; Rossnagel, P; Burggraf, S; Huber, H; & Stetter, KO: *Ferroglobus placidus* gen. nov., sp. nov., a novel hyperthermophilic archaeum that oxidizes Fe^{2+} at neutral pH under anoxic conditions. *Archives of Microbiology*, 166:308–314, 1996.

Hallbeck, L & Pedersen, K: Benefits associated with the stalk of *Gallionella ferruginea*, evaluated by comparison of a stalk-forming and a non-stalk-forming strain and biofilm studies in-situ. *Microbial Ecology*, 30:257–268, 1995.

Heising, S; Richter, L; Ludwig, W; & Schink, B: *Chlorobium ferrooxidans* sp nov., a phototrophic green sulfur bacterium that oxidizes ferrous iron in coculture with a *"Geospirillum"* sp strain. *Archives of Microbiology*, 172:116–124, 1999.

Heising, S & Schink, B: Phototrophic oxidation of ferrous iron by a *Rhodomicrobium vannielii* strain. *Microbiology*, 144:2263–2269, 1998.

Johnson, KJ; Ams, DA; Wedel, AN; Szymanowski, JES; Weber, DL; Schneegurt, MA; & Fein, JB: The impact of metabolic state on Cd adsorption onto bacterial cells. *Geobiology*, 5:211–218, 2007.

Kappler, A & Newman, DK: Formation of Fe(III)-minerals by Fe(II)-oxidizing photoautotrophic bacteria. *Geochimica et Cosmochimica Acta*, 68:1217–1226, 2004.

Kappler, A; Schink, B; & Newman, DK: Fe(III) mineral formation and cell encrustation by the nitrate-dependent Fe(II)-oxidizer strain BoFeN 1. *Geobiology*, 3:235–245, 2005.

Kappler, A & Straub, KL: Geomicrobiological cycling of iron. *Reviews in Mineralogy & Geochemistry*, 59:85–108, 2005.

Kasting, JF: Earth's early athmosphere. *Science*, 259:920–926, 1993.

Kasting, JF: Earth history. the rise of atmospheric oxygen. *Science*, 293:819–20, 2001.

Kasting, JF & Siefert, JL: Life and the evolution of earth's atmosphere. *Science*, 296:1066–1068, 2002.

Klausen, J; Trober, SP; Haderlein, SB; & Schwarzenbach, RP: Reduction of substituted nitrobenzenes by Fe(II) in aqueous mineral suspensions. *Environmental Science & Technology*, 29:2396–2404, 1995.

Konhauser, K: *Introduction to Geomicrobiology* (Blackwell Publishing, Malden, MA, USA), 1st ed., 2007.

Konhauser, KO: Bacterial iron biomineralization in nature. *FEMS Microbiology Reviews*, 20:315–326, 1997.

Konhauser, KO; Amskold, L; Lalonde, SV; Posth, NR; Kappler, A; & Anbar, A: Decoupling photochemical Fe(II) oxidation from shallow-water BIF deposition. *Earth and Planetary Science Letters*, 258:87–100, 2007.

Konhauser, KO; Fyfe, WS; Schultze-Lam, S; Ferris, F; & Beveridge, TJ: Iron phosphate precipitation by epilithic microbial biofilms in arctic canada. *Canadian Journal of Earth Science*, 31:1320–1324, 1994.

Konhauser, KO; Jones, B; Phoenix, V; Ferris, G; & Renaut, R: The microbial role in hot spring silicification. *Ambio*, 33:552–558, 2004.

Lane, DJ; Harrison, AP; Stahl, D; Pace, B; Giovannoni, SJ; Olsen, GJ; & Pace, NR: Evolutionary relationships among sulfur-oxidizing and iron-oxidizing eubacteria. *Journal of Bacteriology*, 174:269–278, 1992.

Lovley, DR: Dissimilatory Fe(III) and Mn(IV) reduction. *Microbiology and Molecular Biology Reviews*, 55:259–287, 1991.

Madigan, MT; Martinko, JM; & Brock, TD: *Brock biology of microorganisms* (Pearson Prentice Hall, Upper Saddle River, NJ), 11th ed., 2006.

Miot, J; Benzerara, K; Morin, G; Kappler, A; Bernard, S; Obst, M; Férard, C; Skouri-Panet, F; Guigner, JM; Posth, NR; Galvez, M; Brown, GE, JR.; & Guyot, F: Iron biomineralization by neutrophilic iron-oxidizing bacteria. *Geochimica et Cosmochimica Acta*, 73:696–711, 2009a.

Miot, J; Benzerara, K; Obst, M; Kappler, A; Hegler, F; Schaedler, S; Bouchez, C; Guyot, F; & Morin, G: Extracellular iron biomineralization by photoautotrophic iron-oxidizing bacteria. *Applied and Environmental Microbiology*, 75:5586–5591, 2009b.

Myers, CR & Nealson, KH: Bacterial manganese reduction and growth with manganese oxide as the sole electron-acceptor. *Science*, 240:1319–1321, 1988.

Pham, AN; Rose, AL; Feitz, AJ; & Waite, TD: Kinetics of Fe(III) precipitation in aqueous solutions at pH 6.0-9.5 and 25 degrees C. *Geochimica Et Cosmochimica Acta*, 70:640–650, 2006.

Phoenix, VR; Adams, DG; & Konhauser, KO: Cyanobacterial viability during hydrothermal biomineralisation. *Chemical Geology*, 169:329–338, 2000.

Phoenix, VR & Konhauser, KO: Benefits of bacterial biomineralization. *Geobiology*, 6:303–308, 2008.

Planavsky, N; Rouxel, O; Bekker, A; Shapiro, R; Fralick, P; & Knudsen, A: Iron-oxidizing microbial ecosystems thrived in late paleoproterozoic redox-stratified oceans. *Earth and Planetary Science Letters*, 286:230–242, 2009.

Posth, NR; Huelin, S; Konhauser, K; & Kappler, A: Size, density and composition of cell-mineral aggregates formed during anoxigenic phototrophic Fe(II) oxidation: Impact on modern and ancient environments. *Geochimica Et Cosmochimica Acta*, 74:3476–3493, 2010.

Pringsheim, EG: Iron bacteria. *Biological Reviews of the Cambridge Philosophical Society*, 24:200–45, 1949.

Rose, AL & Waite, TD: Reconciling kinetic and equilibrium observations of iron(III) solubility in aqueous solutions with a polymer-based model. *Geochimica et Cosmochimica Acta*, 71:5605–5619, 2007.

Schaedler, S; Burkhardt, C; Hegler, F; Straub, KL; Miot, J; Benzerara, K; & Kappler, A: Formation of cell-iron-mineral aggregates by phototrophic and nitrate reducing anaerobic Fe(II)-oxidizing bacteria. *Geomicrobiology Journal*, 26:93–103, 2009.

Straub, KL; Benz, M; Schink, B; & Widdel, F: Anaerobic, nitrate-dependent microbial oxidation of ferrous iron. *Applied and Environmental Microbiology*, 62:1458–1460, 1996.

Thompson, JB & Ferris, FG: Cyanobacterial precipitation of gypsum, calcite and magnesite from natural alkaline lake water. *Geology*, 18:995–998, 1990.

Tipping, E: The adsorption of aquatic humic substances by iron oxides. *Geochimica et Cosmochimica Acta*, 45:191–199, 1981.

Touati, D: Iron and oxidative stress in bacteria. *Archives of Biochemistry and Biophysics*, 373:1–6, 2000.

Tufano, KJ & Fendorf, S: Confounding impacts of iron reduction on arsenic retention. *Environmental Science and Technology*, 42:4777–4783, 2008.

Urrutia Mera, M; Kemper, M; Doyle, R; & Beveridge, TJ: The membrane-induced proton motive force influences the metal binding ability

of *Bacillus subtilis* cell walls. *Applied Environmental Microbiology*, 58:3837–3844, 1992.

van der Zee, J; Krootjes, BBH; Chignell, CF; Dubbelman, TMAR; & van Steveninck, J: Hydroxyl radical generation by light-dependent fenton reactions. *Free Radical Biology & Medicine*, 14:105–113, 1993.

Wächtershäuser, G: Evolution of the first metabolic cycles. *Proceedings of the National Academy of Sciences of the United States of America*, 87:200–204, 1990.

Wächtershäuser, G: Origin of life: Life as we don't know it. *Science*, 289:1307–1308, 2000.

Waite, TD; Sompongchaiyakul, P; & Pham, AN: Kinetics of Fe(II) removal from seawater in the absence and presence of organic matter. *Abstracts of Papers of the American Chemical Society*, 220:U337–U337, 2000.

Weber, KA; Achenbach, LA; & Coates, JD: Microorganisms pumping iron: anaerobic microbial iron oxidation and reduction. *Nature Reviews: Microbiology*, 4:752–764, 2006.

Widdel, F; Schnell, S; Heising, S; Ehrenreich, A; Assmus, B; & Schink, B: Ferrous iron oxidation by anoxygenic phototrophic bacteria. *Nature*, 362:834–836, 1993.

Williams, RJP & Fraústo da Silva, JJR: *The chemistry of evolution: the development of our ecosystem* (Elsevier, Amsterdam; Boston), 1st ed., 2006.

Winogradsky, S: Über Eisenbacterien. *Botanische Zeitung*, 17:261–270, 1888.

Zerkle, AL; House, CH; & Brantley, SL: Biogeochemical signatures through time as inferred from whole microbial genomes. *American Journal of Science*, 305:467–502, 2005.

Zhang, Y & Gladyshev, VN: General trends in trace element utilization revealed by comparative genomic analyses of Co, Cu, Mo, Ni and Se. *Journal of Biological Chemistry*, 285:3393–405, 2010.

4 Does a low pH-microenvironment around Fe(II)-oxidizing phototrophs prevent cell encrustation by Fe(III) minerals?

Florian Hegler[1], Caroline Schmidt[1], Heinz Schwarz[2], Andreas Kappler[1] **FEMS Microbiology Ecology, 74: 592 – 600, 2010**

[1]Center for Applied Geoscience – Geomicrobiology, Eberhard Karls University Tübingen, Sigwartstrasse 10, 72076 Tübingen, Germany
[2]MPI Tübingen, Spemannstrasse 35, 72076 Tübingen, Germany

4.1 Abstract

Neutrophilic Fe(II)-oxidizing bacteria precipitate positively charged Fe(III) minerals that are expected to sorb to the negatively charged cell surface leading to encrustation and thus limiting the cells' accessibility to substrates and nutrients. However, electron-microscopy analysis of phototrophic iron-oxidizing *Thiodictyon* sp. strain F4 cells showed no encrustation but mineral precipitation in distance to the cell surface. In-situ fluorescence microscopy analysis of F4 cells using a pH-sensitive fluorescent dye revealed a low cell surface pH (6.0 ± 0.1) in contrast to the bulk pH (6.6 ± 0.1). Biogeochemical modeling showed that the pH-difference lowers Fe(III) sorption and Fe(III) precipitation rates at the cell surface therefore directing mineral formation away from the cells. The results from this study therefore suggest that the establishment of a cell pH microenvironment could provide a mechanism for photoferrotrophs to successfully prevent Fe(III) mineral precipitation on the cell surface.

4.2 Introduction

While Fe(II) is relatively soluble at neutral pH, Fe(III) preferentially occurs in the solid phase as $Fe(III)_{ppt}$ with maximum aqueous concentrations of dissolved Fe(III) [$Fe(III)_{aq}$] of approximately 1×10^{-10} mol L^{-1} (Stumm & Morgan, 1995) . Iron(III) (oxy)hydroxides [$Fe(III)_{ppt}$] are produced chemically and biologically in the environment (Emerson, 2000, Ehrlich & Newman, 2009) by microbial and chemical iron(II) [Fe(II)] oxidation at neutral pH (Widdel et al., 1993, Hafenbradl et al., 1996, Straub et al., 1996, Emerson, 2000, Canfield, 2005). The phenomenon of microbial

Fe(II) oxidation was discovered already in the early days of microbiology in the 19^{th} century (Ehrenberg, 1836, Winogradsky, 1888). At that time though, the interaction of iron(III) oxides [Fe(III) oxides] with bacteria could only be observed visually, but neither the corresponding metabolism nor the mechanism behind could be explained.

While aerobic neutrophilic Fe(II)-oxidizers *Gallionella* and *Leptothrix* thrive at low concentrations of oxygen, phototrophic Fe(II)-oxidizing bacteria, as well as nitrate-reducing Fe(II)-oxidizers, convert Fe(II) under anoxic conditions. Fe(II)-oxidizing bacteria can access the dissolved substrate ($Fe(II)_{aq}$) easily at circumneutral pH. However, under such pH conditions the cells may be harmed by the poorly soluble product ($Fe(III)_{ppt}$) of their metabolism since $Fe(III)_{aq}$, as well as the positively charged $Fe(III)_{ppt}$ strongly sorb to the negatively charged bacterial cell surfaces. Consequently cells are expected to encrust with $Fe(III)_{ppt}$ leading to a limited exchange of metabolites with their environment. In particular, the Fe(II)-oxidizing nitrate-reducing *Acidovorax* sp. strain BoFeN1 was shown to encrust heavily with $Fe(III)_{ppt}$ at circumneutral pH (Miot et al., 2009a, Schaedler et al., 2009).

In this study, we focus on a photoferrotrophic strain which oxidize Fe(II) according to the following equation:

$$4Fe^{2+} + HCO_3^- + 10H_2 + h\nu \rightarrow 4Fe(OH)_3 + < CH_2O > +7H^+ \tag{4.1}$$

(Widdel et al., 1993). It has been shown that all electrons stemming from Fe(II) oxidation are used by phototrophic Fe(II)-oxidizing bacteria for CO_2 fixation and thus biomass generation (Widdel et al., 1993). Recently, it was suggested for two different strains of phototrophic Fe(II)-oxidizing bacteria that the oxidation of Fe(II) occurs in the periplasm of the cells (Croal et al., 2007, Jiao & Newman, 2007). In contrast to chemotrophic Fe(II)-oxidizing strains, none of the known photoferrotrophs encrusts with Fe(III) minerals (Miot et al., 2009b, Schaedler et al., 2009). It is particularly essential for phototrophic Fe(II)-oxidizing strains to avoid cell encrustation as the mineral coatings may not only limit the exchange of nutrients and metabolites of the cell with its environment. Additionally, the amount of light available for photosynthesis decreases due to the mineral crust, and therefore reduces the overall energy available to the cell.

Various mechanisms have been suggested to explain why some Fe(II)-oxidizing strains do not encrust: a) Organic exopolymers, similar to those observed for *Gallionella* spp., could help to localize precipitation away from the cell (Chan et al., 2009, Schaedler et al., 2009, and references therein). Still, this mechanism does not explain why released $Fe(III)-aq$ does not immediately bind to the negatively charged cell surface after Fe(II) oxidation. b) Shedding of parts of the cell surface covered with Fe-precipitates could remove the precipitates from the surface (Emerson & Revsbech, 1994). c) Fe(III) complexation by organic ligands allows Fe(III) to stay in solution and prevents precipitation (Croal et al., 2004a). However, in case of autotrophic organisms, CO_2 reduction for synthesis of such ligands is quite costly in terms of Fe-requirement. Four atoms of Fe(II) have to be oxidized to reduce a single CO_2 to biomass (e.g. usable in a complexing

molecule keeping Fe(III) in solution) (eq. 4.1). Several carbon atoms are usually required per ligand. For example, 36 Fe(II) would have to be oxidized to produce a single ligand molecule with 6 carbon atoms (with a C oxidation state of 0) and this carbon would not be available for cell biomass while it could complex only one Fe(III) atom. Organic ligands (such as oxalate) requiring very few electrons for their synthesis from CO_2 could potentially be suitable as complexing agent. However, although oxalic acid would fulfill this requirement by needing only two electrons to be synthesized from two CO_2 molecules, an effective recycling of any of these ligands is unlikely, mainly due to photoreactivity of many organic Fe(III) ligands leading to degradation of the ligands (Barbeau et al., 2001). Therefore, this mechanism seems not very plausible. d) The amount of negatively charged (and therefore Fe(III) binding) functional groups on the cell surface could be reduced or the cell surface charge could even be reversed from negative to positive to avoid primary precipitation (Beveridge & Murray, 1980, Urrutia Mera et al., 1992). This has been shown only for cyanobacteria (McConnaughey & Whelan, 1997, Martinez et al., 2010) but it is unknown whether photoferrotrophs are also able to change their surface charge. e) Fe(III) precipitation at the cell surface could be delayed, lowered, or even prevented by acidifying the cell microenvironment (Sobolev & Roden, 2001, Kappler & Newman, 2004, Schaedler et al., 2009).

An environment of enhanced proton activity around the cell (termed "low pH-microenvironment" in this study) has the advantage for a cell that it does not require additional biomass to be produced for complexation of Fe(III) by organic ligands, shedding of parts of the cell or localization of precipitates on exopolymers (e.g. stalks). In the case of phototrophic Fe(II)-oxidizing bacteria, acidification around colonies of cells has previously been observed (Kappler & Newman, 2004). However, it is unclear whether this acidification stems from the formation of $Fe(OH)_3$ from Fe^{3+}_{aq} that would release protons (according to equation 4.1) where Fe(II) oxidation is coupled to CO_2 fixation) or whether the lower pH was actively caused by the cells via proton translocation.

Therefore the objectives of this study were i) to analyze the pH at the single-cell level compared to the bulk medium using the phototrophic Fe(II)-oxidizing bacterium *Thiodictyon* sp. F4, a gram negative, γ-proteobacterium (Croal et al., 2004b)and ii) to evaluate whether and how the establishment of a single-cell pH-microenvironment influences Fe(III) sorption and Fe(III) mineral precipitation. Sub-micrometer pH measurements were achieved by a combination of confocal laser scanning microscopy (CLSM) and a pH-dependent fluorescent dye. Geochemical modeling was used to determine the pH dependence of Fe(III) sorption and precipitation, and evaluate whether an actively sustained pH microenvironment might prevent encrustation.

4.3 Material and Methods

4.3.1 Medium, chemicals and growth conditions

The phototrophic Fe(II) oxidizer *Thiodictyon* sp. strain F4 (Croal et al., 2004b) was grown in mineral medium buffered with 22 mM bicarbonate at pH 6.8-6.9. The addition of 10 mM $FeCl_2$ as electron donor decreased the pH slightly to pH 6.6. For a detailed description of the growth conditions see (Hegler et al., 2008). The fluorescent dye SNARF®-4F 5-(and-6)-carboxylic acid (SNARF4F) (Invitrogen, 2003, Marcotte & Brouwer, 2005) by Molecular Probes was dissolved in water (2 mM) and aliquots were frozen and used not longer than 4 months to avoid potential hydrolytic degradation of the dye. Samples of *Thiodictyon* sp. strain F4 cultures were taken at the end of the exponential growth phase and 500 μL sample were mixed with 1 μL of the dye solution in an anoxic glovebox (100% N_2) in order to avoid oxygen exposure (final concentration of the dye: 4 μL). Although some association of the dye and the cell wall may occur, we chose this dye because it does not penetrate the cell itself (Invitrogen, 2003). The potential association of the dye with the cell surface was not expected to affect its pH-dependent fluorescence (Invitrogen, 2003).

4.3.2 Microscopic analysis of single cell pH-microenvironment

An oxygen-tight microscopy chamber covered with a coverslip was used to avoid physical pressure to the minerals and to keep the sample anoxic during microscopy. The chambers were prepared by gluing a coverslip onto the microscopy slide with epoxy-based glue (Uhu plus schnellfest, UHU GmbH & Co. KG, Germany) including two syringe needles as inlet and outlet. They were washed with double-distilled water prior to use.

The chambers were filled with the culture/dye mixture and incubated for 45 min before microscopic analysis at light saturation. This time allows CCCP to deenergize the membranes. As it was recently suggested that Fe(II) oxidation occurs in the periplasm of phototrophic Fe(II)-oxidizing bacteria (Croal et al., 2007, Jiao & Newman, 2007), no active (energy-requiring) uptake of Fe(II) into the cytoplasm is needed and therefore Fe(II) oxidation did not stop immediately after addition of CCCP. However, reducing equivalents accumulate due to the oxidation of Fe(II) but cannot be re-oxidized, hence finally Fe(II) oxidation will stop due to the lack of electron acceptors.

Microscopy was performed at a Leica TCS SP2 confocal scanning laser microscope. The dye was excited at 488 nm, and the fluorescence measured at emission wavelengths of 580-590 nm and 650-660 nm (figure 4.1 A-C). The ratio of the two wavelengths was used to calculate the pH according to a calibration curve. Continuous spectra for dye calibration were measured in 20 mM PBS buffer with a pH between 5 and 7.5 using a Jena Analytics FlashScan 550 fluorescence plate reader at an excitation of 488 nm. The ratio between the individual wavelength (580-590 nm and 650-660 nm) was calculated depending on pH. We fitted the curve to account for the non-linear

parts of the curve away from the pKa of the dye. The ratio between the individual wavelengths and its correlation to the pH was used to calculate the pH values in the microscopy images.

In order to determine whether the establishment of the ΔpH in the cell microenvironment is an active or passive process, carbonyl cyanide 3-chlorophenylhydrazone (CCCP, Sigma Aldrich, Germany) was used – a protonophore that decouples the proton motive force across the membrane (Harold, 1972).

4.3.3 Electron microscopy

For scanning electron microscopy, samples were prepared as described previously (Schaedler et al., 2008).

4.3.4 Calculation of Fe(II) oxidation rate per cell

In order to calculate the amount of Fe(II) oxidized per cell per unit time, we quantified the decrease of total Fe(II) over time as described (Hegler et al., 2008). Additionally, cells were counted microscopically: 1 mL culture was fixed with glutaraldehyde (final concentration of 2.5%) followed by dissolution of the minerals at pH 3 with oxalic acid ($15\,\mathrm{g\ L^{-1}}$) oxalate ($28\,\mathrm{g\ L^{-1}}$). After dissolution of the $\mathrm{Fe(III)_{ppt}}$ and staining of the cells with 4',6-Diamidino-2-phenylindol (DAPI), a subsample was passed through a Nucleopore-filter (0.22 μm pore size, Millipore) and the amount of cells per filter area was counted in an epi-fluorescence microscope. The data allowed calculating maximum Fe(III) production rates per cell, which were used for calculating the sorption of Fe(III) onto the cell surface. The bulk Fe(III) formation rate was determined by following Fe(II) oxidation over time (which is equal to Fe(III) formation) and calculating the turnover in the entire culture over the complete oxidation phase of 218 h. The release of Fe(III) per second was calculated to be $4.3 \times 10^{-7}\,\mathrm{mM\ s^{-1}}$.

4.3.5 Modeling

The resolution of the microscope did not allow resolving the expected pH gradient between the cell surface and the bulk medium. Thus, a gradient of proton activity was interpolated between cell surface and the bulk medium for modeling. Additionally, geochemical modeling was applied to evaluate sorption of ferric iron to the cell surface. Unfortunately cell surface titrations could not be used to quantify the different functional groups involved in mineral sorption processes at the cell surface of the Fe(II)-oxidizing strain since the Fe(III) minerals (produced during Fe(II) oxidation) interfered with the titrations. Microscopic analysis revealed (data not shown) that dissolving the minerals killed the cells, partially destroyed cell integrity and increased the amount of (titratable) functional groups originating from the cell interior likely falsifying the titration measurements. Additionally, sorption of Fe(III) ions to cell surfaces cannot be quantified directly at circumneutral pH due to low solubility of the Fe(III) at this pH. However, it has

been shown that as an alternative approach a general model for site densities and pK_a-values can be employed to model adsorption of metals to cell surfaces (Fein et al., 2001). Yee & Fein (2003) showed that the adsorption behavior of different physiological and phylogenetic groups of bacteria, gram-positive as well as gram-negative, and cell mixtures is very similar for various metals. The most abundant cell surface moieties are carboxyls (Borrok et al., 2004). Other functional groups such as protonated amines deprotonate at pH values well above 7 and are thus positively charged at circumneutral pH-values. Following the approach of Yee & Fein (2003) we quantified the cell surface interaction of Fe^{3+}_{aq} with the most abundant functional group (carboxyl group).

4.3.6 Calculation of Fe(III) solubility

Geochemists Workbench 6.04 by Rockware was used to calculate the speciation and thus the solubility of Fe(III) in the medium. A matrix including all chemical compounds present in the medium was set up, see table 4.1. For the thermodynamic equilibrium calculations the dissolved ferric iron concentration ($Fe(III)_{aq}$) was defined as follows (including the most dominant Fe(III) species):

$$\begin{aligned} Fe(III)_{aq} = {} & Fe(OH)^0_3 + Fe(OH)^+_2 + FeHPO^+_4 + Fe(OH)^-_4 + FeOH^{2+} + FeCO^+_3 \\ & + Fe_3(OH)^{5+}_4 + FeH_2PO^{2+}_4 + Fe_2(OH)^{4+}_2 + FeSO^+_4 + Fe^{3+} + ... \end{aligned} \tag{4.2}$$

4.3.7 Calculation of iron-cell-surface interaction

The following equation was applied to calculate sorption of Fe(III) to the carboxylic groups of the cell surface:

$$[ML] = \frac{[site_{max}]\, K_a K_{ads} \left(\frac{M}{H^+}\right)}{1 + K_a K_{ads} \left(\frac{M}{H^+}\right)} \tag{4.3}$$

with ML being the ligand-metal complex, K_a is the carboxyl-equilibrium constant, K_{ads} represents the adsorption constant while M is the metal concentration and H+ the proton concentration; $site_{max}$ gives the maximal surface site concentration. The maximal site concentration ($site_{max}$) represents approximately the total amount of -COOH surface sites at pH >5.

Here we shortly derive eq. 4.3 with the already introduced abbreviations: Deprotonation of carboxylic groups is described by

$$R{-}COOH \rightleftharpoons R{-}COO^- + H^+ \tag{4.4}$$

Replacing $R{-}COO^-$ by L^- and $R{-}COOH$ by L and calculating the deprotonated ligand

Table 4.1: Settings and concentrations of all chemical compounds included in the matrix used to calculate the solubility of $Fe(III)_{aq}$ in mineral medium over the pH-range from 6 to 7. The resulting graph depicts all dissolved $Fe(III)_{aq}$ species (figure 4.2).

compound added	
1 kg H_2O	
4.4 mmol L^{-1} $H_2PO_4^-$	swap $H_2PO_4^-$ for PO_4^{3-}
22 mmol L^{-1} HCO_3^-	swap HCO_3^- for CO_3^{2-}
0.68 mmol $L^{-1}Ca^{2+}$	
4.4 mmol L^{-1} K^+	
2 mmol $L^{-1}Mg^{2+}$	
22 mmol $L^{-1}Na^+$	
30.2 mmol L^{-1} Cl^-	
2 mmol L^{-1} SO_4^{2-}	
6.6 mmol L^{-1} NH_4^+	
10 mmol $L^{-1}Fe^{3+}$	
1e-50 mmol L^{-1} $O^2_{(aq)}$	
pH 6.0 slide pH to 7.0	
decouple Fe^{2+} and HS^-	
suppress H_2S(aq) and $FeHS^+$	
balance off	

concentration, L^- yields

$$L^- = \frac{[K_a]\,[L]}{[H+]} \tag{4.5}$$

This formula determines the concentration of the deprotonated ligands at the cell surface with respect to pH. The adsorption equilibrium can be expressed by

$$M + L^- \rightleftharpoons LM \tag{4.6}$$

which can be used to calculate the metal-ligand concentration

$$[ML] = K_{ads}K_a\,[M]\,[L^-] \tag{4.7}$$

The substitution of L^- of eq. 4.5 in eq. 4.7 leads to

$$L^- = \frac{[K_a]\,[L]}{[H+]} \tag{4.8}$$

which – after constraining the maximal sorption with a Langmuir isotherm – yields eq. 4.3. A list for all parameters used in the calculations is compiled in table 4.2.

In the calculations we did not consider abiotic processes that may initiate or stimulate precipitation such as for example the initial presence of nucleation sites (e.g. by the presence of

siderite and vivianite crystallites in the growth medium).

4.3.8 Calculation of the precipitation kinetics of $Fe(III)_{ppt}$

For kinetic precipitation modeling the same speciation setup (table 4.1) was used while the reaction rate constant for precipitation ($k_{precipitation} = 2.0 \times 10^7\,M^{-1}s^{-1}$, for comparison reaction rate constant for diffusion $k_{diffusion} = 7.9 \times 10^9\,M^{-1}s^{-1}$) was taken from Pham et al. (2006). In order to determine the precipitation kinetics, we measured the rate of Fe(III) production for *Thiodictyon* sp. strain F4 (7.9×4.3^{-7} mM s^{-1}) in a growth experiment (table 4.2). The rate of precipitation at the cell surface (at pH 6.0) and in the bulk (at pH 6.6) was calculated accounting for a constant $Fe(III)_{aq}$ release of 4.3×10^{-7} mM s^{-1} (per second).

Table 4.2: Compilation of parameters used to calculate sorption of Fe(III) to carboxylic cell surface functional groups.

parameter	value	reference
K_a	1.0×10^{-5}	Fein et al. (1997)
K_{ads}	1.0×10^{-4}	Yee & Fein (2003)
mol R-COOH/cell	1.8×10^{-16}	Yee & Fein (2003)
cells/L at max. oxidation rate $8.0 \times 10^{+10}$	measured	
$site_{max}$ mol L^{-1}	1.44×10^{-5}	calculated
Fe(III) production rate mM s^{-1} at the bulk	4.3×10^{-7}	measured

4.4 Results and Discussion

4.4.1 Absence of encrustation and establishment of a pH microenvironment around phototrophic Fe(II)-oxidizing *Thiodictyon* sp. strain F4 cells

Scanning electron microscopy showed that cells of the phototrophic Fe(II)-oxidizing *Thiodictyon* strain sp. F4 do not become encrusted when oxidizing Fe(II) at neutral pH (figure 4.1). This suggests that this strain might be able to minimize or even avoid sorption of $Fe(III)_{aq}$ to the cell surface in order to avoid precipitation of $Fe(III)_{ppt}$ on its cell surface. To determine whether a low cell surface pH exists for F4 cells and is possibly involved in preventing cell encrustation, we incubated the cells with a dye that shows pH-dependent variations in fluorescence-emission.

We determined the pH in the bulk medium with the fluorescent dye in comparison to the values obtained using a standard pH-electrode and obtained a value of 6.6 ± 0.1 with both independent methods. As can be seen in figure 4.1, for most active cells we detected that the cell surface pH was at least 0.6 ± 0.1 units lower compared to the bulk medium of the phototrophic Fe(II)-oxidizing strain *Thiodictyon* sp. F4. The same effect was observed for approximately 16 out of 20 investigated cells. However, we even found some cells with a larger shift of 0.8 ± 0.1 pH units between surface and bulk pH, although cells with such a larger pH shift were less frequent (about 10-15% of all cells). A few cells (10%) showed only a very small pH-difference

from the bulk pH possibly representing inactive microbial cells. The cells with the highest and lowest pH-variation were not considered in the subsequent geochemical calculations.

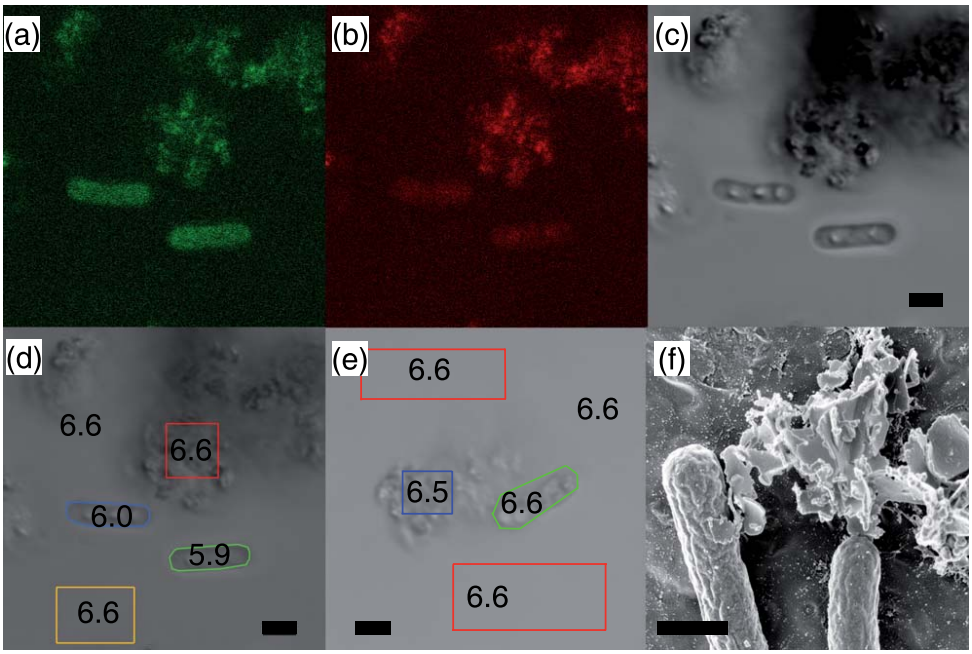

Figure 4.1: Confocal laser scanning microscopy (CLSM) imaging of *Thiodictyon* sp. F4 cells stained with a pH-dependent fluorescent dye, demonstrating the presence of a cell pH-microenvironment. (a-c): CLSM pictures of cells stained with SNARF4. A: 580-590 nm, (b) 650-660 nm, (c) grey-scale image. The ratio of A/B allows calculating the pH. (d): pH-microenvironment around cells of *Thiodictyon* sp. F4, the pH was 6.6 ± 0.1 at the background (yellow box) and mineral (red box), bulk-measurements with a pH-electrode confirmed the values determined with the pH-dependent dye. The pH at the cell level was 5.9 ± 0.1 (green cell) and 6.0 ± 0.1 (blue cell). (e) Red: background, green: cell, blue: mineral, CCCP used to decouple the proton gradient. The pH was 6.6 ± 0.1 at the cell level, the background also pH 6.6 ± 0.1 for both areas, the pH at the mineral was 6.5 ± 0.1 while the whole frame had a pH of 6.6 ± 0.1. Bulk measurements with a pH-electrode confirmed these values. Scale-bar in all images A-E is 2 μm. (f) scanning electron micrograph of *Thiodictyon* sp. F4, scalebar 1 μm. The cell is associated with Fe(III) minerals, but not encrusted.

In order to test whether an active cell metabolism is necessary to establish the low cell surface pH, we decoupled the membranes with CCCP (carbonyl cyanide 3-chlorophenylhydrazone), a protonophore (Harold, 1972). As a consequence of the exposure to CCCP, the cells were no longer able to maintain different proton concentrations at both sides of the membrane. In contrast to the untreated cells, we did not see a lower cell surface pH of these treated cells (figure 4.1 E), suggesting that active cell metabolism is required for establishing and maintaining the observed low cell surface pH. The measured ΔpH is consistent with ΔpH values compiled by (Padan et al., 1981) for the proton motive force (PMF) and with pH values calculated from the differences in sorption of metals to alive and dead cells using surface complexation constants (Johnson et al., 2007). These authors approximated that the difference of metal sorption between active and

inactive cells reflected the decrease of sorption capacity due to a pH decrease of approximately one pH unit at the cell surface.

Such pH-gradients across cell membranes are utilized e.g. for ATP-generation or driving the motor units of flagella (Mitchell, 1979, Nicholls & Ferguson, 2002). In phototrophic organisms protons and positive charges move outside of the cell driven by light energy during cyclic photophosphorylation, acidifying the periplasm and potentially also the close proximity of a bacterial cell surface. If enough light is present, a single electron that comes from one oxidized Fe(II) can theoretically be used several times in the cyclic electron flow to generate the pH-gradient across the membrane by pumping protons and creating a higher pH outside of the cell. These electrons stem from the oxidation of Fe(II) (eq. 4.1). However, electrons from Fe(II) (reducing equivalents, NAD(P)H) are also needed to produce biomass by fixing CO_2. Therefore, continuous oxidation of Fe(II) is necessary for cell growth. Due to the fact that photosynthetic Fe(II)-oxidizers can transport protons several times from the inside to the periplasm using light quanta as energy source and the same electron in cyclic photophosphorylation, it is expected that these cells can release more or less as many protons as needed to establish a low cell surface pH if sufficient light is available. However, they cannot fix an unlimited amount of CO_2 to build biomass.

4.4.2 Effect of the pH microenvironment on sorption, precipitation and dissolution of Fe(III)

After oxidation of Fe(II) by the cell and the release of Fe^{3+}_{aq}, the cation either adsorbs to the negatively charged cell surface functional groups or diffuses away from the cell. The Fe(II)-oxidizing enzymes likely release Fe^{3+}_{aq} and not a hydrolysed Fe(III) species. The interaction of metals and metalloids with cell surfaces can be described as sorption followed by precipitation of the metal ions as minerals (Beveridge & Murray, 1976). Thus, we calculated the sorption of Fe^{3+}_{aq} (as released initially by the cell) to cell surface functional groups. In the initial adsorption-step, metal ions, such as iron, compete directly with protons for binding sites at carboxyl- and phosphoryl-functional groups. Calculations for carboxylic functional groups showed that sorption of Fe^{3+} to carboxylic surface functional groups decreases by more than 80% with a pH drop of 0.6 (figure 4.2). These results agree well with other studies that showed that Co^{2+}, Nd^{3+}, Ni^{2+}, Sr^{2+}, Zn^{2+} (Fein et al., 2001), and Fe(III) (Warren & Ferris, 1998) adsorb less to cell surfaces at lower pH. Additionally, Urrutia Mera et al. (1992) showed that cells of *Bacillus subtilis* bind heavy metals like U and Sc substantially less to their cell surface when the cells were alive (with a functioning pmf). Less adsorption of metals due to competition with H+ leads to fewer potential nucleation sites for mineral precipitation (Urrutia Mera et al., 1992, Fein et al., 2001).

The lower pH not only influences the competition of the $Fe(III)_{aq}$ ions with protons for the cell surface binding sites, it also changes the solubility of Fe(III) itself. Since the concentration of $Fe(III)_{aq}$ ions and therefore the solubility of the Fe(III) determine the kinetics and extent of precipitation (Grundl & Delwiche, 1993, Pham et al., 2006, Rose & Waite, 2007), we determined

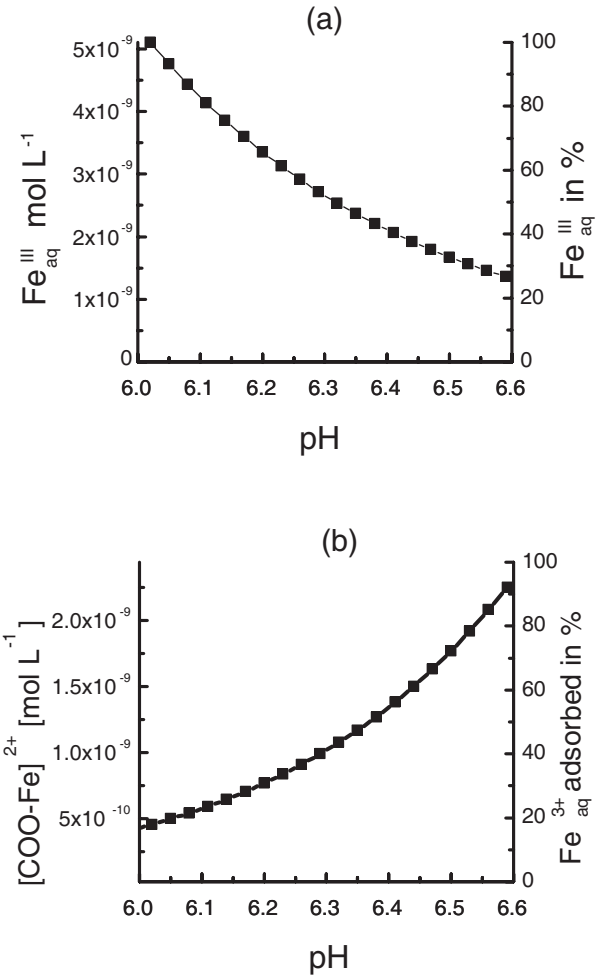

Figure 4.2: (a) Change of $Fe(III)_{aq}$ (in mol L-1 and in %) as a function of pH over a range from pH 6.0 to 6.6 based on thermodynamic equilibrium calculations with Geochemists Workbench relative to the $Fe(III)_{aq}$ concentration at pH 6 that was set to 100% for comparison. (b) Decrease of initial sorption of Fe(III) to carboxylic functional groups at the cell surface over the pH-range 6.0 to 6.6. For comparison, sorption at pH 6.6 was set to 100%.

the effect of a pH change of 0.6 from pH 6.6 to pH 6.0 on the solubility of Fe(III) (figure 4.2). Geochemical modeling showed that a lower pH of 6.0, which is present at the cell surface, will increase the fraction of Fe(III) that is in solution ($Fe(III)_{aq}$) approximately five-fold compared to the bulk pH of 6.6, i.e. the concentration of $Fe(III)_{aq}$ is only 20% at pH 6.6 compared to pH 6.0. Similar as for chemical Fe(II) oxidation, probably also during microbial Fe(II) oxidation, the rate limiting step in the transition from $Fe(II)_{aq}$ to $Fe(III)_{ppt}$ via $Fe(III)_{aq}$ is the nuclation and precipitation of the Fe(III) mineral (Grundl & Delwiche, 1993). The precipitation rate of Fe(III) therefore decreases with decreasing pH. At pH 6.0 (cell) the precipitation rate was determined to be 8.3×10^{-10} mM s^{-1} whereas at pH 6.6 (bulk) the rate increased to 1.3×10^{-9} mM s^{-1}.

All in all, equlibrium calculations showed that the $Fe(III)_{aq}$ concentration is higher at lower pH. Additionally, precipitation of Fe(III) minerals in the bulk medium is faster because the pH in the bulk is higher than at the cell surface. Therefore, a concentration gradient of $Fe(III)_{aq}$ establishes between the cell surface and the bulk with a higher $Fe(III)_{aq}$ concentration at the lower pH at the cell surface and a lower $Fe(III)_{aq}$ concentration at the higher pH in the bulk medium. The concentration gradient of $Fe(III)_{aq}$ drives diffusion of $Fe(III)_{aq}$ from low pH-zones at the cell surface (low precipitation, higher $Fe(III)_{aq}$) to high pH-regions further away from the cell (faster precipitation, low $Fe(III)_{aq}$, high mineral content) (figure 4.3).

4.4.3 Consequences of the cell pH-microenvironment for cell encrustation and metal binding in photoferrotrophs and implications for chemotrophic Fe(II)-oxidizers

In this study we demonstrated the establishment of a single-cell low pH-microenvironment at the cell surface of the phototrophic Fe(II)-oxidizer *Thiodictyon* sp. strain F4 using an in-situ approach with a pH-dependent fluorescent dye in combination with confocal laser scanning microscopy. The observed pH decrease at the cell surface has three consequences for the cell: i) a successful competition of protons with the $Fe(III)_{aq}$ for sorption sites at the cell surface leading to less binding of Fe(III) to the cell surface, ii) an increase in Fe(III) solubility, and iii) a lower precipitation rate of $Fe(III)_{ppt}$ at the cell surface (figure 4.3). This suggests that the establishment of a cell pH microenvironment could provide a mechanism for photoferrotrophs to successfully prevent Fe(III) mineral precipitation on the cell surface. The results of this study may therefore explain why none of the known phototrophic Fe(II)-oxidizing strains encrusts (e.g. figure 4.1). An exception is the purple non-sulfur bacteria, *Rhodomicrobium vannielii*, which differs from the other photoferrotrophs in that it is a mixotrophic Fe(II)-oxidizer, i.e. it needs an organic substrate in addition to the Fe(II), and it is not clear whether this strain benefits from Fe(II) oxidation at all (Heising & Schink, 1998, Schaedler et al., 2009). The benefits for a cell to avoid encrustation are obvious since i) more light can reach the cell surface leading to a higher metabolic rate and ii) the uptake of nutrients from the environment and release of toxic metabolites to the surrounding is not hampered.

For chemotrophic Fe(II)-oxidizing strains, other mechanisms to prevent cell encrustation are expected, because these microorganisms depend solely on the energy provided by the chemotrophic oxidation of Fe(II) with either O2 or nitrate as electron acceptor. Protons can therefore not be pumped using light energy as by the phototrophs in cyclic photophosphorylation where a single electron can be used multiple times to pump protons as long as light energy is available. In chemotrophic Fe(II)-oxidizers, proton translocation is directly coupled to chemotrophic Fe(II) oxidation and electron transport phosphorylation where one electron stemming from oxidation of Fe(II) runs through the electron transport chain once finally being used to reduce O_2 or nitrate. It has been shown that some nitrate-reducing mixotrophic Fe(II)-oxidizing bacteria encrust with $Fe(III)_{ppt}$ on the cell surface (Miot et al., 2009a, Schaedler et al., 2009). Although these bacteria

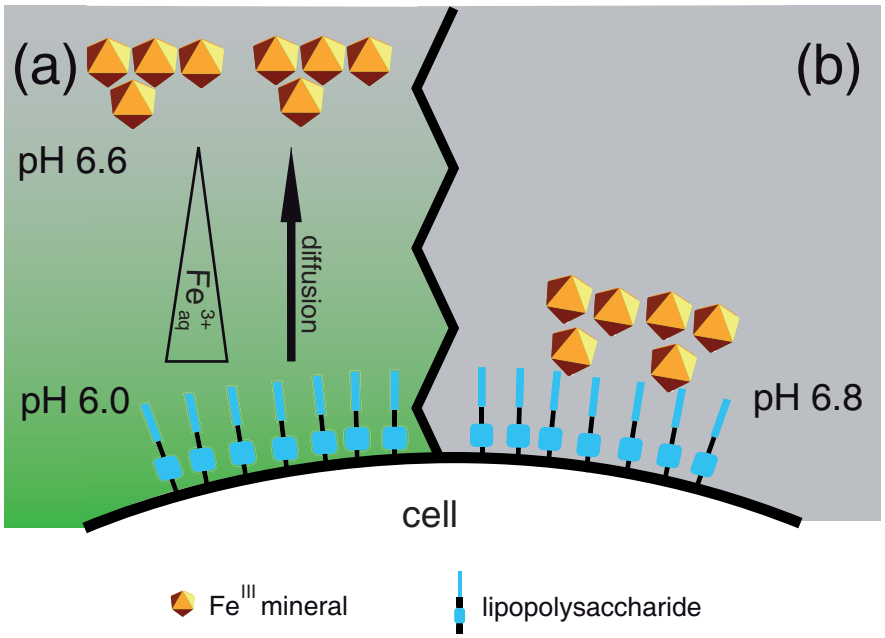

Figure 4.3: Scheme of a gram-negative microbial cell interacting with dissolved Fe(III) species and Fe(III) minerals. (a): Active metabolism with a pH-microenvironment around the cell. Fe(III) remains in solution in cell pH-microenvironment directing precipitation to the bulk medium. (b): Scenario illustrating Fe(III) interaction with the cell surface in the absence of a pH-microenvironment with Fe(III) preferentially binding and precipitating at the cell surface.

also utilize the PMF to generate ATP and to produce reducing equivalents, the energy available to these bacteria is much less compared to the phototrophic strains because phototrophic organisms can tap the energy source of the solar radiation. In contrast, chemotrophic organisms (such as nitrate-reducing and microaerophilic Fe(II)-oxidizing bacteria) are limited by the energy that can be obtained from Fe(II) oxidation, which makes the generation of a large proton gradient less likely or even impossible.

The results presented here shed light on a long lasting enigma: already in 19^{th} century Ehrenberg (1836), Winogradsky (1888) had observed biogenic Fe(III) minerals and speculated on their formation and the influence of bacteria. Although many open questions remain, today, almost 200 years later, we understand the complexity of the interaction between bacteria and the Fe(III) minerals better. The presence of pH microenvironments around phototrophic Fe(II)-oxidizers provides a possible explanation why and how phototrophic Fe(II)-oxidizing bacteria avoid encrustation by Fe(III) minerals. Additionally, the light dependence of this metabolism potentially explains why phototrophic Fe(II)-oxidizers use a different strategy to avoid cell encrustation than the microaerophilic Fe(II)-oxidizing bacteria, like *Gallionella* and *Leptothrix*.

Acknowledgements

We would like to thank Jürgen Berger for his help with confocal scanning laser microscopy; Sebastian Behrens and Nicole Posth are acknowledged for reading the manuscript and helpful comments. We would also like to thank the University of Tübingen for partially funding FH (Promotionsverbund Grenzflächen), the German Research Foundation (DFG) and the Stifterverband der Wissenschaft for funding AK and the Max-Planck Society for supporting HS. We also thank two anonymous reviewers for their helpful comments improving the quality of the manuscript.

Bibliography

Barbeau, K; Rue, EL; Bruland, KW; & Butler, A: Photochemical cycling of iron in the surface ocean mediated by microbial iron(III)-binding ligands. *Nature*, 413:409–13, 2001.

Beveridge, TJ & Murray, RG: Uptake and retention of metals by cell walls of *Bacillus subtilis*. *Journal of Bacteriology*, 127:1502–1518, 1976.

Beveridge, TJ & Murray, RG: Sites of metal deposition in the cell wall of *Bacillus subtilis*. *Journal of Bacteriology*, 141:876–887, 1980.

Borrok, D; Fein, JB; Tischler, M; O'Loughlin, E; Meyer, H; Liss, M; & Kemner, KM: The effect of acidic solutions and growth conditions on the adsorptive properties of bacterial surfaces. *Chemical Geology*, 209:107–119, 2004.

Canfield, DE: The early history of atmospheric oxygen: Homage to robert a. garrels. *Annual Review of Earth and Planetary Sciences*, 33:1–36, 2005.

Chan, CS; Fakra, SC; Edwards, DC; Emerson, D; & Banfield, JF: Iron oxyhydroxide mineralization on microbial extracellular polysaccharides. *Geochimica et Cosmochimica Acta*, 73:3807–3818, 2009.

Croal, LR; Gralnick, JA; Malasarn, D; & Newman, DK: The genetics of geochemistry. *Annual Review of Genetics*, 38:175–202, 2004a.

Croal, LR; Jiao, Y; & Newman, DK: The fox operon from *Rhodobacter* strain SW2 promotes phototrophic fe(II) oxidation in *Rhodobacter capsulatus* sb1003. *Journal of Bacteriology*, 189:1774–1782, 2007.

Croal, LR; Johnson, CM; Beard, BL; & Newman, DK: Iron isotope fractionation by Fe(II)-oxidizing photoautotrophic bacteria. *Geochimica et Cosmochimica Acta*, 68:1227–1242, 2004b.

Ehrenberg, CG: Vorläufige Mitteilungen über das wirkliche Vorkommen fossiler Infusorien und ihre grosse Verbreitung. *Poggendorfs Annalen der Physik und Chemie*, 38:213–227, 1836.

Ehrlich, HL & Newman, DK: *Geomicrobiology* (CRC Press, New York), 5th ed., 2009.

Emerson, D: Microbial oxidation of Fe(II) and mn(ii) at circumentural pH. In *Environmental Microbe-Metal Interactions*, Environmental Microbe-Metal Inteactions (Wiley-VCH), 2000.

Emerson, D & Revsbech, NP: Investigation of an iron-oxidizing microbial mat community located near Aarhus, Denmark: Field studies. *Applied and Environmental Microbiology*, 60:4022–4031, 1994.

Fein, JB; Daughney, CJ; Yee, N; & Davis, TA: A chemical equilibrium model for metal adsorption onto bacterial surfaces. *Geochimica et Cosmochimica Acta*, 61:3319–3328, 1997.

Fein, JB; Martin, AM; & Wightman, PG: Metal adsorption onto bacterial surfaces: Development of a predictive approach. *Geochimica et Cosmochimica Acta*, 65:4267–4273, 2001.

Grundl, T & Delwiche, J: Kinetics of ferric oxyhydroxide precipitation. *Journal of Contaminant Hydrology*, 14:71–97, 1993.

Hafenbradl, D; Keller, M; Dirmeier, R; Rachel, R; Rossnagel, P; Burggraf, S; Huber, H; & Stetter, KO: *Ferroglobus placidus* gen. nov., sp. nov., a novel hyperthermophilic archaeum that oxidizes Fe^{2+} at neutral pH under anoxic conditions. *Archives of Microbiology*, 166:308–314, 1996.

Harold, FM: Conservation and transformation of energy by bacterial membranes. *Bacteriological Reviews*, 36:172–230, 1972.

Hegler, F; Posth, NR; Jiang, J; & Kappler, A: Physiology of phototrophic iron(II)-oxidizing bacteria – implications for modern and ancient environments. *FEMS Microbiology Ecology*, 66:250–260, 2008.

Heising, S & Schink, B: Phototrophic oxidation of ferrous iron by a *Rhodomicrobium vannielii* strain. *Microbiology*, 144:2263–2269, 1998.

Invitrogen: SNARF pH indicators: user manual. 2003.

Jiao, Y & Newman, DK: The pio operon is essential for phototrophic Fe(II) oxidation in rhodopseudomonas palustris tie-1. *Journal of Bacteriology*, 189:1765–1773, 2007.

Johnson, KJ; Ams, DA; Wedel, AN; Szymanowski, JES; Weber, DL; Schneegurt, MA; & Fein, JB: The impact of metabolic state on Cd adsorption onto bacterial cells. *Geobiology*, 5:211–218, 2007.

Kappler, A & Newman, DK: Formation of Fe(III)-minerals by Fe(II)-oxidizing photoautotrophic bacteria. *Geochimica et Cosmochimica Acta*, 68:1217–1226, 2004.

Marcotte, N & Brouwer, AM: Carboxy SNARF-4F as a fluorescent pH probe for ensemble and fluorescence correlation spectroscopies. *The Journal of Physical Chemistry B*, 109:11819–11828, 2005.

Martinez, RE; Gardés, E; Pokrovsky, OS; Schott, J; & Oelkers, EH: Do photosynthetic bacteria have a protective mechanism against carbonate precipitation at their surfaces? *Geochimica et Cosmochimica Acta*, 74:1329–1337, 2010.

McConnaughey, TA & Whelan, JF: Calcification generates protons for nutrient and bicarbonate uptake. *Earth-Science Reviews*, 42:95–117, 1997.

Miot, J; Benzerara, K; Morin, G; Kappler, A; Bernard, S; Obst, M; Férard, C; Skouri-Panet, F; Guigner, JM; Posth, NR; Galvez, M; Brown, GE, JR.; & Guyot, F: Iron biomineralization by neutrophilic iron-oxidizing bacteria. *Geochimica et Cosmochimica Acta*, 73:696–711, 2009a.

Miot, J; Benzerara, K; Obst, M; Kappler, A; Hegler, F; Schaedler, S; Bouchez, C; Guyot, F; & Morin, G: Extracellular iron biomineralization by photoautotrophic iron-oxidizing bacteria. *Applied and Environmental Microbiology*, 75:5586–5591, 2009b.

Mitchell, P: Keilin's respiratory chain concept and its chemiosmotic consequences. *Science*, 206:1148–1159, 1979.

Nicholls, DG & Ferguson, SJ: *Bioenergetics 3* (Academic Press, Amsterdam, London), 3rd ed., 2002.

Padan, E; Zilberstein, D; & Schuldiner, S: pH homeostasis in bacteria. *Biochimica et biophysica acta*, 650:151–166, 1981.

Pham, AN; Rose, AL; Feitz, AJ; & Waite, TD: Kinetics of Fe(III) precipitation in aqueous solutions at pH 6.0-9.5 and 25 degrees C. *Geochimica Et Cosmochimica Acta*, 70:640–650, 2006.

Rose, AL & Waite, TD: Reconciling kinetic and equilibrium observations of iron(III) solubility in aqueous solutions with a polymer-based model. *Geochimica et Cosmochimica Acta*, 71:5605–5619, 2007.

Schaedler, S; Burkhardt, C; Hegler, F; Straub, KL; Miot, J; Benzerara, K; & Kappler, A: Formation of cell-iron-mineral aggregates by phototrophic and nitrate reducing anaerobic Fe(II)-oxidizing bacteria. *Geomicrobiology Journal*, 26:93–103, 2009.

Schaedler, S; Burkhardt, C; & Kappler, A: Evaluation of electron microscopic sample preparation methods and imaging techniques for characterization of cell-mineral aggregates. *Geomicrobiology Journal*, 25:228–239, 2008.

Sobolev, D & Roden, EE: Suboxic deposition of ferric iron by bacteria in opposing gradients of Fe(II) and oxygen at circumneutral pH. *Applied and Environmental Microbiology*, 67:1328–1334, 2001.

Straub, KL; Benz, M; Schink, B; & Widdel, F: Anaerobic, nitrate-dependent microbial oxidation of ferrous iron. *Applied and Environmental Microbiology*, 62:1458–1460, 1996.

Stumm, W & Morgan, JJ: *Aquatic chemistry: chemical equilibria and rates in natural waters* (Wiley-Interscience, New York), 3rd ed., 1995.

Urrutia Mera, M; Kemper, M; Doyle, R; & Beveridge, TJ: The membrane-induced proton motive force influences the metal binding ability of *Bacillus subtilis* cell walls. *Applied Environmental Microbiology*, 58:3837–3844, 1992.

Warren, LA & Ferris, FG: Continuum between sorption and precipitation of Fe(III) on microbial surfaces. *Environmental Science & Technology*, 32:2331–2337, 1998.

Widdel, F; Schnell, S; Heising, S; Ehrenreich, A; Assmus, B; & Schink, B: Ferrous iron oxidation by anoxygenic phototrophic bacteria. *Nature*, 362:834–836, 1993.

Winogradsky, S: Über Eisenbacterien. *Botanische Zeitung*, 17:261–270, 1888.

Yee, N & Fein, JB: Quantifying metal adsorption onto bacteria mixtures: A test and application of the surface complexation model. *Geomicrobiology Journal*, 20:43–60, 2003.

5 Cell surface properties of Fe(II)-oxidizing bacteria – to encrust or not to encrust?

Florian Hegler[1], Iso Christl[2], Florian Latteyer[3], Nadine Göring[4], Andreas Peschel[4], Andreas Kappler[1]

[1]Center for Applied Geoscience – Geomicrobiology, Eberhard Karls University Tübingen, Sigwartstr. 10, 72076 Tuebingen, Germany
[2]Institute for Biogeochemistry and Pollutant Dynamics, Eidgenössische Technische Hochschule, Universitätstr. 16, 8092 Zürich, Switzerland
[3]Institute for Physical and Theoretical Chemistry, Eberhard Karls University Tübingen, Auf der Morgenstelle 18, 72076 Tübingen, Germany
[4]Medical Microbiology and Hygiene Department, Eberhard Karls University Tübingen, Elfriede-Aulhorn-Str. 6, 72076 Tübingen, Germany

5.1 Abstract

Iron is ubiquitous in the environment and bacteria are often associated with iron minerals. While Fe(II) is quite soluble at circumneutral pH, Fe(III) is only poorly soluble under these conditions. Therefore, bacteria oxidizing Fe(II) to Fe(III) face the challenge of a poorly soluble product of their metabolism. Fe(III) may precipitate on the cell surface and form minerals – the cells would ultimately be covered with a mineral crust. The exchange of nutrients as well as light for phototrophs reaching the cell would then be reduced if not inhibited entirely. Therefore, it is vital for a cell to avoid encrustation by Fe(III) minerals. No photoautotrophic Fe(II)-oxidizing bacteria is known that encrusts, in contrast, most of the described nitrate-reducing Fe(II)-oxidizing cells as well as cells of *Rhodomicrobium vannielii* (which is likely photoheterotrophic) (Heising & Schink, 1998) do encrust. The difference in cell surface properties as well as the properties of the precipitating minerals are key to determining how phototrophic Fe(II)-oxidizing cells can avoid encrustation while chemotrophic Fe(II)-oxidizing cells are heavily encrusted by minerals. Sorption of metal ions to cell surfaces is governed by functional groups available at the cell surfaces which interact directly with the immediate surrounding of the cell.

Therefore, we determined the concentration and average pK_a of the cell surface functional groups of the nitrate-reducing Fe(II)-oxidizing *Acidovorax* sp. strain BoFeN1 and the photoferrotroph *"Rhodobacter ferrooxidans"* strain SW2 by acid-base titrations. Additionally, the surface charge of the bacteria was calculated from titration data. Furthermore, we determined the isoelectric point of Fe(III) minerals stemming from the bacterial Fe(II) oxidation which we found to be negative in contrast to chemically precipitated Fe(III)(oxy)hydroxyides.

We found an overall negative surface charge for both tested strains. The overall negative surface charge was significantly less for *Acidovorax* sp. strain BoFeN1 compared to *"Rhodobacter ferrooxidans"* strain

SW2. Additionally, we showed that the biogenically precipitated Fe(III) minerals are negatively charged at circumneutral pH.

5.2 Introduction

5.2.1 Fe(III) minerals and Fe(II)-oxidizing bacteria

In the environment, bacteria are often found in close association with iron minerals (Schultze-Lam et al., 1996, Fortin et al., 1998, Fortin & Langley, 2005, Haaijer et al., 2008). This phenomenon has intrigued researchers for nearly 200 years (Ehrenberg, 1836, Winogradsky, 1888, Pringsheim, 1949). Nevertheless, bacteria are not only associated with minerals, they might even be covered with minerals on the cell surface and thus being encrusted with minerals (Fortin et al., 1997, Kappler et al., 2005a, Schaedler et al., 2009, Miot et al., 2009b, Hegler et al., 2010). The importance of mineral transformation for environmental processes such as sorption and degradation of contaminants is well recognized (Klausen et al., 1995, Tufano & Fendorf, 2008, Gadd, 2010) and the role of bacteria in redox transformation of iron minerals is well documented (Lovley & Phillips, 1988, Kappler & Straub, 2005, Emerson et al., 2010).

In anoxic environments, two metabolic pathways of Fe(II) oxidation are known:
a) Phototrophic Fe(II) oxidizers, such as *"Rhodobacter ferrooxidans"* strain SW2, have the following metabolism (equation 5.1) (Widdel et al., 1993):

$$HCO_3^- + 4\,Fe^{2+} + 10\,H_2O \longrightarrow <CH_2O> + 4\,Fe(OH)_3 + 7\,H_2O \tag{5.1}$$

b) Nitrate-reducing bacteria – such as *Acidovorax* strain sp. BoFeN1 (Kappler et al., 2005b) oxidize Fe(II) according to equation 5.2 (Miot et al., 2009b):

$$2\,Fe^{2+} + 5\,H_2O + NO_3^- \longrightarrow 2\,Fe(OH)_3 + 4\,H^+ + NO_2^- \tag{5.2}$$

Microorganisms may exploit the redox conditions available and can either reduce ferric iron [Fe(III)] (Lovley & Phillips, 1988) or oxidize ferrous iron [Fe(II)] (Kappler & Straub, 2005, Borch et al., 2010, Emerson et al., 2010). While ferric iron is stable under oxic conditions, ferrous iron will oxidize with rapidly at circumneutral pH to Fe(III)with molecular oxygen (Cornell & Schwertmann, 2003, Rose & Waite, 2007). Additionally, Fe(II) is rather soluble at circumneutral pH while Fe(III) is only poorly soluble under these conditions (1×10^{-10} mol L^{-1}).

Ferric iron may precipitate on the cell surfaces of bacteria and form a mineral crust. Such a crust may not only hinder the exchange of metabolites and nutrients with the environment but also reduce light reaching the cell which is crucial for phototrophic organisms. Ultimately, Fe(III) precipitation would lead to a complete encrustation of the cell and potentially to cell death (Schaedler et al., 2008, Miot et al., 2009a,b,c, Schaedler et al., 2009, Hegler et al., 2010).

It has been shown for phototrophic Fe(II) oxidizers, that the oxidation of Fe(II) likely happens in the periplasm of the cell (Croal et al., 2007). The same is true for the nitrate-reducing bacterium *Acidovorax* strain sp. BoFeN1 (Miot et al., 2009b). Despite the low solubility of Fe(III) and the location of Fe(II) oxidation in the periplasm, Fe(II)-oxidizing bacteria are not necessarily encrusted by Fe(III) minerals. So far, none of the phototrophic strain is known to encrust while nitrate-reducing strain *Acidovorax* sp. BoFeN1 (Kappler et al., 2005a) is heavily encrusted by minerals (Miot et al., 2009b, Schaedler et al., 2009). *Rhodomicrobium vanielii* Heising & Schink (1998) is an exception of phototrophic Fe(II)-oxidizing strains because it encrusts with Fe(III) minerals. The difference to the other photoferrotrophs is, that it cannot be cultured continuously with Fe(II) as electron donor and might thus not be considered a true photoferrotroph.

Several mechanisms play a role for the interaction of cells and minerals.

- Exopolymers may work as a template and relocate the precipitation away from the cell (Miot et al., 2009c, Schaedler et al., 2009, and references therein). This mechanism has been suggested for *Gallionella* (Chan et al., 2009). Nonetheless, there have been no suggestions as to how the $Fe(III)_{ppt}$ is transported to the exopolymers and why it does not precipitate directly on the cell surface.
- Emerson & Revsbech (1994) suggested a shedding of the encrusted cell surface and thus a freeing of the cell surface from the mineral crust.
- Fe(III)-complexing ligands could be excreted by the cells to keep Fe(III) in solution (Croal et al., 2004). However, substantial amounts of carbon would need to be fixed in order to produce such ligands. Additionally, Fe(III) complexes are oftentimes light sensitive and degrade over time (Barbeau et al., 2001). A typical iron specific ligand is a siderophore. Even a small siderophore contains dozens of carbon atoms (e.g. Barbeau et al., 2001). Much smaller but also less specific ligands for iron are organic acids, such as citrate. In the case of citrate, six carbon atoms would need to be fixed in order to produce one citrate molecule which then could complex one Fe(III). A total of 4×6 Fe(II) would need to be oxidized to fix the six carbon atoms. Thus, complexation of Fe(III) does not seem likely because the production of ligands is probably too costly for the cell.
- A low pH at the cell surface may keep Fe(III) in solution at the cell surface which directs precipitation away from the cell (Hegler et al., 2010).
- Cells may adjust the cell surface charge in order to avoid interaction with the positively charged Fe(III) ions and thus avoid the interaction of cell surfaces with Fe(III) ions (Beveridge & Murray, 1980, Urrutia Mera et al., 1992). It has been shown for cyanobacteria, that they successfully adapt their cell surface charge to control their interaction with carbonate (McConnaughey & Whelan, 1997, Martinez et al., 2010).
- The properties of the precipitating minerals also need to be accounted for in cell-mineral interactions, especially the charge of the mineral surfaces is vital. The overall charge of the mineral depends on the geochemical conditions, for example background electrolytes (Tipping, 1981, Deo et al., 2001, Cornell & Schwertmann, 2003).

The cell surface charge of Gram negative bacteria is usually negative and is determined by the lipopolysaccharides (LPS) and proteins (Beveridge & Murray, 1980, Beveridge, 1983, 1989). The functional groups are mainly carboxyl-groups, phosphoryl-groups and amino-groups (Beveridge & Murray, 1980, Borrok et al., 2005). The cell surface functions as a template for sorption of metal ions followed by precipitation of minerals (Beveridge & Murray, 1976, 1980, Beveridge, 1983, 1989). Thus, cell surface properties of Fe(II)-oxidizing bacteria, especially the distribution and abundance of the functional groups, are crucial to understand cell-mineral interaction (Beveridge, 1988, 1989). Cell surface properties have so far never been determined for Fe(II)-oxidizing bacteria.

Not only cell surface properties matter to understand cell-mineral interactions. Mineral properties have to match those of the cell surface in order to interact. Therefore, cell-mineral interaction is minimized and encrustation potentially avoided if the cell surfaces and mineral surfaces repel each other, for example by the same charge. Chemically synthesized Fe(III) minerals such as ferrihydrite and goethite have usually a positive surface charge at circumneutral pH (Schwertmann & Cornell, 2000, Cornell & Schwertmann, 2003).

The charge of minerals strongly depend on the geochemical conditions under which they form (Tipping, 1981, Deo et al., 2001, Cornell & Schwertmann, 2003) and less on the bacteria forming the mineral (Larese-Casanova et al. (2010) and chapter 6). Ions in the medium in which the mineral precipitates influence the surface charge profoundly, e.g. phosphate, bicarbonate or humic substances can decrease the point of zero charge (pzc) of ferrihydrite to 5 and below (Tipping, 1981, Dzombak & Morel, 1990, Deo et al., 2001). The surface charge of biogenic Fe(III) minerals is not know.

Therefore, we determined the cell surface properties of two different bacteria: *Acidovorax* sp. strain BoFeN1 that encrusts heavily with Fe(III) minerals and *"Rhodobacter ferrooxidans"* strain SW2 that has been shown not to encrust (Schaedler et al., 2009). We performed acid-base titrations of both strains and modeled the titration results with distinct pK_a-sites representing the cell surface functional groups. Furthermore, the isoelectric point of the Fe(III) minerals precipitated by bacteria was determined.

5.3 Material and Methods

5.3.1 Growth of the strains

Minimal mineral medium was prepared according to Hegler et al. (2008) and cultures were grown as described therein. *"Rhodobacter ferrooxidans"* strain SW2 and *Acidovorax* sp. strain BoFeN1 were taken from the lab collection. The phototrophic Fe(II)-oxidizing strain *"Rhodobacter ferrooxidans"* was grown either using H_2/CO_2 (80:20 v:v) for iron-free cultures or with 10 mmol L^{-1} $FeCl_2$ for cultures grown with Fe(II) as electron donor. The nitrate-reducing *Acidovorax* sp. strain BoFeN1 was grown with 10 mmol L^{-1} $NaNO_3$ and 5 mmol L^{-1} sodium acetate. In case of iron as co-substrate, 10 mmol L^{-1} $FeCl_2$ was added additionally.

5.3.2 Mineral preparation

Minerals for the determination of the iep were prepared either chemically or taken from bacterial cultures. Fe(III) minerals were precipitated chemically in medium by oxidizing 10 mmol L^{-1} Fe(II) with molecular oxygen. Additionally, the iep of chemically synthesized ferrihydrite, which was prepared in a pure system, was determined (Schwertmann & Cornell, 2000). The gas-phase of the freshly prepared ferrihydrite was exchanged to N_2 after the synthesis by cycles of evacuation and gas-addition for 3×20 min.

5.3.3 Stock solutions for titrations

All solutions were prepared according to standard analytical methods (Harris, 1995) under a constant stream of N_2 gas. Solutions of 0.1 mol L^{-1} were prepared in water (conductivity 55.5 μS) and purged with N_2 for at least 30 min. The 0.1 mol L^{-1} solution of NaOH was calibrated against dried potassium hydrogen phthalate (Sigma, Germany, pro analysi) (Eaton et al., 2005). The solution of 0.1 mol L^{-1} HCl was calibrated against the calibrated 0.1 mol L^{-1} NaOH solution (Eaton et al., 2005).

5.3.4 Titrations

Four independent titration setups were used: living cells grown without Fe(II); killed cells grown without Fe(II); killed cells grown without Fe(II) treated with oxalate or finally killed cells grown with Fe(II) and treated with oxalate. For each titration setup, either 250 mL of the Fe(III) mineral free culture or

500 mL of Fe(II) grown culture were harvested at 8000 × g. Cells were killed by adding 0.06% (w/v) NaN_3 for at least 12 hours. Cell death was verified microscopically by the dead-live stain (Molecular Probes, Invitrogen). Microscopic analysis were routinely performed on a Zeiss Axioskop2 plus epi-fluorescence microscope (Zeiss, Germany) with a 100-fold oil-immersion objective lens.

In order separate cells and minerals to titrate cells only, oxalate solution was used to remove Fe(III) minerals. The solution is a mixture of 0.22 mol L^{-1} ammonium oxalate and 0.17 mol L^{-1} oxalic acid (pH 3). 10 mmol L^{-1} ferrous ethylenediammonium sulfate served as catalyst. Cells or cell-mineral pellets were harvested and incubated for 10 min with oxalate solution with periodic shaking before washing the cells as described below. Subsequently, the harvested biomass was washed with degassed 0.1 mol L^{-1} NaCl solution in order to remove remaining ions from the growth medium or from the oxalic acid treatment (three times 7000 × g for 10 min).

Acid-base titrations allow to determine the pK_a values and concentrations of functional groups in a titrated solution. Therefore, the harvested wet biomass was resuspended in 35 mL of 0.1 mol L^{-1} NaCl solution and added to a titration flask prefitted with a pH glass electrode (Profitrode, Mettler Toledo) calibrated freshly for each experiment. The titration beaker was constantly flushed with N_2. All titrations were performed with an automatic titrator (Titrino 836, Mettler Toledo) equipped with a 840 touch control. Initially, the pH of the cell suspension was adjusted to pH 3 with an end-point titration and the suspension was allowed to equilibrate for 30 min. The dynamic titrations were done with 0.1 mV min^{-1} stability criterion to the end point at pH 11. The cell suspension was collected after the titration (7000 ×g for 10 min) and dried at 60 °C for at least 24 hours. The dry weight of the biomass was then determined.

Data evaluation of the cell surface titrations

Raw data of the titrations was treated by removing data points that were very close together which allowed a better mathematical fit of the data with Protofit software (Turner & Fein, 2006). The raw titration data used for pK_a modeling, e.g. the amount of acid against the pH, was from the low starting pH of 3 up to pH 10.5. Modeling of the apparent pK_a (pK_a^{app}) of the cell surface functional groups was done with two independent methods. The first method (Smith & Ferris, 2001, Martinez et al., 2002, Smith & Ferris, 2003) automatically fitted the data with a number of pK_a sites and determined a Gaussion distribution of the concentration of cell surface functional groups. The second method (Turner & Fein, 2006) required an initial guess of pK_a and the corresponding concentration but is optimized to achieve highest comparability of independent titration data sets obtained under slightly different conditions (Turner & Fein, 2006).

5.3.5 Geochemical modeling with Geochemists Workbench

The React module of Geochemists Workbench 6.05 was used to calculate the mineral surface charge of Fe(III) (hydr)oxides in mineral medium. The main medium components were added to the input matrix. Redox reactions of Fe(II)/Fe(III) and HS^-/SO_4^{2-} were blocked in the model. Mineral surface charge was calculated over a pH range from pH 5.5 to 8.4. The properties of the Fe(III) minerals (hydrous ferric oxides) were taken from the database based on the work by Dzombak & Morel (1990).

5.3.6 Determination of the isoelectric point

The isolectric point (iep) of cells and Fe(III) minerals was determined on a Zeta Plus (BTC Brookhaven Instruments) and the PALS Zeta Potential analyzer software was used to analyze the raw data. The mobility of the particles in an electric field was determined over a pH range between 3 and 9.

The surface charge of cells of *"Rhodobacter ferrooxidans"* strain SW2 and *Acidovorax* sp. BoFeN1 grown without iron was qualitatively evaluated. Measurements of the surface charge had substantial background noise and thus only allowed a qualitative assessment if the cell surface charge was positive or negative and if the cell surface charge was different between the strains. Furthermore, the iep of minerals precipitated by the cells as well as chemically synthesized minerals was determined.

Cells and minerals were washed the same way as for the titrations in order to obtain comparable data (section 5.3.4).

The iep of the minerals was calculated by fitting a non-linear function to the mobility values of the particles with Origin 8 (OriginLabs).

5.4 Results and Discussion

5.4.1 Cell surface titration results

Cell surface titrations of *"Rhodobacter ferrooxidans"* strain SW2 and *Acidovorax* sp. BoFeN1 allow to draw conclusions on the cell-mineral interaction, e.g. why strain SW2 does not encrust while BoFeN1 does encrust with Fe(III) minerals.

Evaluation of the raw titration data for the four independent setups was done twice: once with the method of Smith & Ferris (2001), Martinez et al. (2002) and Smith & Ferris (2003) and once with the method by Turner & Fein (2006). Using both methods yielded a more robust evaluation of the data and furthermore allows a higher comparability to previously published results (Smith & Ferris, 2001, Martinez et al., 2002, Smith & Ferris, 2003, Turner & Fein, 2006).

Evaluation with the first method (Smith & Ferris, 2001, Martinez et al., 2002, Smith & Ferris, 2003) showed, that living cells and cells killed with sodium azide express only minor differences in cell surface functional group abundance and pK_a^{app} for *"Rhodobacter ferrooxidans"* strain SW2 (fig 5.1 A and B) and *Acidovorax* sp. strain BoFeN1 (fig 5.2 A and B). Therefore, killing the cells did not affect the availability of cell surface functional groups for protons. Although Johnson et al. (2007) had shown that the Cd^{2+} sorption onto metal surfaces was affected by the metabolic state of the cells, these results are not in disagreement since we measured the proton sorption to the cell wall by pH titration while Johnson et al. (2007) determined Cd^{2+} sorption only at pH 7 for dead and living cells. Proton sorption to cell surface functional groups – as in pH-titrations – is likely not affected by the metabolic state of the cell.

Cell-mineral aggregates cannot be titrated since it is impossible to mathematically separate the individual contribution of cells and minerals to the titration. Therefore, Fe(III) minerals needed to be removed from the cell-mineral aggregates so that cells could be titrated separately. Different methods to dissolve Fe(III) minerals to achieve a separation of cell-mineral aggregates were evaluated in order to determine which method affected the cell surfaces the least. Microscopic analysis showed that a reduction of Fe(III) and thus removal of Fe(III) minerals with hydroxylamine-hydrochloride leads to a destabilization of the cell and finally cell lysis. Dissolving the Fe(III) minerals with $1\,\mathrm{mol\ L^{-1}}$ HCl yielded the same result as a treatment with hydroxylamine-hydrochloride.

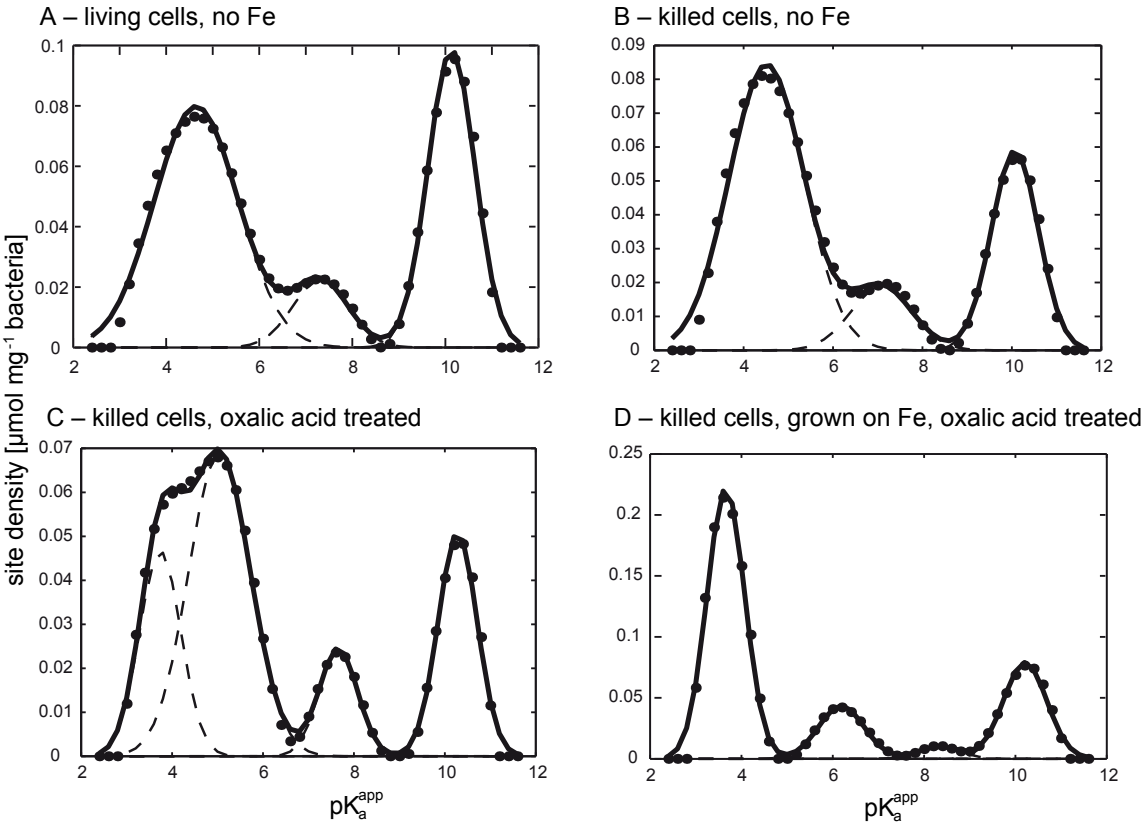

Figure 5.1: Modeled titration of *"Rhodobacter ferrooxidans"* strain SW2. Solid line – overall fit, points – calculated data from titration. Data evaluation was done according to Smith & Ferris (2001), Martinez et al. (2002) and Smith & Ferris (2003). For each set the cells were treated differently prior to titration: A: living cells, no iron in culture; B: killed cells, no iron in culture; C: killed cells treated with oxalic acid, no iron in culture; D: killed cells, treated with oxalic acid, Fe(II) growth substrate.

Another method how to separate cells and minerals is to grow cells in media supplemented with ethylenediaminetetraacetic acid (EDTA) or nitrilotriacetic acid (NTA). Nonetheless, complexing agents like NTA and EDTA also complex other two-valent cations like Ca^{2+} and Mg^{2+}. These ions are needed by Gram-negative bacteria for stabilizing their outer membranes and thus likely the addition of NTA or EDTA leads to the exposure of additional functional groups at the cell surface. This would falsify the results of the titration. Additionally, growing cultures of photoferrotrophs such as *"Rhodobacter ferrooxidans"* strain SW2 in medium supplemented with NTA or EDTA causes additional disadvantages: NTA and EDTA photolytically degrade in systems containing Fe(III) (Stolzberg & Hume, 1975, Svenson et al., 1989). Thus, it is oftentimes not even clear how the photoferrotrophs acquire carbon when growing in systems containing NTA and iron because the carbon could stem from the degradation products of NTA (Caiazza et al., 2007).

Therefore, the treatment with oxalate solution at pH 3 proved to be the most feasible for removing Fe(III) minerals. We did not observe cell lysis microscopically. Furthermore, the pH in this treatment is the same as the lowest pH during titrations. In order to test if the treatment with oxalic acid leads to a change in cell surface properties we titrated killed cells treated with oxalic acid. In order to determine

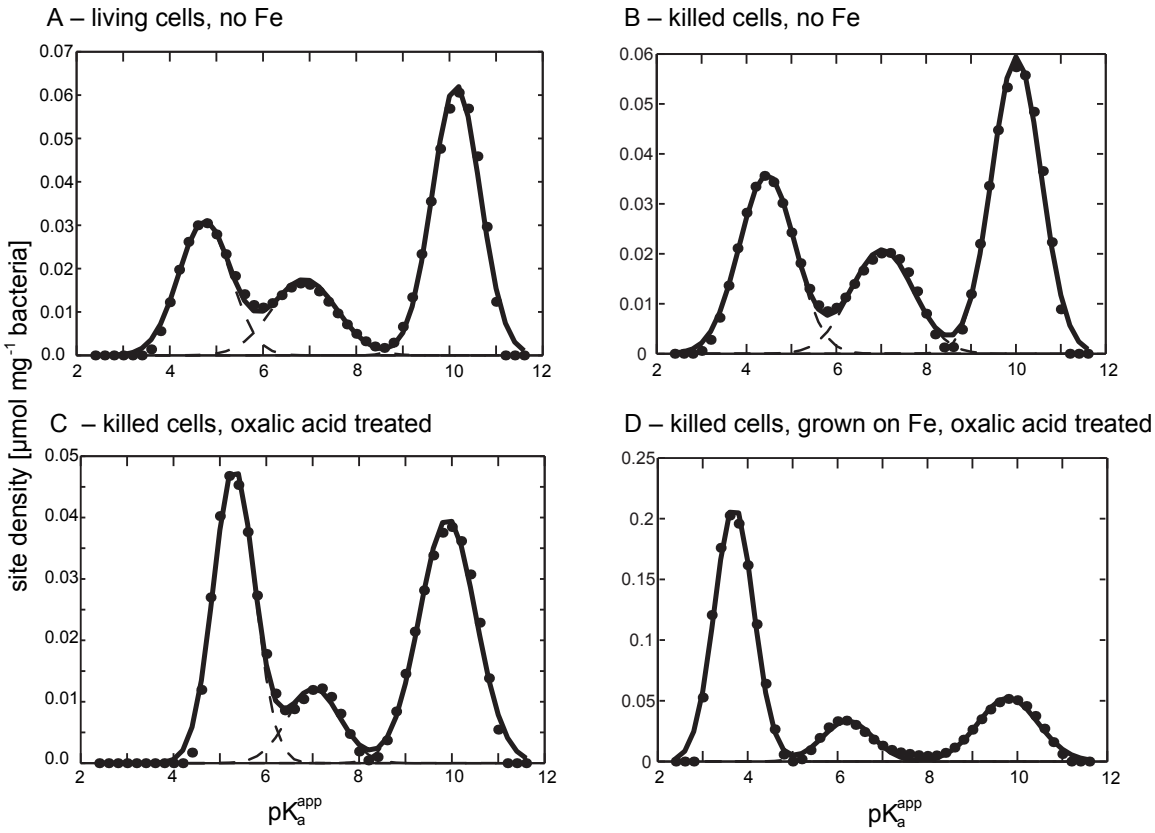

Figure 5.2: Modeled titration of *Acidovorax* sp. strain BoFeN1. Solid line – overall fit, points – calculated data from titration. Data evaluation was done according to Smith & Ferris (2001), Martinez et al. (2002) and Smith & Ferris (2003). For each set the cells were treated differently prior to titration: A: living cells, no iron in culture; B: killed cells, no iron in culture; C: killed cells treated with oxalic acid, no iron in culture; D: dead cells, treated with oxalic acid, Fe(II) growth substrate.

the influence of oxalic acid treatment on the cell surface properties, cells grown without iron were washed with oxalic acid and titrated afterwards. The results suggest (figure 5.1 C and figure 5.2 C) that either oxalic acid was still present or that oxalic acid formed a complex with the cell surface functional groups and thus was titrated as well. The pK_{a2} of oxalic acid is 4.3 (Stumm & Morgan, 1995) which is reflected by a higher concentration of cell surface functional groups at the low pK_a site of the titration (figure 5.1 C and 5.2 C). Potentially, additional functional groups were exposed by the treatment with oxalic acid. Oxalic acid also complexes other ions which stabilize the cell wall such as Ca^{2+} and Mg^{2+} (Straub et al., 2001) which may also change the apparent concentration and distribution of pK_a sites.

Finally, titrations of cells grown with Fe(II) as electron donor and subsequent removal of the Fe(III) minerals by oxalic acid solution also showed a significant peak at the low pK_a values (figure 5.1 D and 5.2 D). This again suggests a significant contribution of oxalic acid, either as cell surface complexes, in this case stabilized by Fe(III), or because it could not be removed entirely from the cell surfaces. The distribution of the higher apparent pK_a values did not change significantly and may be compared to cells grown without iron (figure 5.1 A and D and 5.2 A and D).

Therefore, it is – to our understanding – not possible to remove Fe(III) minerals from medium without

disturbing the cell surfaces with the methods tested by us. Hence, it is not possible to draw conclusions on cell surface properties at low pK_a sites for Fe(II) oxidizing bacteria growing with Fe(II) as electron donor. Nonetheless, the abundance and pK_a^{app} of the functional groups at higher pK_a values did not change significantly between the different setups, e.g. figure 5.1 A-D and 5.2 A-D.

Table 5.1: pK_a values and the concentration of the functional groups modeled with Protofit (Turner & Fein, 2006) of cell surfaces of *Acidovorax* sp. strain BoFeN1 and *"Rhodobacter ferrooxidans"* strain SW2. For each set of titrations the cells were treated differently prior to titration: living cells, no iron in culture; killed cells, no iron in culture; killed cells treated with oxalic acid, no iron in culture; dead cells, treated with oxalic acid, Fe(II) growth substrate.

	Acidovorax sp. strain BoFeN1		*"Rhodobacter ferrooxidans"* strain SW2	
	pK_a	$-log c$ [μmol mg^{-1}]	pK_a	$-log c$ [μmol mg^{-1}]
living	4.9	0.17	4.0	0.46
	6.6	0.13	5.3	0.52
	8.7	0.11	7.0	0.25
			10.1	0.51
dead	4.6	0.23	4.0	0.39
	6.6	0.14	5.2	0.43
	8.0	0.06	6.8	0.18
	9.2	0.11	10.2	0.30
dead, treated with oxalate	4.8	0.22	3.9	0.30
	6.4	0.14	5.2	0.43
	8.6	0.10	7.1	0.15
			9.5	0.11
Fe grown	3.7	0.98	3.7	1.02
	5.4	0.23	5.5	0.25
	7.0	0.15	6.8	0.14
	8.9	0.14	8.8	0.12

Both methods, e.g. (Smith & Ferris, 2001, Martinez et al., 2002, Smith & Ferris, 2003) as well as the method of (Turner & Fein, 2006), showed similar results in respect to the apparent pK_a^{app} values of the surface functional groups (table 5.2). The two methods fitted the titration data with different algorithms. Depending on the algorithm, one site was sometimes modeled as two pK_a sites with the other model. Overall, the independent sites can be compared.

Site densities of the cell surface functional groups cannot be compared among the two methods: The first method (Smith & Ferris, 2001, Martinez et al., 2002, Smith & Ferris, 2003) fits the pK_a^{app} of the surface sites and their respective concentration with a Gaussian distribution. This means that the concentration of the site is The second method (Turner & Fein, 2006) does not calculate a distribution but a distinct pK_a value and the respective concentration for each site. Therefore, the concentration of cell surface functional groups calculated with the second method (Turner & Fein, 2006) is in all cases higher and thus cannot be compared to the results of the first method (Smith & Ferris, 2001, Martinez et al., 2002, Smith & Ferris, 2003).

Table 5.2: Comparison of the pK_a values for determined for *"Rhodobacter ferrooxidans"* strain SW2 and *Acidovorax* sp. strain BoFeN1 with two independent methods. Data evaluation was done according to the method of Smith & Ferris (2001), Martinez et al. (2002), Smith & Ferris (2003) (first method) as well as the method of (Turner & Fein, 2006) (second method).

	pK_a, method 1	pK_a, method 2
living SW2	4.6 ± 0.7	4.0
	6.9 ± 0.9	5.3
	10.1 ±0.5	7.0
		10.1
dead SW2	4.5 ± 0.8	4.0
	7.1 ± 0.7	5.2
	10.1 ± 0.5	6.8
		10.2
dead, treated SW2	3.7 ± 0.5	3.9
with oxalate SW2	5.0 ± 0.7	5.2
	7.7 ± 0.4	7.1
	10.3 ± 0.4	9.5
Fe grown SW2	3.6 ± 0.4	3.7
	6.2 ± 0.5	5.5
	8.3 ± 0.5	6.8
	10.2 ± 0.5	8.8
living BoFeN1	4.7 ± 0.6	4.9
	6.9 ± 0.7	6.6
	10.1 ± 0.5	8.7
dead BoFeN1	4.5 ± 0.6	4.6
	7.0 ± 0.7	6.6
	10.0 ±0.5	8.0
		9.2
dead, treated BoFeN1	5.3 ± 0.4	4.8
with oxalate BoFeN1	7.0 ± 0.6	6.4
	9.9 ±0.6	8.6
Fe grown BoFeN1	3.7 ± 0.4	3.7
	6.2 ± 0.6	5.4
	9.8 ± 0.7	7.0
		8.9

Cell surface charge

The cell surface charge was calculated from the titration data using Protofit (Turner & Fein, 2006). The surface charge of *"Rhodobacter ferrooxidans"* strain SW2 is significantly lower than the surface charge of *Acidovorax* sp. strain BoFeN1 for all cases in which cells were grown without Fe(II) as substrate (figure 5.3). Fe(III) minerals could not be removed without changing the cell surface functional group availability in titrations. The disturbance of the cell surface is reflected by a higher calculated cell surface charge for each strain, e.g. more functional groups being available during the titration. This may have several reasons: the sorption of oxalic acid to the cell surface and the exposure of additional cell surface functional groups caused by the removal of cations when treated with oxalic acid seem likely. Furthermore, an incomplete removal of oxalic acid during washing is possible.

The overall negative cell surface charge is more negative for *"Rhodobacter ferrooxidans"* strain SW2 than for *Acidovorax* sp. strain BoFeN1 (figure 5.3) which was qualitatively confirmed by direct measurements of the cell surface charge.

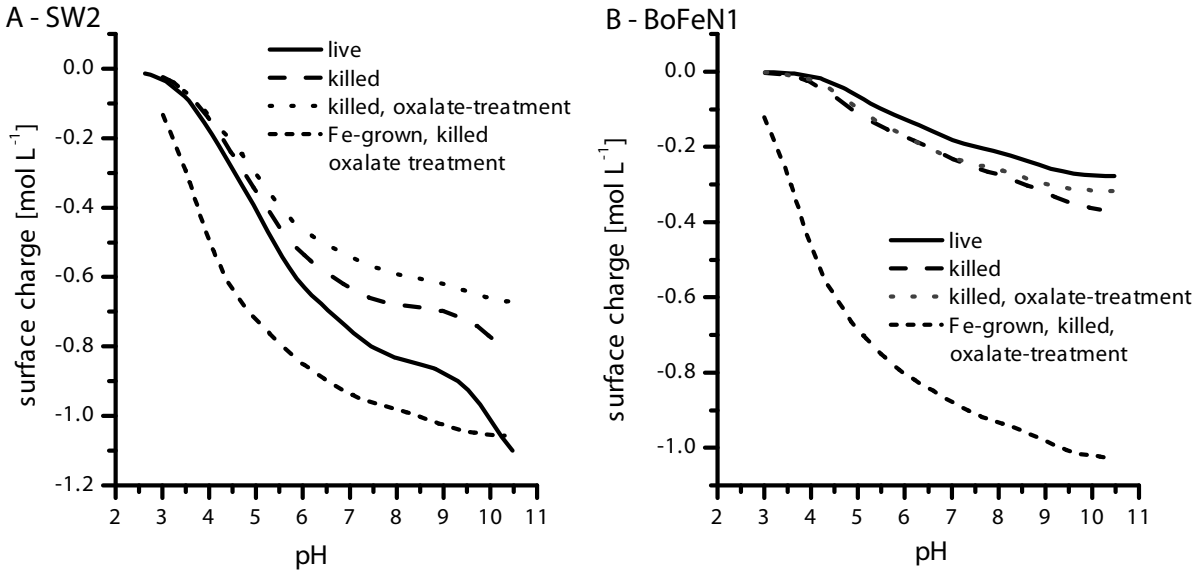

Figure 5.3: Surface charge of A: *"Rhodobacter ferrooxidans"* strain SW2 and B: *Acidovorax* sp. strain BoFeN1 calculated with Protofit (Turner & Fein, 2006). Titrations performed either with living cells, iron free growth medium (solid line); killed cells, iron free growth (dashed line); killed cells treated with oxalic acid, iron free growth (dotted line) and cells grown with Fe(II) as substrate killed and treated with oxalic acid to remove Fe-minerals (short dashed line).

5.4.2 Mineral properties: iep and modeling

The iep of the Fe(III) minerals that were biologically formed in medium through the oxidation of Fe(II) by *Acidovorax* sp. strain BoFeN1 and *"Rhodobacter ferrooxidans"* strain SW2 differ substantially from Fe(III) minerals precipitated in medium through the oxidation by O_2 (table 5.3). This is likely due to the cells present in the system which decrease the iep of the cell-mineral aggregates. Cells release organic matter to which the minerals then bind during precipitation: *"Rhodobacter ferrooxidans"* strain SW2 (Miot et al.,

2009c) and *Acidovorax* sp. strain BoFeN1 (Miot et al., 2009b) were shown to form extracellular fibers. In both cases, these fibers likely contributed to an decrease in the iep in systems containing cells and minerals compared to systems containing minerals only. The iep for chemically synthesized ferrihydrite in ion-free water (table 5.3) agrees well with previously published values of 7.8-7.9 (Cornell & Schwertmann, 2003). The values for the iep in this study are slightly higher, likely because adsorbed CO_2 – which is known to decrease the iep of minerals – was removed by purging the ferrihydrite with N_2 (Cornell & Schwertmann, 2003).

Table 5.3: iep of Fe(III) minerals precipitated in mineral medium and of chemically synthesized ferrihydrite.

mineral	iep
chemically precipitated minerals in medium	3.8 ± 0.2
mineral precipitated by *"Rhodobacter ferrooxidans"* strain SW2	4.4 ± 0.2
mineral precipitated by *Acidovorax* sp. strain BoFeN1	4.4 ± 0.2
chemically synthesized ferrihydrite	8.8 ± 0.2

Geochemical modeling for Fe(III) minerals showed that their surface charge strongly depends on the ions present in the system (figure 5.4). Modeling showed that phosphate and bicarbonate have the strongest influence on the mineral surface charge resulting in an overall negative mineral surface charge when present (figure 5.4). The negative iep of minerals determined agrees well with previous studies who determined a strong influence of carbonate (Evans et al., 1979) and also humic substances (Tipping, 1981) on the surface charge of Fe(III) minerals.

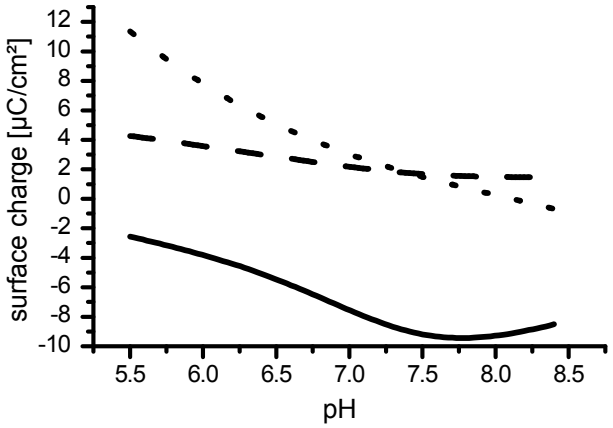

Figure 5.4: Model of the surface charge of hydrous ferric oxides over the pH range of cell growth calculated with Geochemist's Workbench. Solid line: minerals including all medium components according to Hegler et al. (2008); dashed line: minerals in medium excluding phosphate and bicarbonate; dotted line: ferrihydrite in water.

5.4.3 Implications of cell surface properties and mineral charge on cell encrustation

The negative surface charge of cells (figure 5.3) and minerals (figure 5.4 and table 5.3) suggest, that the cells and minerals should not aggregate due to electrostatic repulsion. The surface charge of cells of

Acidovorax sp. strain BoFeN1 is less negative than that of cells of *"Rhodobacter ferrooxidans"* strain SW2 (figure 5.3). Therefore, the repulsion between minerals and cells is expected to be higher for *"Rhodobacter ferrooxidans"* strain SW2 than the repulsion between minerals and cells of *Acidovorax* sp. strain BoFeN1.

Additionally, phototrophic cells are expected to have a low pH at the cell surface (Hegler et al., 2010) while *Acidovorax* sp. strain BoFeN1 may not have a low cell surface pH at all times (chapter 6). This effect could favor the precipitation of minerals on the cell surface of *Acidovorax* sp. strain BoFeN1.

The Fe(III) mineral precipitation for *Acidovorax* sp. strain BoFeN1 starts in the periplasm (Miot et al., 2009b). Once, nucleation sites are present, further Fe(III) ions likely adsorb and thus mineral formation is directed towards the cell surface (Beveridge & Murray, 1980, Beveridge, 1988, 1989).

In contrast, cells that manage to release Fe(III) from the cell without its immediate precipitation on the cell surface, as in the case of photoferrotrophs (for example Hegler et al., 2010), may benefit from the repulsion of negatively charged Fe(III) minerals and negatively charged cell surfaces. Mineral precipitation on their cell surface would not be observable – as in the case of *"Rhodobacter ferrooxidans"* strain SW2.

It has been shown previously that cells and minerals *"Rhodobacter ferrooxidans"* strain SW2 aggregate (Posth et al., 2010) although encrustation by Fe(III) minerals can be ruled out (Schaedler et al., 2009). The surface properties of the Fe(III) minerals not only influence the encrustation behavior. Furthermore, they likely influence the sorption of ions and thus ultimately the fate and transport of contaminants, such as arsenic and cadmium, in the environment (Borch et al., 2010, Gadd, 2010).

5.5 Outlook

Further experiments are needed to determine the exact mechanism of cell-mineral interaction of *"Rhodobacter ferrooxidans"* strain SW2 and *Acidovorax* sp. strain BoFeN1. The properties of the precipitating minerals, especially the surface charge, has not been focused on yet. Therefore, the contribution of geochemistry, e.g. phosphate and bicarbonate as well as organic matter (stemming from cell lysis but also cell exudates) on the biogenic Fe(III) mineral properties, needs to be determined. This would not only enhance the understanding of the cell-mineral interaction but also increase the understanding of the fate and transport of heavy metals in the environment – today and in the past.

Separating the contribution of the geochemistry from biology can be achieved by precipitating Fe(III) minerals – both, chemically and microbially –in medium buffered by Good's buffer (Yu et al., 1997). These buffers have the advantage of interacting only very little with metal ions and thus reducing the effect carbonate and phosphate on the mineral properties. Generally, the precipitation of Fe(III) minerals in carbonate-phosphate free medium allows to minimize the effect of ion-interaction with the minerals. Mineral precipitation can be achieved in cell suspension experiments rather than growth experiments.

The interaction of cells and minerals can also be determined by precipitating Fe(III) in the presence of cells in an otherwise ion-free solution similarly to the experiments of (Châtellier et al., 2004).

Additionally, the exact cell surfaces properties on a molecular basis of cells grown with Fe(II) as substrate have to be determined. It seems vital to me to detect not only cell surface functional groups – which can be achieved by titrations – but additionally the macromolecules present at the cell surface – for example peptides and polysaccharides. To my knowledge there is no technique available that allows a separation of cells from Fe(III) minerals without disturbing the cell surface to an unknown extent and thus falsifying potential results. Therefore, microscopic analysis can help to overcome this gap. For example confocal laser scanning microscopy with various dyes as well as SEM, TEM and STXM-microscopy can

help to overcome this gap. The major disadvantage of dyes used in microscopy are often the unknown properties of these dyes, especially their interaction with the Fe(III) minerals.

Acknowledgments

We would like to thank Raul Martinez for his help with setting up the titrations. We also thank Emily-Denise Melton for her help in improving the quality of the manuscript. I would also like to thank Nadine Göring and Florian Latteyer who helped with several less successful to determine cell-surface properties of the mentioned bacteria which are not shown here.

Bibliography

Barbeau, K; Rue, EL; Bruland, KW; & Butler, A: Photochemical cycling of iron in the surface ocean mediated by microbial iron(III)-binding ligands. *Nature*, 413:409–13, 2001.

Beveridge, TJ: Mechanisms of the binding of metallic ions to bacterial walls and the possible impact on the microbial ecology. In CA Reddy & MJ Klug, eds., *Current perspectives in microbial ecology proceedings of the 3. International Symposium on Microbial Ecology, Michigan State University, 7 - 12 August 1983*, pp. 601–607 (Michigan State University, Washington), 1983.

Beveridge, TJ: The bacterial surface: general considerations towards design and function. *Canadian Journal of Microbiology*, 34:363–372, 1988.

Beveridge, TJ: Role of cellular design in bacterial metal accumulation and mineralization. *Annual Review of Microbiology*, 43:147–171, 1989.

Beveridge, TJ & Murray, RG: Uptake and retention of metals by cell walls of *Bacillus subtilis*. *Journal of Bacteriology*, 127:1502–1518, 1976.

Beveridge, TJ & Murray, RG: Sites of metal deposition in the cell wall of *Bacillus subtilis*. *Journal of Bacteriology*, 141:876–887, 1980.

Borch, T; Kretzschmar, R; Kappler, A; Cappellen, PV; Ginder-Vogel, M; Voegelin, A; & Campbell, K: Biogeochemical redox processes and their impact on contaminant dynamics. *Environmental Science and Technology*, 44:15–23, 2010.

Borrok, D; Turner, BF; & Fein, JB: A universal surface complexation framework for modeling proton binding onto bacterial surfaces in geologic settings. *American Journal of Science*, 305:826–853, 2005.

Caiazza, NC; Lies, DP; & Newman, DK: Phototrophic Fe(II) oxidation promotes organic carbon acquisition by *Rhodobacter capsulatus* SB1003. *Applied Environmental Microbiology*, 73:6150–6158, 2007.

Chan, CS; Fakra, SC; Edwards, DC; Emerson, D; & Banfield, JF: Iron oxyhydroxide mineralization on microbial extracellular polysaccharides. *Geochimica et Cosmochimica Acta*, 73:3807–3818, 2009.

Châtellier, X; West, MM; Rose, J; Fortin, D; Leppard, GG; & Ferris, FG: Characterization of iron-oxides formed by oxidation of ferrous ions in the presence of various bacterial species and inorganic ligands. *Geomicrobiology Journal*, 21:99–112, 2004.

Cornell, RM & Schwertmann, U: *The iron oxides: structure, properties, reactions, occurrences and uses* (VCH, Weinheim, Cambridge), 2nd ed., 2003.

Croal, LR; Gralnick, JA; Malasarn, D; & Newman, DK: The genetics of geochemistry. *Annual Review of Genetics*, 38:175–202, 2004.

Croal, LR; Jiao, Y; & Newman, DK: The fox operon from *Rhodobacter* strain SW2 promotes phototrophic fe(II) oxidation in *Rhodobacter capsulatus* sb1003. *Journal of Bacteriology*, 189:1774–1782, 2007.

Deo, N; Natarajan, KA; & Somasundaran, P: Mechanisms of adhesion of *Paenibacillus polymyxa* onto hematite, corundum and quartz. *International Journal of Mineral Processing*, 62:27–39, 2001.

Dzombak, DA & Morel, F: *Surface complexation modeling: hydrous ferric oxide* (Wiley, New York), 1990.

Eaton, A; Clesceri, L; Rice, E; & Greenberg, A: *Standard methods for the Examination of Water and Wastewater* (American Public Health Association, Maryland), 21st ed., 2005.

Ehrenberg, CG: Vorläufige Mitteilungen über das wirkliche Vorkommen fossiler Infusorien und ihre grosse Verbreitung. *Poggendorfs Annalen der Physik und Chemie*, 38:213–227, 1836.

Emerson, D; Fleming, EJ; & McBeth, JM: Iron-oxidizing bacteria: an environmental and genomic perspective. *Annual Review of Microbiology*, 64:561–83, 2010.

Emerson, D & Revsbech, NP: Investigation of an iron-oxidizing microbial mat community located near Aarhus, Denmark: Field studies. *Applied and Environmental Microbiology*, 60:4022–4031, 1994.

Evans, U; Leal, J; & Arnold, P: The interfacial electrochemistry of goethite (α-FeOOH) especially the effect of CO_2 contamination. *Journal of Electroanalytical Chemistry*, 105:161–167, 1979.

Fortin, D; Ferris, FG; & Beveridge, TJ: Surface-mediated mineral development by bacteria. *Reviews in Mineralogy and Geochemistry*, 35:161–180, 1997.

Fortin, D; Ferris, FG; & Scott, SD: Formation of Fe-silicates and Fe-oxides on bacterial surfaces in samples collected near hydrothermal vents on the Southern Explorer Ridge in the northeast Pacific Ocean. *American Mineralogist*, 83:1399–1408, 1998.

Fortin, D & Langley, S: Formation and occurrence of biogenic iron-rich minerals. *Earth-Science Reviews*, 72:1–19, 2005.

Gadd, GM: Metals, minerals and microbes: geomicrobiology and bioremediation. *Microbiology*, 156:609–643, 2010.

Haaijer, SC; Harhangi, HR; Meijerink, BB; Strous, M; Pol, A; Smolders, AJ; Verwegen, K; Jetten, MS; & Op den Camp, HJ: Bacteria associated with iron seeps in a sulfur-rich, neutral pH, freshwater ecosystem. *ISME Journal*, 2:1231–42, 2008.

Harris, DC: *Quantitative chemical analysis* (Freeman), 5th ed., 1995.

Hegler, F; Posth, NR; Jiang, J; & Kappler, A: Physiology of phototrophic iron(II)-oxidizing bacteria – implications for modern and ancient environments. *FEMS Microbiology Ecology*, 66:250–260, 2008.

Hegler, F; Schmidt, C; Schwarz, H; & Kappler, A: Does a low pH-microenvironment around phototrophic Fe(II)-oxidizing bacteria prevent cell encrustation by Fe(III) minerals? *FEMS Microbiology Ecology*, accepted:accepted, 2010.

Heising, S & Schink, B: Phototrophic oxidation of ferrous iron by a *Rhodomicrobium vannielii* strain. *Microbiology*, 144:2263–2269, 1998.

Johnson, KJ; Ams, DA; Wedel, AN; Szymanowski, JES; Weber, DL; Schneegurt, MA; & Fein, JB: The impact of metabolic state on Cd adsorption onto bacterial cells. *Geobiology*, 5:211–218, 2007.

Kappler, A; Pasquero, C; Konhauser, KO; & Newman, DK: Deposition of banded iron formations by anoxygenic phototrophic Fe(II)-oxidizing bacteria. *Geology*, 33:865–868, 2005a.

Kappler, A; Schink, B; & Newman, DK: Fe(III) mineral formation and cell encrustation by the nitrate-dependent Fe(II)-oxidizer strain BoFeN 1. *Geobiology*, 3:235–245, 2005b.

Kappler, A & Straub, KL: Geomicrobiological cycling of iron. *Reviews in Mineralogy & Geochemistry*, 59:85–108, 2005.

Klausen, J; Trober, SP; Haderlein, SB; & Schwarzenbach, RP: Reduction of substituted nitrobenzenes by Fe(II) in aqueous mineral suspensions. *Environmental Science & Technology*, 29:2396–2404, 1995.

Larese-Casanova, P; Haderlein, S; & Kappler, A: Biomineralization of lepidocrocite and goethite by nitrate-reducing Fe(II)-oxidizing bacteria: Effect of pH, bicarbonate, phosphate and humic acids. *Geochimica Et Cosmochimica Acta*, 74:3721–3734, 2010.

Lovley, DR & Phillips, EJ: Novel mode of microbial energy metabolism: organic carbon oxidation coupled to dissimilatory reduction of iron or manganese. *Applied and Environmental Microbiology*, 54:1472–80, 1988.

Martinez, RE; Gardés, E; Pokrovsky, OS; Schott, J; & Oelkers, EH: Do photosynthetic bacteria have a protective mechanism against carbonate precipitation at their surfaces? *Geochimica et Cosmochimica Acta*, 74:1329–1337, 2010.

Martinez, RE; Smith, DS; Kulczycki, E; & Ferris, FG: Determination of intrinsic bacterial surface acidity constants using a donnan shell model and a continuous pK_a distribution method. *Journal of Colloid and Interface Science*, 253:130–9, 2002.

McConnaughey, TA & Whelan, JF: Calcification generates protons for nutrient and bicarbonate uptake. *Earth-Science Reviews*, 42:95–117, 1997.

Miot, J; Benzerara, K; Morin, G; Bernard, S; Larquet, E; Ona-Nguema, G; Kappler, A; & Guyot, F: Transformation of vivianite by anaerobic nitrate-reducing iron-oxidizing bacteria. *Geobiology*, 7:373–384, 2009a.

Miot, J; Benzerara, K; Morin, G; Kappler, A; Bernard, S; Obst, M; Férard, C; Skouri-Panet, F; Guigner, JM; Posth, NR; Galvez, M; Brown, GE, JR.; & Guyot, F: Iron biomineralization by

neutrophilic iron-oxidizing bacteria. *Geochimica et Cosmochimica Acta*, 73:696–711, 2009b.

Miot, J; Benzerara, K; Obst, M; Kappler, A; Hegler, F; Schaedler, S; Bouchez, C; Guyot, F; & Morin, G: Extracellular iron biomineralization by photoautotrophic iron-oxidizing bacteria. *Applied and Environmental Microbiology*, 75:5586–5591, 2009c.

Posth, NR; Huelin, S; Konhauser, K; & Kappler, A: Size, density and composition of cell-mineral aggregates formed during anoxigenic phototrophic Fe(II) oxidation: Impact on modern and ancient environments. *Geochimica Et Cosmochimica Acta*, 74:3476–3493, 2010.

Pringsheim, EG: Iron bacteria. *Biological Reviews of the Cambridge Philosophical Society*, 24:200–45, 1949.

Rose, AL & Waite, TD: Reconciling kinetic and equilibrium observations of iron(III) solubility in aqueous solutions with a polymer-based model. *Geochimica et Cosmochimica Acta*, 71:5605–5619, 2007.

Schaedler, S; Burkhardt, C; Hegler, F; Straub, KL; Miot, J; Benzerara, K; & Kappler, A: Formation of cell-iron-mineral aggregates by phototrophic and nitrate reducing anaerobic Fe(II)-oxidizing bacteria. *Geomicrobiology Journal*, 26:93–103, 2009.

Schaedler, S; Burkhardt, C; & Kappler, A: Evaluation of electron microscopic sample preparation methods and imaging techniques for characterization of cell-mineral aggregates. *Geomicrobiology Journal*, 25:228–239, 2008.

Schultze-Lam, S; Fortin, D; Davis, BS; & Beveridge, TJ: Mineralization of bacterial surfaces. *Chemical Geology*, 132:171–181, 1996.

Schwertmann, U & Cornell, RM: *Iron oxides in the laboratory : preparation and characterization* (Wiley-VCH, Weinheim), 2nd ed., 2000.

Smith, DS & Ferris, FG: Proton binding by hydrous ferric oxide and aluminum oxide surfaces interpreted using fully optimized continuous pk_a spectra. *Environmental Science & Technology*, 35:4637–4642, 2001.

Smith, DS & Ferris, FG: Specific surface chemical interactions between hydrous ferric oxide and iron-reducing bacteria determined using pk_a spectra. *Journal of Colloid and Interface Science*, 266:60–67, 2003.

Stolzberg, RJ & Hume, DN: Rapid formation of iminodiacetate from photochemical degradation of iron(III) nitrilotriacetate solutions. *Environmental Science & Technology*, 9:654–656, 1975.

Straub, KL; Benz, M; & Schink, B: Iron metabolism in anoxic environments at near neutral pH. *FEMS Microbiology Ecology*, 34:181–186, 2001.

Stumm, W & Morgan, JJ: *Aquatic chemistry: chemical equilibria and rates in natural waters* (Wiley-Interscience, New York), 3rd ed., 1995.

Svenson, A; Kaj, L; & Björndal, H: Aqueous photolysis of the iron (III) complexes of NTA, EDTA and DTPA. *Chemosphere*, 18:1805–1808, 1989.

Tipping, E: The adsorption of aquatic humic substances by iron oxides. *Geochimica et Cosmochimica Acta*, 45:191–199, 1981.

Tufano, KJ & Fendorf, S: Confounding impacts of iron reduction on arsenic retention. *Environmental Science and Technology*, 42:4777–4783, 2008.

Turner, BF & Fein, JB: Protofit: A program for determining surface protonation constants from titration data. *Computers & Geosciences*, 32:1344–1356, 2006.

Urrutia Mera, M; Kemper, M; Doyle, R; & Beveridge, TJ: The membrane-induced proton motive force influences the metal binding ability of *Bacillus subtilis* cell walls. *Applied Environmental Microbiology*, 58:3837–3844, 1992.

Widdel, F; Schnell, S; Heising, S; Ehrenreich, A; Assmus, B; & Schink, B: Ferrous iron oxidation by anoxygenic phototrophic bacteria. *Nature*, 362:834–836, 1993.

Winogradsky, S: Über Eisenbacterien. *Botanische Zeitung*, 17:261–270, 1888.

Yu, Q; Kandegedara, A; Xu, Y; & Rorabacher, DB: Avoiding interferences from good's buffers: A contiguous series of noncomplexing tertiary amine buffers covering the entire range of pH 3-11. *Analytical biochemistry*, 253:50–56, 1997.

6 Influence of pH on microbially produced Fe(III) minerals: identity and localization

Florian Hegler[1], Jennyfer Miot[2], Philip Larese-Casanova[1,3*], Karim Benzerara[2], Christoph Berthold[2], Andreas Kappler[1]

[1]Center for Applied Geoscience – Geomicrobiology, Eberhard Karls University Tübingen, Sigwartstr. 10, 72076 Tübingen, Germany
[2]Institut de Minéralogie et de Physique des Milieux Condensés, UMR 7590, CNRS, Universités Paris 6 et Paris 7, et IPGP, 140, rue de Lourmel, 75 015 Paris, France
[3]current address: Department of Civil and Environmental Engineering, 469 Snell Engineering Center, 360 Huntington Avenue, Northeastern University, Boston, Massachusetts 02115, USA
[4]Institute for Geoscience – Applied Mineralogy, Eberhard Karls University Tübingen, Wilhelmstr. 56, 72074 Tübingen, Germany

6.1 Abstract

Iron mineral formation in biotic as well as in abiotic systems depends on complexing agents and solution chemistry. One of the dominant determinants for Fe(III) mineral identity and crystallinity is pH. Furthermore, the solubility of Fe(III) is lowest at circumneutral pH. Hence, bacteria oxidizing Fe(II) to Fe(III) face the challenge of a poorly soluble product of their metabolism which is expected to precipitate on the cell surface ultimately leading to encrustation and cell death.

pH may vary by more than 2 units over time in environmental systems, for example during diurnal cycles and thus influence mineralogy as well as cell-mineral interaction. In order to understand the influence of pH on cell-mineral interaction as well as mineral crystallinity and mineral phase, we determined the interaction of Fe(III) minerals with cells from pH 6.2 to 7.4 for the nitrate-reducing Fe(II)-oxidizing *Acidovorax* sp. strain BoFeN1. Cell-mineral interactions and co-localization were visualized by scanning transmission electron microscopy and scanning electron microscopy. Element distribution maps of phosphorous, iron and oxygen were taken by scanning energy dispersive X-ray spectroscopy. We also determined Fe(III) mineral identity and crystallinity depending on pH by μXRD and Mössbauer spectroscopy.

We found poorly ordered Fe(III) hydroxides or nano-goethite additionally to an unidentified Fe(II) phase. The abundance and crystallinity of the mineral phases did not change with a change of one pH unit. Additionally, we did not find evidence that the localization of the minerals on the cell surface depends on the pH despite the higher solubility of Fe(III) at lower pH.

The results of these study will further increase our understanding of the factors governing Fe(III) mineral identity and crystallinity in systems of microbially induced Fe(II) oxidation as well as increasing the understanding of the influences pH has on cell-mineral interaction.

6.2 Introduction

6.2.1 Iron mineralogy at circumneutral pH in the environment

Iron(III) oxides [$Fe(III)_{ppt}$] can be very abundant in the environment (James & Ferris, 2004). They play a key role in sorption of heavy metals (Borch et al., 2010, Gadd, 2010) such as arsenic (Tufano & Fendorf, 2008) as well as in organic pollutant degradation (Klausen et al., 1995). Sorption and degradation of the pollutants depend strongly on the mineral phase and crystallinity. Additionally, bacteria are known to be closely associated with iron particles in the environment (Ehrenberg, 1836, Winogradsky, 1888, Pringsheim, 1949, Schultze-Lam et al., 1996, Fortin et al., 1998, Fortin & Langley, 2005). But not only are bacteria associated with minerals, bacteria are also involved in reduction of Fe(III) to Fe(II) or oxidation of Fe(II) to Fe(III) and its subsequent precipitation. Crystallinity and mineral phase determine how easily Fe(III) minerals may be re-reduced and re-oxidized and thus how often an iron atom undergoes oxidation and precipitation before it would be removed from the elemental cycle of iron (e.g. 300 times as suggested by Canfield & Des Marais, 1993).

Additionally challenging for iron-metabolizing bacteria is, that the concentration of Fe(III) in solution ($Fe(III)_{aq}$) depends strongly on pH with the lowest solubility at circumneutral pH (1×10^{-10} mol L^{-1}) and increasing towards lower and higher pH-values (Cornell & Schwertmann, 2003). Fe(II) behaves differently to Fe(III) under these conditions. Its maximum concentration in solution is much higher (1×10^{-3} mol L^{-1}; Cornell & Schwertmann, 2003). Fe^{3+}, which is the primary ion after the oxidation of Fe(II), will quickly hydrolyze according to equation 6.1. Due to the poor solubility of Fe(III) at pH 7, minerals precipitate quickly from $Fe(III)_{aq}$ (Millero et al., 1986, Rose & Waite, 2007).

$$Fe^{3+} + 3\,H_2O \longrightarrow Fe(OH)_3 + 3\,H^+ \tag{6.1}$$

Especially bacteria oxidizing Fe(II) at circumneutral pH have to deal with the poor solubility of Fe(III). Fe(III) may sorb and finally form minerals on the cell surface which would lead to encrustation of the cells. Exchange of nutrients would be limited and light reaching the cell would be reduced. Ultimately cells would die due to encrustation.

pH-changes towards lower or higher pH values increase the solubility of Fe(III) and thus influence the encrustation of cells. In the environment, especially in microbial mats, pH can change substantially over 2 pH units during the course of the day (Revsbech et al., 1983, Pierson et al., 1999). While the influence of geochemical parameters – such as pH – during chemical mineral precipitation on the mineral phase and crystallinity is well established (Schwertmann & Cornell, 2000, Cornell & Schwertmann, 2003) an influence of pH on microbially produced minerals is not clear yet.

6.2.2 Properties of biogenic iron minerals

The Fe(III) mineral phase of bacterial Fe(II) oxidation does not seem to depend on the identity of the bacteria but rather on the geochemical conditions under which the minerals precipitate (Châtellier et al., 2001, 2004, Larese-Casanova et al., 2010). Zegeye et al. (2010) determined a correlation between the cell number of *Shewanella putrefaciens* and the mineral phase resulting from Fe(III) (lepidocrocite) reduction (green rust or magnetite). From this study it is not clear if the high cell number changed the geochemical conditions so other minerals form, for example by a higher reduction rate.

Nonetheless, some characteristics are common for minerals precipitated by microorganisms through redox-processes for energy generation (biogenic minerals):

- the content of incorporated ions from the medium or environment is high, especially in comparison to a pure system containing only the salts needed in chemical synthesis of the minerals. Some ions that are essential for cell growth – like phosphate and carbonate – disturb or drive mineral formation in a certain direction (Cornell & Schwertmann, 2003, Fortin & Langley, 2005, Larese-Casanova et al., 2010);
- biogenic minerals contain a substantial amount of cells and organic molecules which were initially released by cells (Fortin & Langley, 2005) and form cell-mineral aggregates;
- the particle density of biogenic minerals is lower due to the biomass incorporated in the particles (Posth et al., 2010);
- the mineral phase is usually determined by the geochemical conditions prevailing (Larese-Casanova et al., 2010)

Compared to chemical synthesis the factors described above result in a lower crystallinity (Châtellier et al., 2001, 2004) additionally to a higher amount of ions incorporated in the minerals (Cornell & Schwertmann, 2003, Fortin & Langley, 2005).

So far it has not been shown that Fe(II)-oxidizing bacteria influence on the mineral identity. Therefore, various mineral phases have been described as product of various Fe(II)-oxidizing bacteria. The minerals found so far are goethite (α-FeOOH; Kappler & Newman, 2004, Miot et al., 2009b), lepidocrocite (γ-FeOOH; Kappler & Newman, 2004, Larese-Casanova et al., 2010) or poorly crystalline ferrihydrite (Lack et al., 2002, Croal et al., 2004). At the same time, reports also suggest that not only pure but mixed phases can form: magnetite and green rust (Chaudhuri et al., 2001). Others found a goethite/nano-goethite-ferrihydrite mixture (Senko et al., 2005, Hohmann et al., 2010) but also Fe(III) phosphates have been detected (Miot et al., 2009b). Larese-Casanova et al. (2010) clearly showed that medium composition directed mineral formation. Therefore, likely in all the described cases, mineral identity was determined by the geochemical conditions under which the minerals formed and not by the bacteria present in the system. Additionally, the published protocols for Fe(III) mineral synthesis (Schwertmann & Cornell, 2000, Cornell & Schwertmann, 2003) agree well with the published conditions for mineral formation in the bacterial cultures. Therefore, it is vital to determine the geochemical factors that can influence mineral identity in the medium.

6.2.3 Geochemical factors influencing mineral formation

Geochemical factors influencing the mineral product formation are ion composition of the solution in which the mineral precipitates. While, bicarbonate favors the formation of goethite over lepidocrocite (Schwertmann & Cornell, 2000), pH determines between the formation of goethite/lepidocrocite and maghemite (Schwertmann & Cornell, 2000). Additionally, particle size of the minerals that precipitate, depends on the solubility product of the forming minerals (Cornell & Schwertmann, 2003). The solubility product again strongly depends on the pH of the solution. Particle size is thus expected to decrease with lower pH (Cornell & Schwertmann, 2003). pH also influences the precipitation kinetics of Fe(III) ions which form the Fe(III) minerals: the lower the pH the slower Fe(III) will form (Pham et al., 2006, Rose & Waite, 2007).

Ions in the solution in which Fe(III) minerals precipitate can also have a profound influence on the minerals forming (Cornell & Schwertmann, 2003). At circumneutral pH, carbonates direct mineral formation towards goethite (Schwertmann & Cornell, 2000). In contrast, phosphates can prevent this favoring process (Torrent & Barron, 2000). Lepidocrocite is favored if the ratios of Fe/P are high enough although the crystallinity decreased with increasing phosphate concentration (Cornell & Schwertmann, 2003, and references therein). These factors – together with the higher solubility of Fe(III) at lower pH – could have a profound influence on the localization of the precipitating minerals on the cell surface and thus the encrustation of bacteria. Therefore, in this study three distinct pH values were chosen for the experiments (6.2, 6.9 and 7.4) spanning common environmental pH conditions at circumneutral pH as well as the physiological range for typical phototrophic Fe(II)-oxidizing bacteria (Hegler et al., 2008).

6.2.4 Bacterial Fe(II) oxidation

For Fe(II)-oxidizing bacteria, different metabolic pathways are known. At circumneutral pH, Fe(II) can be oxidized by phototrophic Fe(II)-oxidizers (Widdel et al., 1993), nitrate-reducing Fe(II)-oxidizers (Straub et al., 1996) or microaerophilic Fe(II)-oxidizers competing with chemical oxidation by oxygen (Emerson & Moyer, 1997). The forming Fe(III) minerals may precipitate at the cell surface (Kappler et al., 2005b, Miot et al., 2009b,c, Schaedler et al., 2009, Hegler et al., 2010). Additionally, it has been shown that phototrophic Fe(II)-oxidizing bacteria do not have substantial Fe(III) mineral precipitates on the cell surface (Schaedler et al., 2009, Hegler et al., 2010). Hegler et al. (2010) showed that a low pH at the cell surface of phototrophic Fe(II) oxidizers could explain how these bacteria avoid encrustation by Fe(III) minerals. In contrast to photoferrotrophic bacteria, *Acidovorax* sp. strain BoFeN1 oxidizes Fe(II) coupled to the reduction of nitrate (Kappler et al., 2005a) according to the following reaction:

$$10\,Fe^{2+} + 2\,NO_3^- + 24\,H_2O \longrightarrow <CH_2O> + 10\,Fe(OH)_3 + 18\,H^+ + N_2 \tag{6.2}$$

This strain is not autotrophic and requires acetate as carbon source (Kappler et al., 2005b). Kappler et al. (2005a) showed that the oxidation of acetate and that of iron are sequential with a small temporal overlap. Thus, potentially only after acetate is used up the strain benefits from the oxidation of Fe(II) (compare fig 2B in (Kappler et al., 2005a). Fe(II) oxidation additionally to acetate oxidation yields about 10% more cells (Muehe et al., 2009). Acetate is built into biomass according to equation 6.3.

$$CH_3COO^- + H^+ \longrightarrow 2 < CH_2O > \tag{6.3}$$

Before the oxidation of Fe(II) *Acidovorax* sp. strain BoFeN1 oxidizes acetate with nitrate (Kappler et al., 2005b) (eq. 6.4).

$$8\,NO_3^- + 3\,H^+ + 5\,CH_3COO^- \longrightarrow 4N_2 + 4\,H_2O + 10\,HCO_3^- \tag{6.4}$$

Both, nitrate reduction with acetate as electron donor and the mixotrophic growth using acetate as carbon source for biomass consumes protons.

6.2.5 Goals

Despite the abundance of nitrate reduction and the formation of Fe(III) minerals by Fe(II)-oxidizing bacteria in the environment (Straub et al., 1996, Kappler et al., 2005a) it is still unclear, why cells of

Fe(II)-oxidizing nitrate-reducers encrust heavily with Fe(III) minerals (Kappler et al., 2005a, Miot et al., 2009b, Muehe et al., 2009) and how pH affects the Fe(III) minerals in these systems.

Therefore the goals of this study are

- to identify the bulk minerals precipitated by the the nitrate-reducing Fe(II)-oxidizing *Acidovorax* sp. strain BoFeN1 at various pH (Kappler et al., 2005a, Muehe et al., 2009);
- to determine crystallinity at varying pH conditions;
- to determine how the pH affects the localization of the minerals relative to the cells;
- to determine differences in the interaction of phosphate ions with the precipitated Fe(III) minerals.

Mineral phases were analyzed using XRD and Mössbauer spectroscopy and thus complementing the mineralogical analysis. Cell-mineral aggregates were visualized by scanning transmission electron microscopy (STEM), while maps of the elemental distribution by energy dispersive X-ray spectroscopy (EDX) allow to determine the interaction of cells with minerals. Elemental maps of phosphate and iron allowed to determine the location of the most dominant elements of the mineral phases.

6.3 Material and Methods

6.3.1 Reagents

All reagents were of high purity, typically ACS grade or higher. Anoxic solutions were prepared by boiling Millipore water for 2 min and cooling it while bubbling with N_2 gas. HCl-solution was prepared by diluting N_2 purged concentrated HCl with deoxygenated water.

6.3.2 Medium and growth conditions

Acidovorax sp. strain BoFeN1 was used from the lab collection and was grown in minimal mineral medium as described by Hegler et al. (2008) and Muehe et al. (2009). Briefly, the medium contained 0.6 g L^{-1} potassium phosphate (KH_2PO_4), 0.3 g L^{-1} ammonium chloride (NH_4Cl); 0.5 g L^{-1} magnesium sulphate ($MgSO_4 \times 7H_2O$) and 0.1 g L^{-1} calcium chloride ($CaCl_2 \times 2H_2O$) as well as 22 mM bicarbonate buffer. Also, 10 mmol L^{-1} $FeCl_2$, 10 mmol L^{-1} $NaNO_3$ and 5 mmol L^{-1} Na-acetate were added from sterile, anoxic 1 mol L^{-1} stock solutions. Additionally, trace elements and vitamins were added (Hegler et al., 2008). Batch cultures of 250 mL were grown in 0.5 L Schott bottles containing 50% headspace of N_2/CO_2 (80:20) in order to obtain enough material for mineral analysis. The pH was adjusted with anoxic, sterile 1 mol L^{-1} NaOH or 1 mol L^{-1} HCl in the butyl rubber stoppered bottles. In order to allow for equilibration of the bicarbonate buffer and the headspace after adjusting the pH we waited at least 12 hours. Before inoculation, the pH was checked again and if necessary readjusted with an equlibration time of 12 hours.

Previous to inoculation, cells of *Acidovorax* sp. strain BoFeN1 were transferred twice in medium free of Fe(II), containing only acetate and nitrate in order to obtain cultures that were free of mineral nucleation sites (Schaedler et al., 2008) which could potentially influence mineral formation (Cornell & Schwertmann, 2003).

The medium was – in contrast to previous studies (Miot et al., 2009b, Hohmann et al., 2010) – not filtered. This technique has been used previously to remove Fe(II) minerals that precipitate initially due to the over-saturation with regards to Fe(II) carbonates and Fe(II) phosphates in the mineral medium.

6.3.3 Sampling techniques and sample preparation

In this study, we chose an experimental approach, in which the cells were growing over time and we followed Fe(II) oxidation over time with the ferrozine assay (Stookey, 1970, Hegler et al., 2008). Samples for the iron-test were either taken in the glovebox and resuspended in 1 mol L^{-1} HCl or at the lab-bench with N_2-flushed syringes and extracted in 1 mol L^{-1} HCl. Both sampling methods yielded comparable results. Samples for STEM and mineral analysis by Mössbauer spectroscopy and XRD were taken 7-8 days after inoculation.

In order to obtain samples for X-ray diffraction analysis (XRD analysis), several mL of culture were centrifuged in an anoxic glovebox. The pellet was washed once with anoxic double distilled water in order to remove salts from the medium. Samples were stored in the anoxic glovebox until measurement. Prior to the measurement the sample was resuspended in ethanol, further ground in the glovebox with a small mortar and finally added onto a Si-waver. After evaporation of the ethanol the waver was sealed by plastic wrap to avoid potential Fe(II) oxidation during data acquisition (Amstaetter et al., 2010). Miot et al. (2009b) showed for strain BoFeN1 that not all Fe(II) was oxidized at the end of growth and thus anoxic measurements were necessary. The plastic-cover yielded two distinct broad peaks (marked in gray in the diffractogram) at 17-28 and 40-43 2θ. Despite the broad peaks we were still able to analyze the diffractogram and identify the dominating minerals in the system.

Samples for Mössbauer spectroscopy were prepared in an anoxic glovebox by filtering a mineral sample on a 13 mm membrane filter (mixed cellulose esters, 0.45 μm). The filter with the sample was enclosed in oxygen impermeable Kapton® tape for ^{57}Fe specific Mössbauer analysis.

6.3.4 Geochemical modeling

Geochemical modeling was performed with the React module of Geochemists Workbench 6.05. The MINTEQ database was used for the geochemical parameters and constants. The main salts of the medium were included in the matrix while trace metals and vitamins were ignored due to their low concentration in the medium. In order to obtain the aqueous fraction of Fe(II) and Fe(III), respectively, all concentrations of dissolved species were added and plotted as $Fe(III)_{aq,tot}$ and $Fe(II)_{aq,tot}$.

Additionally, sorption of the major ions, e.g. phosphate and bicarbonate, onto ferrihydrite was modeled with the React module of Geochemists Workbench 6.05. The separate MINTEQ database, which is based on the data of Dzombak & Morel (1990), was used for modeling the sorption of ions to hydrous ferrous oxides.

6.3.5 Microscopy

Scanning transmission electron microscopy (STEM) and X-ray energy-dispersive spectrometry (XEDS) samples were prepared as described previously (Miot et al., 2009b). Imaging was done on a JEOL2100 at the IPGP in Paris in the same way as described in Miot et al. (2009b).

6.3.6 Mineral identification – Mössbauer spectroscopy and XRD

The XRD patterns were acquired with a Bruker D8 Discovery μ-X-ray diffractometer with a Co Kα radiation at 30 kV, 30 mA connected to a polycapillary focused to a spot size of 300 μm. For μXRD, a monocapillary with the same settings was used with a monocapillary with a spot-size of 50 μm. Three

overlapping frames of 30° 2θ with a collection time of 1 min per frame were acquired with a GADDS area detector. For μXRD, only the first frame with 30° 2θ with a collection time of up to 5 min was acquired. Diffrac plus EVA© 10.0.1.0-software (Bruker) was used for merging the frames and identifying the mineral phases using the PDF-database (ICDD – International Center for Diffraction Data).

Mössbauer samples were analyzed with a ^{57}Co-source at room temperature while linear acceleration was used in transmission mode. We varied the temperature of the sample with a Janis cryostat to 77 K and 5 K. The calibration of the spectra was done with a α-Fe(0) foil. The Recoil© software was used for spectra analysis.

6.4 Results and Discussion

6.4.1 Growth of the bacteria and oxidation of Fe(II)

Acidovorax sp. strain BoFeN1 was grown as described and oxidized 10 mmol L^{-1} Fe(II) within 3-4 days (fig. 6.1). Quantification of Fe(II) and Fe(total) with the ferrozine method showed, that Fe(II) was completely oxidized to Fe(III) at the end of the experiment. Samples for mineral analysis were taken at the last measurement point about 7-8 days after inoculation in order to sample always in the stationary phase of the culture. The oxidation rates did not differ significantly for the three setups at pH 6.2, 6.9 and 7.4.

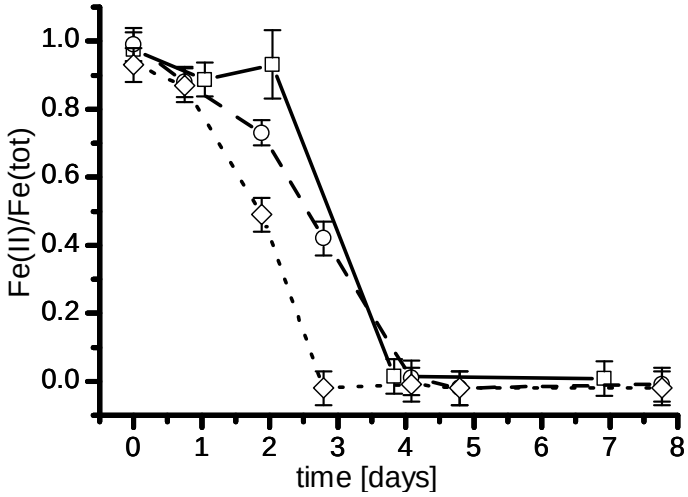

Figure 6.1: Fe(II) oxidation over time by *Acidovorax* sp. strain BoFeN1 for three different pH-values. The results were normalized to Fe_{total}. Culture grown at pH 6.2 □, pH 6.9 ◊ and pH 7.4 ◯.

6.4.2 Identification of the minerals

Minerals were identified, both with XRD and Mössbauer spectroscopy. While XRD allows to determine bulk mineralogy with a detection limit of 5-10%, Mössbauer spectroscopy is iron mineral selective. Mössbauer spectroscopy has the advantage over XRD that even poorly crystalline mineral fractions can be detected and identified. The disadvantage of Mössbauer is that other non-iron minerals that could potentially be present in the system can not be detected. Hence, XRD and Mössbauer spectroscopy

complement each other in the mineral analysis in respect to Fe-minerals.

XRD did not show clear reflections of minerals (figure 6.2). The broad reflections result from the plastic cover used to keep the sample oxygen free, the small reflection is a reflection of the Si-waver at 66 2θ (fig. 6.2).

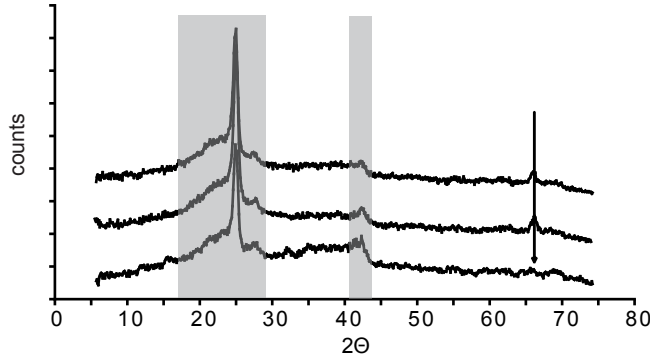

Figure 6.2: XRD of minerals produced by the Fe(II)-oxidizing *Acidovorax* sp. strain BoFeN1; bottom: pH 6.2, middle: pH 6.9 and top pH 7.4. The x-rays were focused with a polycapillary. Gray shaded areas result from cover of the samples with a plastic wrap avoiding their oxidation; the arrow shows a reflection of the Si-waver and is not due to the sample.

In contrast to XRD, the spot size of μXRD is much smaller (50 μm in contrast to 300 μm). μXRD revealed a small peak at 15° 2θ for a mineral sample obtained from a culture grown at pH 6.9 (figure 6.3). This reflection can be attributed to the major reflection of vivianite (see the reference reflections of vivianite in figure 6.3). Minor reflections are likely hidden in the background noise of the measurement. The reflection was only observable for some parts of the ground powder and was not homogeneously distributed throughout the sample. Additionally, the crystal causing the vivianite-reflection was likely small and poorly crystalline as otherwise the reflection would have been observable also with bulk measurements. Additionally, a higher crystallinity would also be observable by more reflections from the crystal and not only the main reflection (e.g. figure 6.2 and 6.3 A).

Mössbauer spectra indicate ferrihydrite or nano-crystalline goethite as Fe(III) minerals that formed as the product of Fe(II) oxidation under the conditions of the setup (figure 6.4). Schwertmann & Cornell (2000) and Cornell & Schwertmann (2003) showed that the mineral phase of Fe(III) minerals is driven towards goethite if bicarbonate is present in the system. Thus, nano-crystalline goethite is more likely in our bicarbonate buffered system.

Additionally, Mössbauer spectroscopy showed that Fe(II) was still present although a clear identification of the mineral phase was not possible (figure 6.4). Vivianite, siderite or even green rust may theoretically be in the system. Mössbauer spectra modeling was not trivial and thus a mixture of these Fe(II) mineral phases is likely. This agrees well with μXRD measurements which indicated small amounts of vivianite which was not homogeneously distributed in the powder (figure 6.3). It is unclear, why the ferrozine-method did not indicate Fe(II) being present, especially since the samples for Mössbauer analysis were taken at the same time-points as all other samples and were measured immediately after sampling. It is expected that poorly crystalline Fe(II) minerals such as vivianite would easily dissolve in 1 mol L^{-1} HCl. An oxidation through oxygen can be excluded.

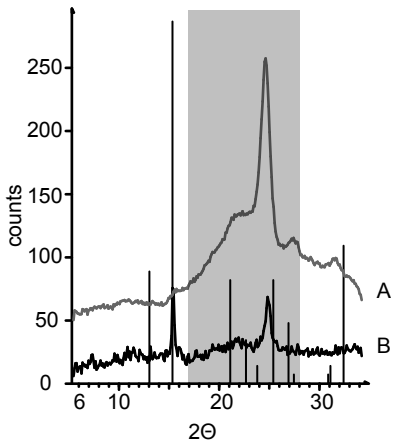

Figure 6.3: XR-diffractograms of minerals produced by BoFeN1 at pH 6.9. Both diffractograms were collected from the same sample. A: The X-ray was focused with a polycapillary allowing for a spot-size of about 300 μm as in figure 6.2. B: μXR-diffractogram of minerals produced by BoFeN1 at pH 6.9. The X-ray was focused with a monocapillary allowing for a spot-size of about 30 μm. Only the first frame was measured up to 33 2θ. The gray shaded area results from cover of the samples by a plastic wrap used to avoid the oxidation of the sample. The black bars show the reflections of vivianite (pdf-reference number of the ICDD for vivianite 00-030-662).

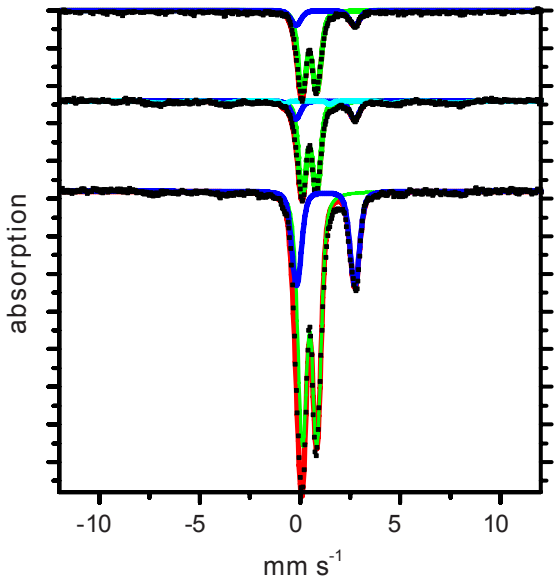

Figure 6.4: Mössbauer spectroscopy of Fe-minerals produced by BoFeN1 at pH 6.2 (bottom), 6.9 (middle) and 7.4 (top) measured at 77 K. Black: measured values, red: overall fit, green: Fe(II) doublet, blue: Fe(III) doublet, cyan: hyperfine field distribution.

Crystallinity of the minerals

Mössbauer spectroscopy showed that the crystal size was small and only poorly ordered (table 6.4) due to the incomplete peak splitting at 4 K (data not shown). Thus, Fe(III) minerals are in all cases indistinguishable between ferrihydrite or nano-goethite although the high bicarbonate content in the medium is expected to favor goethite (Schwertmann & Cornell, 2000). These results are supported by X-ray diffraction data as no clear reflections of the X-rays in XRD measurements indicate only poorly crystalline minerals or very small minerals. These results do not allow to determine the crystal size of the minerals, especially it is not possible to correlate crystal size or crystallinity to pH. This is likely due to the high concentrations of phosphate but also bicarbonate which disturb Fe(III) mineral formation (Cornell & Schwertmann, 2003, Larese-Casanova et al., 2010).

6.4.3 Solubility of Fe(III) minerals

In order to determine how the pH affects the solubility of Fe(II) and Fe(III), we modeled the concentration of $Fe(II)_{aq}$ and $Fe(III)_{aq}$ in the growth medium. The solubility of iron ions is strongly dependent on the pH (Cornell & Schwertmann, 2003). Additionally, a lower pH can lead to less precipitation of $Fe(III)_{ppt}$ on the cell surface (Hegler et al., 2010). The solubility of Fe(II) and Fe(III) in mineral medium was modeled with Geochemists Workbench (figure 6.5) taking all species present in the medium into account. The model shows that the solubility of both, $Fe(II)_{aq}$ and $Fe(III)_{aq}$ increases with a lower pH.

Although the predicted solubility increase of Fe(II) and Fe(III) suggested an influence of pH on the minerals precipitated in the system we did not observe a change in the crystallinity and identity.

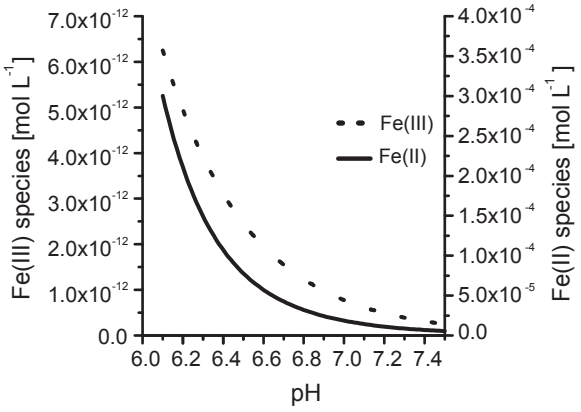

Figure 6.5: Geochemical modeling by Geochemists Workbench for total $Fe(II)_{aq}$ and $Fe(III)_{aq}$ in mineral medium.

6.4.4 Localization of the minerals to the cells and phosphate sorption to the minerals

The primary interaction of Fe(III) ions with the cell surface would be reduced in the case of a bulk lower pH at the cell surface or in the bulk medium (Hegler et al., 2010). Therefore, subsequent precipitation of Fe(III) minerals is expected to be slower the lower the pH (Beveridge & Murray, 1980, Beveridge, 1983, 1989, Hegler et al., 2010). Additionally, the precipitation kinetics are slower the lower the pH (Rose & Waite, 2003, Pham et al., 2006, Rose & Waite, 2007). Furthermore, modeling predicts a higher solubility

of Fe(III) with lower pH and thus a less mineral precipitation onto the cell surfaces is expected.

Therefore, we determined a potential influence of the bulk pH in the growth medium on encrustation of the cells of *Acidovorax* sp. strain BoFeN1 using SEM and STEM for visualizing the association of cells and minerals (figure 6.6 A). We found no evidence for less adsorption of Fe(III) to the cells or less mineral precipitation onto the cells' surface depending on a lower bulk pH of the medium. Fe(III) ions interact strongly with the cell surface functional groups, mainly phosphoryl and carboxylic groups (Beveridge, 1989, Fein et al., 1997, 2001).

Phosphate influences mineral formation and crystallinity remains low (Cornell & Schwertmann, 2003). Therefore, we visualized the interaction of precipitating iron minerals with the phosphate ions of the medium (figure 6.6 B and C). The strong interaction of phosphate ions with the iron minerals observable agrees well with high modeled phosphate-Fe(III) mineral interaction (figure 6.7).

Acidovorax sp. strain BoFeN1 not only oxidizes Fe(II) but at the same time reduces nitrate with acetate (eq. 6.4) and uses acetate as carbon source for biomass (eq. 6.3). The latter two processes consume protons (eq. 6.3 and 6.4). Therefore, potentially for this strain, a low cell surface pH is only present when Fe(II) is oxidized and protons stem from the formation of Fe(III) hydroxides. Thus, the growth of *Acidovorax* sp. strain BoFeN1 may be separated in phases: initially the strain grows with nitrate and acetate while after two days, when the concentration of acetate is low, Fe(II) oxidation starts (e.g. Kappler et al., 2005b, fig 2B).

Thus, even a high pH at the cell surface or even the same pH may be present in the early phase of the batch culture when the strain oxidizes acetate and not iron (eq. 6.3 and 6.4). This is in contrast to photoferrotrophic bacteria for which a low pH at the cell surface was found for the *Thiodyction* strain sp. F4 (Hegler et al., 2010). In the intermediate stage of growth of*Acidovorax* sp. BoFeN1, acetate and Fe(II) oxidation happen at the same time. Therefore, no or only a very small change of the cell surface pH compared to the bulk pH would be expected at that timepoint. However, initially and especially in the intermediate stage, Fe(III) ions will adsorb to the cell surface (Beveridge, 1983) forming the basis for further adsorbing Fe(III) ions, heavy encrustation of the cells would be expected. Only in the second stage could a low cell surface pH potentially establish due to the precipitation of Fe(III) minerals (eq. 6.1). Once Fe(III) minerals precipitated at the cell surface, more Fe(III) ions will adsorb and minerals will form leading to encrustation.

If a low pH at the cell surface was missing or even a high cell surface pH was present a continuous precipitation of Fe(III) minerals on the cell surface would be higher than for photoferrotrophs. This is consistent with the observations of high mineral precipitation on the cell surface at all bulk pH values (fig 6.6 A). This agrees also well with other studies where heavy encrustation of *Acidovorax* sp. strain BoFeN1 with Fe(III) minerals was found (Kappler et al., 2005b, Miot et al., 2009c,b, Schaedler et al., 2009). These observations are also in agreement with a small pH increase of the medium after seven days between 0.1-0.2 pH units for cultures grown with Fe(II) and between 0.2-0.3 pH units for cultures grown only with acetate and nitrate (personal communication Claudia Pantke).

6.4.5 Differences to previously published results

Various results have been published previously for similar systems with *Acidovorax* sp. strain BoFeN1 (Miot et al., 2009b, Larese-Casanova et al., 2010, Hohmann et al., 2010). Nonetheless, the setups in the experiments presented here were different and thus the results in these experiments reflect new aspects in microbial Fe(II) oxidation and resulting mineral precipitation. Miot et al. (2009b) used filtered medium

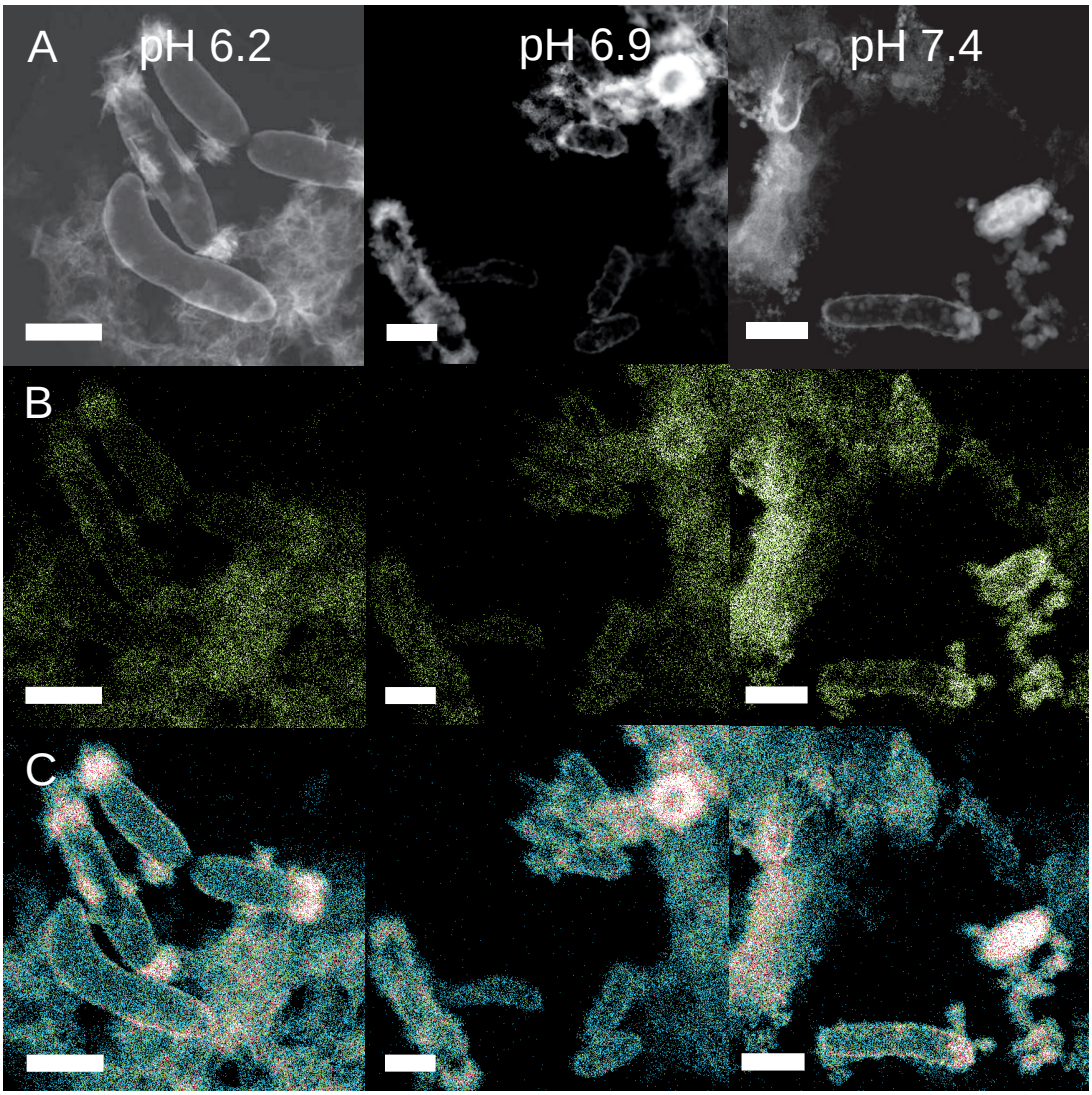

Figure 6.6: *Acidovorax* sp. strain BoFeN1 grown at three different pH values (6.2, 6.9, 7.4): (A) Scanning transmission electron microscopy image (dark field mode), (B) scanning energy dispersive X-ray spectroscopy of phosphate and (C) scanning energy dispersive X-ray spectroscopy of iron. The scalebar represents 1 μm.

where the Fe(II) minerals that precipitate initially were removed. (Miot et al., 2009a) used a very high inoculum of 10% (v/v) and thus high cell numbers. High cell numbers have been described to have an effect on the mineralogy (Zegeye et al., 2010). Larese-Casanova et al. (2010) used cell suspension experiments without phosphate and only minor concentrations of carbonate. Hohmann et al. (2010) reduced the phosphate concentration in the medium to a few μmolar.

Adding the Fe(II) source to the medium leads to an immediate precipitation of a white mineral phase identified as poorly crystalline vivianite (Miot et al., 2009b). Potentially, also some Fe(II) carbonate precipitated at the same time. These primary minerals were removed in some experiments (Miot et al., 2009b, Hohmann et al., 2010) by filtering the medium with a 0.22 μm filter (e.g. Hegler et al., 2008). The medium is in this case oversaturated in respect to Fe(II).

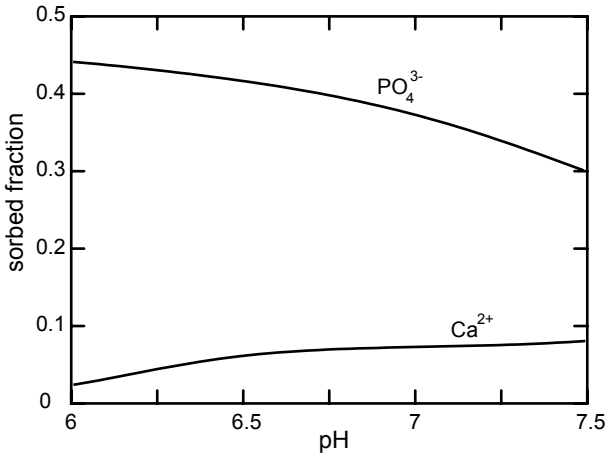

Figure 6.7: Modeling of the sorbed fraction of phosphate and Mg^{2+} onto Fe(III) minerals over the pH range from 6.2 to 7.5.

The filtration has the disadvantage that even small changes in initial pH will lead to strong differences in the medium composition and the amount and properties of the precipitating minerals. The pK_a of bicarbonate (pK_{a1}= 6.35) and phosphate (pK_{a2} = 7.2) (Stumm & Morgan, 1995) are close to the circumneutral pH of the medium (6.8 to 7). Small changes in pH may thus not only direct the formation of either vivianite (e.g. Miot et al., 2009a) or also carbonates as suggested previously (Hegler et al., 2008). Depending on the initial pH (e.g. 6.2, 6.8 or 7.4), the amount of phosphate or carbonate precipitated from the medium as primary Fe(II) phosphates and Fe(II) carbonates differs and therefore the experiments would be difficult to compare. Additionally, not only phosphates and carbonates form but also vitamins and trace metals adsorb and co-precipitate with the primary Fe(II) minerals and are subsequently removed by filtration. The differences between filtrates become even more significant when the pH-values of the experiments are between 6.2 and 7.4 spanning pK_a values of phosphate and bicarbonate. Experiments would hence not be comparable in phosphate, trace metal and vitamin content additionally to the buffer capacity and bicarbonate concentration in the medium as well as the primary minerals that form. It is thus difficult to compare results of experiments with filtered and unfiltered medium in respect to sorption of phosphate and mineral identity due to the different concentration of phosphate.

The experiments of Larese-Casanova et al. (2010) were performed with a MOPS buffer system as cell suspension experiments where most ions present in growth medium were removed. MOPS buffer – as some of the buffers described by Good et al. (1966) – interacts only little or not at all with metal ions such as iron (Yu et al., 1997). In the experiment of Larese-Casanova et al. (2010), the geochemical influence of the solution chemistry on the mineral identity was therefore identified. The mineral formation in the experiments of Larese-Casanova et al. (2010) is difficult to compare to growth experiments as the very high cell number used in these experiments (1×10^{10} cells mL^{-1}) may influence mineral formation (e.g. Zegeye et al., 2010).

However, the experiments of Larese-Casanova et al. (2010) clearly indicate the geochemical influence on the minerals formed by bacteria. But these experiments cannot yield indications on the interaction of cells and minerals in growth experiments. Cell numbers were very high and sorption of minerals to the cell surface and subsequent precipitation of Fe(II) and Fe(III) (Beveridge & Murray, 1976) may only result from a high cell number or may lead to a different mineral phase (Zegeye et al., 2010).

Miot et al. (2009c) showed that the oxidation of Fe(II) by *Acidovorax* sp. strain BoFeN1 happens in the periplasm and that the oxidation of Fe(II) is completed after six days. In these experiments the medium was filtered and thus initial precipitates consisiting of poorly crystalline vivianite (Miot et al., 2009a) were removed. Therefore, it is possible that the Fe(II) minerals detected in this study were removed by filtering in the study of Miot et al. (2009c). Likely, higher concentrations of poorly soluble Fe(II) minerals formed in this study due to the adjustment of pH to the values 6.2, 6.9 and 7.4 (see section 6.3.2). Therefore, further studies are needed to evaluate the primary mineral formation of potentially poorly soluble Fe(II) mineral phases.

6.4.6 Conclusion

The bulk mineralogy does not change over the typical physiological pH-range of Fe(II)-oxidizing bacteria from pH 6.2 to 7.4 (Hegler et al., 2008) despite the higher solubility of Fe(III) in solution at pH 6.2. This is likely due to the high HCO_3^- content of the medium of 22 mM additional to the high phosphate content of 4.4 mmol L^{-1}. These results agree well with previous studies showing a strong geochemical influence of the medium on mineral formation (Larese-Casanova et al., 2010). The crystallinity is low, most likely due to the high phosphate and carbonate concentration in the medium and because mineral free inoculum was added. We could not show, that a low bulk pH could reduce cell encrustation, rather cells interacted strongly with Fe(III) minerals. This observation can be explained by the metabolism of *Acidovorax* sp. strain BoFeN1 which oxidizes acetate additionally to nitrate which leads to an overall increase of the bulk pH.

These results suggest, that in environmental systems the Fe(III) mineral phase forming through the oxidation of Fe(II) is comparable over the pH range of this study. Diurnal cycles causing a change in pH of up to 2 units (Revsbech et al., 1983, Pierson et al., 1999) will change the rate of Fe(II) oxidation (Hegler et al., 2008) but they will likely not change the overall mineral product.

Acknowledgments

We would like to thank Katja Amstätter for the XRD-measurements and the Eberhard Karls University of Tübingen for funding FH as well as Martin Obst, Claudia Pantke and Urs Dippon for helpful and interesting discussions as well as UD and CP for help with improving the quality of the manuscript.

Bibliography

Amstaetter, K; Borch, T; Larese-Casanova, P; & Kappler, A: Redox transformation of arsenic by Fe(II)-activated goethite (α-FeOOH). *Environmental Science & Technology*, 44:102–8, 2010.

Beveridge, TJ: Mechanisms of the binding of metallic ions to bacterial walls and the possible impact on the microbial ecology. In CA Reddy & MJ Klug, eds., *Current perspectives in microbial ecology proceedings of the 3. International Symposium on Microbial Ecology, Michigan State University, 7 - 12 August 1983*, pp. 601–607 (Michigan State University, Washington), 1983.

Beveridge, TJ: Role of cellular design in bacterial metal accumulation and mineralization. *Annual Review of Microbiology*, 43:147–171, 1989.

Beveridge, TJ & Murray, RG: Uptake and retention of metals by cell walls of *Bacillus subtilis*. *Journal of Bacteriology*, 127:1502–1518, 1976.

Beveridge, TJ & Murray, RG: Sites of metal deposition in the cell wall of *Bacillus subtilis*. *Journal of Bacteriology*, 141:876–887, 1980.

Borch, T; Kretzschmar, R; Kappler, A; Cappellen, PV; Ginder-Vogel, M; Voegelin, A; & Campbell, K: Biogeochemical redox processes and their impact on contaminant dynamics. *Environmental Science and Technology*, 44:15–23, 2010.

Canfield, DE & Des Marais, DJ: Biogeochemical cycles of carbon, sulfur, and free oxygen in a microbial mat. *Geochimica et Cosmochimica Acta*, 57:3971–3984, 1993.

Châtellier, X; Fortin, D; West, MM; Leppard, GG; & Ferris, FG: Effect of the presence of bacterial surfaces during the synthesis of Fe oxides by oxidation of ferrous ions. *European Journal of Mineralogy*, 13:705–714, 2001.

Châtellier, X; West, MM; Rose, J; Fortin, D; Leppard, GG; & Ferris, FG: Characterization of iron-oxides formed by oxidation of ferrous ions in the presence of various bacterial species and inorganic ligands. *Geomicrobiology Journal*, 21:99–112, 2004.

Chaudhuri, SK; Lack, JG; & Coates, JD: Biogenic magnetite formation through anaerobic biooxidation of Fe(II). *Applied and Environmental Microbiology*, 67:2844–2848, 2001.

Cornell, RM & Schwertmann, U: *The iron oxides: structure, properties, reactions, occurrences and uses* (VCH, Weinheim, Cambridge), 2nd ed., 2003.

Croal, LR; Johnson, CM; Beard, BL; & Newman, DK: Iron isotope fractionation by Fe(II)-oxidizing photoautotrophic bacteria. *Geochimica et Cosmochimica Acta*, 68:1227–1242, 2004.

Dzombak, DA & Morel, F: *Surface complexation modeling: hydrous ferric oxide* (Wiley, New York), 1990.

Ehrenberg, CG: Vorläufige Mitteilungen über das wirkliche Vorkommen fossiler Infusorien und ihre grosse Verbreitung. *Poggendorfs Annalen der Physik und Chemie*, 38:213–227, 1836.

Emerson, D & Moyer, C: Isolation and characterization of novel iron-oxidizing bacteria that grow at circumneutral pH. *Applied and Environmental Microbiology*, 63:4784–4792, 1997.

Fein, JB; Daughney, CJ; Yee, N; & Davis, TA: A chemical equilibrium model for metal adsorption onto bacterial surfaces. *Geochimica et Cosmochimica Acta*, 61:3319–3328, 1997.

Fein, JB; Martin, AM; & Wightman, PG: Metal adsorption onto bacterial surfaces: Development of a predictive approach. *Geochimica et Cosmochimica Acta*, 65:4267–4273, 2001.

Fortin, D; Ferris, FG; & Scott, SD: Formation of Fe-silicates and Fe-oxides on bacterial surfaces in samples collected near hydrothermal vents on the Southern Explorer Ridge in the northeast Pacific Ocean. *American Mineralogist*, 83:1399–1408, 1998.

Fortin, D & Langley, S: Formation and occurrence of biogenic iron-rich minerals. *Earth-Science Reviews*, 72:1–19, 2005.

Gadd, GM: Metals, minerals and microbes: geomicrobiology and bioremediation. *Microbiology*, 156:609–643, 2010.

Good, NE; Winget, GD; Winter, W; Connolly, TN; Izawa, S; & Singh, RMM: Hydrogen ion buffers for biological research. *Biochemistry*, 5:467–477, 1966.

Hegler, F; Posth, NR; Jiang, J; & Kappler, A: Physiology of phototrophic iron(II)-oxidizing bacteria – implications for modern and ancient environments. *FEMS Microbiology Ecology*, 66:250–260, 2008.

Hegler, F; Schmidt, C; Schwarz, H; & Kappler, A: Does a low pH-microenvironment around phototrophic Fe(II)-oxidizing bacteria prevent cell encrustation by Fe(III) minerals? *FEMS Microbiology Ecology*, accepted:accepted, 2010.

Hohmann, C; Morin, G; Ona-Nguema, G; Guigner, JM; Brown, GEJ; & Kappler, A: Molecular-level modes of As binding to iron (oxy)hydroxides precipitated by the anaerobic nitrate-reducing iron(II)-oxidizing *Acidovorax* sp. strain BoFeN1, 2010. Submitted.

James, RE & Ferris, FG: Evidence for microbial-mediated iron oxidation at a neutrophilic groundwater spring. *Chemical Geology*, 212:301–311, 2004.

Kappler, A & Newman, DK: Formation of Fe(III)-minerals by Fe(II)-oxidizing photoautotrophic bacteria. *Geochimica et Cosmochimica Acta*, 68:1217–1226, 2004.

Kappler, A; Pasquero, C; Konhauser, KO; & Newman, DK: Deposition of banded iron formations by anoxygenic phototrophic Fe(II)-oxidizing bacteria. *Geology*, 33:865–868, 2005a.

Kappler, A; Schink, B; & Newman, DK: Fe(III) mineral formation and cell encrustation by the nitrate-dependent Fe(II)-oxidizer strain BoFeN 1. *Geobiology*, 3:235–245, 2005b.

Klausen, J; Trober, SP; Haderlein, SB; & Schwarzenbach, RP: Reduction of substituted nitrobenzenes by Fe(II) in aqueous mineral suspensions. *Environmental Science & Technology*, 29:2396–2404, 1995.

Lack, JG; Chaudhuri, SK; Chakraborty, R; Achenbach, LA; & Coates, JD: Anaerobic biooxidation of Fe(II) by *Dechlorosoma suillum*. *Microbial Ecology*, 43:424–431, 2002.

Larese-Casanova, P; Haderlein, S; & Kappler, A: Biomineralization of lepidocrocite and goethite by nitrate-reducing Fe(II)-oxidizing bacteria: Effect of pH, bicarbonate, phosphate and humic acids. *Geochimica Et Cosmochimica Acta*, 74:3721–3734, 2010.

Millero, FJ; Sotolongo, S; & Izaguirre, M: The oxidation kinetics of Fe(II) in seawater. *Geochimica et Cosmochimica Acta*, 51:793–801, 1986.

Miot, J; Benzerara, K; Morin, G; Bernard, S; Larquet, E; Ona-Nguema, G; Kappler, A; & Guyot, F: Transformation of vivianite by anaerobic nitrate-reducing iron-oxidizing bacteria. *Geobiology*, 7:373–384, 2009a.

Miot, J; Benzerara, K; Morin, G; Kappler, A; Bernard, S; Obst, M; Férard, C; Skouri-Panet, F; Guigner, JM; Posth, NR; Galvez, M; Brown, GE, JR.; & Guyot, F: Iron biomineralization by neutrophilic iron-oxidizing bacteria. *Geochimica et Cosmochimica Acta*, 73:696–711, 2009b.

Miot, J; Benzerara, K; Obst, M; Kappler, A; Hegler, F; Schaedler, S; Bouchez, C; Guyot, F; & Morin, G: Extracellular iron biomineralization by photoautotrophic iron-oxidizing bacteria. *Applied and Environmental Microbiology*, 75:5586–5591, 2009c.

Muehe, EM; Gerhardt, S; Schink, B; & Kappler, A: Physiology of mixotrophic ferrous iron oxidation by a nitrate-reducing *Acidovorax* strain isolated from a freshwater lake sediment. *FEMS Microbiology Ecology*, 70:335–343, 2009.

Pham, AN; Rose, AL; Feitz, AJ; & Waite, TD: Kinetics of Fe(III) precipitation in aqueous solutions at pH 6.0-9.5 and 25 degrees C. *Geochimica Et Cosmochimica Acta*, 70:640–650, 2006.

Pierson, BK; Parenteau, MN; & Griffin, BM: Phototrophs in high-iron-concentration microbial mats: Physiological ecology of phototrophs in an iron-depositing hot spring. *Applied and Environmental Microbiology*, 65:5474–5483, 1999.

Posth, NR; Huelin, S; Konhauser, K; & Kappler, A: Size, density and composition of cell-mineral aggregates formed during anoxigenic phototrophic Fe(II) oxidation: Impact on modern and ancient environments. *Geochimica Et Cosmochimica Acta*, 74:3476–3493, 2010.

Pringsheim, EG: Iron bacteria. *Biological Reviews of the Cambridge Philosophical Society*, 24:200–45, 1949.

Revsbech, NP; Jørgensen, BB; & Blackburn, TH: Microelectrode studies of the photosynthesis and O_2, H_2S and pH profiles of a microbial mat. *Limnology and Oceanography*, 28:1062–1074, 1983.

Rose, AL & Waite, TD: Kinetics of hydrolysis and precipitation of ferric iron in seawater. *Environmental Science and Technology*, 37:3897–3903, 2003.

Rose, AL & Waite, TD: Reconciling kinetic and equilibrium observations of iron(III) solubility in aqueous solutions with a polymer-based model. *Geochimica et Cosmochimica Acta*, 71:5605–5619, 2007.

Schaedler, S; Burkhardt, C; Hegler, F; Straub, KL; Miot, J; Benzerara, K; & Kappler, A: Formation of cell-iron-mineral aggregates by phototrophic and nitrate reducing anaerobic Fe(II)-oxidizing bacteria. *Geomicrobiology Journal*, 26:93–103, 2009.

Schaedler, S; Burkhardt, C; & Kappler, A: Evaluation of electron microscopic sample preparation methods and imaging techniques for characterization of cell-mineral aggregates. *Geomicrobiology Journal*, 25:228–239, 2008.

Schultze-Lam, S; Fortin, D; Davis, BS; & Beveridge, TJ: Mineralization of bacterial surfaces. *Chemical Geology*, 132:171–181, 1996.

Schwertmann, U & Cornell, RM: *Iron oxides in the laboratory : preparation and characterization* (Wiley-VCH, Weinheim), 2nd ed., 2000.

Senko, JM; Dewers, TA; & Krumholz, LR: Effect of oxidation rate and Fe(II) state on microbial nitrate-dependent Fe(III) mineral formation. *Applied and Environmental Microbiology*, 71:7172–7177, 2005.

Stookey, LL: Ferrozine – a new spectrophotometric reagent for iron. *Analytical Chemistry*, 42:779–781, 1970.

Straub, KL; Benz, M; Schink, B; & Widdel, F: Anaerobic, nitrate-dependent microbial oxidation of ferrous iron. *Applied and Environmental Microbiology*, 62:1458–1460, 1996.

Stumm, W & Morgan, JJ: *Aquatic chemistry: chemical equilibria and rates in natural waters* (Wiley-Interscience, New York), 3rd ed., 1995.

Torrent, J & Barron, V: Key role of phosphorus in the formation of the iron oxides in Mars soils? *Icarus*, 145:645–647, 2000.

Tufano, KJ & Fendorf, S: Confounding impacts of iron reduction on arsenic retention. *Environmental Science and Technology*, 42:4777–4783, 2008.

Widdel, F; Schnell, S; Heising, S; Ehrenreich, A; Assmus, B; & Schink, B: Ferrous iron oxidation by anoxygenic phototrophic bacteria. *Nature*, 362:834–836, 1993.

Winogradsky, S: Über Eisenbacterien. *Botanische Zeitung*, 17:261–270, 1888.

Yu, Q; Kandegedara, A; Xu, Y; & Rorabacher, DB: Avoiding interferences from good's buffers: A contiguous series of noncomplexing tertiary amine buffers covering the entire range of pH 3-11. *Analytical biochemistry*, 253:50–56, 1997.

Zegeye, A; Mustin, C; & Jorand, F: Bacterial and iron oxide aggregates mediate secondary iron mineral formation: green rust versus magnetite. *Geobiology*, 8:209–222, 2010.

7 Extracellular Iron Biomineralization by Photoautotrophic Iron-Oxidizing Bacteria

Jennyfer Miot[1], Karim Benzerara[1], Martin Obst[2], Andreas Kappler[2], Florian Hegler[2], Sebastian Schädler[2], Camille Bouchez[1], Francois Guyot[1], Guillaume Morin[1] **Applied and Environmental Microbiology, 75:5586 – 5591, 2009**

[1]Institut de Minéralogie et de Physique des Milieux Condensés, UMR 7590, CNRS, Universités Paris 6 et Paris 7, et IPGP, 140, rue de Lourmel, 75 015 Paris, France
[2]Center for Applied Geoscience – Geomicrobiology, Eberhard Karls University Tübingen, Sigwartstrasse 10, 72076 Tübingen, Germany

7.1 Abstract

Iron oxidation at neutral pH by the phototrophic anaerobic iron-oxidizing bacterium Rhodobacter sp. strain SW2 leads to the formation of iron-rich minerals. These minerals consist mainly of nano-goethite (μ-FeOOH), which precipitates exclusively outside cells, mostly on polymer fibers emerging from the cells. Scanning transmission X-ray microscopy analyses performed at the C K-edge suggest that these fibers are composed of a mixture of lipids and polysaccharides or of lipopolysaccharides. The iron and the organic carbon contents of these fibers are linearly correlated at the 25 nm scale, which in addition to their texture suggests that these fibers act as a template for mineral precipitation, followed by limited crystal growth. Moreover, we evidence a gradient of the iron oxidation state along the mineralized fibers at the submicrometer scale. Fe minerals on these fibers contain a higher proportion of Fe(III) at cell contact, and the proportion of Fe(II) increases at a distance from the cells. All together, these results demonstrate the primordial role of organic polymers in iron biomineralization and provide first evidence for the existence of a redox gradient around these nonencrusting, Fe-oxidizing bacteria.

7.2 Introduction

Fe(II) can serve as a source of electrons for phylogenetically diverse microorganisms that precipitate iron minerals as products of their metabolism (see, e.g. (Benz et al., 1998, Chan et al., 2004, Schaedler et al., 2009, Widdel et al., 1993)). For example, mixotrophic or autotrophic bacteria can couple the oxidation of Fe(II) to the reduction of nitrate in anoxic and neutral-pH environments. With Fe(III) being highly insoluble at neutral pH, this metabolism leads to the formation of poorly to well-crystallized iron minerals (Benz et al., 1998, Kappler et al., 2005, Straub et al., 1996, Straub & Buchholz-Cleven, 1998) that precipitate partly within the cell periplasm for some strains (Miot et al., 2009b). Similar Fe minerals are also synthesized by autotrophic bacteria that perform anoxygenic photosynthesis, using Fe(II) as an

electron donor and light as a source of energy for CO_2 fixation (Ehrenreich & Widdel, 1994, Heising & Schink, 1998, Widdel et al., 1993), according to the equation

$$HCO_3^- + 4Fe^{2+} + 10H_2O \rightleftharpoons < CH_2O > +4Fe(OH)_3 + 7H_2O \quad (7.1)$$

However, the biological mechanisms of iron oxidation in these bacteria and in particular the way they cope with the formation of minerals within their ultrastructures are still not fully understood. Indeed, iron minerals are potentially lethal since their precipitation may alter cellular ultrastructures but also catalyze the production of free radicals (Auffan et al., 2008). Recent genetic studies of the phototrophic, iron-oxidizing bacteria *Rhodobacter* sp. strain SW2 (Croal et al., 2007) and *Rhodopseudomonas palustris* strain TIE-1 (Jiao & Newman, 2007) have identified genes (fox and pio operons, respectively) encoding proteins specific for iron oxidation. Interestingly, Jiao and Newman Jiao & Newman (2007) suggested that one of these proteins could have a periplasmic localization. However, in contrast to what has been observed in some other phototrophic iron oxidizers (Schaedler et al., 2009) and in some nitrate-reducing, iron oxidizing bacteria (Miot et al., 2009b), no iron-mineral precipitation occurs within the periplasm of the purple nonsulfur iron-oxidizing bacterium *Rhodobacter* sp. strain SW2 (Benz et al., 1998). Similarly to some other anaerobic neutrophilic (Miot et al., 2009b, Schaedler et al., 2009) and microaerobic ironoxidizing bacteria (Chan et al., 2004, Hallberg & Ferris, 2004), this strain seems indeed to have the ability to localize iron biomineralization at a distance from the cells, leaving large areas of the cells free of precipitates (Kappler & Newman, 2004, Schaedler et al., 2009). While it has been shown that the *Gallionella* and *Leptothrix* genera, for example, produce extracellular polymers that facilitate the nucleation of iron minerals outside cells (see, e.g. (Chan et al., 2004, Emerson & Revsbech, 1994), only a little is known about the existence and function of such polymers in anaerobic, neutrophilic ironoxidizing bacteria and particularly in the phototrophic strain SW2. In the present study, we investigate iron biomineralization by the photoautotrophic iron-oxidizing bacterium *Rhodobacter* sp. strain SW2. We use scanning transmission X-ray microscopy (STXM) to map and identify organic polymers produced by the cells as well as the redox state of iron at the 25 nm scale regularly during a 2 week-period. These results demonstrate the primordial role of organic polymers in iron biomineralization and provide the first evidence for the existence of a redox gradient around SW2 cells.

7.2.1 Materials and Methods

Bacterial strain and growth conditions. The phototrophic Fe(II)-oxidizing bacterium *Rhodobacter* sp. strain SW2 (Widdel et al., 1993) was cultivated in batch freshwater mineral medium prepared according to the work of Ehrenreich and Widdel Ehrenreich & Widdel (1994) and buffered at pH 6.8 with bicarbonate in equilibrium with a N_2-CO_2 (80:20) atmosphere. SW2 was grown in this medium, with Fe(II) as an electron donor. For experiments using Fe(II) as an electron donor, Fe(II) was added as $FeCl_2$ at a total concentration of 10 mM, which led to the precipitation of a white phase characterized as vivianite $Fe_3(PO_4)_2$ (Miot et al., 2009b). This vivianite precipitate was removed prior to inoculation by filtration through 0.22 mum Millipore filters in an anoxic glove box [$p(O_2)$ 50 ppm, where $p(O_2)$ is the partial pressure of O_2 in the glove box]. After filtration, the medium contained 4.5 mM dissolved Fe(II) and less than 0.5 mM phosphate. In uninoculated controls, no further precipitation was observed over the time of the experiment. SW2 was inoculated at a 1/100 dilution ratio from a H_2-pregrown

or an Fe(II)-pregrown culture in stationary phase. Cultures were incubated at 20 °C under permanent illumination. Growth was followed in duplicate experiments (two independent cultures). For STXM analyses, samples of the same culture were collected in an O_2-free glove box [p(O_2)50 ppm] at several subsequent time steps (3 h and 4, 7, 11, and 15 days).

Dissolved Fe(II) and Fe(III) measurement. The concentration of dissolved iron was followed over the time courses of the cultures. For that purpose, 200 *mu*L of a culture suspension was sampled with a syringe and filtered through a 0.22 *mu*m Millipore filter in an anoxic glove box. The dissolved Fe(II) content of the filtrate after dilution in 1 M HCl was determined using the ferrozine assay (Viollier et al., 2000). The presence of dissolved Fe(III) was evaluated as the difference between dissolved Fe(II) concentrations after and before reduction with excess hydroxylamine hydrochloride. No measurable dissolved Fe(III) was evidenced in any sample.

Synthesis of model compounds for Fe redox analyses. To determine the Fe oxidation state in the samples by STXM at the Fe $L_{2,3}$-edges, a pure Fe(II) end member and a pure Fe(III) end member are needed, both of which need a structure as close as possible to that of the phases produced by SW2. Pure Fe(II)-vivianite [$Fe_3(PO_4)_2$] obtained after addition of 10 mM Fe(II) to the culture medium was used as the Fe(II) end member. Nano-goethite (α-FeOOH) obtained from the SW2 culture after 15 days of incubation was used as the Fe(III) end member. The mineralogical purity of these compounds was checked by X-ray diffraction (XRD), and the redox state of Fe in both compounds was also controlled by bulk X-ray absorption near-edge spectroscopy (XANES) at the Fe K-edge. Both reference minerals were rinsed twice with degassed distilled water and dried under vacuum inside an anoxic glove box.

Mineral characterization by XRD. The bulk mineralogical composition of the solid phases formed in SW2 cultures was determined by XRD measurement and compared to those of vivianite and goethite model compounds. Samples were prepared under anoxic conditions in an anoxic glove box. The cultures were centrifuged (5,000 × g, 10 min). The solid phases were rinsed twice using degassed distilled water and vacuum dried. The powders were ground in an agate mortar and dispensed in borosilicate capillaries that were sealed with glue before analysis in the diffractometer. This preparation guaranteed strict anoxic conditions for XRD analyses. XRD measurements were performed with CoKα radiation on a Panalytical X -Pert Pro MPD diffractometer mounted in the Debye-Scherrer configuration using an elliptical mirror to obtain a high-flux parallel incident beam and an X-Celerator detector to collect the diffracted beam. Data were recorded in the continuous-scan mode within the 5-80 degree 2 θ range with a step of 0.03 degrees and a counting time of 12 to 24 h per sample.

Scanning electron microscopy. Twenty-eight-day-old samples were chemically fixed using a half-strength Karnovsky solution (Kiernan, 2000); placed on holey, carboncoated, electron microscopy copper grids; dehydrated in subsequent steps with an increasing concentration of isopropanol; and finally dried in a Bal-Tec CPD030 critical point dryer. A detailed description of the sample preparation steps is given by (Schaedler et al., 2008). Dried samples were mounted on aluminum stubs using double-sided carbon tape. For enhanced electrical conductivity, the edges of the electron microscopy grids were painted with conductive silver paste. Samples that showed strong surface charging were coated in a Bal-Tec SCD 40 sputter coater (Bal-Tec, Balzers, Liechtenstein) with a thin layer of Au-Pd (90%-10%, wt/wt). The coating thickness was approximately 20 nm, as determined in focused ion beam cross sections and by a surface texture analyzer (results not shown).

Imaging was performed with a Zeiss Gemini 1550VP field emission scanning electron microscope (SEM) and a Zeiss Gemini 1540XB focused ion beam/field emission SEM. Both microscopes were equipped with Everhart-Thornley secondary electron detectors and in-lens detectors and were optimized to a lens

aperture of 30 μm. Images were recorded in a format of 1,024 by 768 pixels at integration times between 15 μs and 45 μs per pixel.

STXM. The samples were constantly kept under an anoxic atmosphere from preparation to transfer and analysis within the STXM microscope, according to the method described in detail in (Miot et al., 2009b). The entire preparation was performed on samples of the SW2 cultures (or of reference compounds) collected at different stages of the culture (3 h to 15 days). STXM experiments were performed on two independent cultures, and two images at least were analyzed for each time point.

Some of the STXM observations at the Fe L_2,3-edges were performed at Swiss Light Source (SLS; Villigen, Switzerland) on the PolLuX beamline. Some of the observations at the Fe L_2,3-edges and all the observations at the C K-edge were performed at the spectromicroscopy 10ID-1 beamline at Canadian Light Source (CLS; Saskatoon, Canada). Additional information on the PolLuX beamline can be found in the work of Bernard et al. (Bernard et al., 2007) The 10ID-1 beamline at CLS was described in detail by citepKaznatcheev.2007. The energy scales for this study were calibrated using the well-resolved 3p Rydberg peak of gaseous CO_2 for the C K-edge and the major peak of hematite at 708.7 eV for the Fe L_3-edge.

Image sequences (stacks) were acquired across the C K-edge and the Fe L_2,3-edges. as described by (Miot et al., 2009b). No significant beam damage could be observed for typical dwell times used during analyses of the samples (i.e., around 0.8 ms per energy and image point). The aXis2000 software package (Hitchcock, 2008) was used for processing image stacks and XANES spectra according to the procedure described by (Miot et al., 2009b). Normalized Fe L_2,3-edge XANES spectra of selected regions were fitted with linear combinations of the normalized reference spectra of the Fe(II)-phosphate and goethite model compounds. Standard deviations were calculated from the deviation between the fit and the data and were systematically less than 1%. Fe(III)/total Fe ratio profiles were obtained using the Fe(III) and Fe(II) optical density (OD) maps derived from the stack fits (see Fig. S3 in the supplemental material).

Spectra of reference albumin (protein), xanthan (polysaccharide), and 1,2-dipalmitoyl-sn-glycero-3-phosphocholine (lipid) (Dynes et al., 2006) were recorded at the C K-edge. All these spectra were normalized to an OD corresponding to a 1 nm layer of the compound. Therefore, the measured reference spectra were scaled to match the absorption in the pre- and postedge regions predicted from the elemental composition, densities, and tabulated atomic scattering factors (Henke et al., 1993). Model spectra were set to an absolute linear absorbance scale (OD per nm of thickness). Spectra recorded at the Fe L_2,3-edges were normalized as described before. Using aligned stacks recorded at the C K-edge and at the Fe L_2,3-edges on the same area as well as the normalized reference spectra, we calculated C and Fe speciation maps by singular-value decomposition using the stack fit routine in aXis2000. The algorithm fits the spectra of each individual pixel with a linear combination of the normalized reference spectra plus a constant, accounting for the absorption background of all elements absorbing at lower X-ray energies. We subsequently obtained numbers that were proportional to the amount of organic carbon and to the amount of Fe(III) (though with a different proportion constant) for each pixel of this area. Both series of values were then used to plot the amount of C (polysaccharides on fibers or proteins on cells) relatively to the amount of Fe [Fe(III)] for each pixel of the area (2,500 pixels in total) and assess the existence of possible correlations (see reference (Wan et al., 2007) for additional explanations).

7.3 Results

Association of iron minerals with organic carbon. Fe(II) was almost completely consumed (oxidized) within 10 days in cultures of SW2 (see Fig. 7.1). In contrast, no significant oxidation could be detected in abiotic controls over the same period. Consistently with the results obtained by (Kappler & Newman, 2004), XRD analyses indicate that the end product of iron oxidation by SW2 is crystalline and consists of nanocrystalline goethite (α-FeOOH) (see Fig. 7.2).

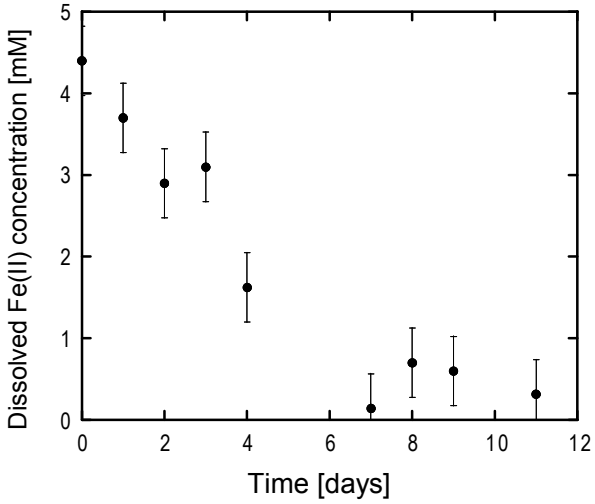

Figure 7.1: Plot of the concentration of dissolved Fe(II) in the SW2 culture versus time over a 12 day period (initial Fe(II) concentration of 4.5 mM). Values represent the mean and error bars the standard deviation calculated from two independent cultures.

Cell-mineral assemblages were imaged by SEM (see Fig. 7.3A). In addition, iron-rich minerals were localized with respect to the cells by analyzing the cultures using STXM at the Fe L_2,3-edges. Maps of Fe(II) and Fe(III) were obtained by fitting stacks with a linear combination of Fe(II) and Fe(III) reference compounds. As shown in Fig. 7.3A and E, iron-rich minerals are exclusively localized outside the cells, mostly on extracellular fibers and in a very low proportion at the cell surface. Extracellular fibers are usually attached to the cell and measure up to a few mum in length and a few nm in diameter (Fig. 7.3A). Moreover, maps of organic carbon reveal that these ironbearing fibers are rich in organic carbon (Fig. 7.3C and D). XANES spectra at the C K-edge obtained for these regions exhibit maxima of absorption at 285.2 eV, 287.4 eV, and 288.6 eV, which can be attributed to alkene (CAC), aliphatic (COC) or carbonyl (CAO), and carboxylic (COOH) groups, respectively (Fig. 7.3F) (Hitchcock et al., 2007). The biochemical indexation of such spectra is more difficult, given the significant variations of the XANES signatures within some biochemical groups, such as lipids and polysaccharides (A. P. Hitchcock, personal communication). However, the XANES spectrum of the fibers can reasonably well be fitted using a linear combination of a polysaccharide (xanthan) and a fully saturated lipid (1,2-dipalmitoyl-sn-glycero-3-phosphocholine). The peak at 285.2 eV that is not well fitted in intensity with our set of reference spectra can be attributed to additional unsaturated C=C bonds that may be present on the aliphatic tail of the fatty acid. Thus, our results suggest that organic fibers attached to SW2 cells consist of a mixture of partially unsaturated lipids and polysaccharides or of lipopolysaccharides. A maximum of 3% of the total mass of carbon may be accounted for by proteins in these fibers. In contrast, XANES spectra at the C K-edge obtained on

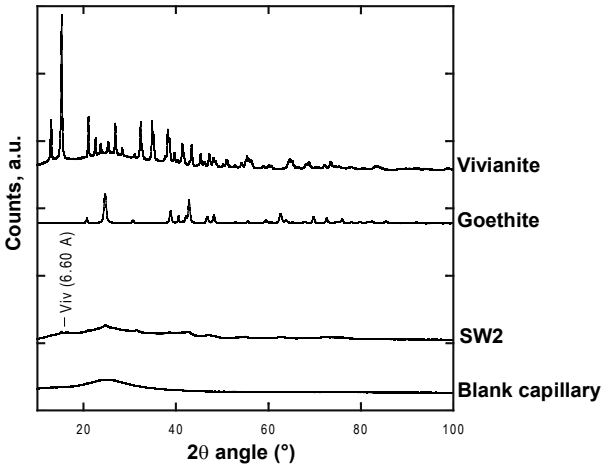

Figure 7.2: X-ray diffraction patterns of 1^{st} the precipitates collected from a 15 day old culture of SW2 (SW2), 2^{nd} reference goethite, 3^{rd} reference vivianite used for STXM analyses and 4^{th} a blank capillary. In the "SW2" pattern, a vivianite peak is observed (Viv); all other broad peaks correspond to peaks of goethite. The large width of the peaks indicates that goethite particles are few nanometers in size. The broad background in all samples but goethite is due to the glass capillary (blank capillary).

bacteria have a dominant absorption maximum at 288.2 eV that is unambiguously attributed to the absorption by the peptidic bond, characteristic of proteins.

The existence of a correlation between the Fe and organic carbon contents on cells and on extracellular mineralized fibers has been investigated separately (Fig. 7.4) by plotting the OD levels measured on each pixel of the region of interest on the Fe(III) map and on the organic carbon map. Interestingly, the Fe(III) and organic carbon contents are correlated on the mineralized fibers (Fig. 7.4A) according to a linear relation, [Fe] = 2.5 [C] + 100 (r = 0.98). This relation suggests that the amount of Fe(III) precipitated is proportional to the amount of organic carbon on the same area.

The Fe content is also related to the amount of organic carbon on the cells according to a linear relation, [Fe] = 0.1 [C] + 25 (r = 0.62). It can be noted that the concentration of iron on the cells is, however, much lower than on the fibers (Fig. 7.4B), which might correspond to Fe adsorbed to the cells.

Iron oxidation state at the nanoscale. The evolution of the iron redox state in these extracellular iron-rich minerals was followed regularly during a 2 week period (3 h to 15 days of culture) using STXM at the Fe $L_{2,3}$-edges. XANES spectra recorded on these samples were fit with a linear combination of a reference Fe(II) compound (vivianite) and a reference Fe(III) compound (goethite) (see Fig. 7.6; table 7.1. Numerical results of these fits indicate that the minerals that form initially in SW2 cultures are composed of mixed-valence iron [the Fe(III)/total Fe ratio was 0.39 after 3 h of culture]. Over time, iron contained in these minerals becomes increasingly oxidized (see Fig. 7.5 and 7.6; table 7.1). After 7 days of culture, iron-rich minerals are mostly composed of Fe(III) [Fe(III)/total Fe = 0.84], and the end product of iron bio-oxidation by SW2 is a pure Fe(III) compound (nano-goethite obtained after 15 days) (see Fig. 7.2).

Local heterogeneities of the redox state of Fe were investigated at different stages of the culture (Fig. 7.7). Therefore, Fe(II), Fe(III), and total Fe intensity profiles were derived from Fe(II) and Fe(III) OD maps of the bacteria and associated extracellular iron-rich minerals. The resulting Fe(III)/total

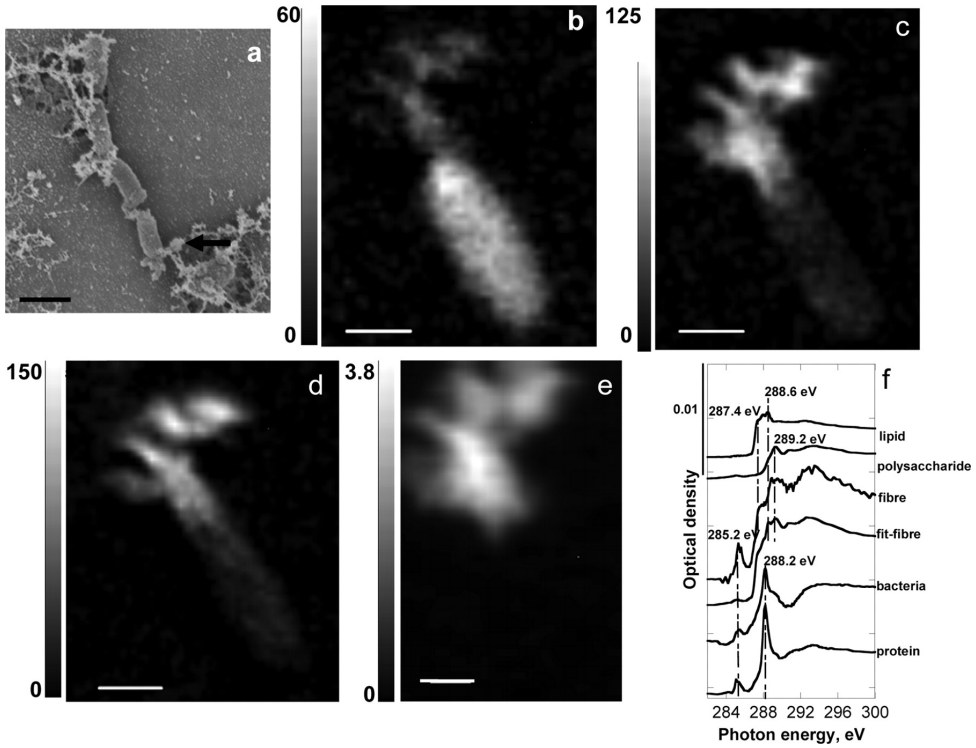

Figure 7.3: (a) SEM micrograph showing mineralized fibers (arrow) emerging from SW2 cells. Minerals are located mostly on the fibers, and the surface of SW2 cells remains largely free of precipitates. Scale bar, 1 μm. (b, c, d, e, and f) STXM analyses of a single SW2 cell with mineralized fibers (3 day old culture). The three different organic carbon maps (b, c, and d) were obtained by fitting an energy sequence of images (stack) with a linear combination of albumin (protein), 1,2-dipalmitoyl-sn-glycero-3-phosphocholine (lipid-fatty acid), and xanthan (polysaccharide). Scale bars, 500 nm. (b) Map of proteins. The cell is clearly visible on this map. (c) Map of lipids. The extracellular fiber is clearly visible on this map. (d) Map of polysaccharides. (e) Fe(III) (goethite) map derived from the stack at the Fe $L_{2,3}$-edges. (f) XANES spectra at the C K-edge obtained on the cell (bacteria) and the extracellular fiber (fibre), compared with the spectra of reference protein, lipid, and polysaccharide. The XANES spectrum of the fiber was fitted with a linear combination of the lipid and the polysaccharide (fit-fibre) and yielded proportions of 50% each.

Fe profiles along the mineralized fibers from the bacterial pole (pole A) toward the end of the fiber at distance of the cell (pole B) are displayed in (Fig. 7.7B) at different time points (5 h and 11 days). This analysis reveals a gradient of the Fe oxidation state along the mineralized fibers [Fe(III)/total Fe = 0.67 - 0.26x (r = 0.88) (in the 5 h-old sample)] (Fig. 3b), iron being systematically more oxidized at the cell contact than at a distance from the cells. This gradient was observed at all sampling times, and the average iron oxidation state on the filaments increased over time (see (Fig. 7.6); table 7.1). Toward the end of the experiment, when iron was almost completely oxidized, the redox gradient was attenuated (11 days) [Fe(III)/total Fe = 0.98 - 0.10x (r = 0.82) (in the 11 day old sample)] (Fig. 7.7B).

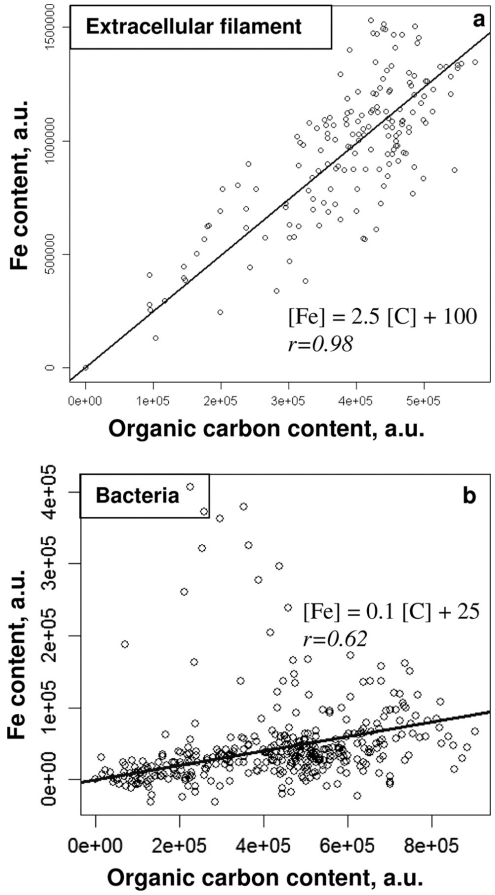

Figure 7.4: Correlation analysis of iron contents versus organic carbon contents on extracellular fibers (a) and bacteria (b) from a 3 day old SW2 culture. Fe and organic carbon contents were estimated at each pixel of the STXM image presented in Fig. 7.3 B to e from the Fe(III), the polysaccharide (for the extracellular fibers), and the protein (for the cell) maps. These results indicate that Fe(III) content is proportional to organic carbon content on extracellular fibers (a) and that cells are covered by a small amount of Fe (b). a.u., arbitrary units.

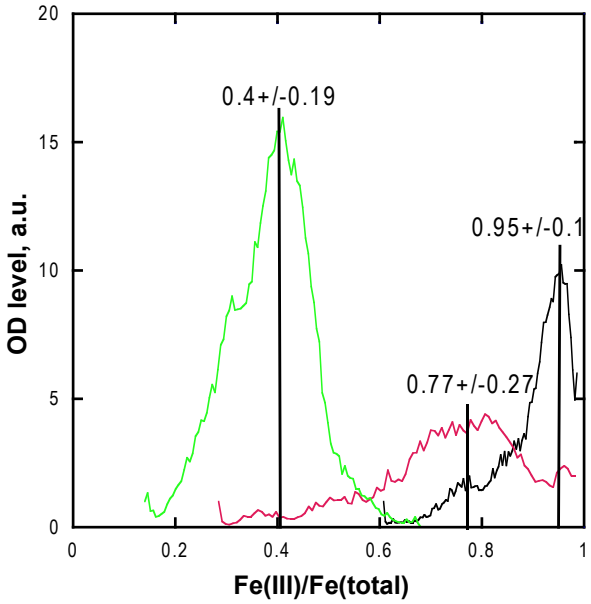

Figure 7.5: Spatial variability of the Fe(III)/Fe(total) ratio within SW2 cultures at different stages of the culture: (green): 3 h, (pink): 4 days, (black): 7 days. Numbers are means ± width at mid-height of the peaks.
METHOD: Fe(II) and Fe(III) maps were used to evaluate the variability of the Fe(III)/Fe(total) ratio within each sample (i.e. at each stage of the culture): the Fe(II)-map was multiplied by the 4/5 correction factor (24) and added to the Fe(III)-map to obtain a Fe(total) map. The Fe(III)-map was subsequently divided by the Fe(total) map. A histogram of the resulting map was plotted, showing the number of pixels for each Fe(III)/Fe(total) ratio. This histogram allowed discriminating the major areas with different Fe redox states within the image. The mean Fe(III)/Fe(total) ratios were calculated as the maxima of each peak in the histogram and the variability as the width at mid-height of the peak.

Table 7.1: Fe(III)/total Fe quantification obtained from the fit of Fe $L_{2,3}$-edge XANES spectra[a]

culture time	Mean Fe(III)/total Fe	SD
3 h	0.39	0.006
4 days	0.66	0.005
7 days	0.84	0.005
11 days	0.84	0.004
15 days	1	–[b]

[a] Spectra were extracted from stacks on precipitates collected at different stages of SW2 culture. Fe(III)/total Fe values result from at least two spectrum fits. Standard deviations were calculated as the standard deviations of the fit to the data. SD, means of the standard deviations obtained for each fit.
[b] No standard deviation [reference Fe(III) end member]

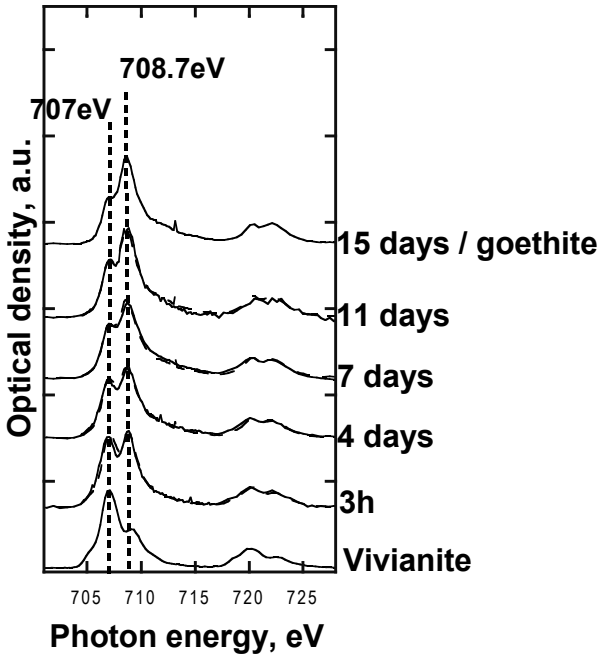

Figure 7.6: Evolution of iron redox state in SW2 cultures over time. Solid lines show the data and dashed lines the best fits of the Fe $L_{2,3}$-edges XANES spectra recorded on minerals formed in SW2 cultures over time. Numerical results of the best fits showing the progressive oxidation of Fe(II) to Fe(III) in SW2 cultures are displayed in Table 7.1. Spectra of 4 to 11 day old samples were fit with a linear combination of reference goethite (absorption maximum for Fe(III) at 708.7 eV) and vivianite (absorption maximum for Fe(II) at 707 eV). The spectrum of the sample collected after 3 h of culture was fit with a linear combination of reference Fe(III)-phosphate and vivianite.

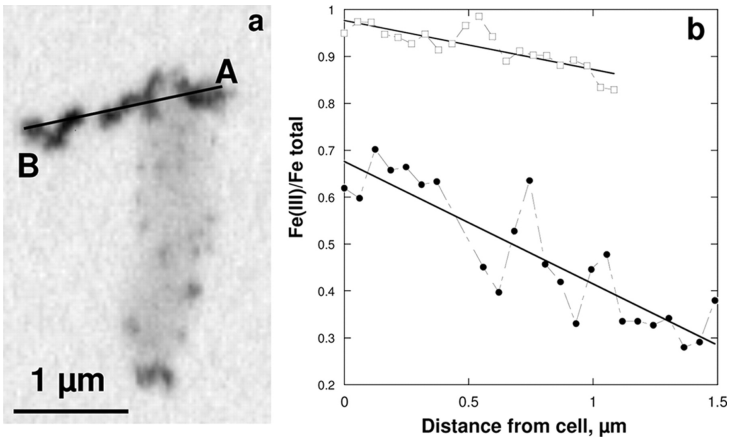

Figure 7.7: STXM observations of gradients of the iron oxidation state along mineralized fibers. (a) STXM image (absorption scale) taken at 702 eV (below the Fe L3-edge) and showing a bacterium and associated extracellular fiber after 5 h. (b) Fe(III)/total Fe ratios along the pole A-pole B profile displayed in panel a (•) and on a fiber from a 11 day old culture (□) and corresponding linear-curve fits (solid lines). A is the point closest to the pole, and B is the point closest to the tip of the fiber. Fe is more oxidized at the cell contact than at a distance from the cells, and the Fe oxidation state gradient is attenuated with time.

7.4 Discussion

Lipopolysaccharidic fibers act as a template for iron biomineralization. Iron biomineralization by the phototrophic SW2 strain occurs outside the cells (Kappler & Newman, 2004, Schaedler et al., 2009). The resulting Fe minerals are located mostly on extracellular fibers and partly as patches at the cell surface, but large areas are left uncovered Fig. 7.3. This pattern of extracellular iron mineralization differs from that produced by the anaerobic nitrate-reducing BoFeN1 strain, cultured in the same medium, but that was shown to mineralize iron within its periplasm (Miot et al., 2009b, Schaedler et al., 2009). In SW2 cultures, extracellular fibers emerging from the cells (Fig. 7.3A) show a XANES spectrum at the C K-edge similar to that of a mixture of partly unsaturated lipids and polysaccharides (Fig. 7.3). Processes of iron oxide particle assembly on organic carbon-containing fibrils have been widely described in the case of iron biomineralization in association with polysaccharides (Chan et al., 2004, Nesterova et al., 2003). It has been suggested that heterogeneous nucleation of iron oxides at the surface of and within exopolysaccharides proceeds through binding to functional groups (Nesterova et al., 2003). Such mechanisms could eventually lead to mineral-organic-compound assemblages with morphologies similar to those evidenced in SW2 cultures. Similar hypotheses can be driven for lipids. Indeed, it has been shown (Archibald & Mann, 1993) that precipitation of positively charged iron oxides at the surfaces of negatively charged lipid microstructures can lead to tubular organic-inorganic composites (Archibald & Mann, 1993). In particular, iron oxide (ferrihydrite, magnetite, lepidocrocite, or goethite) precipitation is activated by addition of low levels of sulfated derivatives on galactocerebroside microtubules that serve as a template for mineral assembly (Archibald & Mann, 1993). These sugar-based lipids exhibit a high negative charge that enhances the binding of cationic Fe(III) species by electrostatic attraction. These binding sites may thus serve as initial foci for mineral nucleation (Archibald & Mann, 1993). Fibers identified in SW2 cultures may exhibit different types of hydrophilic moieties that could bind Fe(III) (possibly phosphate, sulfate, and hydroxyl groups) and serve as templates for mineral nucleation. This could explain the organic-mineral assemblages of iron oxide nanoparticles clustered at the surface of the organic fibers that are observed in SW2 cultures. This hypothesis is further supported by the linear relationship between Fe and the organic C content on these mineralized fibers (Fig. 7.4). The following scenario for iron precipitation can thus be proposed. Fe is initially adsorbed onto the fibers proportionally to the amount of organic carbon (acting as binding ligands) present at the surface of the fibers. The linear relationship between Fe and C contents can be preserved after the nucleation step as long as the size of the minerals remains small, as observed in the present study. In contrast, crystal growth would increase the Fe/C ratio, leading in turn to a wide range of Fe concentrations at a given organic carbon concentration. Such a process might account for the presence of a few spots exhibiting a higher Fe content on the cells (Fig. 7.4B). As shown by Nesterova et al. (Nesterova et al., 2003), organic polymers can stabilize very small mineral particles and inhibit further growth.

The organic fibers that act as a template for iron biomineralization in SW2 cultures are elongated appendages (Fig. 7.3A). XANES spectroscopy suggests that a maximum of 3% in mass of total carbon may be accounted for by proteins in these fibers. In contrast to pili or flagella, which are composed mostly of proteins, fibers observed in SW2 cultures are composed mainly of lipids and polysaccharides. Further analyses will be required to elucidate the origin and the detailed biochemical composition and function of SW2 fibers.

Mineralized fibers exhibit a gradient of Fe oxidation state. The Fe minerals precipitated along the organic fibers record the redox conditions along a section across the microenvironment surrounding

SW2 cells. Fe(II) is progressively oxidized to Fe(III), resulting in the formation of nano-goethite in the latest stages (see 7.2), in agreement with the observations reported (Kappler & Newman, 2004). As observed (Kappler & Newman, 2004), at intermediate stages of SW2 cultures (less than 15 days), mixedvalence Fe minerals (see Fig. 7.6; table 7.1) might be more amorphous, before transforming into the crystalline end product (nano-goethite) (see Fig. 7.2) (Kappler & Newman, 2004). In the present study, a gradient of the Fe oxidation state was observed along these organic fibers, with more-oxidi zed iron minerals in close proximity to the cell and more-reduced iron minerals precipitating at a distance from the cell. Over time, as dissolved Fe(II) becomes completely oxidized, this redox gradient is attenuated and mostly Fe(III) minerals are observed attached to the organic fibers at a distance from the cells. Eventually, the biomineralization process leads to the precipitation of Fe(III)-containing minerals nucleated on the lipopolysaccharidic template. Further biochemical and structural analyses of the fibers produced in SW2 cultures will help in the future in elucidating these mechanisms of iron biomineralization. In particular, additional studies aimed at localizing the sites of iron oxidation, whether it occurs within the periplasm (Croal et al., 2007), at the cell surface (Hegler et al., 2008, Kappler & Newman, 2004, Miot et al., 2009a), or at the fiber surface, are needed.

Acknowledgement

We gratefully acknowledge the support of an ANR Jeunes Chercheurs Grant (J.M. and K.B.). CLS is supported by the NSERC, the CIHR, the NRC, and the University of Saskatchewan. The contributions from A.K., F.H., and S.S. were funded by an Emmy-Noether fellowship and, additionally, by the German Research Foundation (DFG) as well as by the University of Tuebingen (Promotionsverbund Bakterien-Material Interaktionen). We thank Emmanuelle Porcher (MNHN, Paris, France) for correlation analyses. The STXM measurements were performed at CLS, Saskatoon, Canada, and at SLS, Paul Scherrer Institut, Villigen, Switzerland. We thank Konstantine Kaznatcheev, Chithra Karunakaran, and Drew Bertwistle for their expert support of the STXM at CLS. We thank Joerg Raabe and George Tzvetkov for their expert support of the STXM at SLS. We also thank Olivier Beyssac and Sylvain Bernard (ENS, Paris, France) for their help in data collection at SLS. We acknowledge Claus Burkhardt from the NMI Reutlingen for his support in taking the SEM images. This is IPGP contribution 2536.

Bibliography

Archibald, DD & Mann, S: Template mineralization of self-assembled anisotropic lipid microstructures. *Nature*, 364:430–433, 1993.

Auffan, M; Achouak, W; Rose, J; Roncato, MA; Chaneac, C; Waite, DT; Masion, A; Woicik, JC; Wiesner, MR; & Bottero, JY: Relation between the redox state of iron-based nanoparticles and their cytotoxicity toward escherichia coli. *Environmental Science & Technology*, 42:6730–6735, 2008.

Benz, M; Brune, A; & Schink, B: Anaerobic and aerobic oxidation of ferrous iron at neutral pH by chemoheterotrophic nitrate-reducing bacteria. *Archives of Microbiology*, 169:159–165, 1998.

Bernard, S; Benzerara, K; Beyssac, O; Menguy, N; Guyot, F; Brown, G; & Goffé, B: Exceptional preservation of fossil plant spores in high-pressure metamorphic rocks. *Earth and Planetary Science Letters*, 262:257–272, 2007.

Chan, CS; de Stasio, G; Welch, SA; Girasole, M; Frazer, BH; Nesterova, MV; Fakra, S; & Banfield, JF: Microbial polysaccharides template assembly of nanocrystal fibers. *Science*, 303:1656–1658, 2004.

Croal, LR; Jiao, Y; & Newman, DK: The fox operon from *Rhodobacter* strain SW2 promotes phototrophic fe(II) oxidation in *Rhodobacter capsulatus* sb1003. *Journal of Bacteriology*, 189:1774–1782, 2007.

Dynes, JJ; Lawrence, JR; Korber, DR; Swerhone, GDW; Leppard, GG; & Hitchcock, AP: Quantitative mapping of chlorhexidine in natural river biofilms. *Science of the Total Environment*, 369:369–383, 2006.

Ehrenreich, A & Widdel, F: Anaerobic oxidation of ferrous iron by purple bacteria, a new type of phototrophic metabolism. *Applied and Environmental Microbiology*, 60:4517–4526, 1994.

Emerson, D & Revsbech, NP: Investigation of an iron-oxidizing microbial mat community located near Aarhus, Denmark: Field studies. *Applied and Environmental Microbiology*, 60:4022–4031, 1994.

Hallberg, R & Ferris, F: Biomineralization by *Gallionella*. *Geomicrobiology Journal*, 21:325–330, 2004.

Hegler, F; Posth, NR; Jiang, J; & Kappler, A: Physiology of phototrophic iron(II)-oxidizing bacteria – implications for modern and ancient environments. *FEMS Microbiology Ecology*, 66:250–260, 2008.

Heising, S & Schink, B: Phototrophic oxidation of ferrous iron by a *Rhodomicrobium vannielii* strain. *Microbiology*, 144:2263–2269, 1998.

Henke, BL; Gullikson, EM; & Davis, JC: X-ray interactions - photoabsorption, scattering, transmission, and reflection at e=50-30,000 ev, z=1-92. *Atomic Data and Nuclear Data Tables*, 54:181–342, 1993.

Hitchcock, AP: axis2000 - analysis of x-ray images and spectra. 2008.

Hitchcock, AP; Li, J; Reijerkerk, S; Foley, P; Stover, HDH; & Shirley, I: X-ray absorption spectroscopy of polyureas and polyurethanes and their use in characterizing chemical gradients in thin-walled polyurea capsules. *Journal of Electron Spectroscopy and Related Phenomena*, 156:Ciii–Civ, 2007.

Jiao, Y & Newman, DK: The pio operon is essential for phototrophic Fe(II) oxidation in rhodopseudomonas palustris tie-1. *Journal of Bacteriology*, 189:1765–1773, 2007.

Kappler, A & Newman, DK: Formation of Fe(III)-minerals by Fe(II)-oxidizing photoautotrophic bacteria. *Geochimica et Cosmochimica Acta*, 68:1217–1226, 2004.

Kappler, A; Schink, B; & Newman, DK: Fe(III) mineral formation and cell encrustation by the nitrate-dependent Fe(II)-oxidizer strain BoFeN 1. *Geobiology*, 3:235–245, 2005.

Kiernan, JA: Formaldehyde, formalin, paraformaldehyde and glutaraldehyde: What they are and what they do. *Microscopy today*, 8:8–12, 2000.

Miot, J; Benzerara, K; Morin, G; Bernard, S; Larquet, E; Ona-Nguema, G; Kappler, A; & Guyot, F: Transformation of vivianite by anaerobic nitrate-reducing iron-oxidizing bacteria. *Geobiology*, 7:373–384, 2009a.

Miot, J; Benzerara, K; Morin, G; Kappler, A; Bernard, S; Obst, M; Férard, C; Skouri-Panet, F; Guigner, JM; Posth, NR; Galvez, M; Brown, GE, JR.; & Guyot, F: Iron biomineralization by neutrophilic iron-oxidizing bacteria. *Geochimica et Cosmochimica Acta*, 73:696–711, 2009b.

Nesterova, M; Moreau, J; & Banfield, JF: Model biomimetic studies of templated growth and assembly of nanocrystalline feooh. *Geochimica et Cosmochimica Acta*, 67:1177–1187, 2003.

Schaedler, S; Burkhardt, C; Hegler, F; Straub, KL; Miot, J; Benzerara, K; & Kappler, A: Formation of cell-iron-mineral aggregates by phototrophic and nitrate reducing anaerobic Fe(II)-oxidizing bacteria. *Geomicrobiology Journal*, 26:93–103, 2009.

Schaedler, S; Burkhardt, C; & Kappler, A: Evaluation of electron microscopic sample preparation methods and imaging techniques for characterization of cell-mineral aggregates. *Geomicrobiology Journal*, 25:228–239, 2008.

Straub, KL; Benz, M; Schink, B; & Widdel, F: Anaerobic, nitrate-dependent microbial oxidation of ferrous iron. *Applied and Environmental Microbiology*, 62:1458–1460, 1996.

Straub, KL & Buchholz-Cleven, BEE: Enumeration and detection of anaerobic ferrous iron-oxidizing, nitrate-reducing bacteria from diverse european sediments. *Applied and Environmental Microbiology*, 64:4846–4856, 1998.

Viollier, E; Inglett, PW; Hunter, K; Roychoudhury, AN; & Van Cappellen, P: The ferrozine method revisited: Fe(II)/Fe(iii) determination in natural waters. *Applied Geochemistry*, 15:785–790, 2000.

Wan, J; Tyliszczak, T; & Tokunaga, TK: Organic carbon distribution, speciation, and elemental correlations within soil micro aggregates: Applications of stxm and nexafs spectroscopy. *Geochimica et Cosmochimica Acta*, 71:5439–5449, 2007.

Widdel, F; Schnell, S; Heising, S; Ehrenreich, A; Assmus, B; & Schink, B: Ferrous iron oxidation by anoxygenic phototrophic bacteria. *Nature*, 362:834–836, 1993.

8 Formation of Cell-Iron-Mineral Aggregates by Phototrophic and Nitrate-Reducing Anaerobic Fe(II)-Oxidizing

S. Schädler[1], C. Burkhardt[2], F. Hegler[1], K. L. Straub[1,3*], J. Miot[4], K. Benzerara[4], A. Kappler[1] **Geomicrobiology Journal, 26:93 – 103, 2009**

[1]Center for Applied Geoscience – Geomicrobiology, Eberhard Karls University Tübingen, Sigwartstrasse 10, 72076 Tuebingen, Germany
[2]Naturwissenschaftliches und Medizinisches Institut an der Universität Tübingen, Markwiesenstr. 55, 72770 Reutlingen, Germany
[3]current address: Department of Environmental Geosciences, University of Vienna, Althanstraße 14, 1090 Vienna, Austria
[4]Institut de Minéralogie et de Physique des Milieux Condensés, UMR 7590, CNRS, Universités Paris 6 et Paris 7, et IPGP, 140, rue de Lourmel, 75 015 Paris, France

8.1 Abstract

Microbial anaerobic Fe(II) oxidation at neutral pH produces poorly soluble Fe(III) which is expected to bind to cell surfaces causing cell encrustation and potentially impeding cell metabolism. The challenge for Fe(II)-oxidizing prokaryotes therefore is to avoid encrustation with Fe(III). Using different microscopic techniques we tracked Fe(III) minerals at the cell surface and within cells of phylogenetically distinct phototrophic and nitrate-reducing Fe(II)-oxidizing bacteria. While some strains successfully prevented encrustation others precipitated Fe(III) minerals at the cell surface and in the periplasm. Our results indicate differences in the cellular mechanisms of Fe(II) oxidation, transport of Fe(II)/Fe(III) ions, and Fe(III) mineral precipitation.

8.2 Introduction

Some prokaryotes have the ability to utilize iron as electron donor or electron acceptor for energy conservation in enzymatically catalyzed redox reactions (Ghiorse, 1984, Kappler & Straub, 2005, Weber et al., 2006, Ehrlich & Newman, 2009). Iron redox transformation significantly affects many other biogeochemical cycles (e.g. carbon, phosphorous, sulfur) and influences the mobilization, immobilization and transformation of organic and inorganic pollutants Stumm & Sulzberger (1992), Thamdrup (2000), Cornell & Schwertmann (2003), Neubauer et al. (2007).

The oxidation of Fe(II) by molecular oxygen is very slow at acidic pH but it can be catalyzed effectively by acidophilic microorganisms (Blake et al., 1993). At neutral pH, Fe(II) is oxidized by O2 within minutes

(Stumm & Morgan, 1995) and neutrophilic aerobic Fe(II)-oxidizers have to compete with this abiotic reaction (Emerson & Moyer, 1997). In anoxic environments, Fe(II) is relatively stable since neither nitrate nor sulfate react chemically with Fe(II) at appreciable rates at low temperature and only Mn(IV) and high concentrations of nitrite have been shown to be relevant chemical oxidants for Fe(II) (Buresh & Moraghan, 1976, Rakshit et al., 2008). Therefore, anaerobic Fe(II)-oxidizing microbes represent the most important catalysts for Fe(II) oxidation under anoxic conditions (Kappler & Straub, 2005).

Microorganisms catalyze the oxidation of Fe(II) under pH-neutral anoxic conditions either with light as energy source (Widdel et al., 1993) or with nitrate as electron acceptor (Straub et al., 1996) according to the following equations: Photosynthetic Fe(II) oxidation:

$$4\,Fe^{2+} + CO_2 + 11\,H_2O + h\nu \rightarrow {<}CH_2O{>} + 4\,Fe(OH)_3 + 8\,H^+ \tag{8.1}$$

Nitrate-dependent Fe(II) oxidation:

$$10\,Fe^{2+} + 2\,NO_3^- + 24\,H_2O + 10\,Fe(OH)_3 + N_2 + 18\,H^+ \rightarrow < CH2O > +4\,Fe(OH)_3 + 8\,H^+ \tag{8.2}$$

where $<CH_2O>$ is an approximate formula of biomass. At circumneutral pH, both aerobic and anaerobic iron oxidizers face the problem of very poor solubility of one end product of their metabolism, i.e., Fe(III), with concentrations of dissolved Fe(III) in the nM to μM range (Stumm & Morgan, 1995).

At neutral pH, ferric iron (hydr)oxides are expected to precipitate more or less instantly as Fe(III) is formed due to its low solubility under these conditions. This precipitation depends on the geochemical conditions and Fe(III) concentrations and in many cases it occurs even directly where the Fe(III) is formed (i.e., likely on a membrane). Furthermore, the formed particles are positively charged due to their high points of net zero charge (ZPC): e.g., pH 7.9 for ferrihydrite, pH 9.0 - 9.4 for goethite (Schwertmann & Cornell, 2000) (7.5 - 9.5 depending on the literature), and pH 8.5 for hematite (Jeon et al., 2004). If present in the proximity of cells, Fe(III) ions, Fe(III) colloids and Fe(III) minerals would therefore be expected to adsorb to prokaryotic cell surfaces that are in general negatively charged due to a high content of carboxylic, phosphoryl and/or hydroxyl groups. Formation of mineral crusts would potentially limit the diffusion of substrates and nutrients to the cell, impair uptake of these compounds across the membrane, and as a consequence lead to the stagnation of cell metabolism and eventually to cell death.

For stalk-or sheath-forming aerobic Fe(II)-oxidizing bacteria of the genera *Gallionella* and *Leptothrix* it was suggested that microbially produced and excreted organic matrices are used for extra-cellular capture of Fe(III) minerals produced during aerobic Fe(II) oxidation (Hanert, 2006, Emerson & Revsbech, 1994). It has to be kept in mind that Fe(II) oxidation by *Leptothrix* is not associated with energy production and the site of Fe(II) oxidation therefore may be determined not by the need to produce maximum energy, but rather by the need to deposit Fe(III) in a particular location (i.e., sheath) or by the properties of the sheath itself. Nevertheless, the following questions remain unanswered: i) where the Fe(II) is oxidized (in the cytoplasm, in the periplasm or at the cell surface) and, ii) in the case of intracellular oxidation, how the Fe(III) is transported from the cytoplasm to the cell surface and the organic templates.

Even less is known about the mechanisms of Fe(II) oxidation in neutrophilic anaerobic Fe(II)-oxidizing bacteria. In particular it is unknown how those species avoid encrustation of the cell surface with the Fe(III) minerals that they produce. It was suggested that phototrophic Fe(II)-oxidizing bacteria oxidize Fe(II) at the cell surface (Kappler & Newman, 2004), posing questions of how the electrons are then transported from the outside to the inside of the cell and why the positively charged Fe(III) does not bind to the

negatively charged cell surface. Recently it was proposed that Fe(II) oxidation by the photoautotrophic strains *Rhodobacter ferrooxidans* strain SW2 and *Rhodopseudomonas palustris* strain TIE-1, happens in the periplasm of the cells (Croal et al., 2007, Jiao & Newman, 2007). Since cell en-crustation was observed for neither of the strains (Kappler & Newman, 2004, Jiao et al., 2005), this raises the question how Fe(III) is transported to the cell exterior and then away from the cells following periplasmic Fe(II) oxidation. The possibility of a pH microenvironment was suggested for strain SW2 (Kappler & Newman, 2004) and neutrophilic aerobic Fe(II)-oxidizers (Sobolev & Roden, 2001). A lower pH would potentially keep the Fe(III) in solution in close cell proximity and lead to controlled Fe(III)mineral precipitation at a certain distance from the cell surface. Alternatively, the use of organic ligands as complexing and solubilization agents has been suggested (Croal et al., 2004), although no evidence for such molecules has yet been found. In summary, presently it is not known where Fe(II) oxidation takes place in neutrophilic Fe(II) oxidizers (at the surface of the outer membrane, in the periplasm or even in the cytoplasm).

In order to identify the Fe(II) oxidation and Fe-transport mechanisms of neutrophilic anaerobic Fe(II)-oxidizing bacteria, it is necessary to evaluate whether various Fe(II)-oxidizing strains show differences in the localization of Fe(II) oxidation sites, in transport of Fe(II) and Fe(III) ions, and in Fe(III) mineral precipitation. In this study, we characterized cell-mineral aggregates formed by phototrophic and nitrate-reducing anaerobic Fe(II)-oxidizing bacteria using different microscopic techniques. In particular, the objective of this work was to determine the spatial allocation of Fe(III) minerals relative to the cells that produced these minerals.

8.3 Methods and materials

8.3.1 Bacterial cultures

The following anoxygenic phototrophic Fe(II)-oxidizing cultures from our own culture collection including representatives from the phylum *Proteobacteria* and from the phylum *Chlorobi* were used: the purple sulfur bacterium (PSB) *Thiodictyon* sp. strain F4, a highly enriched culture (Croal et al., 2004), the green sulfur bacterium (GSB) *Chlorobium ferrooxidans* sp. strain KoFox, growing in a defined coculture with *Geospirillum* KoFum sp. (Heising et al., 1999), and the purple non-sulfur bacterium (PNSB) *"Rhodobacter ferrooxidans"* strain SW2 (Ehrenreich & Widdel, 1994). In addition to these phototrophic strains, we chose a lithotrophic nitrate-reducing Fe(II)-oxidizing enrichment culture (Straub et al., 1996) and *Acidovorax* sp. strain BoFeN1, a mixotrophic nitrate-reducing Fe(II)-oxidizing strain (Kappler et al., 2005) for our experiments. By this selection we cover both nitrate-reducing and phototrophic Fe(II)-oxidizing bacteria including autotrophic and mixotrophic strains from different phylogenetic groups.

8.3.2 Growth Medium and Cultivation Conditions

Bacteria were cultivated in freshwater mineral medium with Fe(II), hydrogen, or acetate as electron donor at pH 6.8.7.0, as described previously (Straub et al., 1996, Kappler & Newman, 2004, Hegler et al., 2008). Phototrophic Fe(II)-oxidizing cultures were incubated at 20 °C and light saturation (>700 lux). Nitratereducing Fe(II)-oxidizing bacteria were incubated at 28 °C in the dark. Fe(II) oxidation was followed by quantification of remaining Fe(II) in the cultures by a spectrophotometric test with ferrozine as described previously (Kappler & Newman, 2004).

8.3.3 Sampling and Sample Preparation for Light and Electron Microscopy

Samples were taken at the late exponential growth phase when Fe(II) was almost completely oxidized. For light and scanning electron microscopy (SEM), 1 mL of a culture was taken with sterile syringes that had been flushed with N_2 / CO_2. Light microscopy images of the samples were taken with a Zeiss AxioVison microscope equipped with an oil immersion object lens. For SEM, samples were chemically fixed using a half-strength Karnovsky solution (Kiernan, 2000), placed on holey carbon-coated EM-copper-grids, dehydrated in subsequent steps with an increasing concentration of isopropanol, and finally dried in the Critical Point Dryer Bal-Tec CPD030, as previously described (Schaedler et al., 2008). Dried samples were mounted on aluminum stubs using double-sided carbon tape. For enhanced electrical conductivity, the edges of the EM grids were painted with conductive silver paste. Samples that showed strong surface charging were coated in a Balzers sputter coater SCD 40 (Bal-Tec, Balzers, Liechtenstein) with a thin layer of Au/Pd (90%/10% w/w). The coating thickness was approximately 20 nm (determined in focused ion beam cross-sections and by a surface texture analyzer; results not shown).

For transmission electron microscopy (TEM), cells were fixed for at least 2 hours in 1 to 3% (v/v) glutaraldehyde at 4 °C, centrifuged for a few minutes at 6500 rpm and subsequently washed 3 times in distilled water or sodium cacodylate buffer (pH 7.2).

8.3.4 Electron Microscopy Techniques

Scanning Electron Microscopy

Imaging was performed with a Zeiss Gemini 1550VP FE-SEM, a Zeiss Gemini 1540XB FIB/FE-SEM, and a Zeiss Ultra 55, SEM-FEG microscope. A dual-beam focused ion beam (FIB) mounted on a Zeiss Gemini 1540XB was used for simultaneous milling and imaging at a working distance (SEM) of approx. 5 mm. Both microscopes were equipped with Everhart-Thornley SE detectors and in-lens detectors and were optimized to a lens aperture of 30 μm. Images were recorded in a format of 1024 × 768 pixels, at integration times between 15 μs and 45 μs per pixel.

Transmission Electron Microscopy and Scanning Transmission Electron Microscopy.

For transmission electron microscopy, one half of each sample was stained in either 1% or 2% osmium tetroxide for at least 90 min and rinsed 3 times in distilled water. Stained and unstained samples were then dehydrated in increasing concentrations of either acetone or graded ethanol and propylene oxide-1,2 and embedded in epoxy resin. After 24 h at 60 μs, samples were cut on aMT-X Ultramicrotome or a LEICA ultramicrotome (EM-UC6) with a 55° Diatome diamond knife to a 60 or 70 nm thickness. Ultrathin sections were placed on 200 mesh copper grids.

The prestained samples were subsequently poststained with 2% uranyl acetate for 5 min and lead citrate (2 g L^{-1}) for 7 min before final imaging. An Akashi EM-002B microscope operating at 100 kV was used for microscopy and energydispersive X-ray spectroscopy EDS. The area sampled by the Oxford spectrum analyzer is approximately 8.8 nm at 83 kV. Acquisition rates were maintained at 10 - 20% dead time with 60 s live time. The electron beam was defocused at the condenser lens to maintain counting rates below 1 kHz and live time efficiency >95%. The EDS patterns were recorded on an INCA 3.04 Microanalysis Suite and digitized for analysis.

For scanning transmission electron microscopy (STEM), whole cells were deposited on a carbon-coated 200-mesh copper grid after two rinsing steps in degassed distilled water in an anoxic glove-box. STEM

observations were performed with a JEOL2100 Microscope at IMPMC operating at 200 kV in darkfield (DF) mode.

8.4 Results

8.4.1 Association of Fe(II)-Oxidizing Cells with Fe(III) Minerals – Observations Using Light Microscopy

Light microscopy was performed in order to get a first overviewof the spatial relation between cells and mineral phases in the cultures (figure 8.1). This inspection showed clear differences between the arrangements of cells with respect to iron mineral precipitates for the different strains investigated in this study. Only cells of the mixotrophic nitrate-reducing Fe(II)-oxidizing strain BoFeN1 (figure 8.1 a) were mainly observed in association with iron precipitates. In cultures of all other Fe(II)-oxidizing strains – including the lithotrophic nitrate-reducing enrichment culture – most cells were not associated with iron precipitates (figures 8.1 b, c, d).

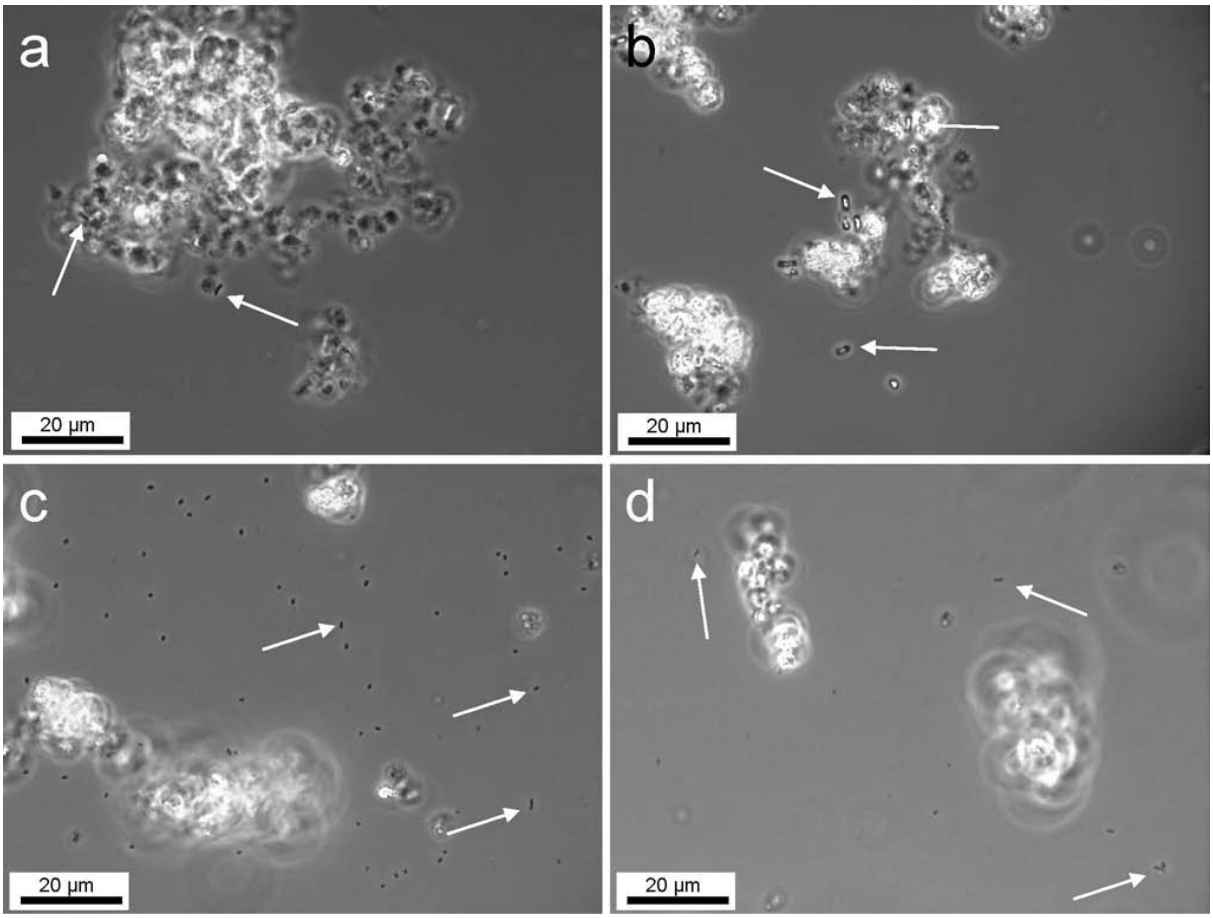

Figure 8.1: Light microscopy images showing iron precipitates and cells (arrows) in cultures of Acidovorax sp. strain BoFeN1(a), *Thiodictyon* sp. strain F4 (b), *Chlorobium ferrooxidans* strain KoFox (c), and *"Rhodobacter ferrooxidans"* strain SW2 (d).

8.4.2 Localization of Fe(III) Minerals – Visualization by Scanning Electron Microscopy

As compared to light microscopy, the higher resolution of scanning electronmicroscopy (SEM) allows amore detailed survey of cell surfaces and cell-mineral associations. Scanning electron micrographs of the mixotrophic anaerobic Fe(II)-oxidizing nitrate-reducing bacterium Acidovorax sp. strain BoFeN1, cultured in the presence of acetate and dissolved Fe(II), showed cell surfaces partly or entirely covered by globular iron mineral particles (figures 8.2 a, b). Cells that were covered to a different extent with iron globules of varying size (up to 150 nm)probably represented different growth stages of cells. Similarly shaped but smaller sized globular particles were described on coated SEM samples and attributed to sputter coating artefacts (Folk & Lynch, 1997). Besides the different size of our structures compared to these sputtering artefacts, our observations of these particles were confirmed by transmission electron micrographs of uncoated samples, and neither the varying globule sizes nor the different extent of the encrustation can be explained by such artefacts.

In contrast, cells from the lithotrophic nitrate-reducing Fe(II)-oxidizing enrichment culture (figures 8.3 a, b) and cells of the Fe(II)-oxidizing phototrophs *Chlorobium ferrooxidans* strain KoFox (Figures 8.3 c, d) and *Thiodictyon* strain F4 (figure 8.3 e) to a large extent remained free of iron particles. The wrinkled cell surfaces of *Thiodictyon* strain F4 cells generally remained completely free of iron particles in all samples. Planktonic cells were observed, as were cells loosely associated with iron precipitates (figure 8.3 e). In cultures of *Rhodobacter* strain SW2, iron minerals were often observed along filamentous structures, which seemed to originate from the cell poles (figure 8.3 f). Sporadically SW2 cell surfaces were partially covered with iron particles (figures 8.3 g, h). When present at the surface of SW2 cells, the Fe(III) minerals seemed to develop at the cell poles first (figures 8.3 g, h).

In the coculture of *Chlorobium ferrooxidans* with *Geospirillum* sp. KoFum, we observed a significant difference: The surfaces of the Fe(II)-oxidizing *Chlorobium ferrooxidans* cells remained largely free of iron particles, with the exception of sparse, flat mineral particles that we will refer to as patches. In contrast, cell surfaces of *Geospirillum* sp. KoFum were observed to have a thin crust of globular particles with diameters in the order of several tens and up to one hundred nanometres (figures 8.3 c, d). Clearly, in this coculture only the Fe(II)-oxidizing strain was able to avoid encrustation.

8.4.3 Analysis of the Interior of Bulk Cell-Mineral Aggregates Using a Focused Ion Beam

Milling into bulk cell-mineral aggregates with a focused ion beam (FIB) creates cross-sections that allow for an insight into cell-mineral-aggregates. Bulky mineral structures from all phototrophic cultures and the lithotrophic nitrate-reducing enrichment culture were free of encrusted cells (data not shown). This indicates that none of the cells of these cultures became completely encrusted in iron minerals or deeply embedded in mineral structures. In contrast, the mixotrophic Fe(II)-oxidizing nitrate-reducing *Acidovorax* sp. strain BoFeN1 showed a range of slightly encrusted to heavily encrusted cells (figures 8.2 a, b). The images suggest that cell encrustation started by the formation of few small iron globules (figure 8.2 c), which grew during the course of Fe(II) oxidation ((figures 8.2 d) and finally covered the complete cell surface (figure 8.2 e).

8.4.4 Observation of Cell Internal Structures by (Scanning) Transmission Electron Microscopy

Transmission electron microscopy (TEM) and scanning transmission electron microscopy (STEM) on ultramicrotomy sections revealed details from the cell interior as well as from the cell-mineral interface.

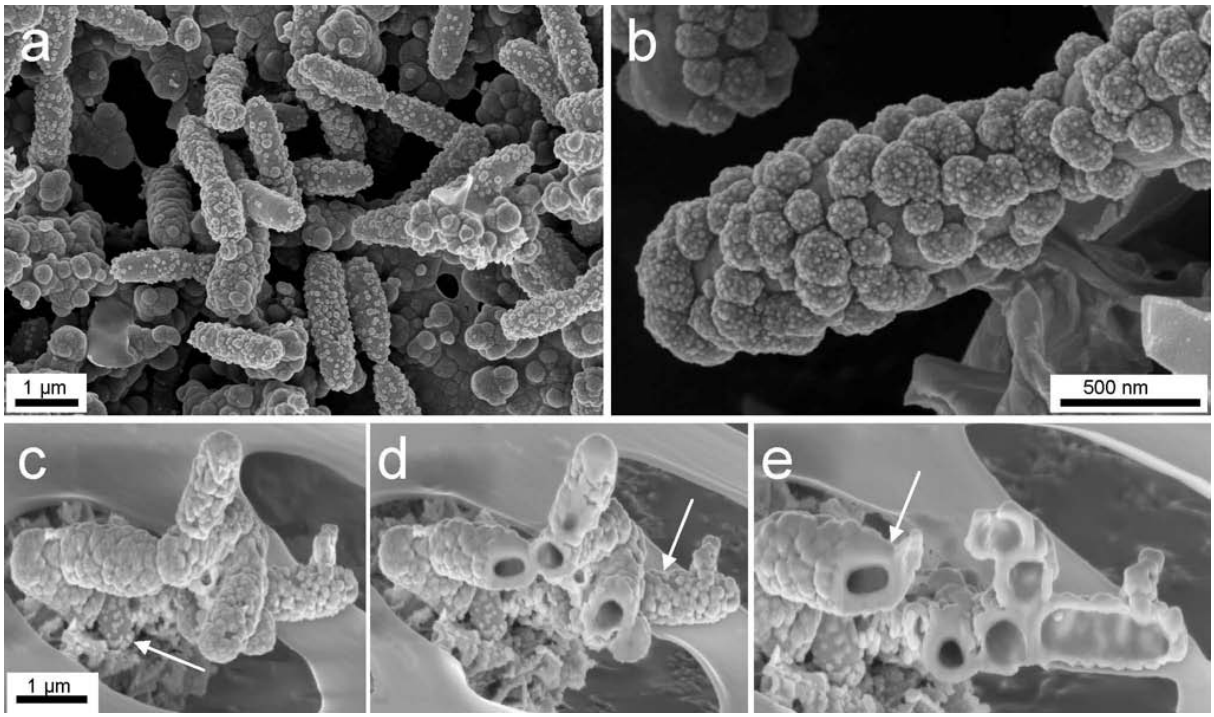

Figure 8.2: Scanning electron micrographs of cells of the nitrate-reducing Fe(II)-oxidizing bacterium *Acidovorax* sp. strain BoFeN1 grown in the presence of Fe(II) (a - c). Images (d, e) show the same cells as (c) after milling with a focused ion beam (FIB). Different stages of encrustation can be observed from almost uncovered cells (c, arrow), partially covered cells (d, arrow), to completely covered cells (e, arrow). FIB milling current 10 pA, images taken using in-lens detectors, acceleration voltage 3 kV. Imaging quality in Figures (c-e) suffers from the ion milling process.

We observed that *Acidovorax* sp. strain BoFeN1 cells contained iron minerals in the periplasm (figures 8.4 a-c, figure 8.5). The thickness of the periplasmic mineral layer is approximately 30-40 nm (figure 8.4 a, figure 8.5). The variations in thickness of the crust may be caused by the compression of samples during the preparation of thin sections; however, in particular the mineral layers at the pole regions appear to be thicker than along the cell body. The thicknesses of the two cell poles vary as well, which cannot be explained by preparation artefacts. Additionally, the presence of globular particles on the surface of the cells as previously observed in scanning electron microscopy was confirmed (figure 8.4 d, figure 8.5).

In contrast, the periplasm of *Rhodobacter* sp. strain SW2 cells did not show any electron dense particles (figures 8.4 e-f), suggesting that the periplasm is free of mineral phases. The iron minerals present in cultures of *Rhodobacter* sp. strain SW2 have a fluffy and poorly crystalline appearance with μm sized primary particles that were rather loosely attached to or associated with the cell surfaces.

8.5 Discussion

Neutrophilic Fe(II)-oxidizing bacteria face the problem of a poorly soluble metabolic end product, i.e., Fe(III). As a first step towards understanding the mechanisms of Fe(II) oxidation, Fe(III) transport, Fe(III) release, and iron mineralization, we investigated cell-mineral aggregates and localized Fe(III)

minerals in the cells and at the cell surface. The responses of diverse strains of anerobic Fe(II)-oxidizing bacteria to the iron minerals they produce during growth were documented.

8.5.1 Cell-Mineral Aggregate Formation and Cell Encrustation

Our results give a first detailed overview of the spatial localization of iron oxides that were produced by 5 phylogenetically distinct cultures of anaerobic Fe(II)-oxidizing bacteria. The response of the cultures to ferric iron can be differentiated into non-encrustation and encrustation. Our study revealed non-encrusting Fe(II)-oxidizing cells in a lithotrophic nitratereducing enrichment culture and in phototrophic cultures of *"Rhodobacter ferrooxidans"* strain SW2, *Chlorobium ferrooxidans* strain KoFox, and *Thiodictyon* sp. strain F4. The surfaces of non-encrusting cells usually remained free of iron minerals with the minerals either loosely attached to the cells or localized at some distance. We observed cells encrusted with ferric iron minerals only in the culture of the nitrate-reducing *Acidovorax* sp. strain BoFeN1.

Similarly, cells of the phototroph *Rhodomicrobium vannielii* strain BS-1 were described in an earlier study to encrust heavily with ferric iron minerals when the culture was grown in the presence of Fe(II) (Heising & Schink, 1998). These contrasting observations suggest that fundamentally different Fe(II) oxidation and Fe(II)/Fe(III) transportmechanisms are present in non-encrusting and encrusting anaerobic Fe(II)-oxidizing bacteria. Furthermore, these differences cannot be related to a type of energy metabolism, i.e., respiration or photosynthesis.

The cell appendices observed in some samples of *"Rhodobacter ferrooxidans"* strain SW2 suggest that these cells excrete a fibrous extracellular material on which iron precipitates, possibly similar to *Gallionella* spp. cells that have been reported to produce extracellular organic fibers, forming twisted stalks and acting as a precipitation template for iron oxides (Emerson & Revsbech, 1994, Hallberg & Ferris, 2004).

Alternatively, it can be speculated that these extracellular fibres produced by strain SW2 could be involved in electron transfer to the cells in a similar way as described recently for the conductive pili in Fe(III)-reducing microorganisms (Gorby et al., 2006, Reguera et al., 2005): whereas the Fe-reducers putatively use the pili to transport electrons from the cells to the solid-phase electron acceptors (Fe(III) minerals), the Fe(II)-oxidizers could transport electrons from Fe(II) that sorbs to the organic structures to the cells. This would oxidize the Fe(II) to Fe(III) followed by Fe(III) mineral precipitation at the organic structures, thus preventing cell encrustation. Chan et al. (2004) suggested that the similar biologically produced filament structures that they observed, may serve as a precipitation template for mineralization of oxyhydroxides during microbial ferrous iron oxidation. These researchers also discussed the potential benefits of an increased pH gradient across the cell membrane (i.e., up to 4 H+ per ferrous iron oxidized when goethite is formed), which may also be generated and harvested by SW2 cells.

In cocultures of the phototrophic Fe(II)-oxidizing *Chlorobium ferrooxidans* strain KoFox with *Geospirillum* sp. KoFum, only cells of strain KoFum were covered by iron minerals. Small patches of iron minerals at the surface of KoFox cells imply that these cells may produce extracellular precipitation templates (e.g., exopolysaccharides) at their cell surface – which they would need to shed after a certain time – and thus act similarly to the sheath-forming bacterium Leptothrix ochracea that uses an exopolysaccharide slime layer on which minerals are precipitated (Emerson & Revsbech, 1994). Cells of strain KoFum were unable to oxidize ferrous iron (Heising et al., 1999). Hence, KoFum cells cannot encrust intracellularly, but the cell surfaces seemed to act as a passive template for iron biomineralization. The fact that the Fe(II)-oxidizing KoFox cells were not encrusted, but the co-cultureKoFum cells were, potentially rules out a ligand-complexation-driven mechanism to avoid precipitation by the KoFox strain: In the presence

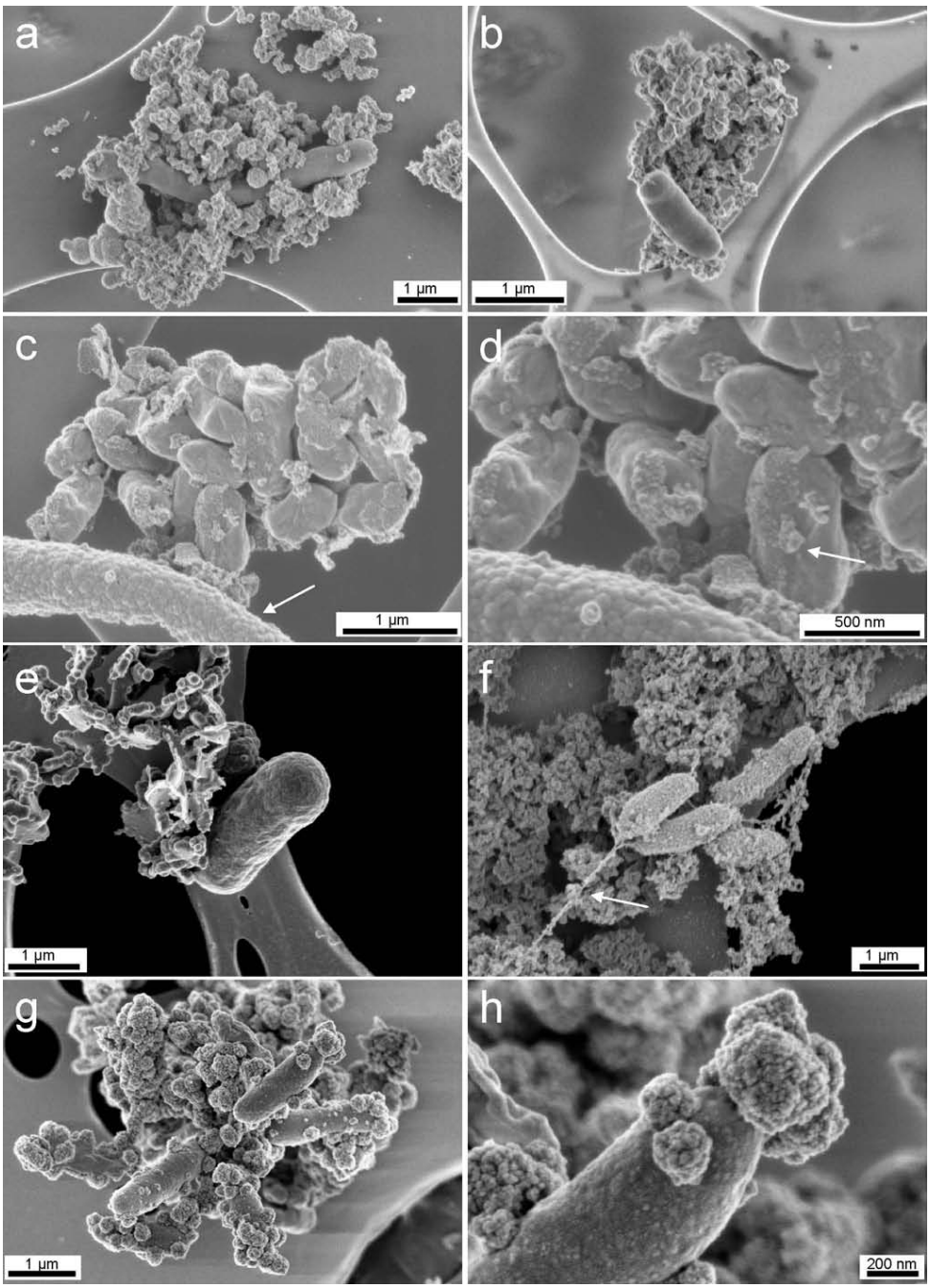

Figure 8.3: Scanning electron micrographs of anaerobic Fe(II)-oxidizing cultures with non-encrusted, different-sized cells of the lithotrophic nitrate-reducing enrichment culture (a, b) and non-encrusted *Chlorobium ferrooxidans* strain KoFox cells with encrusted coculture strain *Geospirillum* sp. strain KoFum (arrow) (c, d). Fig. (d) is a close-up of (c) with focus on iron mineral patches on the cell surface of *Chlorobium ferrooxidans* (arrow). (e) Non-encrusted *Thiodictyon* sp. strain F4. (f) *"Rhodobacter ferrooxidans"* strain SW2 cells (non-encrusted) with filamentous structure (arrow) as well as the rare case of a partly mineral-covered cell surface (g, h). All images taken with in-lens detectors at acceleration voltages of 4 kV (a, b) 1 kV (c, d, f), or 2 kV (e, g, h).

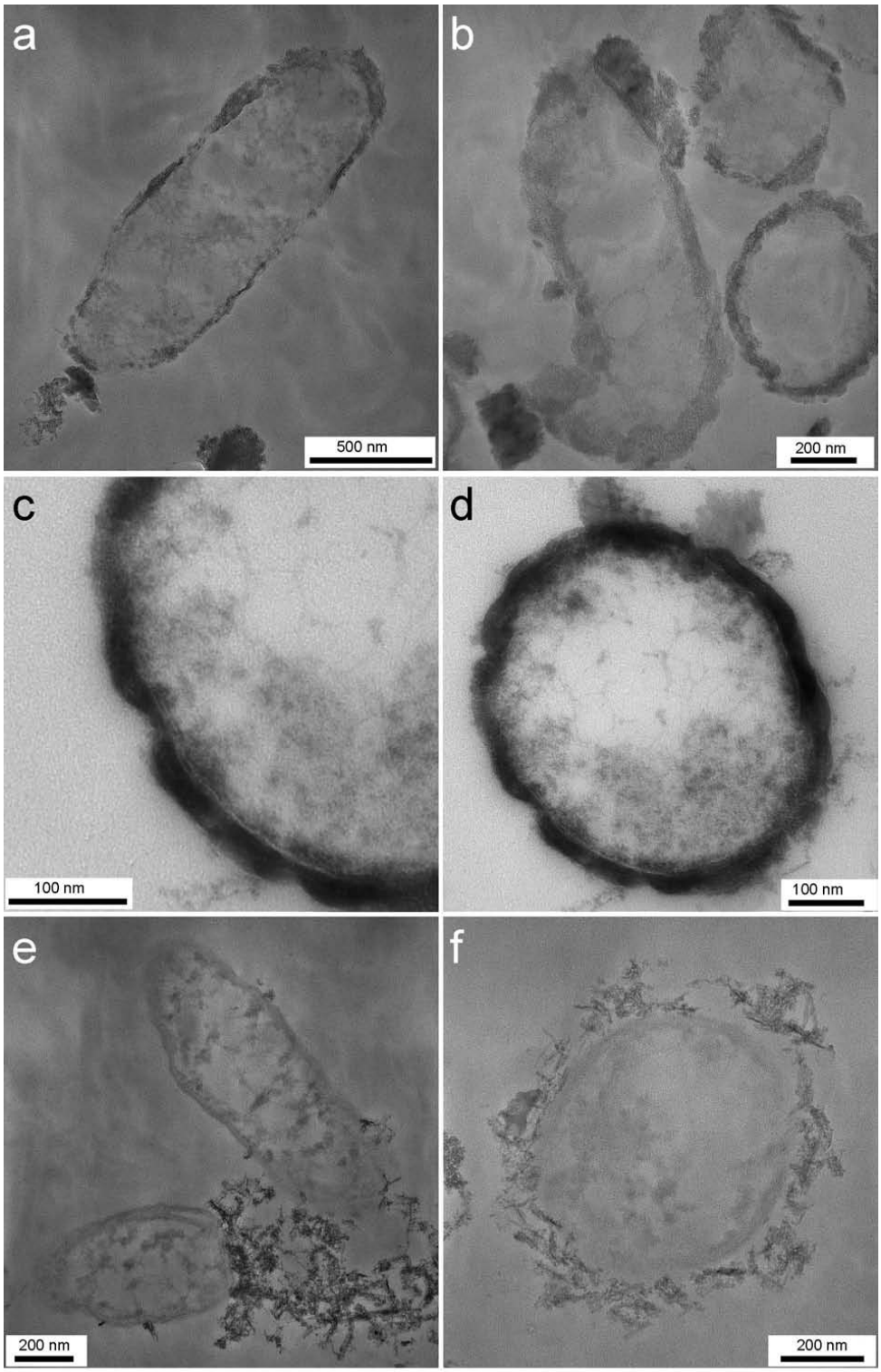

Figure 8.4: Transmission electron micrographs of the nitrate-reducing Fe(II)-oxidizing bacterium *Acidovorax* sp. strain BoFeN1 grown in the presence of Fe(II) (a, b, c, d) showing encrustation of the cell surface and mineral precipitation in the periplasm. In contrast, cells of the phototrophic Fe(II)-oxidizing bacterium *"Rhodobacter ferrooxidans"* strain SW2 (e, f) show no encrustation, but a lose association with mineral particles. Stained samples.

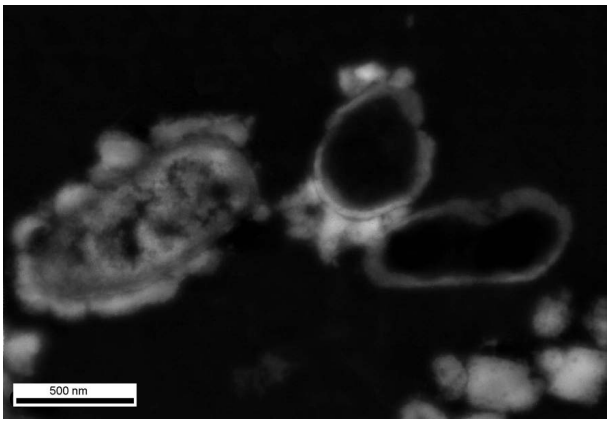

Figure 8.5: Scanning transmission electron micrographs of cells of the nitrate-reducing Fe(II)-oxidizing bacterium *Acidovorax* sp. strain BoFeN1. Bright regions indicate the presence of Fe(III) in the periplasm and at the cell surface.

of Fe(III)-solubilizing ligands encrustation would be expected for neither of the strains present in the culture, assuming similar cell-surface properties.

In cultures of the *Thiodictyon* sp. strain F4, the cells were free of minerals and no Fe(III) precipitation was observed on the cells or on cell appendices. It is evident that these cells manage to precipitate Fe(III) minerals at a certain distance of the cell surface; although the way in which they do is presently unclear. A pH microenvironment keeping the Fe(III) in solution in close cell vicinity, in combination with exopolymers at which the Fe(III) then nucleates and precipitates, could be a potential mechanism (see later).

In contrast to these non-encrusting phototrophic Fe(II)-oxidizers, cells of the encrusting strain BoFeN1 appeared with iron-containing precipitates (possibly Fe(III) (hydr)oxides or Fe(III) phosphates) within the periplasm, as well as a cover of iron-containing globules on the surface. This appearance was similar to what was reported by Emerson & Moyer (1997) for the two neutrophilic Fe(II)-oxidizing strains ES-1 and ES-2. Similar precipitation within the periplasm has been previously observed for other microbial systems such as calcifying bacteria (e.g. Benzerara et al., 2004a,b). However, the replacement of $FeCl_2$ by $CaCl_2$ in the culture medium of BoFeN1 did not lead to calcification (data not shown). These results suggest that the precipitation of Fe minerals in the periplasm is not due to preferential binding of positively charged ions (Ca^2+ or Fe^2+) to the peptidoglycan or other biopolymers within the periplasm but rather due to oxidation of the Fe(II) with concomitant Fe(III) mineral precipitation.

In very few experiments, cells of SW2 cultures showed precipitation of Fe(III) minerals at the cell surface. It seemed that this mineral precipitation starts at the cell poles rather than the cell body. Likewise, the cell poles of BoFeN1 cells also often appeared more densely covered or more closely attached to Fe(III) precipitates and showed a thicker precipitate layer within the periplasm. Several hypotheses can be formulated, meriting further investigations: (1) The cell pole region is better accessible to diffusion of dissolved Fe(II) to and possibly into the cell; (2) It is plausible that the geometry of the spherical poles that yields to a lower surface/volume ratio as compared to the cylindrical cell body could possibly increase the surface charge density at the cell poles and may lead to preferential interaction with the positively charged Fe(III) phases (Shapiro et al., 2002). (3) Finally, it could be related to the older age of one of the poles in a bacterial cell and/or the concomitant higher accumulation of proteins within this

pole that may play a role in periplasmic iron precipitation.

8.5.2 Mechanisms of Fe(II) Oxidation and Fe(III) Transport and Mineralization

Based on our observations, we suggest that different strains use different oxidation and iron transport mechanisms, which lead to the various interactions between iron minerals and the cells. Figure 8.6 1 shows different possibilities of how and where Fe(II) could be oxidized by the cells: dissolved Fe(II) diffuses to the cell surface where it can either be taken up into the periplasm (by diffusive uptake or a transport mechanism, figure 8.6 1a) or bind to the cell surface (figure 8.6 1b). In both cases it will be oxidized by an iron oxidase protein that is located either in the periplasm or at the cell surface respectively. A comparison to manganese-oxidizing bacteria shows that potential candidates for this protein are multi-copper oxidase (MCO)-like enzymes – suggested to be the mechanism of Mn(II) oxidation at bacterial surfaces by Tebo et al. (2004). A c-type cytochrome was suggested as another possibility to be the Fe(II) oxidoreductase in *"Rhodobacter ferrooxidans"* strain SW2 cells, most likely functioning in the cells' periplasm (Croal et al., 2007).

In the case of the Fe(II) oxidase being located in the periplasm, the poorly soluble Fe(III) produced can either leave the cell via an Fe(III) transport system and adsorb to the cell surface, or precipitate directly in the periplasm (figure 8.6 1a). Strains which do not show encrustation obviously have a mechanism to maintain the Fe(III) produced during their metabolism in solution and to displace the position of precipitation of iron(hydr)oxides to a point distant from the cell's surface. Figure 8.6 sums up possible mechanisms. As suggested by (Kappler & Newman, 2004), organic ligands could form a dissolved Fe(III) complex, keeping the Fe(III) in solution, as depicted in figure 8.6 part 2. Alternatively, soluble colloidal Fe(III) species could be produced by the cells (Sobolev & Roden, 2001).

A slightly acidic cell pH microenvironment (Figure 6.2b) was suggested to be generated by the protonmotive force (PMF) (Urrutia Mera et al., 1992). As a consequence of proton pumping, the pH in the cell wall of an actively metabolizing cell in a neutral bulk solution can decrease to pH values below 6 (Johnson et al., 2007). This would increase the solubility of Fe(III) and keep it in solution. As the Fe(III) diffuses away from the cell and thus towards a neutral pH where its solubility decreases, it meets a precipitation nucleus and forms a solid phase. Preventing cell-surface encrustation by diffusion of the positively charged Fe(III) away from the cell could be enhanced by a positively charged cell surface (figure 8.6 part 2c). In these cases (presence of a pH micro-environment, a charged cell surface, or a combination of the two), exopolysaccharides could act as Fe(III) precipitation template (Chan et al., 2004). An exopolymer more negatively charged than the cell surface would be an explanation for precipitation distant to the cell.

8.5.3 Implications of Iron Biomineralization on Biosignature Formation

Several previous studies have looked for traces of Fe(II)-oxidizing bacteria in the geological record and in modern environments (e.g. Ghiorse, 1984, Little et al., 2004, Ivarsson et al., 2008). However, the products and potential biosignatures left by bacteria with such a metabolism have until now been studied for only very few genera, such as *Gallionella* or *Leptothrix* (e.g. Hallberg & Ferris, 2004, Fortin & Langley, 2005). Consequently, our knowledge of the diversity of the biomineralization patterns that can potentially be observed is restricted. Although it is difficult here to presume what can be preserved after diagenesis and metamorphism, the present study offers some clues on the possible fossils that form during biomineralization by Fe(II)-oxidizing bacteria. It clearly shows that a significant diversity of biominerals

exists, although all these strains grow in very similar culture media. Some bacteria can be fossilized as mineral shells corresponding to whole cells (e.g., BoFeN1) with preservation of their morphology and size due to the precipitation of minerals in their periplasm. SW2 cells can form small filamentous mineral structures that resemble pili.

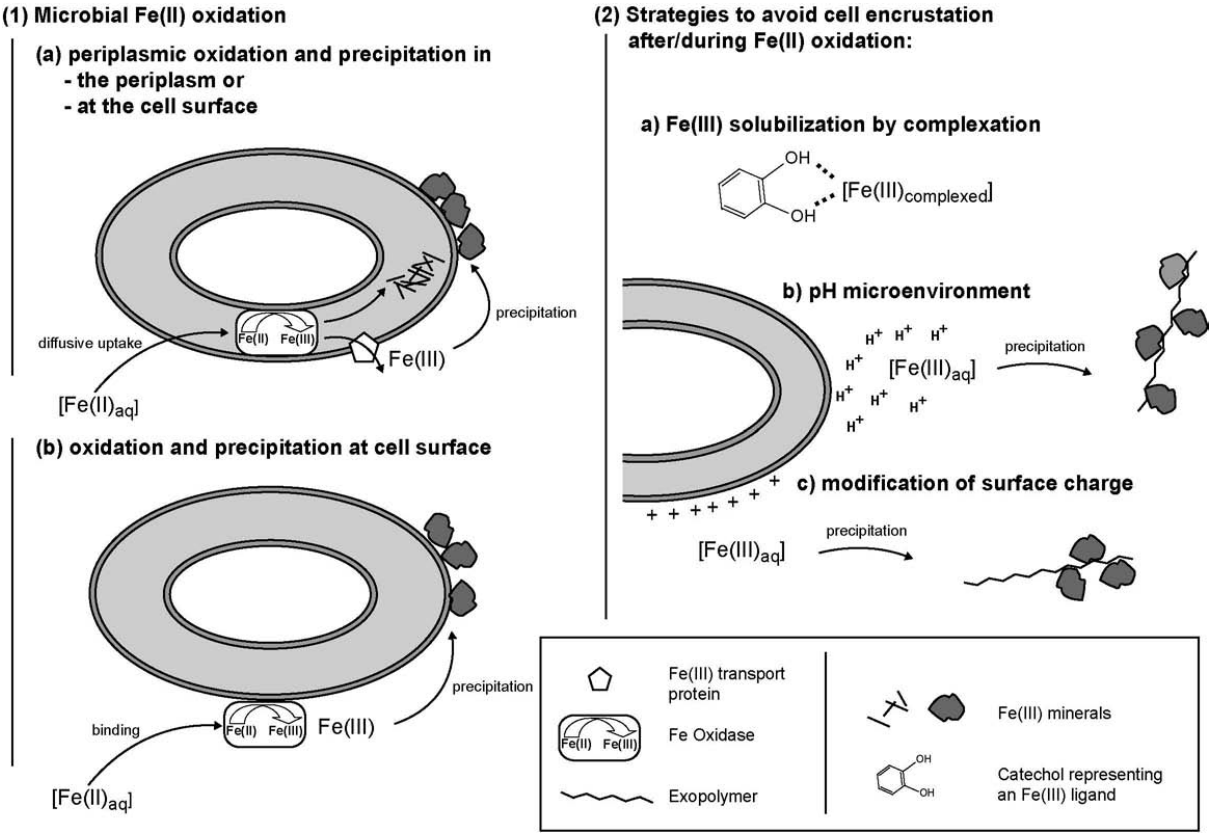

Figure 8.6: Model for anaerobic Fe(II) oxidation (1) and suggested mechanisms that could avoid encrustation (2) by gram-negative cells.

Additional analyses are needed to see whether they are associated with organics similar to the structures observed by (Chan et al., 2004) and may be preserved in the geological record. In contrast, some cells such as *Thiodictyon* sp. strain F4 do not leave any obvious specific signature in the mineral deposits suggesting the possibility of specific biases in the fossil record. Finally, it can be noted that in the case of KoFox and KoFum, interestingly, the one susceptible to leaving a fossil or a trace is not the one that oxidizes iron; therefore, looking for Fe(III)-precipitates associated with potential microfossils may be misleading. In any case, the combination of analyses of the mineralogy and texture of the iron precipitates with analyses of the organic molecules possibly preserved in the microfossils (e.g. Bernard et al., 2007) appears as a necessary approach to investigate the resulting microfossils.

8.6 Conclusions and Possible Further Experiments

Obviously different bacterial Fe(II)-oxidizing strains oxidize Fe(II) at different locations, i.e., at the cell surface or in the periplasm, and show different mechanisms of how to avoid encrustation with ferric iron. Suggested mechanisms are Fe(III) solubilization by complexation, creation of specific cellular pH

microenvironments, modification of the cell surface charge, and production of cellular exopolymers that act as precipitation templates; any combination of these mechanisms is possible. In order to evaluate the suggested mechanisms, further experiments are necessary to identify the Fe(II)-oxidizing mechanisms and enzymes as pioneered in the studies by Croal et al. (2007) and Jiao & Newman (2007). Additionally, potential organic compounds (exopolysaccharides) acting as nucleation sites should be identified (e.g., by scanning transmission X-ray microscopy, STXM), the hypothesized cell pH microenvironment should be attempted to be visualized (e.g., by using a pH-dependent fluorophore), and the cell surface properties (cell surface charge) should be determined via titration.

Bibliography

Benzerara, K; Menguy, N; Guyot, F; Skouri-Panet, F; de Lucca, G; & Huelin, T: Bacteria-controlled precipitation of calcium phosphate by ramlibacter tataouinensis. *Earth and Planetary Science Letters*, 228:439–449, 2004a.

Benzerara, K; Yoon, T; Tyliszczak, T; Constanz, B; Spormann, AM; & Brown, G: Scanning transmission x-ray microscopy study of microbial calcification. *Geobiology*, 2:249–259, 2004b.

Bernard, S; Benzerara, K; Beyssac, O; Menguy, N; Guyot, F; Brown, G; & Goffé, B: Exceptional preservation of fossil plant spores in high-pressure metamorphic rocks. *Earth and Planetary Science Letters*, 262:257–272, 2007.

Blake, RC; Shute, EA; Greenwood, MM; Spencer, GH; & Ingledew, WJ: Enzymes of aerobic respiration on iron. *FEMS Microbiology Reviews*, 11:9–18, 1993.

Buresh, R & Moraghan, J: Chemical reduction of nitrate by ferrous iron. *Journal of Environmental Quality*, 5:320, 1976.

Chan, CS; de Stasio, G; Welch, SA; Girasole, M; Frazer, BH; Nesterova, MV; Fakra, S; & Banfield, JF: Microbial polysaccharides template assembly of nanocrystal fibers. *Science*, 303:1656–1658, 2004.

Cornell, RM & Schwertmann, U: *The iron oxides: structure, properties, reactions, occurrences and uses* (VCH, Weinheim, Cambridge), 2nd ed., 2003.

Croal, LR; Jiao, Y; & Newman, DK: The fox operon from *Rhodobacter* strain SW2 promotes phototrophic fe(II) oxidation in *Rhodobacter capsulatus* sb1003. *Journal of Bacteriology*, 189:1774–1782, 2007.

Croal, LR; Johnson, CM; Beard, BL; & Newman, DK: Iron isotope fractionation by Fe(II)-oxidizing photoautotrophic bacteria. *Geochimica et Cosmochimica Acta*, 68:1227–1242, 2004.

Ehrenreich, A & Widdel, F: Anaerobic oxidation of ferrous iron by purple bacteria, a new type of phototrophic metabolism. *Applied and Environmental Microbiology*, 60:4517–4526, 1994.

Ehrlich, HL & Newman, DK: *Geomicrobiology* (CRC Press, New York), 5th ed., 2009.

Emerson, D & Moyer, C: Isolation and characterization of novel iron-oxidizing bacteria that grow at circumneutral pH. *Applied and Environmental Microbiology*, 63:4784–4792, 1997.

Emerson, D & Revsbech, NP: Investigation of an iron-oxidizing microbial mat community located near Aarhus, Denmark: Field studies. *Applied and Environmental Microbiology*, 60:4022–4031, 1994.

Folk, R & Lynch, F: The possible role of nanobacteria (dwarf bacteria) in clay-mineral diagenesis and the importance of careful sample preparation in high-magnification sem study. *Journal of Sediment Research*, 67:583–589, 1997.

Fortin, D & Langley, S: Formation and occurrence of biogenic iron-rich minerals. *Earth-Science Reviews*, 72:1–19, 2005.

Ghiorse, WC: Biology of iron- and manganese-depositing bacteria. *Annual Review of Microbiology*, 38:515–550, 1984.

Gorby, YA; Yanina, S; McLean, JS; Rosso, KM; Moyles, D; Dohnalkova, A; Beveridge, TJ; Chang, IS; Kim, BH; Kim, KS; Culley, DE; Reed, SB; Romine, MF; Saffarini, DA; Hill, EA; Shi, L; Elias, DA; Kennedy, DW; Pinchuk, G; Watanabe, K; Ishii, S; Logan, B; Nealson, KH; & Fredrickson, JK: Electrically conductive bacterial nanowires produced by shewanella oneidensis strain mr-1 and other microorganisms. *Proceedings of the National Academy of Sciences*, 103:11358–11363, 2006.

Hallberg, R & Ferris, F: Biomineralization by *Gallionella*. *Geomicrobiology Journal*, 21:325–330, 2004.

Hanert, H: *The Genus Gallionella*, vol. Proteobacteria: Delta, Epsilon subclass, pp. 996–997 (Springer), 2006.

Hegler, F; Posth, NR; Jiang, J; & Kappler, A: Physiology of phototrophic iron(II)-oxidizing bacteria – implications for modern and ancient environments. *FEMS Microbiology Ecology*, 66:250–260, 2008.

Heising, S; Richter, L; Ludwig, W; & Schink, B: *Chlorobium ferrooxidans* sp nov., a phototrophic

green sulfur bacterium that oxidizes ferrous iron in coculture with a *"Geospirillum"* sp strain. *Archives of Microbiology*, 172:116–124, 1999.

Heising, S & Schink, B: Phototrophic oxidation of ferrous iron by a *Rhodomicrobium vannielii* strain. *Microbiology*, 144:2263–2269, 1998.

Ivarsson, M; Lindblom, S; Broman, C; & Holm, N: Fossilized microorganisms associated with zeolite-carbonate interfaces in sub-seafloor hydrothermal environments. *Geobiology*, 6:155–170, 2008.

Jeon, B; Dempsey, B; Burgos, W; Royer, R; & Roden, E: Modeling the sorption kinetics of divalent metal ions to hematite. *Water Research*, 38:2499–2504, 2004.

Jiao, Y; Kappler, A; Croal, LR; & Newman, DK: Isolation and characterization of a genetically traceable photoautotrophic Fe(II)-oxidizing bacterium, *Rhodopseudomonas palustris* strain tie-1. *Applied and Environmental Microbiology*, 71:4487–4496, 2005.

Jiao, Y & Newman, DK: The pio operon is essential for phototrophic Fe(II) oxidation in rhodopseudomonas palustris tie-1. *Journal of Bacteriology*, 189:1765–1773, 2007.

Johnson, KJ; Ams, DA; Wedel, AN; Szymanowski, JES; Weber, DL; Schneegurt, MA; & Fein, JB: The impact of metabolic state on Cd adsorption onto bacterial cells. *Geobiology*, 5:211–218, 2007.

Kappler, A & Newman, DK: Formation of Fe(III)-minerals by Fe(II)-oxidizing photoautotrophic bacteria. *Geochimica et Cosmochimica Acta*, 68:1217–1226, 2004.

Kappler, A; Schink, B; & Newman, DK: Fe(III) mineral formation and cell encrustation by the nitrate-dependent Fe(II)-oxidizer strain BoFeN 1. *Geobiology*, 3:235–245, 2005.

Kappler, A & Straub, KL: Geomicrobiological cycling of iron. *Reviews in Mineralogy & Geochemistry*, 59:85–108, 2005.

Kiernan, JA: Formaldehyde, formalin, paraformaldehyde and glutaraldehyde: What they are and what they do. *Microscopy today*, 8:8–12, 2000.

Little, C; Glynn, S; & Mills, R: Four-hundred-and-ninety-million-year record of bacteriogenic iron oxide precipitation at sea-floor hydrothermal vents. *Geomicrobiology Journal*, 21:415–429, 2004.

Neubauer, SC; Toledo-Durán, GE; Emerson, D; & Megonigal, JP: Returning to their roots: Iron-oxidizing bacteria enhance short-term plaque formation in the wetland-plant rhizosphere. *Geomicrobiology Journal*, 24:65–73, 2007.

Rakshit, S; Matocha, CJ; & Coyne, MS: Nitrite reduction by siderite. *Soil Science of America Journal*, 72:1070–1077, 2008.

Reguera, G; McCarthy, KD; Mehta, T; Nicoll, JS; Tuominen, MT; & Lovley, DR: Extracellular electron transfer via microbial nanowires. *Nature*, 435:1099–1101, 2005.

Schaedler, S; Burkhardt, C; & Kappler, A: Evaluation of electron microscopic sample preparation methods and imaging techniques for characterization of cell-mineral aggregates. *Geomicrobiology Journal*, 25:228–239, 2008.

Schwertmann, U & Cornell, RM: *Iron oxides in the laboratory : preparation and characterization* (Wiley-VCH, Weinheim), 2nd ed., 2000.

Shapiro, L; McAdams, HH; & Losick, R: Generating and exploiting polarity in bacteria. *Science*, 298:1942–1946, 2002.

Sobolev, D & Roden, EE: Suboxic deposition of ferric iron by bacteria in opposing gradients of Fe(II) and oxygen at circumneutral pH. *Applied and Environmental Microbiology*, 67:1328–1334, 2001.

Straub, KL; Benz, M; Schink, B; & Widdel, F: Anaerobic, nitrate-dependent microbial oxidation of ferrous iron. *Applied and Environmental Microbiology*, 62:1458–1460, 1996.

Stumm, W & Morgan, JJ: *Aquatic chemistry: chemical equilibria and rates in natural waters* (Wiley-Interscience, New York), 3rd ed., 1995.

Stumm, W & Sulzberger, B: The cycling of iron in natural environments: Considerations based on laboratory studies of heterogeneous redox processes. *Geochimica et Cosmochimica Acta*, 56:3233–3257, 1992.

Tebo, B; Bargar, J; Clement, B; Dick, G; Murray, K; Parker, D; & SM., RVW: Biogenic manganese oxides: Properties and mechanisms of formation. *Annual Reviews of Earth and Planetary Sciences*, 32:287–328, 2004.

Thamdrup, B: Bacterial manganese and iron reduction in aquatic sediments. *Advances in Microbial Ecology, Vol 16*, 16:41–84, 2000.

Urrutia Mera, M; Kemper, M; Doyle, R; & Beveridge, TJ: The membrane-induced proton motive force influences the metal binding ability of *Bacillus subtilis* cell walls. *Applied Environmental Microbiology*, 58:3837–3844, 1992.

Weber, KA; Achenbach, LA; & Coates, JD: Microorganisms pumping iron: anaerobic microbial iron oxidation and reduction. *Nature Reviews: Microbiology*, 4:752–764, 2006.

Widdel, F; Schnell, S; Heising, S; Ehrenreich, A; Assmus, B; & Schink, B: Ferrous iron oxidation by anoxygenic phototrophic bacteria. *Nature*, 362:834–836, 1993.

9 Geomicrobiology of an iron-carbonate spring

Florian Hegler[1], Tina Loesekann[1], Karin Stögerer[1], Kurt Hanselmann[1,2,3], Sebastian Behrens[1], and Andreas Kappler[1] **for submission to Applied Environmental Microbiology**

[1]Center for Applied Geoscience – Geomicrobiology, Eberhard Karls University Tübingen, Sigwartstrasse 10, 72076 Tübingen, Germany
[2]University of Zŕich, Institute of Plant Biology – Microbial Ecology, Zollikerstrasse 107, CH-8008 Zürich, Switzerland
[3] swiss i-research & training, Zuŕich, Switzerland

9.1 Summary

This study describes the geomicrobiology of a bicarbonate-iron(II)-rich, circumneutral mineral water spring (Fuschna) in the Swiss Alps. Dark-green microbial mats at the side of the outflow channel as well as iron(III)(hydr)oxides in the flow channel dominate the spring visually. Gradients of oxygen, iron(II), and bicarbonate establish in the water. To identify the biogeochemical processes occurring at this site, we determined the geochemistry and the mineralogy as a function of space and time. The microbial community members were identified with 16S rRNA gene clone libraries. The influence of changes in geochemistry and the season on the microbial community was determined by a cluster analysis of denaturing gradient gel electrophoresis (DGGE) patterns. Geochemical analysis indicated micro-oxic water at the source which was completely oxygenated downstream (within 2-3 m). Calcite and ferrihydrite were identified by X-ray diffraction and Mössbauer spectroscopy and both methods revealed an increasing mineral crystallinity with distance from the source. In contrast, DGGE banding pattern cluster analysis revealed that the microbial community composition shifted mainly with the season and to a lesser extent along the flowpath. Using comparative 16S rRNA gene sequence analysis, we showed that the microbial communities differ between the water flow channel and the adjacent microbial mat. The microbial mat was dominated by a single cyanobacterium while microaerophilic Fe(II)-oxidizers and Fe(III)-reducers were identified in both the microbial mat and the flow channel. In summary our data suggest that seasonal changes mainly lead to microbial community variations while the geochemical gradients influenced the crystallinity of the minerals.

9.2 Introduction

Chalybeate waters are mineral spring waters containing elevated concentrations of reduced iron of typically up to 200 μmol L^{-1} (Emerson et al., 2010, and references therein). Chalybeate springs offer the opportunity to study geochemical gradients of O_2 and ferrous iron when anoxic Fe(II)-rich groundwater reaches the surface. While the water equilibrates with the environment, mineral precipitation can occur

and bacterial communities can establish and thrive utilizing the geochemical gradient of reduced iron and O_2.

Several microbial guilds gain energy by Fe(II) oxidation, such as photoferrotrophs (Widdel et al., 1993), nitrate-reducing Fe(II)-oxidizers (Straub et al., 1996) and microaerophilic Fe(II)-oxidizers (Emerson & Moyer, 1997). Photoferrotrophs are restricted to habitats with strictly anoxic conditions in the photic zone (Widdel et al., 1993). Nitrate-reducing Fe(II)-oxidizers can live under anoxic conditions, for example in lake sediments (Kappler et al., 2005) or the soils (Ratering & Schnell, 2001), but their occurrence and distribution depends on the availability of nitrate as electron acceptor. While molecular oxygen easily oxidizes Fe(II) chemically at circumneutral pH (Cornell & Schwertmann, 2003), microaerophilic Fe(II)-oxidizers can outcompete chemical oxidation in environments with low concentrations of molecular oxygen, especially in environments of opposing gradients of oxygen and Fe(II) (Emerson & Moyer, 1997). Such habitats can be found at oxic-anoxic interfaces in the environment. Therefore, nitrate-reducing and microaerophilic Fe(II)-oxidizers can populate a wide range of light-independent habitats.

Fe(III) produced by Fe(II) oxidation, either chemically or biologically, is only poorly soluble and will precipitate rapidly (Cornell & Schwertmann, 2003). Fe(III) minerals that precipitate in pure systems are different from iron minerals that precipitate in nature. In the environment as well as in mineral media in the laboratory, iron minerals are usually poorly crystalline and contain substantial amounts of impurities, such as ions from solution but also organic matter of microbial origin (Châtellier & Fortin, 2004, Châtellier et al., 2001, Fortin, 2004, Kappler & Newman, 2004, Fortin & Langley, 2005, Larese-Casanova et al., 2010). These Fe(III) minerals may be used by Fe(III)-reducing bacteria that oxidize organic matter at the same time (Lovley, 1991). Furthermore, it was shown that Fe(III) minerals produced by bacterial Fe(II) oxidation are better electron acceptors for Fe(III) reducing bacteria (Straub et al., 2004). Depending on the availability of organic matter, bacterial Fe(III) reduction can be very fast (Lovley, 1991) leading to an additional supply of Fe(II) for Fe(II)-oxidizing bacteria. Therefore, an interplay between Fe(II) oxidation and Fe(III)-reducing bacteria at locations with high iron concentrations is expected which leads to microbial Fe-cycling (Roden et al., 2004, Kappler & Straub, 2005, Weber et al., 2006, Gault et al., 2011).

To date, only few studies have been published on the geomicrobiology of chalybeate surface waters, i.e. where Fe(II)-rich water reaches the photic zone (James & Ferris, 2004, Wagner et al., 2007, Duckworth et al., 2009, Bruun et al., 2010). The microorganisms and the microbial communities that establish at a habitat with ferruginous surface waters are expected to be well adapted to the conditions prevailing. Previous studies found microaerophilic Fe(II)-oxidizers (James & Ferris, 2004, Wagner et al., 2007, Duckworth et al., 2009, Bruun et al., 2010) but photoferrotrophs or nitrate-reducing Fe(II) oxidizers were scarce. Furthermore, Fe(III)-reducers were detected in some of the studies (Wagner et al., 2007, Duckworth et al., 2009, Bruun et al., 2010). The studies mentioned above focus on the microbiology at the respective field site. Nonetheless, the complex interplay between the geochemical parameters and the precipitating minerals in addition to the microbial community has drawn less attention so far. Furthermore, changes of the microbial community over time and thus varying conditions has – to our knowledge – not been determined for chalybeate waters.

Therefore, in order to elucidate the interaction of geochemistry, mineralogy and microbiology, we evaluate all three at the circumneutral chalybeate bicarbonate-rich Fuschna spring, Engadin (Swiss Alps). This spring is one of several similar springs in the Engadin which are, depending on the geological context in which they occur, also characterized by high bicarbonate and/or sulfate concentrations Carlé (1975), Bissig et al. (2006). CO_2 in the water originates from metamorphic reactions in the earth crust (Schotterer

et al., 1987, Bissig et al., 2006), the other ions result from the interaction and dissolution of minerals (Carlé, 1975). The spring water at this field site is likely comprised of meteoric water (Schotterer et al., 1987).

In order to extend the current knowledge on the geomicrobiology at chalybeate springs, Fuschna samples were extensively studied with an array of geochemical, microscopic, molecular and microbiological tools. The mineralogy and diverse geochemical parameters at the field site were analyzed. Cell numbers were determined by quantitative PCR and most-probable-number counts. The microbial diversity was investigated using comparative sequence analysis of 16S rRNA genes. Shifts in the microbial community composition were monitored with denaturing gradient gel electrophoresis and linked to possible factors which may induce the shifts by clustering methods.

The main goals of this study were to link geochemical parameters to the mineralogy of the field site and elucidate the environmental factors which determine the spatial and temporal distribution of microorganisms at the spring.

9.3 Material and Methods

9.3.1 Location of the spring

The field site is located at 46°47'16.62"N and 10°15'52.28" E near Scuol, Switzerland at an elevation of 1260 m above sea level. The spring is classified as a bicarbonate rich ferrous spring (Wexsteen et al., 1988, Bissig, 2004). The samples were taken five times over the course of one year (April 2009, June 2009, August 2009, February 2010, May 2010).

9.3.2 Sampling

Samples were collected at three different locations at the spring, i.e. at the source (0 m), 1.2 m downstream from the source, and 2.2 m from the source. At all sample locations water flow was sufficient for taking liquid samples for geochemical analyses. At all locations the flow channel and microbial mats at the side were distinctly separated (fig. 9.1A). Samples for geochemical analyses were taken from the flowing water, while samples for community analysis were taken in the center of the flow channel and from the mat at the channels sides. After 2.2 m, the flow channel split up as a delta or even overgrew (fig. 9.1A, right side), therefore, further than 2.2 m from the source no further samples for geochemical analysis were taken and a distinct differentiation between flow channel and mat was difficult.

Geochemical sampling was not possible in February 2010 as the water was frozen. Microbiological samples were collected using sterile tools and frozen immediately on dry ice. In the lab, samples were frozen at -20°C until extraction.

The delivery rate of the spring was determined by measuring the amount of water at the source with a beaker (n=10, 250±20 mL) depending on time.

9.3.3 Geochemical analysis of water samples

pH, oxygen and temperature were measured with mobile field equipment. Oxygen concentrations were measured with a WTW Oxi 315i while temperature and pH measurements were taken with an Eutech pH310 pH-meter.

All samples for laboratory analysis were cooled within minutes after sampling. Bicarbonate and carbonate samples were collected in brown 250 mL gas-tight screw-cap bottles. Titrations for phenolphthalein-alkalinity (i.e. CO_2) and H_2CO_3 were done with a Metrohm Titrino 836 using a dynamic titration. The titrants were either 0.1 N HCl up to pH 4.5 for the total alkalinity and [0.1]N NaOH until pH 8.3 for the phenolphthalein alkalinity (Eaton et al., 2005). Water samples for quantification of ferrous and ferric iron were collected in Eppendorf cups and immediately acidified with 2 mol L^{-1} HCl (final concentration of HCl was 1 mol L^{-1}). Fe(II) and Fetot was quantified as described previously (Hegler et al., 2008). Samples for quantification of dissolved ions by ion chromatography were collected in 50 mL Falcon tubes and analyzed on a Dionex DX-120 ion chromatograph equipped with an autosampler and an AS23 anion column and a CS 12A cation column. Samples were measured in duplicates and analyzed with the chromeleon software package.

9.3.4 Mineral analysis

Mineral samples were stored in 10 mL rubber-stoppered serum flasks and frozen immediately after sampling on dry ice. In order to avoid potential oxidation of Fe(II) minerals, samples were opened and thawed in an anoxic chamber (100% N_2) and dried therein for XRD and Mössbauer analysis. Additional sampling points to the previously described points (0 m, 1.2 m and 2.2 m from the source) were chosen for XRD analysis at intermediate intervals (0.7 m, 1.8 m and 4.0 m).

Fe(II) and Fe(III) in mineral samples were determined by dissolving the minerals with 6 mol L^{-1} HCl in an anoxic glovebox and quantifying the iron concentration of the sample as described in Hegler et al. (2008).

For XRD mineral identification dried samples were resuspended in 500 µL of 100% ethanol, ground in the glovebox with a small mortar and finally added onto a Si-waver. The sample was stored under anoxic conditions until analysis. During the analysis the sample was exposed to oxygen. This did not affect the results as no oxygen sensitive minerals were detected.

The XRD patterns were acquired with a Bruker D8 Discovery X-ray diffractometer with a Co Kα radiation at 30 kV, 30 mA connected to a polycapillary focused to a spot size of 300 µm. Three overlapping frames of 30°C 2θ with a collection time of 1 min per frame were acquired with a GADDS area detector. Diffrac plus EVA 10.0.1.0-software (Bruker) was used for merging the frames and identifying the mineral phases using the PDF-database (ICDD – International Centre for Diffraction Data).

For Mössbauer spectroscopy, the dried mineral samples were enclosed in oxygen-impermeable Kapton tape for ^{57}Fe specific Mössbauer analysis in an anoxic glovebox. The sample was analyzed in a Mössbauer spectrometer (Wissenschaftliche Elektronik GmbH, Germany) with a ^{57}Co-source embedded within a Rhodium matrix at room temperature. Linear acceleration was used in transmission mode using a constant acceleration drive system set to a velocity range of $\pm$ 12 mm sec^{-1} with movement error of $<$ 1%. The absorption was determined with a 1024 multichannel analyzer. We varied the temperature of the sample with a Janis cryostat (Janis Research Company Inc., USA). The calibration of the spectra was done with a α-Fe(0) foil. The Recoil (University of Ottawa, Canada) software was used for spectra analysis. All models were modeled using Voigt based spectral lines.

Mössbauer spectroscopy has the advantage over XRD that it is possible to detect smaller fractions of iron minerals including poorly crystalline iron minerals. The disadvantage is that other non-iron minerals that could potentially be contained in the system cannot be detected. Hence, the approach using XRD and Mössbauer spectroscopy complemented the mineral analysis, especially with the respect to Fe-minerals.

9.3.5 Most probable number counting and Fe(III) reduction rates

In order to determine the number of bacteria that could perform either Fe(III) reduction or Fe(II) oxidation we used the culture-dependent most probable number counting technique (Cochran, 1950). The samples were stored for up to four days at 4°C before the dilution series was set up. Mineral medium was designed to resemble the spring water and contained 1.25 mmol L^{-1} $MgSO_4 \times 7\ H_2O$, 0.07 mmol L^{-1} KH_2PO_4, 0.3 mmol L^{-1} NH_4Cl, 1 mmol L^{-1} $CaCl_2 \times 2H_2O$ and 0.3 mmol L^{-1} $NaNO_3$. Additionally, 0.1 mL L^{-1} sterile-filtered vitamin solution (Widdel & Pfennig, 1981), 1 mL L^{-1} sterile trace element solution (Tschech & Pfennig, 1984) and 1 mL L^{-1} sterile selenate-tungstate solution (Widdel, 1980) were added. 35 mmol L^{-1} $NaHCO_3$ was used as buffer. The pH was adjusted to pH 6.3-6.4. The medium was prepared as described previously (Hegler et al., 2008).

In order to remove excess water from the collected wet samples, the samples were centrifuged for 5 min at 3000 × g and the pellet was resuspended in 10 mL of the designed medium. The dilution series was set up with 10-fold dilutions and seven parallels in 96-deep-well plates (1 mL/well). The setup was done in an anoxic chamber to avoid false-positives through the oxidation of Fe(II) by molecular oxygen. As substrate, 10 mmol L^{-1} ferrihydrite, 5 mmol L^{-1} lactate and 5 mmol L^{-1} acetate were used for the Fe(III) reduction setup. The ferrihydrite was chemically synthesized as described previously (Raven et al., 1998), washed four times with Millipore-water and deoxygenated by repeating evacuation and flushing with N_2. The cell number of Fe(II)-oxidizing bacteria was determined by adding 10 mmol L^{-1} $FeCl_2$ and then exposing the plate to light (photoferrotrophs) or additionally adding 10 mmol L^{-1} Na-nitrate for chemoautotrophic Fe(II)-oxidizers. For chemoheterotrophic Fe(II)-oxidizers, additionally 5 mmol L^{-1} Na-acetate were added. Oxidation and reduction was determined after twelve weeks of incubation at 20°C. Data-evaluation was done according to (Klee, 1993).

The determination of Fe(III) reduction rates was done in 10 mL test-tubes. 1 g of centrifuged sample material (5 min at 3000 × g) was added anoxically to 9 mL spring water. Four different setups with three parallels each prepared. Either 10 mmol L^{-1} ferrihydrite, 5 mmol L^{-1} Na-acetate and 5 mmol L^{-1} Na-lactate or 10 mmol L^{-1} ferrihydrite only or 5 mmol L^{-1} Na-acetate and 5 mmol L^{-1} Na-lactate or no additions at all were added. The concentration of Fe(II) and Fetot was followed over time as described previously (Hegler et al., 2008).

9.3.6 Extraction and amplification of environmental DNA

Total community DNA was extracted from 2.5 g of the sample material using the method of Zhou et al. (1996). Crude DNA extracts were purified with the Wizard DNA Clean-Up Kit (Promega, Madison, Wi, USA). Domain specific primers were used to amplify almost full-length 16S rRNA genes from the extracted chromosomal DNA by PCR (primers: see table 9.2).

PCRs were performed with a final volume of 50 µL: 0.2 µmol L^{-1} of each primer, 200 µmol L^{-1} of deoxyribonucleoside triphosphate, 3.5 mmol L^{-1} $MgCl_2$, 300 mg of bovine serum albumin, 1 × PCR buffer and 1.25U of GoTaq (Promega, Madison, Wi, USA). Template DNA (20 ng μL^{-1}) was added to the reaction mixture.

For denaturing gradient gel electrophoresis (DGGE), PCR cycling conditions were as follows: 1 cycle at 94°C for 2 min; 10 cycles with 94°C for 1 min, 65°C for 1 min with a decrease of 0.5°C after each cycle, and 72°C for 1 min; and 20 cycles with 94°C for 1 min, 55°C for 1 min, and 72°C for 1 min with a final cycle of 72°C for 10 min.

For the clone library, PCR cycling conditions were as follows: start at 70°C, then 1 cycle with 94°C for

5 min; 25 cycles with 95°C for 1 min, 44°C for 1 min, and 72°C for 3 min with a final cycle of 72°C for 10 min. The number of amplification cycles during PCR was reduced as much as possible to reduce PCR biases; however 25 cycles were needed to yield sufficient product.

9.3.7 Quantitative real-time PCR and data analysis

The absolute quantification of bacterial 16S rRNA genes was performed by using the SsoFast Eva Green Supermix (Bio-Rad Laboratories GmbH, Munich, Germany) and gene-specific primers (biomers.net GmbH, Ulm, Germany) on the iQ5 real-time PCR detection system (Bio-Rad Laboratories GmbH, Munich, Germany). The DNA extracts were additionally cleaned by running the extract on a 1% agarose-gel. Bands were cut out and purified with a QIAEX II Gel extraction kit (QIAGEN, Hilden, Germany) and resuspended in 20 µL of water. The forward primer was 341F (Muyzer et al., 1995) and the reverse primer was 797R (Nadkarni et al., 2002) (table 9.3) while specific primers were used for the quantification of 16SR-rNA genes of *Gallionella* species (table 9.2). Each reaction was performed in a final volume of 20 µL consisting of 10 µL SsoFast Eva Green Mix, 0.3 µL 341F (5 µmol L^{-1}), 0.9 µL 797R (5 µmol L^{-1}), 6.8 µL DEPC-treated water (Carl Roth, Karlsruhe, Germany) and 2 µL of sample, standard or DEPC-treated water (NTC) respectively. PCR amplification and detection were conducted as follows: 2 min at 98°C followed by 40 cycles of 5 s at 98°C and 12 s at 60°C and melt curve analysis (1 min at 95°C, 1 min at 60°C and 71 cycles at 60-95°C with temperature increase of 0.5°C per cycle).

The data were analyzed with the iQ5 optical system Software, Version 2.0 (Bio-Rad, 2006) by using plasmid pCR2.1_thio_16S with a fragment of the 16S rRNA gene from *Thiomonas* sp. as a standard. Each qPCR was performed in duplicate or triplicate, respectively.

9.3.8 Denaturing gradient gel electrophoresis (DGGE) – preparation and analysis

In order to analyze cyanobacterial and bacterial community structure, we used denaturing gradient gel electrophoresis (DGGE) (Green et al., 2009). Primers were group specific (table 9.2) and PCR conditions as described above. Briefly, we used a 6% acrylamide gel with a denaturing gradient of formamide and urea ranging from 35 to 60%. Analysis of the banding pattern was done with GelCompare II software version 6.00 (Applied Maths). The UPGMA method (Unweighted Pair Group Method with Arithmetic Mean) was used to analyze the banding pattern of the gels using the following parameters: optimization of 2% and tolerance of 1%.

9.3.9 Clone library construction and analysis

For clone library construction, products of three parallel PCR reactions were combined and purified with the Wizard DNA Clean-Up (Promega, Madison, Wi, USA). PCR products were ligated in the pCR4 TOPO vector (Invitrogen, Carlsbad, CA, USA) and transformed into E. coli TOP10 cells (Invitrogen, Carlsbad, CA, USA) according to the manufacturer's recommendations.

Sequencing was performed by Taq cycle sequencing using vector primers M13F and M13R (biomers.net GmbH, Ulm, Germany). Partial reads were assembled using the program DNA Baser (http://www.dnabaser.com). The presence of chimeric sequences in the clone libraries was determined with the program Bellerophon (http://foo.maths.uq.edu.au/ huber/bellerophon.pl). Potential chimeras were eliminated from subsequent analyses. Sequence data were aligned with the SINA webaligner (Pruesse et al., 2007) (http://www.arb-silva.de/aligner) and analyzed with the software packages ARB (Ludwig et al., 2004) and Mothur (Schloss

et al., 2009).

9.3.10 Microscopy

Light microscopy images were taken on a Zeiss Axioscope 2 plus epifluorescence microscope (Zeiss, Germany) with a 40-fold objective lens. 4',6-diamidino-2-phenylindole (DAPI, final concentration 5 mg L^{-1}) was added as a fluorescent dye. Fluorescent images of DAPI stained samples were taken with an excitation below 395 nm and an emission between 420-470 nm. The autofluorescence of cyanobacteria was detected by exposing the sample to wavelength between 395-440 nm and detecting the emission at wavelength >470 nm. Images of autofluorescence and DAPI-staining were overlain using the FIJI-software-package (http://pacific.mpi-cbg.de).

9.3.11 Geochemical modeling

Thermodynamic geochemical modeling was performed with the Geochemists Workbench 6.0 software package (Rockware) using the React-module. The ion concentrations (table 9.3) were used as input to calculate mineral precipitation under the experimentally determined geochemical conditions. Temperature changes were not considered while the pH-increase of the water was taken into account.

9.4 Results

9.4.1 Geochemistry and mineralogy

The Fuschna spring is an iron-carbonat-rich spring with a water delivery rate between 0.7 ± 0.1 to 1.2 ± 0.1 L min^{-1}. A narrow flow channel of 10 to 15 cm held most of the water (figure 9.1A). At both sides of the stream a 0.5 to 1 cm thick dark-green microbial mat flanked the flow channel (figure 9.1B). With increasing distance from the spring the water channel divided into multiple subchannels. Depending on the season and extent of the flanking microbial mats, no clear channel was distinguishable at about 2.3 m from the source and below. Water samples were collected in April, June, and August 2009 and May 2010. Geochemical sampling of spring water was not possible in February 2010 because the spring was frozen and no liquid water could be collected.

The dissolved oxygen concentration in the spring water rose from 15 µM (microoxic) at the spring source (at the outflow from the ground) to 260 µM (85% oxygen saturated) about 2.3 m from the source (figure 9.2A). The measured oxygen concentration increased with distance from the source and did not vary significantly between sampling campaigns. The water temperature varied between 8.1°C and 10.8°C at the source over the sampling campaign. We detected a temperature increase from 10.8°C to 14.5°C 2.2 m from the source in August 2009 while the temperature did not increase more than 1°C at the other times. The pH at the source ranged between increased from 6.0 and 6.3 and increased to pH 6.7 to 7.0 at 2.3 m from the source. The overall pH-increase over distance from the source was maximum 0.9 pH-units.

The concentration of Fe(II) in the spring water decreased slightly from the source. At the source, 80% of the iron was present as Fe(II). The total concentration of Fe(III) increased with distance from the source to about 40% (figure 9.2B). A complete, representative list of the ions detected in the water in August 2009 is shown in table 9.3 (supplementary information). The ion concentrations in the water did not change significantly over time (data not shown). The main ions were calcium (17.4 mM) and magnesium (2.2 mM). The alkalinity of the water was relatively high ranging between 52 and 58 mEq

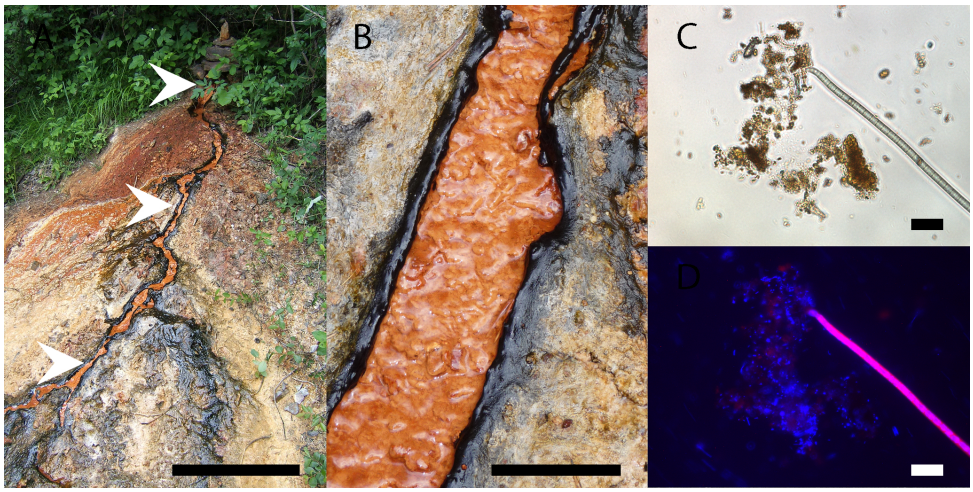

Figure 9.1: Photographs and microscopy images of the Fuschna spring: A: Overview, scale bar represents 1 m, white arrows show sampling locations; B: Close-up of the stream with cyanobacterial mats and minerals precipitates about 1.2 m downstream from the source, scale bar represents 5 cm; C: representative light microscopic micrograph of a sample from the cyanobacterial mat 1.2 m downstream from the source, scale bar represents 25 µm; D: epi-fluorescence micrograph of image C, DAPI-stained (blue) overlaid with the auto-fluorescence signal of cyanobacteria (pink).

L^{-1} (figure 9.2C) as determined by endpoint-titrations. The major component of the spring water was CO_2-bicarbonate with a concentration at the source of 44 mM; the contribution of other ions to the titration was minor due to their relatively low concentrations (e.g. table 9.3 for a complete list of ions).

In order to determine which minerals are expected to precipitate at the geochemical conditions described above, thermodynamic equilibrium modeling for calcite, dolomite and siderite precipitation was done including all ions detected in the water. The model indicated that the main mineral expected to precipitate is calcite ($CaCO_3$) (figure 9.3). This is due to the high concentration of calcium and the high bicarbonate content in the mineral water (table 9.3). Fe(II)-carbonates (e.g. siderite, $FeCO_3$) are only expected to precipitate at pH-values above pH 6.7. Calcite over-saturation was higher than that of dolomite ($CaMg(CO_3)_2$) and siderite, therefore these minerals were predicted to precipitate to a lesser extent than calcite.

X-ray diffraction (XRD) of samples collected at increasing distances from the source confirmed that the main crystalline mineral phase was indeed calcite (figure 9.4). Neither dolomite nor siderite was detected with XRD at any location. With increasing distance from the source a slightly higher crystallinity of calcite was observed as evidenced by the increasing height and sharpness of the reflections at $2\theta = 27$ and 57 (figure 9.4). XRD did not reveal the presence of any iron-containing minerals. The concentration of Fe(III) in dry sediment samples was 1.5-2.5% (w/w) independent of the location (e.g. 0 m from the source to 2.2 m downstream), we did not detect any Fe(II) in these samples. Therefore, we used Mössbauer spectroscopy (table 9.1 and figure 9.5) which is selective for iron and – in contrast to XRD – is also able to detect poorly crystalline mineral phases. Furthermore, iron-minerals can be indentified in a matrix of non-iron minerals (e.g. calcite) and thus the sensitivity for iron-mineral phases is higher. With Mössbauer spectroscopy we could not detect any Fe(II) mineral phases. A poorly crystalline Fe(III) mineral phase was detected. It was fitted best with a chemically synthesized ferrihydrite standard (table 9.1). The

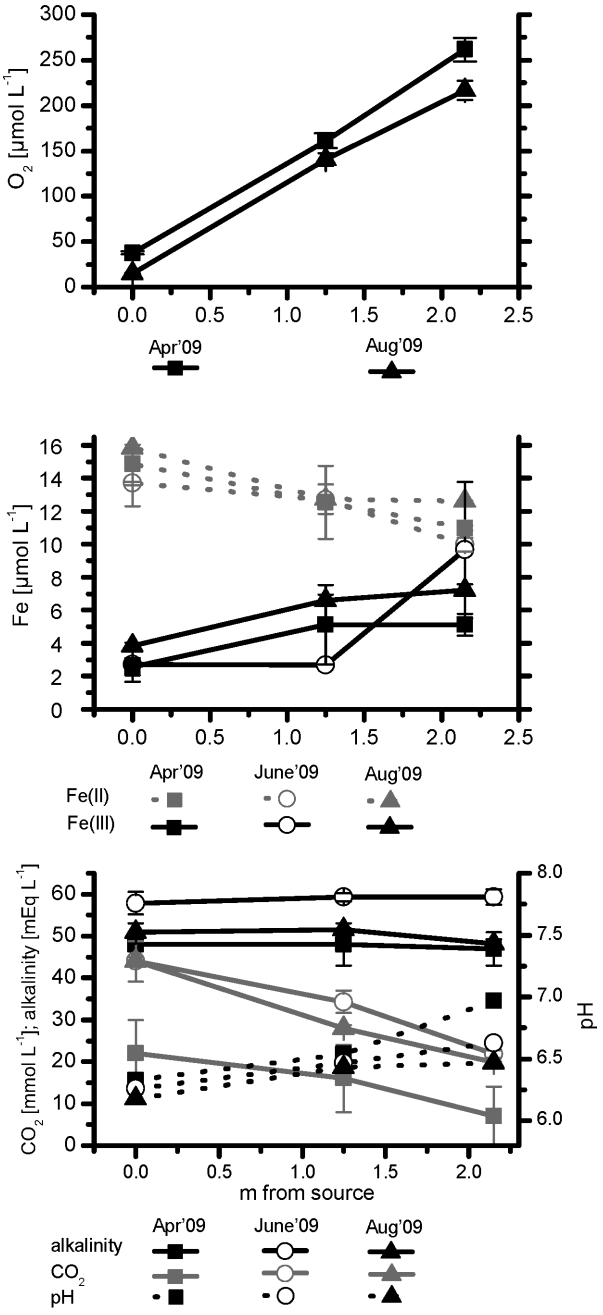

Figure 9.2: Geochemical parameters of the spring water at increasing distance from the source: A: Oxygen concentration in the stream water measured by oxygen electrode at three different time points. B: Fe(II) and Fe(III) determined in the water of the stream at four time points. C: Bicarbonate, CO_2 concentration and pH at three different time points.

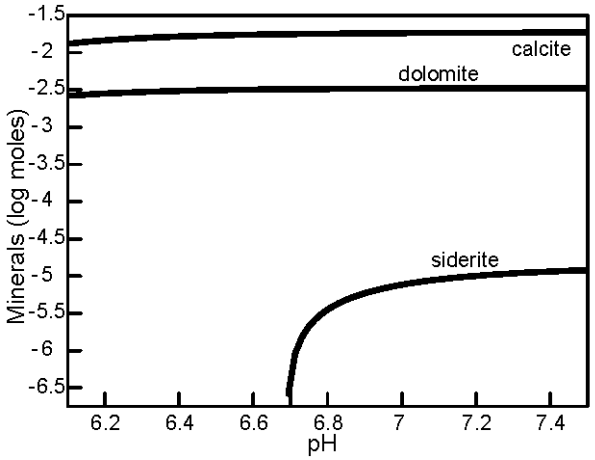

Figure 9.3: Thermodynamic modeling of carbonate mineral precipitation using Geochemist's Workbench. The pH-change along the flow channel was taken into account, temperature was kept constant as by 5°C did not influence the thermodynamic modeling significantly. The ion concentrations of the spring were used in the matrix for the calculation.

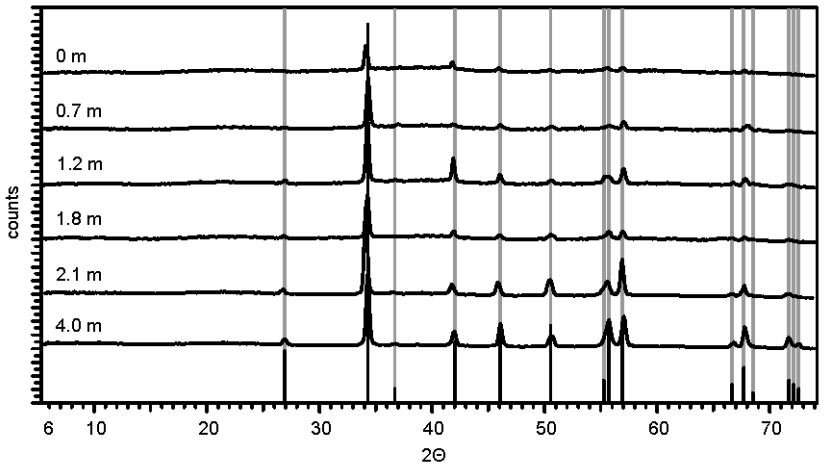

Figure 9.4: Representative XR-diffractograms of mineral samples collected downstream of the source downstream. At the bottom the reference for calcite is shown (powder diffraction file: 00-005-0586). The samples were collected in August 2009.

crystallinity of the Fe(III) minerals increased with distance from the source. This is reflected in the Mössbauer spectra by the peak width. They become narrower resulting in sharper peaks with increasing distance from the source (figure 9.5). These changes can also be calculated and are expressed by the decrease in σ_Δ (table 9.1).

Table 9.1: Modeling results from Mössbauer spectra from samples of August 2009 at three different locations from the source collected at 77K. For the sample collected at 1.2 m an additional spectrum was collected at 4K.

	source	1.2 m downstream	2.3 m downstream	ferrihydrite reference
δ_0 (77K)	0.466	0.475	0.465	0.46
Δ_ε (77K)	0.986	0.938	0.898	0.7
σ_Δ	0.732	0.572	0.474	
δ_0 (5K)		0.491		0.48
ε (5K)		-0.05		-0.02
H (5K)		44.293		45.3 and 49.3

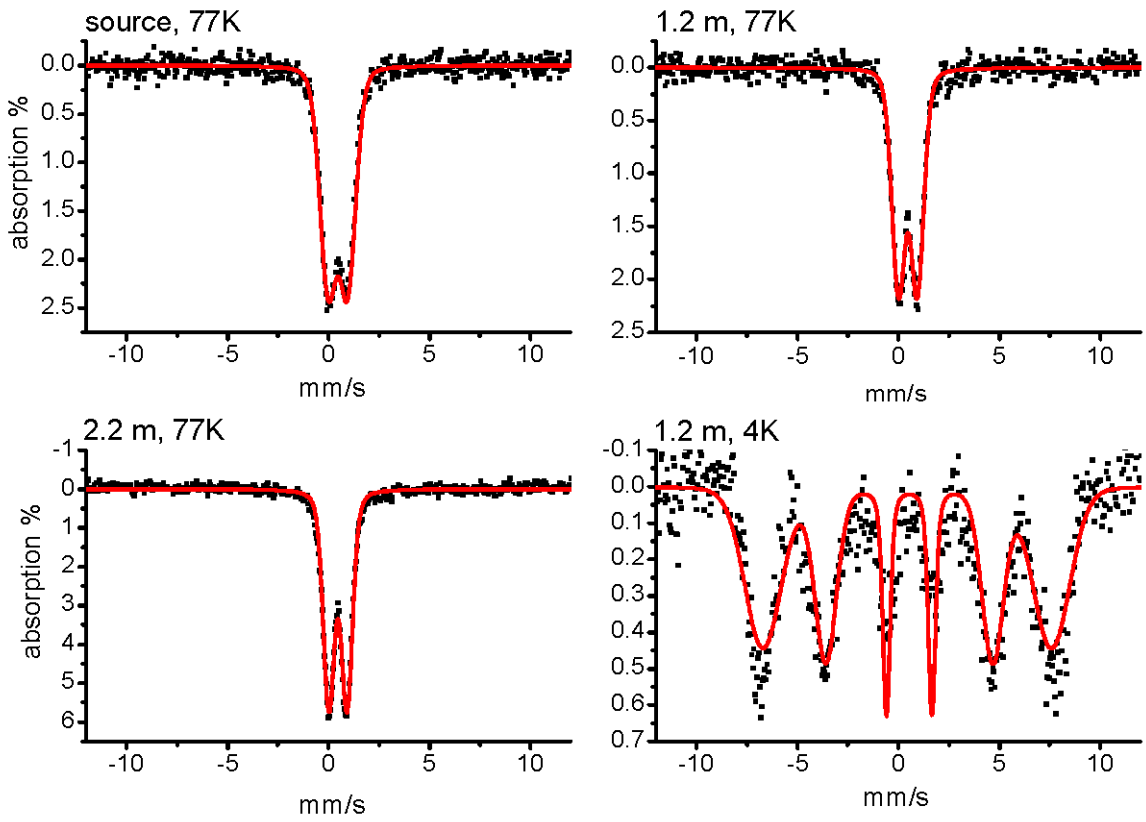

Figure 9.5: Mössbauer spectra from samples of August 2009 at three different locations from the source collected at 77K. For the sample collected at 1.2 m an additional spectrum was collected at 4K. Red line: fitted model results, see table 9.1.

9.4.2 Bacterial cell counts

The water channel at the spring was flanked by dark-green to blackish mats while the mats were usually not observable in the flow channel (figure 9.1B). Upon inspection by eye, the mats were dominated by cyanobacteria. Light and epifluorescence microscopy (figure 9.1C and D) showed the presence of both bacteria and structures of filamentous cyanobacteria in the mat's matrix (figure 9.1C and D).

Bacterial cell numbers were determined with two independent methods: Once with culture dependent most probable number counts where we differentiated between the number of cells capable of a certain metabolic pathway and once with culture independent quantitative real-time PCR (qPCR) where the amplifiable 16S-rRNA gene fragments are detected. We quantified the number of amplifiable, bacterial 16S rRNA genes with qPCR using broad-range bacterial primers (table 9.2). Gene copy numbers were $2.02 \times 10^8 \pm 3.18 \times 10^7$ copies g^{-1} in the middle of the flow channel 1.2 m from the source, while we quantified $1.97 \times 108 \pm 3.05 \times 107$ copies g^{-1} within the microbial mats also 1.2 m from the source. Using specific primers for the 16S-rNA gene of *Gallionella* species (table 9.2) – which are a proxy for microaerophilic Fe(II)-oxidizing bacteria – we found $1.97 \times 10^7 \pm 4.36 \times 10^6$ copies g^{-1} in the middle of the flow channel 1.2 m from the source while the number of amplifiable 16S-rRNA gene copy numbers in

the microbial mat was much lower with $8.34 \times 10^3 \pm 4.21 \times 10^3$ copies g^{-1}.

Using culture-dependent most-probable number (MPN) counts, we distinguished between the number of nitrate-reducing and phototrophic Fe(II)-oxidizers and Fe(III)-reducers. Samples for MPN counts of Fe(II)-oxidizing and Fe(III)-reducing bacteria were taken in late spring and early summer (June 2009 and May 2010) at the three locations corresponding to the geochemical sampling sites, e.g. 0 m, 1.2 m and 2.2 m from the source. Furthermore, at 1.2 m from the source we distinguished between the flanking microbial mat and the middle of the flow channel. At all other locations, only the microbial mat was sampled. The number of microorganisms being able to oxidize Fe(II) – phototrophically or coupled to the reduction of nitrate – was always substantially lower than that of Fe(III)-reducers. Photoferrotrophs were found in concentrations ranging between 10^3 to 10^4 cells g^{-1} sample material. The cell number of the nitrate-reducing Fe(II)-oxidizing bacteria found at all locations ranged between 10^3 to 3×10^4 cells g^{-1} material. At some locations, even no Fe(II)-oxidizers of the described type could be detected.

In contrast to Fe(II)-oxidizing bacteria, Fe(III)-reducers were much more abundant. Cell numbers determined by MPNs were around 10^8 cells g^{-1} material. For samples taken in May 2010 the number of Fe(III)-reducers was significantly higher at the source where the Fe(II) concentration was highest (figure 9.2) and was lower downstream at 2.2 m from the source (figure 9.6). The difference between the number of Fe(III)-reducers at the side and in the middle of the flow channel turned out to be not significant for May 2010 while there is a significant difference between the number of Fe(III) reducers for the samples taken in June 2009 (figure 9.6).

Due to the high numbers of Fe(III)-reducers, we determined the intrinsic Fe(III) reduction for samples from the microbial mat and the middle of the flow channel. The samples were collected in September 2010 at 1.2 m distance from the source. We did not observe a lag time before reduction started in the samples from microbial mat while in contrast two to eight days passed before reduction started in the in the samples collected from the flow channel. The reduction rate of Fe(III) in the microbial mat was fastest when no organic substrates (e.g. acetate and lactate) were added (3.3 ± 0.1 mM Fe(III) day^{-1}). In contrast, the reduction rate was slowest when additional ferrihydrite was added as Fe(III) source (1.1 ± 0.2 mM Fe(III) day^{-1}) (figure 9.7A). The reduction rate was intermediate of organic substrate was added (2.2 ± 0.2 mM Fe(III) day^{-1}) and not significantly faster if additionally to the organic substrate ferrihydrite was added (2.7 ± 0.4 mM Fe(III) day^{-1}). The 1 mol L^{-1} HCl extractable iron was reduced almost completely (figure 9.7A).

In contrast to the iron reduction measured for the microbial mat, the samples collected from the middle of the flow channel showed a prolonged lag-phase of two to eight days (figure 9.7B). The addition of organic substrate (acetate and lactate) reduced the lag-phase and led to almost complete reduction of 1 mol L^{-1} HCl extractable Fe(III) (figure 9.7B). The addition of ferrihydrite without additional organic substrate led to an incomplete reduction of Fe(III). The concentration of electron equivalents already available in the sample that can be used by bacteria to reduce Fe(III) was calculated to be about 4-5 mmol electrons g^{-1} material. This value was determined by the maximum amount of Fe(III) that was reduced in samples that were not supplemented with additional electron donors.

9.4.3 Diversity and identification of the microorganisms

Samples were collected at the same locations as for the geochemical analysis, e.g. at the source, 1.2 m and 2.2 m from the source in April 2009, August 2009 and February 2010.

We used denaturing gradient gel electrophoresis (DGGE) in order to detect shifts in the microbial

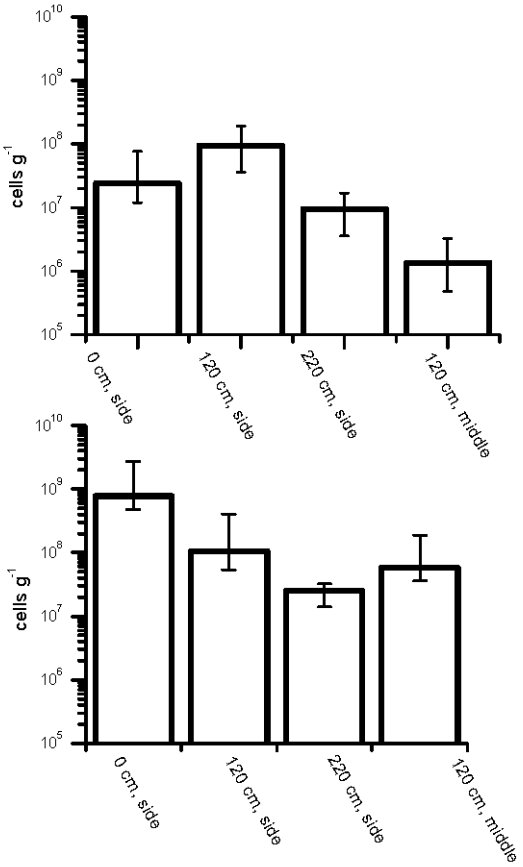

Figure 9.6: Most probable number counts for Fe(III)-reducing bacteria. Fe(III)-reducers were incubated with 30 mmol L^{-1} ferrihydrite, 10 mmol L^{-1} lactate and 10 mmol L^{-1} acetate, n=7. Samples were collected in June 2009 (top) and in May 2010 (bottom) at increasing distance from the source either from the microbial mat at the side of the flow channel or in the middle of the channel. Error bars show the 95% confidence interval.

community. The DNA from the samples was extracted and amplified with broad-range primers for Bacteria, Archaea and most cyanobacteria (table 9.2). With the general archaeal primers no amplicon could be obtained under various PCR conditions (data not shown).

DGGE banding patterns revealed relatively low cyanobacterial diversity in the microbial mats at the side of the flow channel. The banding indicated one prominent band which was accompanied by an additional minor band only in a few cases. A cluster-analysis of the cyanobacterial diversity was therefore not performed.

In contrast to cyanobacteria, bacterial diversity was higher in both the microbial mats and in the middle of the flow channel. In order to determine shifts in the microbial community patterns with time and along the flow path, a cluster analysis was performed (figure 9.8). The cluster diagram indicated that the composition of the microbial community did not change significantly with increasing distance from the source. In contrast, the microbial diversity in the microbial mat samples was clearly different from the flow channel samples. The most drastic community shift was observed by comparing the different

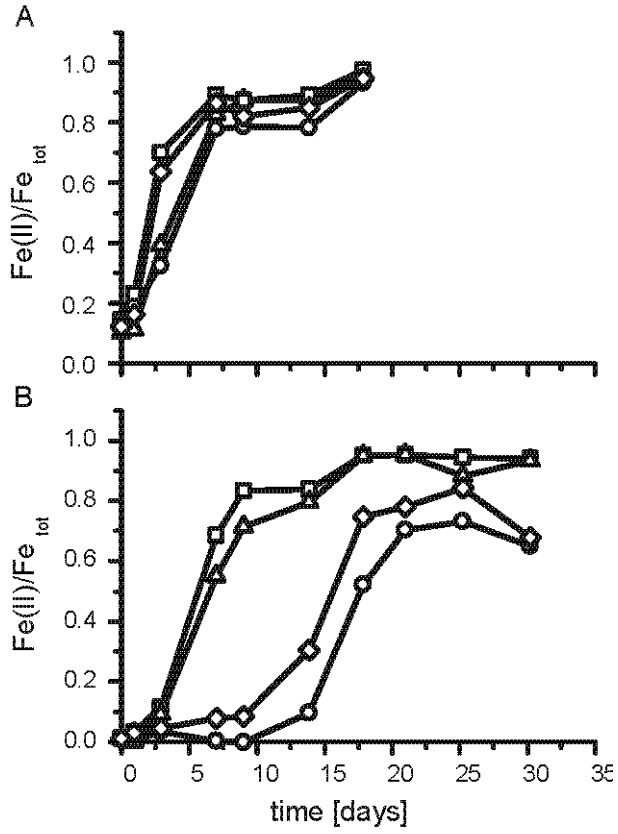

Figure 9.7: Bacterial reduction of Fe(III) by 1 g sample from the spring. A: sample collected from the side of the stream. ◊no addition □addition of 5 mmol L^{-1} lactate and 5 mmol L^{-1} acetate ◯ addition of 10 mmol L^{-1} ferrihydrite △ addition of 5 mmol L^{-1} acetate, 5 mmol L^{-1} lactate and 10 mmol L^{-1} ferrihydrite B: sample collected from the middle of the channel. ◊no addition □addition of 5 mmol L^{-1} lactate and 5 mmol L^{-1} acetate ◯addition of 10 mmol L^{-1} ferrihydrite △addition of 5 mmol L^{-1} acetate, 5 mmol L^{-1} lactate and 10 mmol L^{-1} ferrihydrite. Samples were collected in summer 2010. Due to the slightly different lag-times only one representative out of three parallels is shown.

seasonal sampling dates. The UPGMA diagram (Unweighted Pair Group Method with Arithmetic Mean) (figure 9.8) shows a clear clustering of spring, summer, and winter samples independent of sampling location (microbial mat or flow channel) and distance from the source.

In order to study the microbial diversity in the mats and the flow channel in more detail, bacterial 16S rRNA gene clone libraries were constructed from the samples collected in August 2009 at 1.2 m from the source. In total, 181 clones were analyzed, 96 from the microbial mat and 85 clones from the flow channel. Comparative sequence analysis and calculation of diversity indices were based on a 97% 16S rRNA gene sequence similarity criterion (Hong et al., 2006). In general, the diversity within the microbial mat was higher than in the flow channel. In the flow channel only nine phylotypes were detected, whereas twenty phylotypes were found in the microbial mat sample. Many Fuschna clones showed a high sequence similarity of >97% to sequences of uncultivated microorganisms from other freshwater habitats (table 9.3).

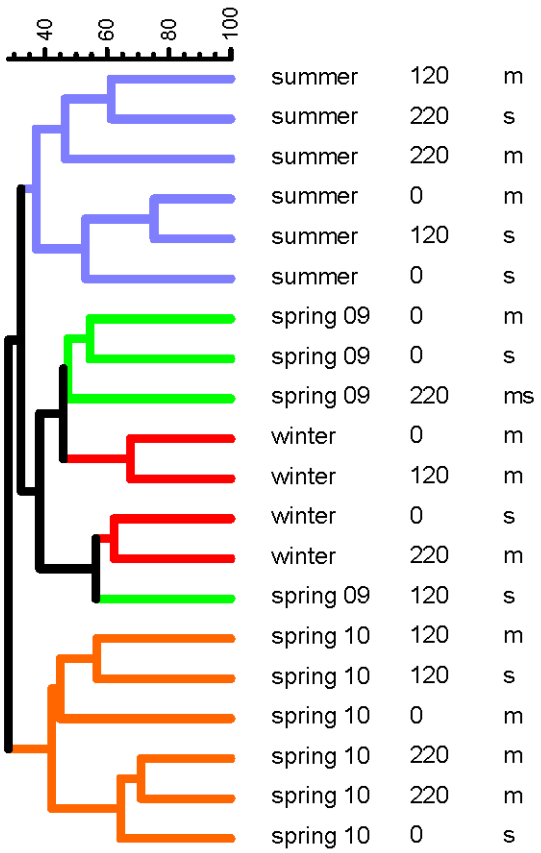

Figure 9.8: Cluster analysis of the microbial communities at alternating seasons by unweighted pair-group mean averaging (UPGMA) depicting the seasonal variations of DGGE banding. Samples were collected three times (spring and summer 2009, winter 2010) either from the microbial mat (side – s) or the flow channel (middle – m).

Clone library coverage based on the Chao-index was 77% for the microbial mat samples and 89% for the flow channel samples, respectively.

Both clone libraries were dominated by proteobacterial sequences with 83% and 87% of total clones, respectively (figure 9.9). However, the diversity within the proteobacteria was higher in the microbial mat samples (10 phylotypes) compared to the flow channel (4 phylotypes). Clones related to bacteria involved in iron cycling were found in both clone libraries: Within the beta-proteobacteria, most clones from the flow channel (1 phylotype) were closely related to known Fe(II)-oxidizers of the genus *Gallionella* (72% of total clones), but only very few clones from the flow channel (2% of total clones) grouped into this phylotype. In contrast, a large fraction of clones from the flow channel (29% of total clones) formed two distinct phylotypes which were affiliated with known Fe(III)-reducers of the genus *Rhodoferax*. Interestingly, *Rhodoferax*-like sequences were only represented by few clones (4% of total clones) in the microbial mat. Additional beta-proteobacterial phylotypes represented by singletons include the uncultivated group H2SRC138 found in the clone library from the flow channel and two phylotypes from the microbial mat which were related to *Ideonella* spp. and *Thiobacter* spp., respectively.

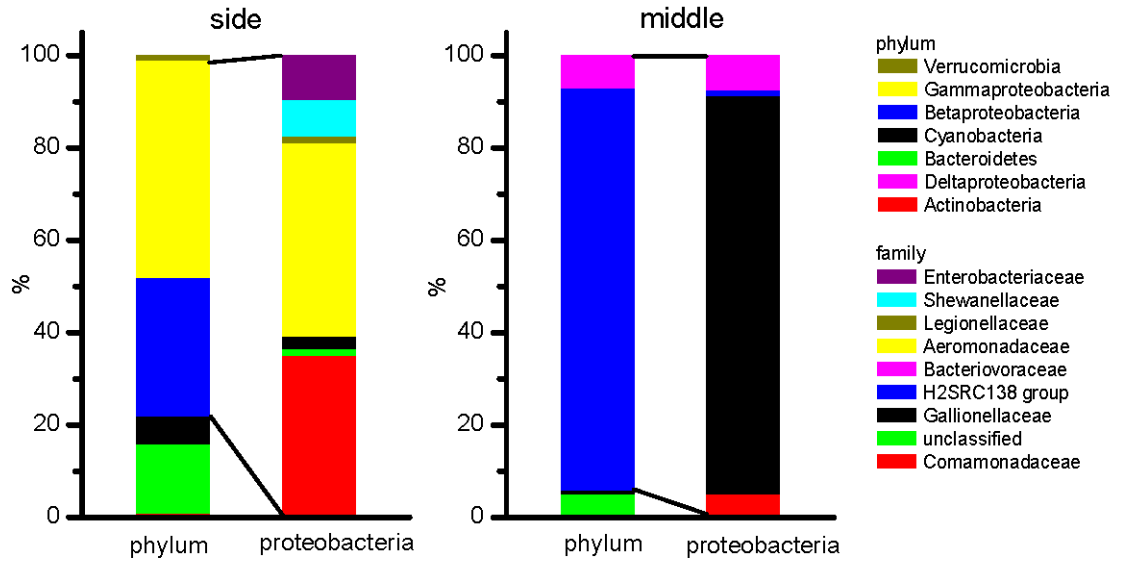

Figure 9.9: Normalized diversity of the bacterial communities determined by a clone library analysis. The samples were collected 1.20 m from the source in August 2009 from either the microbial mat (side) or from the flow channel (middle). The proteobacterial OTUs are shown on the family level. Side: 96 OTUs at phylum level, 74 OTUs for proteobacteria, middle: 85 OTUs at phylum level, 80 OTUs for proteobacteria.)

Within the δ-proteobacteria, one phylotype from the flow channel (6% of total clones) was closely related to the *Bacteriovorax stolpii* (96% sequence similarity). A large fraction of clones from the microbial mat (47% of total clones) was affiliated with the diverse group of gamma-proteobacteria, but no gamma-proteobacterial clone was found in the clone library from the flow channel. One phylotype from the microbial mat (32% of total clones) was affiliated with *Aeromonas punctata* subsp. cavi (Popoff & Veron, 1976). Two other phylotypes, represented by 6% total clones each, were closely related (99% sequence similarity) to the known versatile Fe(III)-reducer *Shewanella putrefaciens* (Nealson & Scott, 2006) and *Buttiauxella noackiae* (Müller et al., 1996), respectively. Additional singletons from the microbial mat grouped with *Plesiomonas* spp. and *Legionella* spp.

All clones related to cyanobacteria fell in subsection III and grouped into one phylotype which was closest related to *Tychonema bourrellyi* (99% sequence similarity) (Anagnostidis & Komárek, 1988, Suda et al., 2002). This phylotype was more abundant in the clone library from the microbial mat than in the clone library from the flow channel where it was only represented by a singleton. We did not expect to detect cyanobacterial DNA within the flow channel because the thick mats were not observable there. Nonetheless, single cyanobacterial cells might have been washed of the mat and thus cyanobacterial DNA was detected within the flow channel. Visual observations suggested though that the cyanobacterial habitat was clearly at the sides of the flow channel. The abundance of the cyanobacterial clones in the library is underestimating the number of cyanobacteria because of the lower number of clones analyzed for this group.

The Bacteroidetes represent the most diverse microbial group found at the Fuschna spring. In total, nine phylotypes dispersed in six microbial families and uncultivated group NS11-12 were detected with the

majority of phylotypes originating from the microbial mat sample. Phylotypes were not shared between sampling sites and each phylotype was only represented by 1-4 clone sequences. Other major microbial lineages which were represented by singletons from the microbial mat include the *Actinobacteria* and *Verrucomicrobia*.

9.5 Discussion

9.5.1 Seasonal and geological controls of spring geochemistry

The geochemical parameters oxygen, Fe(II) concentration and alkalinity were rather stable in spring, summer and autumn (water was frozen in winter and no measurements were done) and their changes along the flow path were similar between sampling campaigns, i.e. the oxygen levels in the water increased to near saturation. Turbulent water flow caused oxygen from the air, but potentially also from cyanobacterial primary production, to mix with the water. Alkalinity – which is a conservative parameter – did not fluctuate strongly between the independent sampling times. This agrees well with the findings of Schotterer et al. (1987), Bissig et al. (2006) that most of the water originates from one source within the host rock while the influence of rain and melt water on the water geochemistry is minor. Therefore, the ion composition of the water mainly results from the host rock and is expected to be comparable over the course of the year (table 9.2). This was supported by the fact that – although the delivery rate of the spring fluctuated between 0.7 L min^{-1} and 1.2 L min^{-1} over the seasons – geochemical parameters did not change strongly during this time.

Concomitant with an increase in dissolved oxygen in the spring water the Fe(II) concentration decreased due to the oxidation of Fe(II) – Fe(III)(oxy)hydroxides formed. The oxidation of Fe(II) is kinetically limited (Davison & Seed, 1983). Therefore, even 2.2 m from the source we still detected Fe(II) despite O_2 was almost saturated in the water and Fe(II) oxidation is thermodynamically favored. Furthermore, Fe(III)-reducing bacteria may have re-reduced Fe(III) to Fe(II) and therefore the decrease in Fe(II) concentration in water would be less than without microbial re-reduction.

In contrast to Fe(II), Fe(III) is only poorly soluble in water at circumneutral pH and precipitates rapidly (Cornell & Schwertmann, 2003). Therefore, no significant amount of dissolved Fe(III) was expected , only colloidal Fe(III) particles prevail. Since we did not filter the water samples used for iron determination in the field we cannot distinguish between particulate and dissolved Fe(III). Furthermore, the stabilization of the water samples in the field with 1 mol L^{-1} HCl led to the dissolution of particulate Fe(III). This explains why the concentration of Fe(III) was in the same range as Fe(II) despite the poor solubility of Fe(III). These results therefore suggest that colloidal Fe(III) particles were transported with the water.

The concentration of calcium (initially >17 mol L^{-1}) is significantly higher than the concentration of Fe(II) (approx. 10-20 µmol L^{-1}). Therefore, a dominance of calcite over other carbonaceous minerals – such as siderite – is expected. Thermodynamic geochemical modeling of mineral precipitation for the ions present in the spring water showed that calcite is expected to precipitate preferentially over dolomite or siderite (figure 9.3). XRD of mineral samples collected at the spring verified the theoretical predictions (figure 9.4) and confirmed the presence of calcite. No other minerals were detected.

The crystallinity of calcite increased with the distance from the source which is likely due to a higher pH (figure 9.2C). The higher pH shifted the geochemical equilibrium towards CO_3^{2-} and thus towards calcite precipitation which is concomitant with a slightly higher crystallinity of the calcite (Stumm & Morgan, 1995). The pH increase with the distance from the source can be attributed to outgasing of CO_2

from the water in combination with the precipitation of calcite (Stumm & Morgan, 1995). The outgasing of CO_2 depends on temperature as well as the partial pressure of CO_2 the air above the water (Stumm & Morgan, 1995). Thus, wind and air temperature affect the rate of CO_2 outgasing and therefore control the concentration of CO_2 and bicarbonate in the water which control the pH. The different outgasing rates may explain the differences in pH-measurements between seasons (figure 9.2C).

Additionally, we determined the total iron concentration in sediment samples collected at the spring. The total concentration of iron in the sediments was only a few weight%. The transport of particulate Fe(III) in the water as well as the reduction of Fe(III) by Fe(III)-reducing bacteria could explain the low concentration of iron in the mineral samples collected.

The crystallinity of Fe(III) mineral phases is known to increase with a decreasing precipitation rate (Schwertmann & Cornell, 2000). Since the Fe(II) concentration in the water decreased with distance from the spring, Fe(III) mineral formation will slow down and thus the crystallinity of the Fe(III) minerals will likely be higher (compare figure 9.2B). Furthermore, interaction of Fe(II) with ferrihydrite could lead to mineral transformation and thus a higher crystallinity (Hansel et al., 2005).

9.5.2 Fe(III) reduction at the field site

Generally the cell number of Fe(III)-reducers determined by the most probable number technique was higher than the cell number of photoferrotrophs and nitrate-reducing Fe(II)-oxidizers. The highest cell number of Fe(III)-reducers was determined in the microbial mat at the source (figure 9.7) and correlates well with the lower crystallinity of the Fe(III) mineral phase (ferrihydrite) at this location (table 9.1, figure 9.5). Due to the lower crystallinity of ferrihydrite at the source we expect Fe(III) being better bioavailable for Fe(III)-reducers. The cell number of Fe(III)-reducers in the middle of the flow channel was not substantially lower than the number in the microbial mats. Potentially, some of the Fe(III)-reducers in the middle were not active or could even switch between Fe(II) oxidation and Fe(III) reduction, similar to *Geobacter metallireducens* (Finneran et al., 2002). The number of active Fe(III)-reducers may be overestimated with the culture-dependent most-probable number cell counts, because cells may live using other electron acceptors of available and only switch to Fe(III) if necessary. *Shewanella putrefaciens* – which was detected at the field site – is well known to be metabolically versatile and thus be able to use other electron acceptors than Fe(III) (Nealson & Scott, 2006, Fredrickson & Zachara, 2008).

The 16S rRNA gene copy number as a proxy for cell number determined with qPCR were in the same order of magnitude as the cell numbers of Fe(III)-reducers determined with most-probable number counting. Therefore, the potential of microbial Fe(III) reduction was likely high in the samples of the field site. Furthermore, the cell number determined with qPCR is similar between samples taken from the microbial mat and from the middle of the flow channel. Most probable number counting showed that more Fe(III)-reducers were present within the microbial mats than in the middle of the flow channel. Therefore, also relatively more Fe(III)-reducers (based on total bacteria determined with qPCR) were present in the microbial mat, thus the potential for Fe(III) reduction is likely even higher in the microbial mats than within the flow channel. Due to the high amount of biomass in the microbial mat we would have expected higher gene copy numbers therein compared to the flow channel. This discrepancy is potentially due to primer-bias underestimating the number of cyanobacteria in the sample.

In order to determine the Fe(III) reduction capacity and rate within the microbial mat and within samples from the flow channel, we set up microcosms supplemented with either electron donor or acceptor and determined the intrinsic Fe(III) reduction kinetics. This allowed determining if the microbial

communities were limited in either electron donor or acceptor at the side or the middle of the flow channel.

In the microbial mats, Fe(III)-reducers were not limited by electron donors (figure 9.7A) and thus cellular Fe(III) reduction in the microcosms started without a significant lag-phase. Electron donors were readily available within the microbial mat due to microbial primary production. Nonetheless, the availability of Fe(III) for Fe(III)-reducers in the microbial mats might be limiting. Two factors control Fe(III) availability: i) the turnover rate, e.g. how fast Fe(II) is re-oxidized, which is directly linked to local oxygen concentrations (e.g., O_2 produced by cyanobacteria in the mats) and ii) the concentration of Fe(III) minerals that are available for bacteria. An increase in Fe(III) in the form of additional ferrihydrite decreased the reduction rate in the microbial mats (figure4A). This showed that iron in the microbial mats was better bioavailable and potentially less crystalline than the chemically synthesized ferrihydrite which was added to the microcosms. This fact, additionally to the very short lag-phase in these experiments, suggested a very active cycling of iron in the microbial mats. These results also agree well with the high fraction (compared to the total copy number of the 16S rRNA gene determined with qPCR) of Fe(III) reducers we determined with MPN counting in the microbial mat while the fraction of Fe(III) reducers of all cells was lower in the middle.

Furthermore, the high reduction rate of Fe(III) in the microbial mats suggests that anoxic zones can prevail in the mat despite the continuous production of O_2 by the cyanobacteria. Heterogeneities in iron speciation in biofilms of *Pseudomonas aeruginosa* have previously been described (Hunter et al., 2008), these heterogeneities could offer the ecological niche for Fe(III) reducers.

In contrast to the microbial mats at the side of the flow channel, we found, that Fe(III)-reducers were not limited in Fe(III) in the middle of the flow channel but rather in electron donors (figure 9.7B). The fixation of carbon in the middle of the flow channel is likely lower than within the microbial mat as only photoferrotrophs as well as microaerophiles are potential primary producers within the flow channel. Other electron donors are only available from the water if organic matter is washed out from the microbial mats at the side of the flow channel.

In order to determine the amount of bioavailable electron donors in the middle of the flow channel, we measured the amount of Fe(III) reduced in these experiments without additional electron donor added (data not shown). 4-5 mmol electrons were bioavailable per gram sediment. This was low and cells might even be inactive due to the limitation in electron donor. The inactivity of cells could also explain the long lag-time before reduction of Fe(III) starts.

9.5.3 Microbial community composition

Cluster analysis of the DGGE band patterns showed that the dominant change in bacterial community composition happened over the course of the seasons and not with increasing distance from the source. Furthermore, bacterial communities of the microbial mat and the middle of the flow path were also different. The differences between side and middle were stronger than the differences with increasing distance from the source (figure 9.8). The increasing distance from the source and the accompanying pH change as well as the changes in geochemical parameters (i.e. CO_2 outgassing) in the water likely influenced the communities less than seasonal variations or the habitat, e.g. growth at the side or in the middle of the flow channel. The strong influence of the seasons is potentially due to the influence of temperature, light and oxygen – especially in winter under a snow-cover. As in most ground-water springs, the water temperature at the source was rather stable over the course of the year (Carlé, 1975). Microbial communities in the flow channel at the source are therefore less affected by the temperature

changes as the communities in the microbial mats (which might for example be frozen in winter). All in all, it is reasonable to assume that the rates of carbon fixation, iron reduction , and iron oxidation will be slower in winter. While the snow covers the water channel, less light could reach the phototrophic microorganisms (Curl et al., 1972). Due to the lack of light, the production of biomass would decrease for phototrophic organisms while chemotrophic bacteria might still thrive. All in all, this likely caused significant microbial community shifts over the course of the year which were reflected in the banding patterns.

In order to better understand the microbial community structure, we constructed 16S rRNA gene clone libraries to identify the microorganisms in the flow channel and in the microbial mat. The samples were collected in August 2009 at 1.2 m from the source. About 30 16S rRNA gene clones sequences were available from a previous, so far unpublished study in 2005 (accession no. from AB475010 to AB475041) by Kurt Hanselmann and co-workers from the University of Zürich. We included these sequences in our analysis although the samples for the 2005 library were taken in October and DGGE analysis revealed a strong shift in microbial community composition with time. However, we do not report the 2005 clone sequences as closest relatives to the 2010 clones because their phylogenetic identification and affiliation have not been described in a publication previously (table 9.4).

A higher diversity in the microbial mat compared to the flow channel is expected since microbial mats are known to host a wide range of microorganisms with various metabolic pathways (Ley et al., 2006). The high number of clones (34% of all proteobacteria) closely related to *Rhodoferax ferrireducens* suggested a high potential for Fe(III) reduction within the microbial mats. This was also confirmed by our microcosm experiments (figure 9.7). Only a few clones related to *Gallionella* suggested microaerophilic Fe(II) oxidation in the microbial mat. This can be expected as microaerophilic Fe(II)-oxidizers require low oxygen concentration (below 10 µmol L^{-1} (Druschel et al., 2008)) in order to be not kinetically outcompeted by the chemical oxidation of Fe(II) with O_2. These results agree well with the qPCR data which show that only 0.004% of the amplifiable 16S-rRNA belongs to *Gallionella* species. Among the *Shewanellaceae* (6% of all bacterial clones in the mat library) many are known Fe(III)-reducers, although they are also known as metabolically versatile microorganisms with the potential to exhibit many different physiologies in a complex stratified mat environment (Nealson & Scott, 2006, Fredrickson & Zachara, 2008). Among the *Aeromonadaceae* are many facultative pathogens which are known to be capable of a variety of different metabolisms including nitrate reduction and the fermentative use of organic acids (Popoff & Veron, 1976). The *Buttiauxella* strains – making up 6% of the total clones in the microbial mats – are known for their versatile metabolism (Müller et al., 1996). These bacteria are often found in the intestines of mollusks (Müller et al., 1996) – thus they might represent a feature originating from snails feeding on the microbial mats.

The clones of the cyanobacteria indicated that the cyanobacteria were all closely related and they were 99% similar to *Tychonema bourrellyi*. These findings agree well with DGGE analysis of the cyanobacterial diversity in the microbial mats which indicated that the mats were dominated by only one species of cyanobacteria. The DGGE results therefore justify the low number of clones (7) sequenced. *Tychonema bourrellyi* – the closest relative – prefers oligotrophic to slightly eutrophic waters in rather cold environments (Anagnostidis & Komárek, 1988, Suda et al., 2002, and references therein). These findings agree well with the geochemical settings at the field site.

The microbial mats established only at the side of the flow channel (figure 9.1A and B). Likely the water flow in the channel is too fast to allow cyanobacterial filaments growing into the channel without them being washed off. Additionally, cyanobacteria may interact with the Fe(III) minerals precipitating

in the flow channel. These could adsorb to the cell surface (Brown et al., 2010) and cells could encrust similarly to some Fe(II)-oxidizing bacteria (Schaedler et al., 2009, and references therein).

In the samples collected from the middle of the flow channel microaerophilic iron-oxidizing *Gallionellaceae* dominated the clone library (81% of all clones). *Gallionella* sp. are known to utilize the oxygen to oxidize Fe(II) microaerophilically (Hanert, 2006). Quantification of amplifiable 16S-RNA with qPCR showed that 10% of all bacterial amplifiable 16S-rRNA belonged to *Gallionella* species. The number of *Gallionella* specific 16S-rRNA gene copies detected with qPCR and the number of *Gallionella*-clones in the clone library within the flow channel is in the same order of magnitude and thus agrees well. These numbers reflect the geochemical conditions (e.g. elevated Fe(II) concentration and initially low O_2) in the flow channel well.

Furthermore, we would expect that the abundance of *Gallionella* decreased further downstream because these bacteria need to outcompete O_2 for the oxidation of Fe(II) which becomes difficult with the increasing oxygen concentration further downstream (figure 9.2 (Druschel et al., 2008, Emerson et al., 2010). The additional clones (8%) found in the flow channel were related to *Bacteriovorax stolpii* (96% similarity) which is a known facultative predatory microorganism living on other bacteria (Baer et al., 2000).

Other geomicrobiological studies on chalybeate surface waters are scarce. James & Ferris (2004) identified microaerophilic Fe(II)-oxidizers in a creek by morphological comparison and found mostly microaerophilic Fe(II)-oxidizers. An enhancement of the Fe(II) oxidation rate by microaerophilic Fe(II)-oxidizers was found in this study. James & Ferris (2004) did neither detect photoferrotrophs or nitrate-reducing Fe(II)-oxidizers nor Fe(III)-reducers, simply because they do not have specific morphological features which would allow their visual identification.

In the study of Wagner et al. (2007) a clone library was constructed for a chalybeate spring with high bicarbonate concentrations similar to the spring described in this study. Wagner et al. (2007) used proteobacterial 16S rRNA gene primers and identified several *Gallionella* and *Leptothrix* clones. Furthermore, Wagner et al. (2007) found sequences of *Rhodoferax fermentans*, an Fe(III)-reducer related to *Rhodoferax ferrireducens* – which we found in our library.

Duckworth et al. (2009) also used bacterial 16S rRNA gene primers and found *Gallionella* and *Leptothrix* related species in the chalybeate creek water of West Berry Creek. A further comparison of the clone libraries of Duckworth et al. (2009) with the library constructed in this study was difficult due to elevated concentrations of total organic carbon (1.8 - 3.0 mg L^{-1}) and the presence of siderophores in the creek. Nonetheless, two independent sampling locations were chosen in their study and a clear difference in the microbial community between the habitats was evident (Duckworth et al., 2009). These results agree with our results which also show significant differences in the microbial community between the microbial mat and the flow channel. The diversity of the microbial communities in the study of Duckworth et al. (2009) was much higher than in our study. This could be related to the more complex habitat with additional carbon and siderophores being present and an unclear influx of organic matter. Duckworth et al. (2009) also detected Fe(III)-reducers and Fe(II)-oxidizers and suggested from this data that the potential for Fe-cycling exists. Other bacteria not involved in iron-cycling were also found which is likely due to the higher concentrations of other substrates (Duckworth et al., 2009).

Finally, Bruun et al. (2010) found microaerophilic Fe(II)-oxidizers of the *Gallionella* and *Sideroxydans* species in an iron-rich freshwater seep while iron-reduction was carried out by *Geobacter* species. They found that a complex mixture of organic substrates was enhancing Fe(III) reduction better than the addition of acetate (Bruun et al., 2010). These findings are comparable to our findings: Fe(III) reduction was delayed in samples collected in the flow channel compared to the Fe(III) reduction in the microbial

mats mats where a more complex mixture of organic substrates is present.

The mentioned studies (James & Ferris, 2004, Wagner et al., 2007, Duckworth et al., 2009, Bruun et al., 2010) and our study suggest a strong contribution of microaerophilic Fe(II)-oxidizers in freshwater habitats while nitrate-reducing Fe(II)-oxidizers and photoferrotrophs likely contribute less to the oxidation of Fe(II).

9.5.4 Conclusions

Overall, the Fuschna spring is a well defined system with a known influx of ions through the spring water. Therefore, all primary biomass production at the spring is based on two distinct processes: phototrophy, e.g. by cyanobacteria and photoferrotrophs, and chemotrophy by microaerophilic oxidation of Fe(II) by bacteria such as Gallionella species. Fe(III) reduction is strictly coupled to the breakdown of molecules produced by microbial primary producers. Therefore, this system is well suited to study microbial iron cycling decoupled from the input of other organic sources.

Furthermore, this system may be used to study the interaction of microbial Fe(II)-oxidation coupled to oxygen production by cyanobacteria - similar to one of the proposed Fe(II) oxidation mechanisms which lead to the formation of banded iron formations in the late Precambrian (Emerson et al., 2010). Even the high bicarbonate concentration in the spring water is similar to the concentration of bicarbonate suggested to be present in the Precambrian oceans (approx. 50 mmol L^{-1} in the spring water to 70 mmol L^{-1} in ocean waters (Grotzinger & Kasting, 1993)).

Overall, the role of iron metabolizing bacteria in past and present may be studied at this field site.

Acknowledgments

We hereby thank Urs Dippon, Christian Schröder, Inga Köhler and Christoph Berthold for help with the mineral identification, Martin Obst and Niko Hagemann for help with the SEM, Ellen Struve for IC-measurements and Petra Kühner for the qPCR.

Bibliography

Anagnostidis, K & Komárek, J: Modern approach to the classification system of cyanophytes. 3-oscillatoriales. *Archiv für Hydrobiologie*, 80:327–472, 1988.

Baer, ML; Ravel, J; Chun, J; Hill, RT; & Williams, HN: A proposal for the reclassification of *Bdellovibrio stolpii* and *Bdellovibrio starrii* into a new genus, *Bacteriovorax* gen. nov. as *Bacteriovorax stolpii* comb. nov. and *Bacteriovorax starrii* comb. nov., respectively. *International Journal of Systematic and Evolutionary Microbiology*, 50:219–24, 2000.

Bissig, P: Die CO_2-reichen Mineralquellen von Scuol-Tarasp (Unterengadin, Kt. GR). *Bulletin für angewandte Geologie*, 9:39–47, 2004.

Bissig, P; Goldscheider, N; Mayoraz, J; Surbeck, H; & Vuataz, FD: Carbogaseous spring waters, coldwater geysers and dry co_2 exhalations in the tectonic window of the Lower Engadine Valley, Switzerland. *Eclogae Geologicae Helvetiae*, 99:143–155, 2006.

Brown, I; Bryant, DA; Casamatta, D; Thomas-Keprta, KL; Sarkisova, SA; Shen, G; Graham, JE; Boyd, ES; Peters, JW; Garrison, DH; & McKay, DS: Polyphasic characterization of a thermotolerant siderophilic filamentous cyanobacterium that produces intracellular iron deposits. *Applied and Environmental Microbiology*, 2010.

Bruun, AM; Finster, K; Gunnlaugsson, HP; Nornberg, P; & Friedrich, MW: A comprehensive investigation on iron cycling in a freshwater seep including microscopy, cultivation and molecular community analysis. *Geomicrobiology Journal*, 27:15–34, 2010.

Carlé, W: *Die Mineral- und Thermalwässer von Mitteleuropa* (Wissenschaftliche Verlagsgesellschaft, Stuttgart), 1975.

Châtellier, X & Fortin, D: Adsorption of ferrous ions onto *Bacillus subtilis* cells. *Chemical Geology*, 212:209–228, 2004.

Châtellier, X; Fortin, D; West, MM; Leppard, GG; & Ferris, FG: Effect of the presence of bacterial surfaces during the synthesis of Fe oxides by oxidation of ferrous ions. *European Journal of Mineralogy*, 13:705–714, 2001.

Cochran, WG: Estimation of bacterial densities by means of the "most probable number". *Biometrics*, 6:105–16, 1950.

Cornell, RM & Schwertmann, U: *The iron oxides: structure, properties, reactions, occurrences and uses* (VCH, Weinheim, Cambridge), 2nd ed., 2003.

Curl, J, Herbert; Hardy, JT; & Ellermeier, R: Spectral absorption of solar radiation in alpine snowfields. *Ecology*, 53:1189–1194, 1972.

Davison, W & Seed, G: The kinetics of the oxidation of ferrous iron in synthetic and natural waters. *Geochimica et Cosmochimica Acta*, 47:67–79, 1983.

Druschel, GK; Emerson, D; Sutka, R; Suchecki, P; & Luther, GW: Low oxygen and chemical kinetic constraints on the geochemical niche of neutrophilic iron(ii) oxidizing microorganisms. *Geochimica et Cosmochimica Acta*, 72:3358–3370, 2008.

Duckworth, OW; Holmstrom, SJM; Pena, J; & Sposito, G: Biogeochemistry of iron oxidation in a circumneutral freshwater habitat. *Chemical Geology*, 260:149–158, 2009.

Eaton, A; Clesceri, L; Rice, E; & Greenberg, A: *Standard methods for the Examination of Water and Wastewater* (American Public Health Association, Maryland), 21st ed., 2005.

Emerson, D; Fleming, EJ; & McBeth, JM: Iron-oxidizing bacteria: an environmental and genomic perspective. *Annual Review of Microbiology*, 64:561–83, 2010.

Emerson, D & Moyer, C: Isolation and characterization of novel iron-oxidizing bacteria that grow at circumneutral pH. *Applied and Environmental Microbiology*, 63:4784–4792, 1997.

Finneran, KT; Housewright, ME; & Lovley, DR: Multiple influences of nitrate on uranium solubility during bioremediation of uranium-contaminated subsurface sediments. *Environmental Microbiology*, 4:510–6, 2002.

Fortin, D: What biogenic minerals tell us. *Science*, 303:1618–1619, 2004.

Fortin, D & Langley, S: Formation and occurrence of biogenic iron-rich minerals. *Earth-Science Reviews*, 72:1–19, 2005.

Fredrickson, JK & Zachara, JM: Electron transfer at the microbe-mineral interface: a grand challenge in biogeochemistry. *Geobiology*, 6:245–253, 2008.

Gault, AG; Ibrahim, A; Langley, S; Renaud, R; Takahashi, Y; Boothman, C; Lloyd, JR; Clark, ID; Ferris, FG; & Fortin, D: Microbial and geochemical features suggest iron redox cycling within bacteriogenic iron oxide-rich sediments. *Chemical Geology*, 281:41–51, 2011.

Green, S; Leigh, M; & Neufeld, J: Denaturing gradient gel electrophoresis (dgge) for microbial community analysis. In K Timmis, ed., *Handbook of Hydrocarbon and Lipid Microbiology.*, pp. 4137–4158 (Springer, Heidelberg, Germany), 2009.

Grotzinger, JP & Kasting, JF: New constraints on precambrian ocean composition. *Journal of Geology*, 101:235–243, 1993.

Hanert, H: *The Genus Gallionella*, vol. Proteobacteria: Delta, Epsilon subclass, pp. 996–997 (Springer), 2006.

Hansel, CM; Benner, SG; & Fendorf, S: Competing fe (ii)-induced mineralization pathways of ferrihydrite. *Environmental Science & Technology*, 39:7147–53, 2005.

Hegler, F; Posth, NR; Jiang, J; & Kappler, A: Physiology of phototrophic iron(II)-oxidizing bacteria – implications for modern and ancient environments. *FEMS Microbiology Ecology*, 66:250–260, 2008.

Heinzel, E; Janneck, E; Glombitza, F; Schlomann, M; & Seifert, J: Population dynamics of iron-oxidizing communities in pilot plants for the treatment of acid mine waters. *Environmental Science and Technology*, 43:6138–44, 2009.

Hong, SH; Bunge, J; Jeon, SO; & Epstein, SS: Predicting microbial species richness. *Proceedings of the National Academy of Sciences*, 103:117–22, 2006.

Hunter, RC; Hitchcock, AP; Dynes, JJ; Obst, M; & Beveridge, TJ: Mapping the speciation of iron in *Pseudomonas aeruginosa* biofilms using scanning transmission X-ray microscopy. *Environmental Science & Technology*, 42:8766–8772, 2008.

James, RE & Ferris, FG: Evidence for microbial-mediated iron oxidation at a neutrophilic groundwater spring. *Chemical Geology*, 212:301–311, 2004.

Kappler, A; Konhauser, KO; & Newman, DK: The potential significance of microbial Fe(III) reduction during deposition of precambrian banded iron formations. *Geobiology*, 3:167–177, 2005.

Kappler, A & Newman, DK: Formation of Fe(III)-minerals by Fe(II)-oxidizing photoautotrophic bacteria. *Geochimica et Cosmochimica Acta*, 68:1217–1226, 2004.

Kappler, A & Straub, KL: Geomicrobiological cycling of iron. *Reviews in Mineralogy & Geochemistry*, 59:85–108, 2005.

Klee, AJ: A computer program for the determination of most probable number and its confidence limits. *Journal of Microbiological Methods*, 18:91–98, 1993.

Larese-Casanova, P; Haderlein, S; & Kappler, A: Biomineralization of lepidocrocite and goethite by nitrate-reducing Fe(II)-oxidizing bacteria: Effect of pH, bicarbonate, phosphate and humic acids. *Geochimica Et Cosmochimica Acta*, 74:3721–3734, 2010.

Ley, RE; Harris, JK; Wilcox, J; Spear, JR; Miller, SR; Bebout, BM; Maresca, JA; Bryant, DA; Sogin, ML; & Pace, NR: Unexpected diversity and complexity of the guerrero negro hypersaline microbial mat. *Applied Environmental Microbiology*, 72:3685–95, 2006.

Li, D; Li, Z; Yu, J; Cao, N; Liu, R; & Yang, M: Characterization of bacterial community structure in a drinking water distribution system during an occurrence of red water. *Applied and Environmental Microbiology*, 76:7171–7180, 2010.

Lovley, DR: Dissimilatory Fe(III) and Mn(IV) reduction. *Microbiology and Molecular Biology Reviews*, 55:259–287, 1991.

Ludwig, W; Strunk, O; Westram, R; Richter, L; Meier, H; Yadhukumar; Buchner, A; Lai, T; Steppi, S; Jobb, G; Forster, W; Brettske, I; Gerber, S; Ginhart, AW; Gross, O; Grumann, S; Hermann, S; Jost, R; Konig, A; Liss, T; Lussmann, R; May, M; Nonhoff, B; Reichel, B; Strehlow,

R; Stamatakis, A; Stuckmann, N; Vilbig, A; Lenke, M; Ludwig, T; Bode, A; & Schleifer, KH: ARB: a software environment for sequence data. *Nucleic Acids Research*, 32:1363–71, 2004.

Müller, HE; Brenner, DJ; Fanning, GR; Grimont, PAD; & Kämpfer, P: Emended description of *Buttiauxella agrestis* with recognition of six new species of *Buttiauxella* and two new species of *Kluyvera*: *Buttiauxella ferragutiae* sp. nov., *Buttiauxella gaviniae* sp. nov., *Buttiauxella brennerae* sp. nov., *Buttiauxella izardii* sp. nov., *Buttiauxella noackiae* sp. nov., *Buttiauxella warmboldiae* sp. nov., *Kluyvera cochleae* sp. nov., and *Kluyvera georgiana* sp. nov. *International Journal of Systematic Bacteriology*, 46:50–63, 1996.

Muyzer, G; Teske, A; Wirsen, CO; & Jannasch, HW: Phylogenetic-relationships of *Thiomicrospira* species and their identification in deep-sea hydrothermal vent samples by denaturing gradient gel-electrophoresis of 16S RDNA fragments. *Archives of Microbiology*, 164:165–172, 1995.

Nadkarni, MA; Martin, FE; Jacques, NA; & Hunter, N: Determination of bacterial load by real-time PCR using a broad-range (universal) probe and primers set. *Microbiology*, 148:257–266, 2002.

Nealson, K & Scott, J: *Ecophysiology of the Genus Shewanella*, vol. Volume 6: Proteobacteria: Gamma Subclass, chap. Section 3.3, pp. 1133–1151 (Springer, New York), 2006.

Nubel, U; Garcia-Pichel, F; & Muyzer, G: Pcr primers to amplify 16s rrna genes from cyanobacteria. *Applied and Environmental Microbiology*, 63:3327–32, 1997.

Popoff, M & Veron, M: A taxonomic study of the *Aeromonas hydrophila- Aeromonas punctata* group. *Journal of General Microbiology*, 94:11–22, 1976.

Pruesse, E; Quast, C; Knittel, K; Fuchs, BM; Ludwig, WG; Peplies, J; & Glockner, FO: Silva: a comprehensive online resource for quality checked and aligned ribosomal rna sequence data compatible with arb. *Nucleic Acids Research*, 35:7188–7196, 2007.

Ratering, S & Schnell, S: Nitrate-dependent iron(II) oxidation in paddy soil. *Environmental Microbiology*, 3:100–109, 2001.

Raven, KP; Jain, A; & Loeppert, RH: Arsenite and arsenate adsorption on ferrihydrite: Kinetics, equilibrium, and adsorption envelopes. *Environmental Science & Technology*, 32:344–349, 1998.

Roden, EE; Sobolev, D; Glazer, B; & Luther, GW: Potential for microscale bacterial fe redox cycling at the aerobic-anaerobic interface. *Geomicrobiology Journal*, 21:379–391, 2004.

Schaedler, S; Burkhardt, C; Hegler, F; Straub, KL; Miot, J; Benzerara, K; & Kappler, A: Formation of cell-iron-mineral aggregates by phototrophic and nitrate reducing anaerobic Fe(II)-oxidizing bacteria. *Geomicrobiology Journal*, 26:93–103, 2009.

Schloss, PD; Westcott, SL; Ryabin, T; Hall, JR; Hartmann, M; Hollister, EB; Lesniewski, RA; Oakley, BB; Parks, DH; Robinson, CJ; Sahl, JW; Stres, B; Thallinger, GG; Van Horn, DJ; & Weber, CF: Introducing mothur: Open-source, platform-independent, community-supported software for describing and comparing microbial communities. *Applied and Environmental Microbiology*, 75:7537–7541, 2009.

Schönhuber, W; Zarda, B; Eix, S; Rippka, R; Herdman, M; Ludwig, W; & Amann, R: In situ identification of cyanobacteria with horseradish peroxidase-labeled, rRNA-targeted oligonucleotide probes. *Applied and Environmental Microbiology*, 65:1259–67, 1999.

Schotterer, U; Siegenthaler, U; Oeschger, H; Riesen, T; MÃ¼ller, I; & Kelts, K: Isotopic geochemistry of the engadine mineral springs of scuol-tarasp, switzerland. In *Isotope Techniques in Water Resources Development (Vienna, 30 March - 3 April 1987)*, pp. 277–286. 1987.

Schwertmann, U & Cornell, RM: *Iron oxides in the laboratory : preparation and characterization* (Wiley-VCH, Weinheim), 2nd ed., 2000.

Straub, KL; Benz, M; Schink, B; & Widdel, F: Anaerobic, nitrate-dependent microbial oxidation of ferrous iron. *Applied and Environmental Microbiology*, 62:1458–1460, 1996.

Straub, KL; Schonhuber, WA; Buchholz-Cleven, BEE; & Schink, B: Diversity of ferrous iron-oxidizing, nitrate-reducing bacteria and their involvement in oxygen-independent iron cycling. *Geomicrobiology Journal*, 21:371–378, 2004.

Stumm, W & Morgan, JJ: *Aquatic chemistry: chemical equilibria and rates in natural waters* (Wiley-Interscience, New York), 3rd ed., 1995.

Suda, S; Watanabe, MM; Otsuka, S; Mahakahant, A; Yongmanitchai, W; Nopartnaraporn, N; Liu, Y; & Day, JG: Taxonomic revision of water-bloom-forming species of oscillatorioid cyanobacteria. *International Journal of Systematic and Evolutionary Microbiology*, 52:1577–1595, 2002.

Tschech, A & Pfennig, N: Growth yield increase linked to caffeate reduction in *Acetobacterium woodii*. *Archives of Microbiology*, 137:163–167, 1984.

Wagner, C; Mau, M; Schlömann, M; Heinicke, J; & Koch, U: Characterization of the bacterial flora in mineral waters in upstreaming fluids of deep igneous rock aquifers. *Journal of Geophysical Research*, 112:1–8, 2007.

Weber, KA; Urrutia, MM; Churchill, PF; Kukkadapu, RK; & Roden, EE: Anaerobic redox cycling of iron by freshwater sediment microorganisms. *Environmental Microbiology*, 8:100–113, 2006.

Wexsteen, P; Jaffé, FC; & Mazor, E: Geochemistry of cold co2-rich springs of the scuol-tarasp region, lower engadine, swiss alps. *Journal of Hydrogeology*, 104:77–92, 1988.

Widdel, F: *Anaerober Abbau von Fettsäuren und Benzoesäure durch neu isolierte Arten*. Ph.D. thesis, Universität Göttingen, Göttingen, 1980.

Widdel, F & Pfennig, N: Studies on dissimilatory sulfate-reducing bacteria that decompose fatty acids. i. isolation of a new sulfate-reducer enriched with acetate from saline environments. description of desulfobacter postgatei gen. nov. sp. nov. *Archives of Microbiology*, 129:395–400, 1981.

Widdel, F; Schnell, S; Heising, S; Ehrenreich, A; Assmus, B; & Schink, B: Ferrous iron oxidation by anoxygenic phototrophic bacteria. *Nature*, 362:834–836, 1993.

Zhou, J; Bruns, MA; & Tiedje, JM: DNA recovery from soils of diverse composition. *Applied and Environmental Microbiology*, 62:316–22, 1996.

Supporting information "Geomicrobiology of an iron-carbonate spring"

Table 9.2: Primers used for the DGGE and clone library are clearly marked while PCRs for the Archaea primers yielded no product in this study (a – for DGGE, b – for clone, c – for qPCR library)

Primer	Target group	Sequence (5'->3')	Reference and notes
Cya359F-GC[a]	Cyanobacteria	CGCCCGGGGCGCGCCCCGGG CGGGGCGGGGGCACGGGGGG GGGGAATYTTCCGCAATGGG	(Nubel et al., 1997)
CYA785R[a]	Cyanobacteria	GACTACWGGGGTATCTAATCC	(Lee et al., 1993)
GC-341-F (GM5-F-GC)[a]	Bacteria	CGCCCGCCGCGCCCCGCGCC CGTCCCGCCGCCCCCGCCCG CCTACGGGAGGCAGCAG	Modified after (Muyzer et al., 1995)
907-R[a]	Bacteria	CCGTCAATTCCTTTRAGTTT	(Muyzer et al., 1993)
GC-ARCH344F[a]	Archaea	CGCCCGCCGCGCGCGGCGGG CGGGGCGGGGGCACGGGGGA CGGGGYGCAGCAGGCGCGA	(Lane, 1991)
ARCH519R[a]	Archaea	GWATTACCGCGGCKGCTG	(Bano et al., 2004)
GC-ARCH357F[a]	Archaea	CGCCCGCCGCGCGCGGCGG GCGGGGCGGGGGCACGGGGG CCCTACGGGGCGCAGCAG	(Yu et al., 2008)
Cya359F-TL1[b]	Cyanobacteria	GRGGAATTTTCCGCAATGGG	modified after (Nubel et al., 1997)
ARCH693R[a]	Archaea	GGATTACARGATTTC	(Yu et al., 2008)
CYA1342R[b]	Cyanobacteria	GACCTGCAATTACTAGCG	(Schönhuber et al., 1999)
GM3-8F[b]	Bacteria	AGAGTTTGATCMTGGCTCAG	(Muyzer et al., 1995)
Uni1392R[b]	Bacteria	ACGGGCGGTGTGTRC	(Pace et al., 1986)
341F[c]	Bacteria	CCTACGGGAGGCAGCAG	For qPCR (Muyzer et al., 1995)
797R[c]	Bacteria	GGACTACCAGGGTATCTAATC CTGTT	For qPCR (Nadkarni et al., 2002)
GAL214F[c]	*Gallionella* spp.	CCTCTCGCTTTCGGAGTGGCCG	For qPCR (Li et al., 2010)
GAL384R[c]	*Gallionella* spp.	GGTATGGCTGGATCAGGC	For qPCR (Heinzel et al., 2009)

Table 9.3: Geochemical parameters of the spring, samples collected in August 2009. Concentrations for sodium, nitrate, nitrite and brome were below the detection limit of the IC.

meter [m]	**°C**	**O_2 [μM]**	**pH**	**Fe(II)/ Fe_{tot}**
0 ± 0.05	10.8 ± 0.1	15 ± 1	6.3 ± 0.05	0.80± 0.03
1.2 ± 0.05	12.5 ± 0.1	140 ± 7	6.5 ± 0.05	0.65± 0.03
2.2 ± 0.05	14.5 ± 0.01	217 ± 11	6.7 ± 0.05	0.6 ± 0.03
P_{total} [μM]	**K [mM]**	**Mg [mM]**	**Ca [mM]**	**F [μM]**
0.09 ± 0.01	0.3 ± 0.03	2.2 ± 0.01	17.4 ± 0.6	32 ± 1
0.24 ± 0.02	0.3 ± 0.01	2.2 ± 0.2	16.0 ± 0.7	28 ± 1
0.21 ± 0.02	0.3 ± 0.01	2.2 ± 0.2	13.4 ± 0.8	19 ± 0.1
Cl [mM]	**SO_4^{2-} [mM]**	**$CaCO_3$ [mM]**	**alkalinity [mM]**	**delivery [L/min]**
0.2 ± 0.003	0.5 ± 0.03	44 ± 1	51 ± 2	1.1 ± 0.05
0.2 ± 0.01	0.8 ± 0.07	28 ± 1	51 ± 2	
0.2 ± 0.01	0.8 ± 0.06	20 ± 0.1	48 ± 2	

Table 9.4: List of clone of each OTU and the best blast hit based on the 16S-rRNA gene for samples collected 1.2 m from the source in August 2009.

				total	middle	side	closest cultured	accession #	similarity %	representative clone of each OTU	remarks	best blast hit	accession #	similarity %
Bacteria				**181**	**85**	**96**								
Actino-bacteria	*Actino-mycetales*	*Micro-bacteria-ceae*		1	0	1	*Salinibacterium amurskyense*	AF-539697	96	Fuschna-P4-H05		clone from unvegetated, perhumid, recently-deglaciated soil	GQ-397018	99
Bactero-idetes	*Bactero-idales*	*Por-phyro-mona-daceae*	OTU1	2	0	2	*Paludibacter propionici-genes*	AB-078842	97	Fuschna-P5-H01		clone from sub-merged biofilm mats of a mon-tane wetland in the Alps close to Cadagno di Fuori, Switzer-land	AB-478675	98
			OTU2	4	0	4	*Paludibacter propionici-genes*	AB078842	95	Fuschna-P5-E06		clone from limestone-corroding stream biofilm, Frasassi cave system, Italy	DQ415777	97
	Flavo-bacter-iales	*Cryo-morph-aceae*		2	2	0	*Owenweeksia hongkongen-sis*	AB-125062	88	Fuschna-P4-G09		clone from ammonia-removing biofilm from a trickling filter at Kollikon, Switzerland	AJ-224942	94

Table 9.4: List of clone of each OTU and the best blast hit based on the 16S-rRNA gene for samples collected 1.2 m from the source in August 2009.

		total	middle	side	closest cultured	accession #	similarity %	representative clone of each OTU	remarks	best blast hit	accession #	similarity %
	Flavobacteriaceae	1	0	1	*Actibacter sediminis*	EF-670651	91	Fuschna-P3-G09		clone from deep sea hydrothermal vent sediment, East Lau spreading center	GQ-848480	94
Sphingobacteriales	*Chitinophagaceae*	3	0	3	*Chitinophaga sancti*	M62795	91	Fuschna-P4-D06		clone from a paper pulp column	EF-562550	98
		2	2	0	*Sediminibacterium salmoneum*	EF-407879	97	Fuschna-P5-C08		clone from lake water, Lake Tanggulha, Tibet	HM-128469	98
	Sphingobacteriaceae	1	0	1	*Solitalea canadensis*	AB-078046	91	Fuschna-P4-H01		clone from lake sediment, Lake Constance, Germany	EU-580471	99
		2	0	2	*Pedobacter terricola*	EF-446147	93	Fuschna-P5-A04		clone from lake sediment, Lake Constance, Germany	EU-580501	95
	NS11-12 marine group	1	0	1	*Solitalea koreensis*	EU-787448	86	Fuschna-P3-C07	→ Mothur: PHOS-HE51	clone from an autotrophic nitrifying bioreactor	FJ-529921	94

Table 9.4: List of clone of each OTU and the best blast hit based on the 16S-rRNA gene for samples collected 1.2 m from the source in August 2009.

				total	middle	side	closest cultured	accession #	similarity %	representative clone of each OTU	remarks	best blast hit	accession #	similarity %
Cyano-bacteria		*Subsection III*		7	1	6	*Tychonema bourrellyi*	AB-045897	99	Fuschna-P5-F06		clone from biofilm on rock surface in karstwater stream, Germany	GQ-324965	99
Beta-proteo-bacteria	*Burk-holder-iales*	*Comamona-daceae*		1	0	1	*Ideonella azo-tifigens*	EU-542576	97	Fuschna-P4-C05		clone from sediment at submerged sinkhole, Lake Huron	GQ-406152	99
			OTU1	26	4	22	*Rhodoferax ferrireducens*	AF-435948	98	Fuschna-P5-D04	$\rightarrow$ 1^{st} non-Fuschna clone: clone from coal tar waste-contaminated groundwater, FJ810573, 97%	clone from Fuschna spring (database release only)	AB-475011	98
			OTU2	3	0	3	*Rhodoferax ferrireducens*	AF-435948	98	Fuschna-P5-G03		clone from low-temperature biodegraded oil reservior, Canada	AY-570588	
		unclassified		1	0	1	*Thiobacter subterraneus*	AB-180657	92	Fuschna-P4-H03		clone from spring water, Wettinquelle, Germany	AM-167943	99

Table 9.4: List of clone of each OTU and the best blast hit based on the 16S-rRNA gene for samples collected 1.2 m from the source in August 2009.

			total	middle	side	closest cultured	accession #	similarity %	representative clone of each OTU	remarks	best blast hit	accession #	similarity %
	Nitroso-monadales	*Gallionellaceae*	71	69	2	*Gallionella ferruginea*	L07897	97	Fuschna-P4-E07	→ 1^{st} non-Fuschna clone: clone from riparian iron oxidizing biofilm, EU937883, 98%	clone from Fuschna spring (database release only)	AB-475021	99
		H2SRC138 group	1	1	0	*n/a*			Fuschna-P4-B09	→ Mothur: Gallionella, '→ 1^{st} non-Fuschna clone: clone from Chesapeake Bay, USA, EU801652, 88%	clone from Fuschna spring (database release only)	AB-475021	89
Delta-proteo-bacteria	*Bdello-vibrionales*	*Bacterio-voraceae*	6	6	0	*Bacteriovorax stolpii*	AJ-288899	96	Fuschna-P5-E09		clone from lake water, Lake Fuchskuhle, Germany	AJ-290009	
Gamma-proteo-bacteria	*Aerom-onadales*	*Aero-monada-ceae*	31	0	31	*Aeromonas punctata subsp. cavi*	X74674	99	Fuschna-P5-C02	→ OTU dispersed on branch, other Aeromonas spp. closer to subset	clone from pond water with fish septicaemia, China	GU-205198	99

Table 9.4: List of clone of each OTU and the best blast hit based on the 16S-rRNA gene for samples collected 1.2 m from the source in August 2009.

			total	middle	side	closest cultured	accession #	similarity %	representative clone of each OTU	remarks	best blast hit	accession #	similarity %
	Alteromonadales	*Shewanellaceae*	6	0	6	*Shewanella putrefaciens*	X81623	99	Fuschna-P4-G01		clone from microbial mats, Zloty Stok gold mine, Poland	GU-191139	99
	Enterobacteriales	*Enterobacteriaceae*	6	0	6	*Buttiauxella noackiae*	AJ293689	99	Fuschna-P5-H02		clone from unidentifiable bacterial isolate	AF-227832	99
			1	0	1	*Plesiomonas shigelloides*	X60418	93	Fuschna-P3-D08	→ double-check w/ BLAST, seq on single branch → Rhanella, Enterobacteriaceae	clone from arctic stream sediment, Alaska	FJ-849420	96
	Legionellales	*Legionellaceae*	1	0	1	*Legionella taurinensis*	DQ-667196	96,3	Fuschna-P5-F02		clone from fouled MF membrane from drinking water treatment plant	FJ-572668	96
Verrucomicrobia	*Verrucomicrobiales*	*Verrucomicrobiaceae*	1	0	1	*Prosthecobacter fusiformis*	U60015	88	Fuschna-P5-F05		clone from lake water, Dongping ecosystem, China	FJ-612153	87

10 Physiology of phototrophic iron(II)-oxidizing bacteria - implications for modern and ancient environments

Florian Hegler[1], Nicole R. Posth[1], Jie Jiang[1], Andreas Kappler[1]
FEMS Microbiology Ecology 66: 250 – 260, 2008

[1]Center for Applied Geoscience – Geomicrobiology, Eberhard Karls University Tübingen, Sigwartstr. 10, 72076 Tuebingen, Germany

Keywords: phototrophic Fe(II) oxidation, iron cycling, banded iron formations, ferrous iron

10.1 Abstract

Phototrophic Fe(II)-oxidizing bacteria are present in modern environments and evidence suggests that this metabolism was present already on early earth. We determined Fe(II) oxidation rates depending on pH, temperature, light intensity and Fe(II) concentration for three phylogenetically different phototrophic Fe(II)-oxidizing strains (purple non-sulfur bacterium *Rhodobacter ferrooxidans* sp. strain SW2, purple sulfur bacterium *Thiodictyon* sp. strain F4, and green sulfur bacterium *Chlorobium ferrooxidans* strain KoFox). While we found the overall highest Fe(II) oxidation rates with strain F4 (4.5 mmole L^{-1} day^{-1}, 800 lux, 20 °C), the lowest light saturation values (at which maximum Fe(II) oxidation occurred) were determined for strain KoFox with light saturation already below 50 lux. The oxidation rate per cell was determined for *Rhodobacter ferrooxidans* strain SW2 to be 32 pmol Fe(II) h^{-1} $cell^{-1}$. No significant toxic effect of Fe(II) was observed at Fe(II) concentrations of up to 30 mmole. All three strains are mesophiles with upper temperature limits of 30 °C. The main pigments were identified to be spheroidene, spheroidenone, OH-spheroidenone (SW2), rhodopinal (F4), and chlorobactene (KoFox). This study will improve our ecophysiological understanding of iron cycling in modern environments and will help to evaluate if phototrophic iron-oxidizers may have contributed to the formation of Fe(III) on early earth.

10.2 Introduction

Fe(III) oxy(hydr)oxides are abundant both in terrestrial and aquatic environments (Canfield, 1989). While Fe(III) can serve as electron acceptor for microorganisms mineralizing organic matter (Lovley, 1991), the product of their metabolism, i.e. Fe(II), can be re-oxidized by Fe(II)-oxidizing microorganisms either under oxic or under anoxic conditions (Kappler & Straub, 2005). At acidic pH, the ferrous iron is relatively stable even in the presence of O_2 due to kinetic limitations ((Stumm & Morgan, 1995) so that

mainly microorganisms, and not chemical oxidation processes, are responsible for the oxidation of iron(II), e.g. in acid mine drainage processes (Baker & Banfield, 2003). At circumneutral pH, however, microbes have to compete with the rapid chemical oxidation of iron(II) by molecular oxygen and thrive best under microoxic conditions (Emerson & Moyer, 1997). In anoxic environments, iron-oxidizing bacteria can oxidize iron either by using nitrate as electron acceptor (Straub et al., 1996) or phototrophically by using light as energy source (Widdel et al., 1993). These tightly coupled microbial iron reduction and oxidation processes allow efficient iron cycling on very small spatial scales as recently demonstrated in several studies (Weber et al., 2006, and references therein). The iron cycle is tightly coupled to carbon, nutrient and trace metal biogeochemical cycles, making its full understanding vital to the interpretation of natural systems (Thamdrup, 2000).

In both freshwater and marine sediments, Fe(III) reduction is controlled by microorganisms and not by chemical reduction of Fe(III) minerals (Thamdrup, 2000). Thus, steady-state Fe(II) concentrations, balanced by microbial Fe(III) reduction and various chemical and microbiological Fe(II) oxidation processes lead to Fe(II) concentrations of 10^{-3} mol L^{-1} in sediments (Canfield, 1989, Stumm & Sulzberger, 1992, Thamdrup, 2000, Gerhardt et al., 2005). It was suggested that each Fe atom undergoes about 100-300 redox cycles until it gets buried in a biounavailable form in the sediment (Canfield et al., 1993).

Furthermore, anaerobic and aerobic iron oxidation, as well as iron reduction, have not only drawn interest because of their presence in modern environments but also because it is likely that these processes were important on early earth about 3.5 to 1.8 Ga ago, possibly even being responsible for the deposition of banded iron formations (BIFs) (Johnson et al., 2003, Kappler et al., 2005). BIFs represent the largest iron deposits worldwide (Beukes et al., 1992), but even until today the mechanism of Fe(II) oxidation of these formations at different time points of earth history is not yet fully understood. As early as 1968, microorganisms were suggested to have played a major role in the deposition of the oldest BIFs (Cloud, 1968) when the atmosphere of the early earth was probably still anoxic (Farquhar et al., 2000). The traditional model assumes that molecular oxygen produced by cyanobacteria was responsible for the oxidation of the iron (Cloud, 1968, Beukes et al., 1992). Phototrophic Fe(II)-oxidizing bacteria were suggested as early as 1973 to have played a major role in BIF Garrels et al. (1973), Hartmann (1984). However, only recent analysis of the genome of anoxygenic phototrophic bacteria showing that anoxygenic photosynthesis likely evolved earlier than oxygenic photosynthesis (Xiong, 2006) in combination with evidence from eco-physiological, biomarker and isotope studies (Johnson et al., 2003, Brocks et al., 2005, Kappler et al., 2005, Rashby et al., 2007) made a strong case for early BIF deposition via phototrophic iron-oxidizing bacteria.

While much is known about the biochemical and ecological role of acidophilic aerobic iron oxidation in acid mine drainage processes (Blake et al., 1993, Baker & Banfield, 2003, e.g.), much less is known about the biochemical mechanism of iron oxidation at circumneutral pH. In the last years, the ecological significance of aerobic Fe(II) oxidation both freshwater and deep sea environments has been investigated intensively and their activity in the environment has been localized and quantified by microsensor studies ((Edwards et al., 2003, Emerson & Weiss, 2004). In contrast, anaerobic iron oxidation has been largely unexplored although it closes a gap in the iron cycle under O_2-free conditions. This group of anaerobic Fe(II)-oxidizing bacteria include nitrate-dependent and phototrophic Fe(II)-oxidizing cultures. As of yet, seven cultures of phototrophic Fe(II) oxidizers are known: the freshwater strains *Rhodobacter ferrooxidans* strain SW2 (Ehrenreich & Widdel, 1994), *Rhodopseudomonas palustris* strain TIE-1 (Jiao et al., 2005), *Chlorobium ferrooxidans* strain KoFox (Heising et al., 1999), *Thiodictyon* sp. strain F4 (Croal et al., 2004), and *Rhodomicrobium vannielii* strain BS-1 (Heising & Schink, 1998) as well as the marine strains

Rhodovulum iodosum, and *Rhodovulum robiginosum* (Straub et al., 1999). These bacteria oxidize Fe(II) according to the following stoichiometry (Ehrenreich & Widdel, 1994):

$$HCO_3^- + 4Fe^{2+} + 10H_2O \rightarrow < CH_2O > +4Fe(OH)_3 + 7H_2O \tag{10.1}$$

Phototrophic iron-oxidizing bacteria metabolize dissolved Fe(II), i.e. Fe^{2+}, and can also oxidize the soluble minerals FeS and $FeCO_3$ but not the poorly soluble Fe_3O_4 and FeS_2 (Kappler & Newman, 2004). So far, these strains have been isolated from both fresh and saltwater settings, notably fresh water ditches (Ehrenreich & Widdel, 1994, Heising et al., 1999), a freshwater marsh (Croal et al., 2004) and North Sea coastal sediments (Straub et al., 1999). Only recently has it been demonstrated that the biochemical pathway(s) of Fe(II) oxidation in the two phototrophic Fe(II)-oxidizing bacteria *Rhodopseudomonas palustris* strain TIE-1 and *Rhodobacter ferrooxidans* strain SW2 involve c-type cytochromes from where the electrons are transported to the photosynthetic reaction center (Croal et al., 2007, Jiao & Newman, 2007). Interestingly, one of these studies even suggested that the Fe(II) is oxidized in the periplasm (Jiao & Newman, 2007) and not at the outer membrane as previously suggested (Kappler & Newman, 2004).

In order to understand the potential ecological role of phototrophic Fe(II)-oxidizing bacteria in various modern and ancient environments, especially with respect to the deposition of Precambrian banded iron formations (BIF), this study aimed to quantify the Fe(II) oxidation rates for this type of microbial metabolism under different conditions regarding pH, light intensity, temperature, and Fe(II) concentration. The overall goal of this study was to help evaluating a potential role of phototrophic Fe(II)-oxidizing bacteria in deposition of Precambrian banded iron formation (e.g. by future modeling studies) by providing relevant Fe(II) oxidation rates at circumneutral pH and different light and temperature conditions. For these experiments, we chose three strains of distinct phylogenetic groups: the α-proteobacteria (*Rhodobacter ferrooxidans* strain SW2), the β-proteobacteria (*Chlorobium ferrooxidans* strain KoFox), and the γ-proteobacteria (*Thiodictyon* sp. strain F4). Additionally, we identified the main carotenoids these strains produce in order to assess if any specific carotenoids are present and can potentially be used as a biomarker for this type of metabolism, especially with respect to the proposed role of these organisms in the deposition of BIFs.

10.3 Materials and methods

10.3.1 Sources of microorganisms

The strains *Rhodobacter ferrooxidans* strain SW2, *Thiodictyon* sp. strain F4, and *Chlorobium ferrooxidans* strain KoFox were kindly originally provided by F. Widdel (Max-Planck Institute Bremen, Germany) and B. Schink (University of Konstanz, Germany) to D.K. Newman (MIT, USA) from where A. Kappler transferred them into his lab strain collection at the University of Tüingen, Germany.

10.3.2 Media and growth conditions

All strains were cultivated in serum bottles (58 mL volume, 25 mL medium) in freshwater medium modified from Ehrenreich & Widdel (1994) containing 0.6 g L−−1 potassium phosphate (KH_2PO_4), 0.3 g L^{-1} ammonium chloride (NH_4Cl); 0.5 g L^{-1} magnesium sulphate ($MgSO_4 \times 7\,H_2O$) and 0.1 g L^{-1} calcium chloride ($CaCl_2 \times 2\,H_2O$). The medium was buffered at pH 6.8-6.9 with 22 mmol L^{-1} bicarbonate which was autoclaved separately under N_2 / CO_2 atmosphere (90:10). The medium was cooled to room

temperature under N_2 / CO_2 atmosphere (90:10) and 1 mL L^{-1} trace element solution (Tschech & Pfennig, 1984), 1 mL L^{-1} selenate-tungstate-solution (Widdel, 1980) and 1 mL L^{-1} sterile filtered vitamin solution (Widdel & Pfennig, 1981) were added. If necessary, the pH was adjusted to pH 6.8 with 0.5 mol L^{-1} Na_2CO_3 or 1 mol L^{-1} HCl. If mineral-free cultures were required, either acetate was added from a 1 mol L^{-1} stock solution to a concentration of 10 mmol L^{-1} or the headspace was flushed with a mixture of dihydrogen and CO_2 (90:10 v/v).

Two different kinds of Fe(II)-containing growth media were used in this study: filtered and unfiltered Fe(II)-containing medium. For unfiltered medium $FeCl_2$ was added (1 mol L^{-1} stock solution of 99.9% ferrous chloride tetrahydrate ($FeCl_2 \times 4H_2O$) dissolved in anoxic water (boiled and then flushed with nitrogen during cooling) to fresh water medium. A greenish-whitish precipitate formed immediately (likely consisting of Fe(II) phosphate, possibly vivianite containing little amounts of Ca and S; personal communication Jennyfer Miot). The unfiltered medium (containing the precipitated Fe(II) minerals) was used for some of the microbial iron(II) oxidation experiments without further treatment. In contrast, the preparation of filtered medium provided medium in which only dissolved Fe(II) was present and neither dissolution processes of Fe(II) minerals nor sorption of Fe(II), Fe(III) or cells to Fe(II) minerals played a role. This medium was filtered in an anoxic chamber with a 0.22 μ m filter (polyethersulfone, Millipore) two hours after the $FeCl_2$ solution was added and Fe(II) minerals precipitated. The pH was checked before filtering and adjusted to pH 6.8 if necessary. Approximately 40% of the Fe(II) of a 10 mM Fe(II) solution stayed in solution (supersaturated with regard to siderite); this medium was stable for about four weeks without any further visible Fe(II) mineral precipitation. Within the typical time-frame of our experiments, loss of iron by photochemical oxidation, precipitation or adsorption to the glass was not observed in non-inoculated controls. Standard incubation conditions were at 20 °C)and {unit[650]lux, the light source was a tungsten light bulb, and the light intensity was varied by changing the distance to the light bulb.

To adjust the pH, 1 M HCl or 0.5 M Na_2CO_3 was added with a syringe to bottles sealed with a rubber stopper already containing Fe(II) in order to avoid a loss of CO_2 in the case of a decreasing pH and thus a loss of buffer. pH was checked at the beginning and the end of the growth experiments and did not change by more than 0.1 pH units.

10.3.3 Analytical techniques

Fe(II) and Fe(III) were quantified by a spectrophotometric assay with ferrozine modified from (Stookey, 1970). Samples of Fe(II)-grown cultures were taken sterilely with a syringe through the butyl-rubber stopper. About 200 μ L culture suspension were withdrawn after vigorous shaking and transferred into an Eppendorf tube. 100 μ L of the sample were taken quickly with a transfer pipette and added to 700 μ L of 1 mol L^{-1} HCl to stabilize Fe(II) and to dissolve the Fe(III) minerals. 20 μ L from this solution were transferred into a well of a microtiter plate containing either 80 μL of 1 mol L^{-1} HCl to quantify Fe(II) or 80 μ L of a solution of the reducing agent hydroxylamine hydrochloride (50% w/v in 1 M HCl) to quantify the total iron content (i.e. Fe(II) plus Fe(III)). Three subsamples were analyzed per sample at each time point for Fe(II) and three for total iron. 100 μ L ferrozine solution (10% w/v ammonium acetate, 0.1% w/v ferrozine) were added after 30 min. The ferrozine was allowed to react for 5 min with the Fe(II) and the absorbance at 562 nm was measured with a FlashScan 550 plate reader (Jena Analytics, Jena, Germany).

Ferrous iron concentration was plotted vs. time. The curve obtained was inverse sigmoidal while the

turning point of this curve denotes the maximum oxidation rate at a given condition, such as pH or temperature. We approximated this by a regression through the visibly steepest part of the curve as shown in 10.1 yielding the oxidation rate per time. Each experiment consists of three parallel cultures. The oxidation rates were determined for each of these parallels, averaged, and the standard deviation calculated. The uninoculated control was used to quantify loss of Fe(II) either by sorption to the glass-wall of the serum bottles or by a possible abiotic oxidation by light.

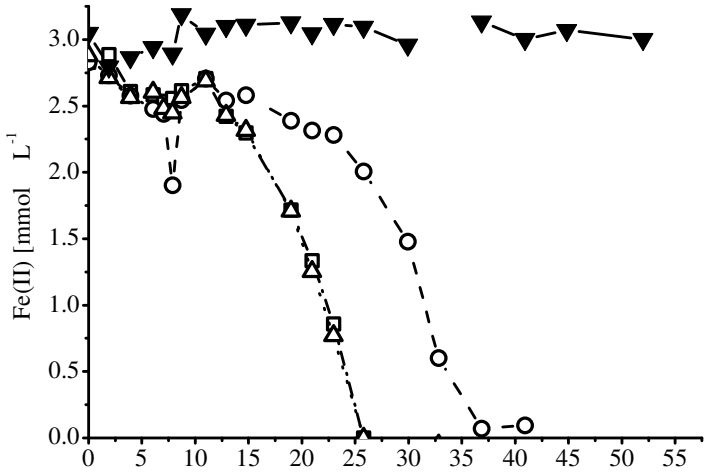

Figure 10.1: Fe(II) concentration plotted over time for three parallel cultures of *Rhodobacter ferrooxidans* strain SW2 (inoculated with the same inoculum) growing in filtered 3 mM Fe(II)-containing medium. Maximum oxidation rates were determined at the steepest part of the Fe(II) curve (indicated by the solid lines). Although the lag-time can differ (probably due to small differences in the inoculation procedure) in the three parallel cultures (□, ○, △), the maximum rate and the total extent of oxidation are similar for the three parallel cultures while in the noninoculated control (▼) no oxidation was observed at all.

Cell numbers were determined by microscopic cell counts. Cells in aliquots of cell-mineral suspensions were fixed with 3.7% formaldehyde (30 min), centrifuged, washed with 0.9% NaCl and resuspended in 1.1 mL of 0.9% NaCl. The Fe(III) minerals were dissolved by addition of 1 mL anoxic ferrous ethylene diammonium sulphate solution (C_2 H_4 (NH_3)$_2$ SO_4) from a 100 mM anoxic stock solution and 8.9 mL oxalate solution (pH 3, autoclaved). 10 μL of 4',6-diamidino-2-phenylindole (DAPI, 5 mg L^{-1} stock) were added as a fluorescent dye and 0.5 - 1 mL of cell suspension was sucked onto a filter (Millipore, polycarbonate filter, 0.22 μm pore size). Cells were counted microscopically (see below).

10.3.4 Microscopy

Light microscopy images were taken with an AxioVison microscope (Zeiss) and an oil immersion objective lens. Scanning electron micrographs were taken on either a Zeiss Leo Gemini 1550 VP or a Zeiss Crossbeam Leo 1540 XB FE-SEM at the Natural and Medical Sciences Institute at the University of Tübingen. Samples were prepared for SEM as described elsewhere (Schaedler et al., 2008).

10.3.5 Data analysis

The data for pH and temperature dependence of Fe(II) oxidation was fitted according to a model published by (Rosso et al., 1995) that can be used to determine minimal, optimal and maximal pH and temperature of microbial metabolism based on experimental data. The data obtained for the light-dependent Fe(II) oxidation rates were modeled with 10.2 with ν = oxidation rate, v_max = maximum oxidation rate, I = light intensity and x_HLS = light intensity at which the oxidation rate equals 50% of v_max. For all data for light-dependent Fe(II) oxidation, half light saturation values x_HLS at which the oxidation rate is at 50% of the maximum rate are reported.

$$\nu = \frac{v_{max} I}{I + x_{HLS}} \tag{10.2}$$

10.3.6 Identification of pigments

Cells from hydrogen- or acetate-grown stationary growth phase cultures were harvested by centrifugation at 7800 $\times g$. The pigments were extracted in the dark with 5 mL of acetone and ethanol (1:1). After sonification for 2 min, the mixture was incubated at 20 °C for 1 hour. The pigments were then transferred to hexane by adding 3 mL of hexane and 0.5 mL of water. The upper hexane phase was exchanged until it remained clear. The hexane extracts were collected, concentrated 10-fold under a stream of nitrogen, and stored at -20 °C. Pigments were separated with a normal-phase thin-layer chromatography system with silica adsorbed (Kieselgel 60, Merck, Darmstadt, Germany) with petrolether and acetone (4:1) as the mobile phase. After scraping the colored bands from the thin-layers, the pigments were extracted with dichloromethane and filtered through glass wool. The pigments were transferred to hexane (see above) and absorbance spectra of the individual pigments were recorded in a spectrophotometer. The pigments were identified by comparison to reference absorption spectra and published TLC-Rf-values (Züllig & Rheineck, 1985, Britton, 1995b). No differences in pigment content between Fe(II)-grown cells and hydrogen-/acetate-grown cells were observed in TLC plates and due to higher cell mass therefore acetate- and H_2-grown cells were used for pigment identification. All steps of the pigment separation and identification were done in the dark or at least with dim light.

10.4 Results

10.4.1 Fe(II) oxidation by phototrophic Fe(II)-oxidizing bacteria

Phototrophic Fe(II)-oxidizing bacteria oxidize Fe(II) and produce Fe(III) that precipitates as Fe(III) mineral (figure 10.2). In the cultures investigated in this study, a significant fraction, but never all cells were associated with the Fe(III) minerals produced during Fe(II) oxidation (figure 10.2). Furthermore, the cells were not encrusted in iron minerals, but rather loosely attached to the Fe(III) minerals.

The maximum rates of Fe(II) oxidation by the strains were determined by analyzing the decrease of Fe(II) over time. In some cases, for the same strain the lag phase of independent or even parallel cultures varied by up to 14 days either due to small differences in culture age, and therefore physiological status of the inoculated cells, or due to slightly different amounts of inoculum, and thus a variation of the number of cells added. Nevertheless, the maximum rates and the extent of Fe(II) oxidation were similar in all cultures (figure 10.1). Therefore, the maximum oxidation rates are dependent on the concentration and

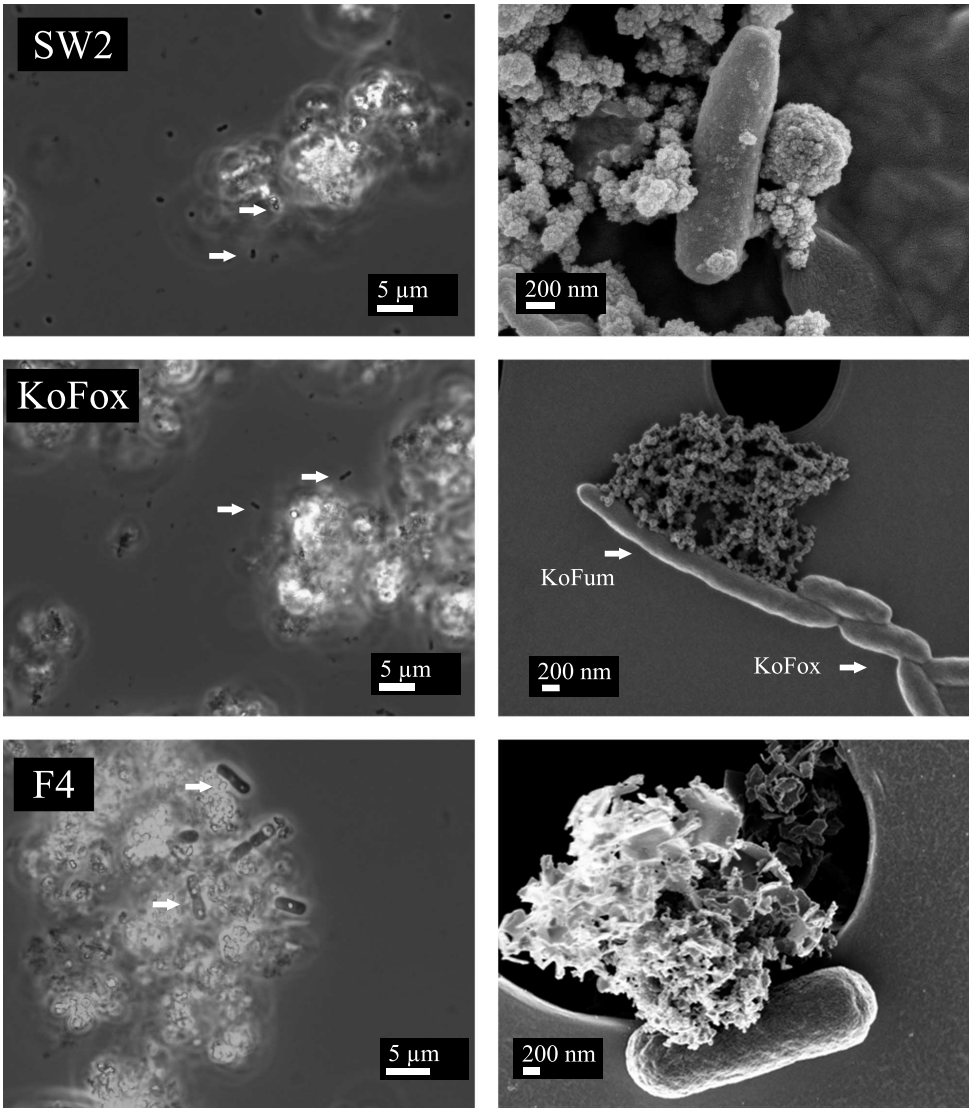

Figure 10.2: Light microscopy (left) and SEM-images (right) of the phototrophic Fe(II)-oxidizing bacteria *Rhodobacter ferrooxidans* strain SW2, *Chlorobium ferrooxidans* strain KoFox (with the co-culture KoFum in the SEM-picture) (Heising et al., 1999), and *Thiodictyon* sp. strain F4. Images were taken of samples from cultures growing with Fe(II) as electron donor. Cells are indicated with arrows.

activity of cells at the point of maximum Fe(II) oxidation and not on the number and physiological status of the inoculated cells. Oxidation rates can thus be compared between independent cultures of the same strain.

10.4.2 Oxidation of dissolved Fe(II) and Fe(II) minerals by anoxygenic phototrophs

The medium used for cultivation of anoxygenic phototrophic Fe(II)-oxidizing bacteria typically contains 20-30 mM bicarbonate as buffer and 4 mM of phosphate as mineral salt (Ehrenreich & Widdel, 1994, Kappler & Newman, 2004). Upon Fe(II) addition, Fe(II) phosphate precipitates form (personal communication Jennyfer Miot). We compared oxidation rates for cultures of *Rhodobacter ferrooxidans* strain SW2 with only dissolved Fe(II) to cultures that contained a mix of dissolved Fe(II) and Fe(II) minerals and observed similar rates of approximately 0.5 mmol L^{-1} h^{-1} at 2 and 4 mM Fe(II) for both filtered and non-filtered medium (figure 10.3). Only at 8 mM Fe(II) was a significant difference found, with higher rates in the precipitate-free medium compared to the Fe(II)-mineral containing medium. All further experiments investigating light, temperature, and pH dependence were done at Fe(II) concentrations of 2-4 mM. As no difference in oxidation rate was found dependent upon presence of Fe(II) minerals at these concentrations, we carried out these experiments in either filtered or non-filtered medium and consider the results as comparable to each other.

10.4.3 Growth yields and oxidation rates per cell

Initial cell numbers and cell numbers after Fe(II) oxidation as well as oxidation rates per cell were determined for *Rhodobacter ferrooxidans* strain SW2. The initial cell number after inoculation was $1.6 \pm 0.1 \times 10^8$ cells mL^{-1}. During oxidation of 4 mM Fe(II) at 20 °C at circumneutral pH and light saturation the cell number increased to $9.8 \pm 0.1 \times 10^8$ cells mL^{-1}. The oxidation rate for these conditions was determined to be 0.75 mmol mL^{-1} day^{-1} which yielded a per-cell oxidation rate of 32 pmol Fe(II) h^{-1} $cell^{-1}$. According to the equation for microbially catalyzed photoautotrophic Fe(II) oxidation (equation 10.1), by oxidation of 4 mM Fe(II) the cells can produce 1 mM $<CH_2O>$ (used as proxy for biomass) meaning about 30 mg biomass. This growth yield in photoautotropic Fe(II)-oxidizing cultures of strain SW2 was confirmed already by others (Ehrenreich & Widdel, 1994).

10.4.4 Concentration dependence of Fe(II) oxidation rates

The dependence of Fe(II) oxidation rates on the amount of Fe(II) initially present was tested with *Rhodobacter ferrooxidans* strain SW2 at concentrations of Fe(II) in the range of 0.2 mM to 30 mM. We observed an increase in oxidation rates from 0.2 to 8 mM Fe(II), with the highest oxidation rate at 8 mM (figure 10.3). At higher concentrations of 15 mM and above, the oxidation rate decreased to about 40-50% of the maximum rate, however, up to 30 mM no substantial toxic effect of Fe(II) was observed.

10.4.5 Light dependence of Fe(II) oxidation rates

In order to determine the light dependence of *Chlorobium ferrooxidans* strain KoFox, *Thiodictyon* sp. strain F4 and *Rhodobacter ferrooxidans* strain SW2, we incubated cultures at various distances from tungsten light bulbs, measured the light intensity, and determined the Fe(II) oxidation rates by quantifying Fe(II) over time. For *Rhodobacter ferrooxidans* strain SW2, we observed a light saturation (light intensity

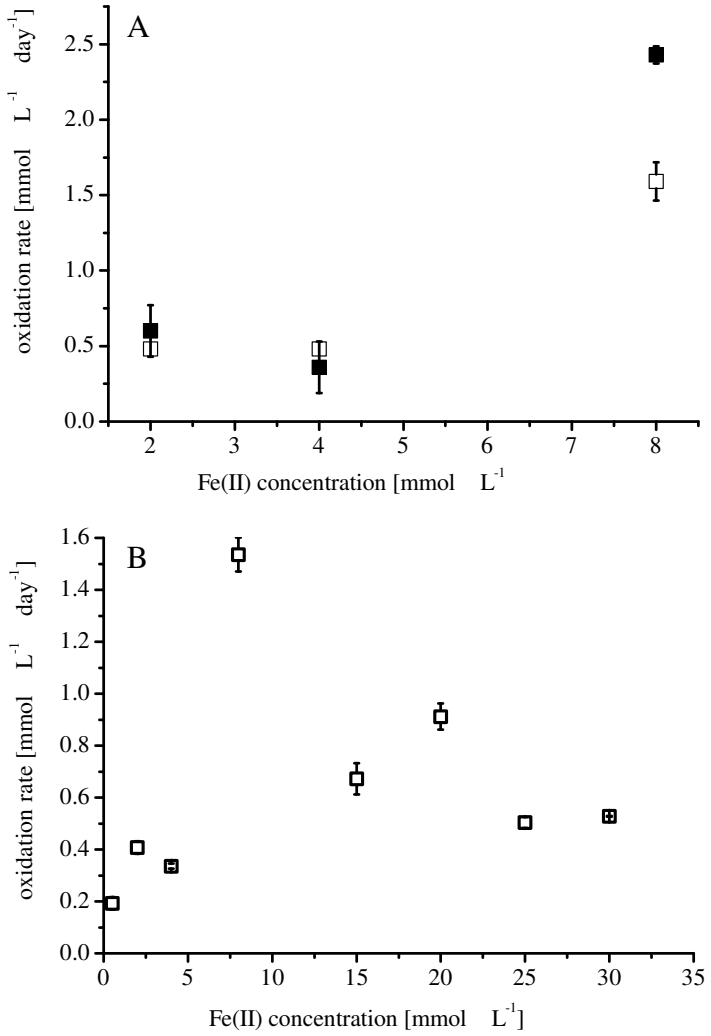

Figure 10.3: Rates of Fe(II) oxidation by *Rhodobacter ferrooxidans* strain SW2 at various Fe(II) concentrations. (A) Comparison of Fe(II) oxidation rates in filtered (■) and non-filtered (□) medium. (B) Fe(II) oxidation rates in non-filtered medium. In both setups each data point represents two experiments with at least four cultures each from which the standard deviation was calculated.

at which maximum oxidation rates are observed) of approximately 400 lux with a half-light saturation (HLS) (light intensity at which we observed 50% of the maximum oxidation rate) of 113 ± 50 lux was determined (figure 10.4). *Thiodictyon* sp. strain F4 has a light saturation of 800 lux with a HLS of 350 ± 68 lux (figure 10.4). In contrast to the purple sulfur and purple non-sulfur strains F4 and SW2, the Fe(II) oxidation rate of the green-sulfur bacterium *Chlorobium ferrooxidans* sp. strain KoFox reaches light saturation already below 50 lux with a HLS of 11 ± 5 lux (figure 10.4).

10.4.6 Temperature dependence of Fe(II) oxidation rates

The optimal and maximal temperatures for phototrophic Fe(II) oxidation were determined for the three strains *Chlorobium ferrooxidans* strain KoFox, *Thiodictyon* sp. strain F4, and *Rhodobacter ferrooxidans* strain SW2 (figure 10.5). We found that all three strains investigated are mesophilic with maximum Fe(II) oxidation rates at 23 °C for strain F4, 26 °C for SW2, and 25 °C for strain KoFox and an upper temperature limit for Fe(II) oxidation of 32 °C for F4, 30 °C for SW2, and 32 °C for KoFox. We also incubated the strains at lower temperatures and observed that strain F4 did not oxidize Fe(II) at 10 °C, but the strains SW2 and KoFox oxidized Fe(II) at appreciable rates even at 5 °C.

10.4.7 pH-dependence of Fe(II) oxidation rates

In order to determine the pH-dependence of *Chlorobium ferrooxidans* strain KoFox, *Thiodictyon* sp. strain F4 and *Rhodobacter ferrooxidans* strain SW2, we incubated the strains in non-filtered medium containing 4 mM Fe(II) at pH 5 to 8. We determined the optimal pH for Fe(II) oxidation for strains F4 and SW2 to be at 6.5, while for strain KoFox we observed maximum oxidation rates at pH 6.9 (table 10.1). The maximum pH at which we observed Fe(II) oxidation was 7.2 for strain F4 and 7.5 for strains SW2 and KoFox. The lowest pH at which the strains oxidized Fe(II) was 5.4 for strains F4 and KoFox and 5.2 for strain SW2.

Strain	$\mathbf{pH}_{opt}$	$\mathbf{pH}_{min}$	$\mathbf{pH}_{max}$	$\mathbf{R}^2$
F4	6.5 ± 0.1	5.4 ± 0.1	7.2 v 0.1	0.98
KoFox	6.9 ± 0.1	5.4 ± 0.1	7.5 ± 0.1	0.97
SW2	6.5 ± 0.0	5.2 ± 0.1	7.5 ± 0.1	0.92

Table 10.1: pH-dependence of Fe(II) oxidation by the phototrophic Fe(II)-oxidizing strains – *Thiodictyon* sp. strain F4, *Chlorobium ferrooxidans* strain KoFox and *Rhodobacter ferrooxidans* strain SW2. Shown are the optimal pH (pH_{opt}) and the lowest and highest pH at which significant Fe(II) oxidation occurred, pH_{min} and pH_{max}, respectively. R^2 indicates the goodness of the fit.

10.4.8 Carotenoids in phototrophic Fe(II)-oxidizing bacteria

We identified the main carotenoids in the phototrophic Fe(II)-oxidizing bacteria *Chlorobium ferrooxidans* strain KoFox, *Thiodictyon* sp. strain F4, and *Rhodobacter ferrooxidans* SW2 (table 10.2). Spheroidene, spheroidenone, OH-spheroidene were identified as the main pigments in the purple non-sulfur strain SW2, whereas rhodopinal was the main pigment in the purple-sulfur strain F4 and chlorobactene in the green sulfur strain KoFox. All pigments identified represented the main pigments in these strains when grown

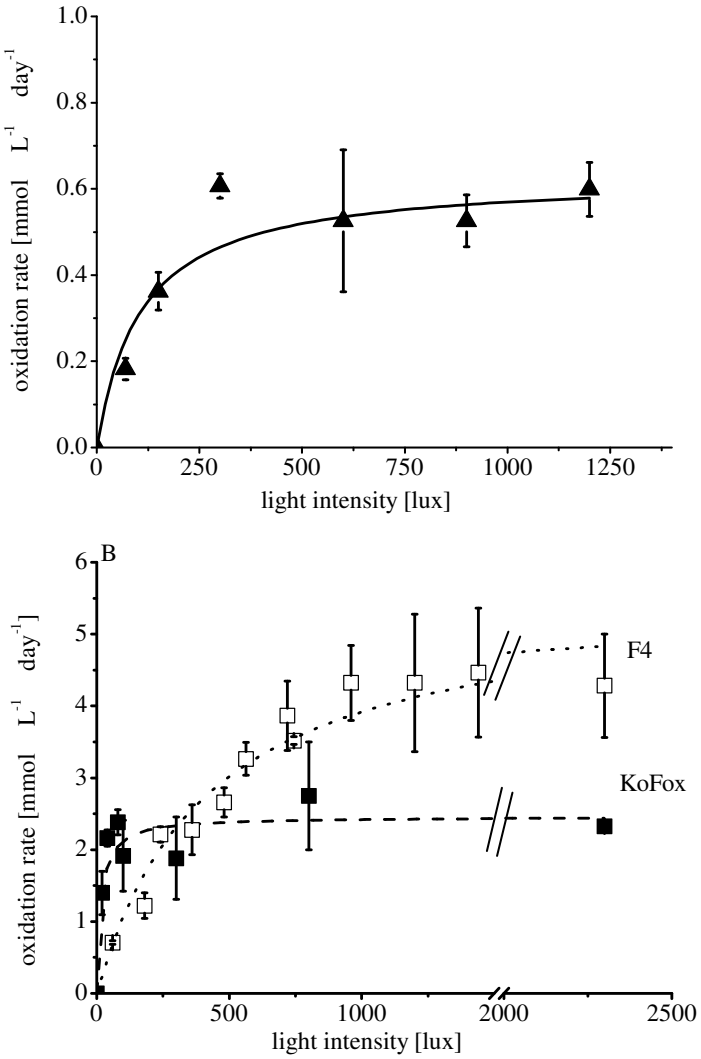

Figure 10.4: Light dependence of Fe(II) oxidation by the phototrophic Fe(II)-oxidizing bacteria *Chlorobium ferrooxidans* strain KoFox (■) and *Thiodictyon* sp. strain F4 (□) (A) and for *Rhodobacter ferrooxidans* strain SW2 (B). The dashed, punctuated, and solid lines represent the light dependence of Fe(II) oxidation modeled with equation 10.2 using the experimentally determined data. Each data point represents at two independent experiments with at least two cultures each. The error bars represent standard deviations calculated from all experiments. The rates were determined for strains KoFox and F4 with a 10 mM Fe(II)-containing unfiltered medium whereas the rates for strain SW2 were determined in filtered medium containing 4 mM dissolved Fe(II). Since we showed that at these Fe(II) concentrations the oxidation rates in filtered and non-filtered Fe(II)-containing medium are similar (figure 10.3A), we consider these experiment to be comparable.

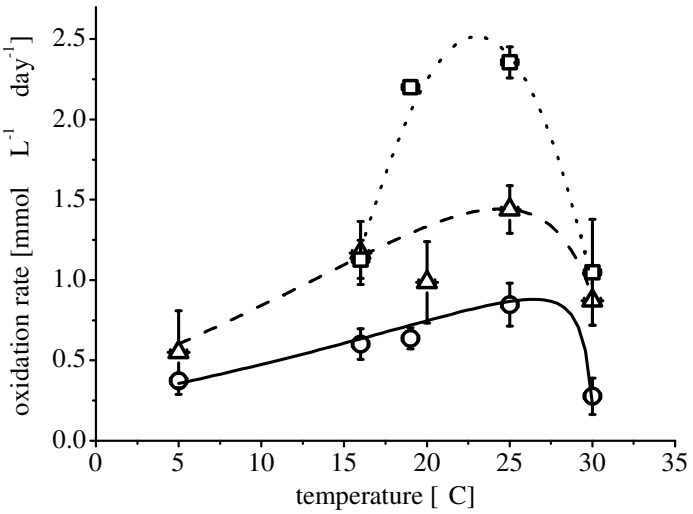

Figure 10.5: Temperature dependence of Fe(II) oxidation rates for *Chlorobium ferrooxidans* strain KoFox (△), *Thiodictyon* sp. strain F4 (□) and *Rhodobacter ferrooxidans* strain SW2 (○). All rates were determined with filtered medium containing 4 mM dissolved Fe(II). The dashed and solid lines are calculated from the data with the model described by (Rosso et al., 1995). Each data point represents two independent experiments with at least four cultures each. The error bars represent standard deviations calculated from all experiments.

either photoautotrophically with Fe(II) as electron source or photoautotrophically, with either H2 (strains SW2 and KoFox) or acetate (strain F4).

Strain	Compound	Absorption maxima (nm)
SW2	spheroidene (yellow)	430, 455, 486
	spheroidenone (pinkish-red)	465, 480, 517
	OH-spheroidene (yellow)	430, 454, 486
KoFox	chlorobactene (yellow)	435, 462, 491
F4	rhodopinal (purple-red)	362, 490-512 (broad)

Table 10.2: Main carotenoids (and their color) – identified in the phototrophic Fe(II)-oxidizing bacteria *Rhodobacter ferrooxidans* sp. SW2, *Chlorobium ferrooxidans* strain KoFox, and *Thiodictyon* sp. strain F4.

10.5 Discussion

10.5.1 Ecophysiology of anoxygenic phototrophic Fe(II)-oxidizers

Understanding the physiological constraints of microbially catalyzed phototrophic Fe(II) oxidation enhances our understanding of the iron cycle over the last 3.5 Ga until today. In modern environments, these organisms close the iron cycle in near surface environments where Fe(II) produced in deeper layers by

Fe(III)-reducing microorganisms reaches the light-exposed surface. With regard to ancient environments, physiology experiments with modern phototrophic Fe(II)-oxidizing bacteria constrain the likely ecological limits for this metabolism in the past. The fact that modern phototrophic Fe(II)-oxidizing bacteria were isolated from environments as varied as a marsh (*Thiodictyon* sp. F4) (Croal et al., 2004), iron-rich ditches (*Chlorobium ferrooxidans* strain KoFox, *Rhodobacter ferrooxidans* strain SW2, *Rhodopseudomonas palustris* strain TIE-1) (Ehrenreich & Widdel, 1994, Heising et al., 1999, Jiao et al., 2005) and ocean sediments (*Rhodovulum iodosum*, and *Rhodovulum robiginosum*) (Straub et al., 1999) highlights the ubiquity and likely environmental significance of this metabolism.

In natural environments, bacteria must cope with temperature, pH and light conditions that change in different time intervals (minutes to months). Especially in anoxic near surface environments required by phototrophic Fe(II)-oxidizers, temperature and light intensity, but also pH, can change rapidly. In this regard, the physiology of the isolated strains reflects the habitats from which they were isolated: moderate temperatures and a circumneutral pH. Two of the strains even grew at temperatures of 4 °C (KoFox and SW2). As of yet, no phototrophic Fe(II)-oxidizing strain is known that is able to oxidize Fe(II) at high temperatures, for example in iron-rich hot springs. Iron-rich, neutrophilic hot springs reflect habitats thought to have been omnipresent on ancient earth. Likewise, attempts made to isolate thermophilic aerobic iron(II)-oxidizing bacteria, to date have also been without success (e.g. Emerson & Weiss, 2004).

10.5.2 Adaptation to pH changes in the environment

When Fe(III) precipitates from solution, protons are formed

$$\mathrm{Fe}^{3+} + 3\,\mathrm{H}_2 \longrightarrow \mathrm{Fe(OH)}_{3,\mathrm{ppt}} + 3\,\mathrm{H}^+ \tag{10.3}$$

and thus the vicinity of a cell can acidify (depending on the buffer capacity of the environment). As a consequence, it is essential for these strains to be able to cope with lower pH values not only because of pH changes caused by environmental processes but also due to metabolism-driven pH changes. It has been previously suggested that the pH for Fe(II) oxidation by *Rhodobacter ferrooxidans* strain SW2 ranges from 5.5 to 7 (Ehrenreich & Widdel, 1994). We found the range to be slightly broader (pH 5.2 to 7.5). The slightly wider range we report here for strain SW2 might be due to adaptation and mutation of the strain or to a slightly different culturing technique (such as the use of other salts that may contain concentrations of a trace element not supplemented with the trace element solution). Yet, the differences between the values reported previously and the values we determined are minor. Also, the other phototrophic Fe(II)-oxidizing bacteria that we have tested (strains F4 and KoFox) showed similar pH ranges to strain SW2 for phototrophic Fe(II) oxidation. Such a relatively wide pH range is essential for such strains considering their environmental habitats. Over the course of the day, the pH in sediments changes due to the generation of protons by the microbial formation of Fe(III) hydroxides (during the day when light is present), but also due to uptake of bicarbonate/CO_2 by the cells. Indeed, a range of pH fitting the limits for the phototrophic Fe(II)-oxidizers described here occur in naturally forming microbial mats (e.g. Pierson et al., 1999).

10.5.3 Consequences of light-dependence for habitat choice of phototrophic Fe(II)-oxidizers

Phototrophic Fe(II)-oxidizing bacteria require very restricted and specialized habitats as they need to be close to the surface to get light but also require a reduced environment devoid of oxygen. In the

presence of O2, the Fe(II) substrate would be oxidized chemically by molecular oxygen rather then by the phototrophic Fe(II)-oxidizing cells. These organisms circumvent this problem either by tolerating low concentrations of oxygen, which allows them to live closer to the surface (requiring that the cells oxidize the Fe(II) faster than the molecular oxygen) or by lowering their requirement for light and being able to live deeper in soils and sediments where the concentration of Fe(II), replenished from below, is higher. In this regard, *Chlorobium ferrooxidans* strain KoFox, which needs the lowest light intensities for highest Fe(II) oxidation rates, has adapted best to living deeper in a sediment or soil. *Rhodobacter ferrooxidans* strain SW2 and *Thiodictyon* strain F4 require higher light intensities for fast Fe(II) oxidation and thus cannot live as deep in sediments as strain KoFox.

In modern microbial iron rich mats, light penetrates on average about 2-3 mm and thus phototrophic bacteria will live in the upper anoxic millimeter of such an environment (e.g. Pierson et al., 1999). The amount of light the phototrophic Fe(II)-oxidizing strains need for maximum Fe(II) oxidation follows the general observation that green-sulfur-bacteria (such as strain KoFox) have a very low light saturation, while purple sulfur and purple non-sulfur bacteria need more light (in our case represented by strains F4 and SW2, respectively) (Overmann & Schubert, 2002).

10.5.4 Oxidation of dissolved Fe(II) and relatively soluble Fe(II) minerals

We found that the oxidation rate is the same at low Fe(II) concentrations (2 and 4 mM Fe(II)) for filtered (no Fe(II) minerals present) and unfiltered medium (including Fe(II) minerals). This suggests that at these concentrations, the dissolution rate of the Fe(II) minerals support iron oxidation rates as fast as the ones obtained with only dissolved Fe(II). In contrast, at higher concentrations (e.g. 8 mM Fe(II)), the oxidation rates were much faster in the presence of only dissolved Fe(II) compared to a setup containing dissolved Fe(II) as well as Fe(II) minerals. This suggests that at such high Fe(II) concentrations, in particular in the presence of high amounts of Fe(II) minerals, the dissolution rate of the Fe(II) minerals limits the overall oxidation rate. This may be due to Fe(III) mineral formation at the surface of the Fe(II) minerals thus reducing the Fe(II) mineral dissolution rate. Additionally, the organisms might directly oxidize Fe(II) minerals by transferring electrons from the mineral surface into the cells and not only dissolved Fe(II) as previously suggested (Croal et al., 2007, Jiao & Newman, 2007). These authors provide evidence that Fe(II) oxidation takes place in the periplasm of phototrophic Fe(II)-oxidizing bacteria which would require a dissolved Fe(II) species to be transported at some step. In contrast, oxidation of Fe(II) minerals does not necessarily require the presence of dissolved Fe(II) and could explain why in the presence of higher amounts of Fe(II) minerals the oxidation rates are lower than in the presence of only dissolved Fe(II). The bulk of the Fe(II) minerals are not accessible to the microbes via direct contact. In order to distinguish the contribution of Fe(II) coming from the poorly crystalline minerals vs. the Fe(II) from solution further experiments are needed.

10.5.5 Pigments in anoxygenic phototrophic Fe(II)-oxidizers

Carotenoids function both as radical detoxifiers and as light harvesting pigments (Britton, 1995b,a), harvesting photons used for energy generation in cyclic photophosphorylation, but also protecting cells from oxidative damage by radicals. Since radical formation is stimulated by Fe-catalyzed Fenton reactions, in particular photosynthetic Fe(II)-oxidizing bacteria are potentially faced with high radical concentrations. As a consequence, it can be speculated that these organisms might contain unique and specialized carotenoids that help the cells to cope with these radicals. We therefore determined the identity

of the main carotenoids in the photosynthetic Fe(II)-oxidizing strains *Rhodobacter ferrooxidans* strain SW2, *Chlorobium ferrooxidans* strain KoFox, and *Thiodictyon* sp. F4. However, the pigments identified (spheroidene, spheroidenone, OH-spheroidene, rhodopinal, chlorobactene) suggest that these organisms use standard carotenoids that are also present in non-Fe(II)-oxidizing relatives of these phototrophic organisms (Britton, 1995b,a). Despite the presence of high concentrations of Fe and exposure to light, radical formation (e.g. due to light catalyzed radical formation and/or Fenton reactions) obviously does not represent a major problem for these organisms.

10.5.6 Potential role of anoxygenic phototrophic Fe(II)-oxidizers on ancient earth

In order to evaluate a potential role of phototrophic Fe(II)-oxidizing bacteria in the formation of Precambrian banded iron formations, eco-physiological studies with modern organisms help constrain the conditions required for such organisms and whether it is plausible that they thrived at all in Precambrian oceans. While it is true that these modern analogue organisms could have acquired new functions via horizontal gene transfer or have evolved over time including adaptation of their physiology to modern environmental conditions, evolutionary phylogenetic studies and eco-physiological studies with modern strains are the only way to constrain possible scenarios in the past.

To date, modeling of ocean pH on early earth yielded a pH value of approximately 7 (Grotzinger & Kasting, 1993) and a wide range of temperatures of 25-70 °C (Knauth & Lowe, 2003, Robert & Chaussidon, 2006, Jaffrés et al., 2007, Shields & Kasting, 2007) with the most recent suggestion of 10-33 °C (Kasting et al., 2006). While certainly not offering direct proof, the physiological data presented in this study for three phylogenetically distant phototrophic Fe(II)-oxidizers supports the notion that these organisms may have lived in a moderate-temperature Precambrian ocean actively contributing to BIF deposition. The Fe(II) oxidation rates provided in the present study even support a recent report in which we used first preliminary physiological data to suggest that the rates of oxidation by phototrophic Fe(II)-oxidizing bacteria can indeed sustain the high Fe(III) precipitation rats required for the deposition of the BIFs (Kappler et al., 2005). Additionally, the oxidation rates provided here for several strains of phototrophic Fe(II)-oxidizers under various environmental conditions allow in future studies not only evaluation of Fe(III) precipitation rates under different conditions. It also allows to better understand modern and ancient Fe cycling as attempted previously by (Konhauser et al., 2005) who used Fe(II) oxidation rates to model the ancient Fe-cycle involved in the deposition of BIFs.

Since the heavily debated upper temperature limit suggested for Precambrian oceans, (see e.g. Jaffrés et al., 2007) is approximately 50-70 °C, the isolation of a thermophilic phototrophic iron-oxidizing strain e.g. from iron-rich hot springs would offer a modern analogue strain which could offer more information about the role of these organisms in BIF deposition at higher temperatures. In addition, the model of BIF deposition by anoxygenic phototrophs assumes that these strains thrived in the water column of the archean ocean (Kappler et al., 2005). As all modern organisms isolated thusfar stem from ditches or sediments, two of them from marine sediments, it would be beneficial to isolate such as strain from the water column. Since unfortunately modern oceans are either oxic or sulfidic, no modern analogue of a Fe(II)-rich ocean exists. However, a number of lakes with seasonal stratification and significant concentrations of dissolved Fe(II) in the water column are good candidates for isolation of Fe(II)-oxidizing organisms from the water column. Interestingly, however, it has been recently demonstrated that even the strains isolated from sediments can maintain a significant concentration of planktonic cells in the water column when grown in batch cultures (Konhauser et al., 2005).

10.6 Conclusions

Knowledge about the physiological limitations of phototrophic Fe(II)-oxidizers better constrains metabolic activities that close the iron cycle under anoxic conditions and in particular microbially-catalyzed processes that lead to the formation of Fe(III) oxides in the upper centimeters of the subsurface. The Fe(II) oxidation rates determined for phototrophic iron-oxidizing bacteria under varying conditions of pH, temperature and light and will help to understand the interactions of iron oxidizers and iron reducers since Fe(II)-oxidizing bacteria provide the Fe(III) for the iron reducers that mineralize organic matter and in turn the iron-reducers provide the Fe(II) that is used by the anoxygenic phototrophs.

The activity of anoxygenic phototrophic Fe(II)-oxidizers is limited to Fe(II)-rich and light-penetrated environments such as the surface of sediments, ditches or soils (although so far no phototrophic Fe(II)-oxidizers were isolated from soils). However, the fact that these organisms can tolerate a wide range of pH values and temperature, can cope with low light intensities and can live with low and high concentrations of Fe(II) suggests that they find niches in many environments. However, further research is needed to determine the full ecological role of this metabolism. Additionally, more biochemical research is needed in order to understand the mechanism of anaerobic Fe(II) oxidation and the strategies that these organisms developed to deal with a poorly soluble metabolic product, i.e. Fe(III) (hydr)oxides.

Acknowledgments

We would like to acknowledge Sonia Huelin for providing data of the pH-dependence of the strains. SEM images were taken by Sebastian Schädler and Claus Burkhardt at the Natural and Medical Sciences Institute at the University of Tübingen. We would like to thank Jennyfer Miot for chemical data regarding the primary precipitates of the mineral medium. We would also like to thank two anonymous reviewers for helpful comments. This study was funded by an Emmy-Noether fellowship and additional funding from the German Research Foundation (DFG) to AK.

Bibliography

Baker, BJ & Banfield, JF: Microbial communities in acid mine drainage. *FEMS Microbiology Ecology*, 44:139–152, 2003.

Beukes, NJ; Klein, C; Holland, HD; Kasting, JF; Kump, LR; & Lowe, DR: *Proterozoic Atmosphere and Ocean*. The Proterozoic Biosphere: a multidisciplenary study (Press Syndicate of the University of Camebridge, New York), 1992.

Blake, RC; Shute, EA; Greenwood, MM; Spencer, GH; & Ingledew, WJ: Enzymes of aerobic respiration on iron. *FEMS Microbiology Reviews*, 11:9–18, 1993.

Britton, G: Structure and properties of carotenoids in relation to function. *FASEB Journal*, 9:1551–1558, 1995a.

Britton, G: *UV/Visible Spectroscopy*. Carotenoids (Birkhäuser, Basel), 1995b.

Brocks, JJ; Love, GD; Summons, RE; Knoll, AH; Logan, GA; & Bowden, SA: Biomarker evidence for green and purple sulphur bacteria in a stratified palaeoproterozoic sea. *Nature*, 437:866–870, 2005.

Canfield, DE: Reactive iron in marine sediments. *Geochimica et Cosmochimica Acta*, 53:619–632, 1989.

Canfield, DE; Thamdrup, B; & Hansen, JW: The anaerobic degradation of organic matter in danish coastal sediments: Iron reduction, manganese reduction, and sulfate reduction. *Geochimica et Cosmochimica Acta*, 57:3867–3883, 1993.

Cloud, PE: Atmospheric and hydrospheric evolution on primitive earth. *Science*, 160:729–737, 1968.

Croal, LR; Jiao, Y; & Newman, DK: The fox operon from *Rhodobacter* strain SW2 promotes phototrophic fe(II) oxidation in *Rhodobacter capsulatus* sb1003. *Journal of Bacteriology*, 189:1774–1782, 2007.

Croal, LR; Johnson, CM; Beard, BL; & Newman, DK: Iron isotope fractionation by Fe(II)-oxidizing photoautotrophic bacteria. *Geochimica et Cosmochimica Acta*, 68:1227–1242, 2004.

Edwards, KJ; McCollom, TM; Konishi, H; & Buseck, PR: Seafloor bioalteration of sulfide minerals: Results from in situ incubation studies. *Geochimica et Cosmochimica Acta*, 67:2843–2856, 2003.

Ehrenreich, A & Widdel, F: Anaerobic oxidation of ferrous iron by purple bacteria, a new type of phototrophic metabolism. *Applied and Environmental Microbiology*, 60:4517–4526, 1994.

Emerson, D & Moyer, C: Isolation and characterization of novel iron-oxidizing bacteria that grow at circumneutral pH. *Applied and Environmental Microbiology*, 63:4784–4792, 1997.

Emerson, D & Weiss, J: Bacterial iron oxidation in circumneutral freshwater habitats: Findings from the field and the laboratory. *Geomicrobiology Journal*, 21:405–414, 2004.

Farquhar, J; Bao, H; & Thiemens, M: Atmospheric influence of earth's earliest sulfur cycle. *Science*, 289:756–758, 2000.

Garrels, RM; Perry, EA, JR; & Mackenzie, FT: Genesis of precambrian iron-formations and the development of atmospheric oxygen. *Economic Geology*, 68:1173–1179, 1973.

Gerhardt, S; Brune, A; & Schink, B: Dynamics of redox changes of iron caused by light-dark variations in littoral sediment of a freshwater lake. *Biogeochemistry*, 74:323–339, 2005.

Grotzinger, JP & Kasting, JF: New constraints on precambrian ocean composition. *Journal of Geology*, 101:235–243, 1993.

Hartmann, H: The evolution of photosynthesis and microbial mats: a speculation on banded iron formations. In Y Cohen; RW Castenholz; HO Halvorson; & CW Boylen, eds., *Microbial Mats - Stromatolites*, pp. 451–453 (Liss, A. R., New York), 1984.

Heising, S; Richter, L; Ludwig, W; & Schink, B: *Chlorobium ferrooxidans* sp nov., a phototrophic green sulfur bacterium that oxidizes ferrous iron in coculture with a *"Geospirillum"* sp strain. *Archives of Microbiology*, 172:116–124, 1999.

Heising, S & Schink, B: Phototrophic oxidation of ferrous iron by a *Rhodomicrobium vannielii* strain. *Microbiology*, 144:2263–2269, 1998.

Jaffrés, JBD; Shields, GA; & Wallmann, K: The oxygen isotope evolution of seawater: A critical review of a long-standing controversy and an improved geological water cycle model for the past 3.4 billion years. *Earth-Science Reviews*, 83:83–122, 2007.

Jiao, Y; Kappler, A; Croal, LR; & Newman, DK: Isolation and characterization of a genetically traceable photoautotrophic Fe(II)-oxidizing bacterium, *Rhodopseudomonas palustris* strain tie-1. *Applied and Environmental Microbiology*, 71:4487–4496, 2005.

Jiao, Y & Newman, DK: The pio operon is essential for phototrophic Fe(II) oxidation in rhodopseudomonas palustris tie-1. *Journal of Bacteriology*, 189:1765–1773, 2007.

Johnson, CM; Beard, BL; Beukes, NJ; Klein, C; & O'Leary, JM: Ancient geochemical cycling in the earth as inferred from fe isotope studies of banded iron formations from the transvaal craton. *Contributions to Mineralogy and Petrology*, 144:523–547, 2003.

Kappler, A & Newman, DK: Formation of Fe(III)-minerals by Fe(II)-oxidizing photoautotrophic bacteria. *Geochimica et Cosmochimica Acta*, 68:1217–1226, 2004.

Kappler, A; Pasquero, C; Konhauser, KO; & Newman, DK: Deposition of banded iron formations by anoxygenic phototrophic Fe(II)-oxidizing bacteria. *Geology*, 33:865–868, 2005.

Kappler, A & Straub, KL: Geomicrobiological cycling of iron. *Reviews in Mineralogy & Geochemistry*, 59:85–108, 2005.

Kasting, JF; Howard, MT; Wallmann, K; Veizer, J; Shields, G; & Jaffrés, J: Paleoclimates, ocean depth, and the oxygen isotopic composition of seawater. *Earth and Planetary Science Letters*, 252:82–93, 2006.

Knauth, LP & Lowe, DR: High archean climatic temperature inferred from oxygen isotope geochemistry of cherts in the 3.5 ga swaziland supergroup, south africa. *Geological Society of America Bulletin*, 115:566–580, 2003.

Konhauser, KO; Newman, DK; & Kappler, A: The potential significance of microbial Fe(III) reduction during deposition of precambrian banded iron formations. *Geobiology*, 3:167–177, 2005.

Lovley, DR: Dissimilatory Fe(III) and Mn(IV) reduction. *Microbiology and Molecular Biology Reviews*, 55:259–287, 1991.

Overmann, J & Schubert, K: Phototrophic consortia: model systems for symbiotic interrelations between prokaryotes. *Archives of Microbiology*, 177:201–208, 2002.

Pierson, BK; Parenteau, MN; & Griffin, BM: Phototrophs in high-iron-concentration microbial mats: Physiological ecology of phototrophs in an iron-depositing hot spring. *Applied and Environmental Microbiology*, 65:5474–5483, 1999.

Rashby, SE; Sessions, AL; Summons, RE; & Newman, DK: Biosynthesis of 2-methylbacteriohopanepolyols by an anoxygenic phototroph. *Proceedings of the National Academy of Sciences*, 104:15099–15104, 2007.

Robert, F & Chaussidon, M: A palaeotemperature curve for the precambrian oceans based on silicon isotopes in cherts. *Nature*, 443:969–972, 2006.

Rosso, L; Lobry, JR; Bajard, S; & Flandrois, JP: Convenient model to describe the combined effects of temperature and pH on microbial-growth. *Applied and Environmental Microbiology*, 61:610–616, 1995.

Schaedler, S; Burkhardt, C; & Kappler, A: Evaluation of electron microscopic sample preparation methods and imaging techniques for characterization of cell-mineral aggregates. *Geomicrobiology Journal*, 25:228–239, 2008.

Shields, GA & Kasting, JF: Palaeoclimatology: Evidence for hot early oceans? *Nature*, 447:E1, 2007.

Stookey, LL: Ferrozine – a new spectrophotometric reagent for iron. *Analytical Chemistry*, 42:779–781, 1970.

Straub, KL; Benz, M; Schink, B; & Widdel, F: Anaerobic, nitrate-dependent microbial oxidation of ferrous iron. *Applied and Environmental Microbiology*, 62:1458–1460, 1996.

Straub, KL; Rainey, FA; & Widdel, F: *Rhodovulum iodosum* sp. nov. and *Rhodovulum robiginosum* sp. nov., two new marine phototrophic ferrous-iron-oxidizing purple bacteria. *International Journal of Systematic Bacteriology*, 49:729–735, 1999.

Stumm, W & Morgan, JJ: *Aquatic chemistry: chemical equilibria and rates in natural waters* (Wiley-Interscience, New York), 3rd ed., 1995.

Stumm, W & Sulzberger, B: The cycling of iron in natural environments: Considerations based on laboratory studies of heterogeneous redox processes. *Geochimica et Cosmochimica Acta*, 56:3233–3257, 1992.

Thamdrup, B: Bacterial manganese and iron reduction in aquatic sediments. *Advances in Microbial Ecology, Vol 16*, 16:41–84, 2000.

Tschech, A & Pfennig, N: Growth yield increase linked to caffeate reduction in *Acetobacterium woodii*. *Archives of Microbiology*, 137:163–167, 1984.

Weber, KA; Achenbach, LA; & Coates, JD: Microorganisms pumping iron: anaerobic microbial iron oxidation and reduction. *Nature Reviews: Microbiology*, 4:752–764, 2006.

Widdel, F: *Anaerober Abbau von Fettsäuren und Benzoesäure durch neu isolierte Arten*. Ph.D. thesis, Universität Göttingen, Göttingen, 1980.

Widdel, F & Pfennig, N: Studies on dissimilatory sulfate-reducing bacteria that decompose fatty acids. i. isolation of a new sulfate-reducer enriched with acetate from saline environments. description of desulfobacter postgatei gen. nov. sp. nov. *Archives of Microbiology*, 129:395–400, 1981.

Widdel, F; Schnell, S; Heising, S; Ehrenreich, A; Assmus, B; & Schink, B: Ferrous iron oxidation by anoxygenic phototrophic bacteria. *Nature*, 362:834–836, 1993.

Xiong, J: Photosynthesis: what color was its origin. *Genome Biology*, 7:245–245, 2006.

Züllig, H & Rheineck, SG: Pigmente phototropher bakterien in seesedimenten und ihre bedeutung für die seenforschung. *Aquatic Sciences - Research Across Boundaries*, 47:87–126, 1985.

11 Trace metal dependence of *"Rhodobacter ferrooxidans"* strain SW2, a Fe(II)-oxidizing bacterium – a model organism?

Florian Hegler[1], Stefanie Lutz[1], Stefan Lalonde[2], Kurt Konhauser[2], Andreas Kappler[1]

[1]Center for Applied Geoscience – Geomicrobiology, Eberhard Karls University Tübingen, Sigwartstr. 10, 72076 Tübingen, Germany
[2]Department of Earth and Atmospheric Sciences, University of Alberta, Edmonton, Alberta, T6G 2E3, Canada

11.1 Abstract

The trace metal content – or metallome – defines an organism to the same extent as the proteome (all proteins of an organism) or the genome (all genes). Only the atoms of the metallome withstand time while both, DNA and proteins, degrade over time. The metallome is hence a good potential tool to determine which organisms could have lived in certain environments in the past. The phototrophic Fe(II)-oxidizing microorganism *"Rhodobacter ferrooxidans"* strain SW2 is used as a model organism to study the deposition of the banded iron formations (BIFs). Therefore, we determined the trace metal content and the trace metal requirements of this organism.

We followed growth of *"Rhodobacter ferrooxidans"* strain SW2 in medium depleted in either molybdenum, nickel, cobalt or vanadium. Additionally, the trace metal content in the cytoplasm of this strain grown with a surplus of trace elements was determined. Geochemical sorption modeling of molybdenum, vanadium, nickel and cobalt to ferrihydrite in minimal mineral medium provided data on the trace metal availability in medium.

"Rhodobacter ferrooxidans" strain SW2 requires cobalt, vanadium and nickel. Molybdenum is required only in traces below experimental limits. The metallome of *"Rhodobacter ferrooxidans"* strain SW2 reflects the trace metal availability in oceans on ancient earth. Thus, the strain potentially conserved metal requirements from the past and is therefore a good model organism for understanding environments on early earth.

11.2 Introduction

11.2.1 Trace element requirements of cells

Any living organism consists ultimately of atoms. The ratio amongst the major elements such as carbon, nitrogen and phosphorous is often very similar between any group of organisms (Redfield et al., 1963, Copin-Montegut & Copin-Montegut, 1983, Downing, 1997, Sterner & Elsner, 2002). For example, in the

case of marine plankton the ratio between carbon, nitrogen and phosphate is 106:16:1 (Redfield et al., 1963).

However, the ratio and abundance of minor elements may differ between species more than the major elements. Such less abundant elements – or trace elements (TE) – are mostly metals that are oftentimes located in the reactive centers of enzymes (Fraústo da Silva & Williams, 2001). Trace elements are chromium, cobalt, copper, iodine, iron, manganese, molybdenum, nickel, selenium, tungsten, vanadium and zinc but probably also other elements. The concentrations of TE within phototrophic cells lies between 0.05-1.5 μmols g^{-1} dry weight (Kassner & Kamen, 1968). The ratio and abundance of TE in the cell is governed by the habitat but also the genome of an organism (Fraústo da Silva & Williams, 2001, Zhang & Gladyshev, 2010). Microorganisms may adapt to their environment by adjusting their enzymes to the metals prevailing in their surrounding. It has been shown, that various groups of organisms require different trace metals depending on their prevailing habitat (e.g. anoxic compared to microaerophilic) (Zhang & Gladyshev, 2010). *Ferroplasma acidiphilum* may for example replace more than 80% of all metals in the reactive centers of enzymes in media supplemented by iron as only TE by just one metal: iron (Ferrer et al., 2007).

However, not only the environmental factors dictate the TE-requirements of an organism. Some TE requirements are deeply rooted in the genome and thus can be stable for billions of years (Fraústo da Silva & Williams, 2001, Zerkle et al., 2005, Anbar, 2008). For example, it is known, that copper remains to be very scarce in archeae which is hypothesized to be due to its low bioavailability on early earth during the peaking of archeae abundance (Fraústo da Silva & Williams, 2001).

11.2.2 Trace element availability in the past

As already hinted above, TE availability to microorganisms changed fundamentally over geological timescales coupled to the geochemical conditions on the earth (Fraústo da Silva & Williams, 2001, Zerkle et al., 2005, 2006, Anbar, 2008). Considering the change from an anoxic to an oxic atmosphere (Kasting & Siefert, 2002, Kasting, 2004) a fundamental change in TE availabilities is to be expected. The oxidation state of trace elements changed over time (Fraústo da Silva & Williams, 2001). But even more importantly, the ocean chemistry changed fundamentally from an anoxic, sulphide rich to an oxic, sulphide poor ocean (Zerkle et al., 2005, Anbar, 2008, Reinhard et al., 2009). The concentrations of certain TE were much lower on ancient earth than today (e.g. Mo and Ni) due to the low solubility of sulphides (Fraústo da Silva & Williams, 2001, Zerkle et al., 2005, Williams & Fraústo da Silva, 2006, Anbar, 2008). Some elements that were abundant in the oceans in the past more than 2.5 Ga ago are today only present as TE, iron is the most prominent example.

Hence, any organism living in ancient earth environments evolved with the metals available while its enzymes evolved according to the geochemically available TE ultimately defining the metallome. As most main enzymes evolved during that time the enzyme's need for certain TE would be fixed in the genome. This information is passed on through time and may change only very little, especially if the evolutionary pressure is low. Therefore, the imprint of the geochemical conditions of the past may be passed on in the genome and may still be found today in the metallome of organisms.

Therefore, the genetic information that determines the TE content of the cell today can result from two fundamentally different conditions: i) the need of a certain element in the reactive center of an enzyme because only this specific element can fulfill the reaction; or ii) even if different metals could perform similarly well in the reactive center of an enzyme, due to the geochemical conditions only certain trace

metals were available and the enzymes evolved that way.

Hence, the genetic mark was passed on through evolution although today the TE availability may have changed (Zerkle et al., 2005, Williams & Fraústo da Silva, 2006, Anbar, 2008). In that case, a higher abundance of some TE within the cell may allow to draw conclusions about the geochemical setting in which certain groups evolved in (Fraústo da Silva & Williams, 2001, Zerkle et al., 2005).

11.2.3 Banded iron formations and phototrophic Fe(II)-oxidizing bacteria

The differences in TE requirements in certain organisms can potentially be used to understand how some of the largest iron-rich deposits (BIFs) on earth formed. It is known that geogenic Fe(II) from hydrothermal vents was oxidized to Fe(III) and finally precipitated as layered silica-iron rich sedimentary deposits of several km^2 (Beukes et al., 1992, Posth et al., 2008). Several hypotheses to explain the oxidation exist:

- The oxidation of Fe(II) by UV-light was suggested (Cairns-Smith, 1978) but suggested to be of minor importance under Archean seawater conditions (Konhauser et al., 2007).
- The oxidation of Fe(II) by molecular oxygen stemming from the reduction of water by cyanobacteria (Cloud, 1968, Beukes et al., 1992, Konhauser et al., 2002)
- The direct oxidation of Fe(II) by phototrophic Fe(II)-oxidizing bacteria (photoferrotrophs) (Garrels et al., 1973, Widdel et al., 1993, Konhauser et al., 2002, Kappler et al., 2005, Hegler et al., 2008, Posth et al., 2008).

It is highly probable now, that BIFs younger than 2.5-2.2 Ga formed by the oxidation of Fe(II) by molecular oxygen. Older BIFs did likely not form by molecular oxygen as larger concentrations of molecular oxygen on early earth developed only between 2.5-2.2 Ga (Canfield, 2005). Nonetheless, small concentrations of oxygen were likely present even before that time although the importance in the oxydation of Fe(II) is still debated (Anbar et al., 2007). Therefore, photoferrotrophs were probably involved in the formation of older BIFs (Kappler et al., 2005, Posth et al., 2008).

In order to determine, how closely a modern photoferrotrophic strain resembles the proposed TE availability on ancient earth we determined the TE utilization pattern for *"Rhodobacter ferrooxidans"* strain SW2 (Widdel et al., 1993, Ehrenreich & Widdel, 1994) for four different trace metals (nickel, vanadium, molybdenum or cobalt). This will allow to determine if *"Rhodobacter ferrooxidans"* strain SW2 is a good model organism for the TE utilization pattern and thus and their link to the past.

11.2.4 Trace metals – from the past until today

While the oxygen concentration in the atmosphere remained low on early earth until 2.5 Ga ago (Bekker et al., 2004, Anbar et al., 2007) the earth's environment was reducing. Elements like cobalt and nickel are especially suited for electron rich environments like the ones on ancient earth rich in CH_4, H_2, CO and H_2S. Today, in contrast, the environment is rather electron poor (e.g. rich in O_2, N_2 and CO_2) which make the use of other, more specific, metals in reactive centers in enzymes better suited (Williams & Fraústo da Silva, 2006). Thus, the use of cobalt and nickel in an organism today points towards the conservation of enzymes that evolved billions of years ago (Williams & Fraústo da Silva, 2006).

Molybdenum on the other hand has been only scarcely available on early earth due to the precipitation of MoS and other species while molybdate at the higher oxidation state of six is more soluble and became only available today (Zerkle et al., 2005, Williams & Fraústo da Silva, 2006, Anbar, 2008). The use of

molybdenum in organisms today thus indicates that the enzymes have likely developed after oxygen levels increased on earth (Williams & Fraústo da Silva, 2006). Vanadium is thought to have fulfilled the same functions in enzymes as molybdenum but was better bioavailable on ancient earth than molybdenum due to the better solubility of vanadium-sulfides (Williams & Fraústo da Silva, 2006). Thus, the use of vanadium in any organism also indicates preserved traits from the past (Williams & Fraústo da Silva, 2006). Hence, the use of vanadium, cobalt, nickel and molybdenum in enzymes by any bacteria is a good indicator if the metallome of a bacterium conserved traits from the past to present.

In order to determine if the photoferrotroph *"Rhodobacter ferrooxidans"* strain sp. SW2 uses trace metals that had been dominantly used on ancient earth, we performed depletion studies in which one of the four trace metals (nickel, vanadium, molybdenum and cobalt) was removed from the medium. Additionally, the whole metallome in cells was measured by supplementing a batch-culture with higher amounts of TE and then determining the concentration of TE that was built into the cells biomass.

11.2.5 Geochemical modeling of trace metal sorption to Fe(III) minerals

Sorption of trace metals to Fe(III) minerals depends on several factors, e.g. the crystallinity, the mineral type and the geochemical conditions under which the minerals precipitate. These factors have been determined for hydrous ferrous oxides (HFO) (Dzombak & Morel, 1990) and goethite (Mathur & Dzombak, 2006). Fe(III) minerals precipitating in mineral medium are poorly crystalline and are likely best resembled HFO. In order to understand the availability of these TE in mineral medium, we modeled sorption of the respective trace metals to HFO (Dzombak & Morel, 1990). These results may be interpolated to the conditions prevailing on early earth.

11.3 Materials and Methods

11.3.1 Medium, strains and growth conditions

"Rhodobacter ferrooxidans" strain SW2 (Widdel et al., 1993, Ehrenreich & Widdel, 1994) was used from the lab strain collection. The mineral medium was prepared according to Hegler et al. (2008). In order to remove potentially adsorbed TE, all glass-ware was washed with 1 mol L^{-1} HCl for 24 hours and after that rinsed for at least 48 hours with ultrapure water (conductivity 55.5 μS) before use.

In order to determine the TE-requirements of the strain, two sets of experiments were performed:

- One of the four trace metals vanadium, nickel, molybdenum or cobalt was limited in the medium while growth of the strain was observed at the same time.
- Trace elements were added in excess while growth was observed and the TE content in the cytoplasm was determined with ICP-MS.

The trace element solution was prepared according to Tschech & Pfennig (1984): 5 mL 25% HCl were added to 495 mL ultrapure water and 70 mg L^{-1} $ZnCl_2$, 100 mg L^{-1} $MnCl_2 \times 4H_2O$, 2 mg L^{-1} $CuCl_2 \times 2H_2O$ and 30 mg L^{-1} H_3BO_3 were supplemented subsequently. The solutions of the four trace metals nickel, vanadium, cobalt and molybdenum were prepared separately. In all cases, 5 mL 25% HCl were added to 495 mL ultrapure water and either 190 mg L^{-1} $CoCl_2 \times 6H_2O$ or 240 mg L^{-1} $NiCl_2 \times 6H_2O$ or 36 mg L^{-1} $Na_2MoO_4 \times 2H_2O$ or 25 mg L^{-1} NH_4VO_3 were added. Additionally, a separate solution of

6 mg L^{-1} $Na_2SeO_3 \times 5H_2O$ and 8 mg L^{-1} $Na_2WO_4 \times 2H_2O$ amended with 0.4 g L^{-1} NaOH was prepared. 1 mL L^{-1} of all TE solutions were added to the medium except the solutions containing the undesired TE.

Two different vitamin solutions were prepared. Solution 1 contained 12 mg L^{-1} d(+)-biotin, 50 mg L^{-1} B1-hydrochloride, 250 mg L^{-1} B6-hydrochloride, 50 mg L^{-1} 4-aminobenzoic acid and 25 mg L^{-1} D-pantothenic acid dissolved in ultrapure water. Solution 2 contained 50 mg L^{-1} cobalamin dissolved in ultrapure water as this vitamin contains cobalt. Thus, vitamin solution 2 was not added when cobalt was omitted as TE. Again, 1 ml L^{-1} vitamin solution was added to the medium.

Although of highest purity, the Fe(II)-salt $FeCl_2$ (99.8%) contained substantial amounts of TE. Hence, the iron solution for adding Fe as trace metal was prepared separately. Elemental iron of ultrapure standard was washed with acetone to remove organic contaminants. The Fe(0) was dissolved and oxidized to Fe(II) in anoxic 1 mol L^{-1} HCl in an anoxic chamber. Fe(II) was added to the medium to a final concentration of 7.5 μmol L^{-1}. Trace metal solutions were autoclaved while vitamin solutions and the Fe(II) solution were sterile-filtered with a 0.2 μm filter (polyethylensulfone, Millipore). The concentrations of all TE-solutions were determined by ICP-MS (chapter 11.3.3).

For experiments in which the trace elements were added in excess, the trace element solution was not prepared separately but as one solution. Also the vitamin-solution was prepared in one and not two solutions. In experiments supplemented with excess trace metals, the amounts of trace metals as stated above were added 0 ×, 0.5 ×, 1 ×, 2 × and 5 × of the described concentrations above.

ICP-MS measurements showed that Millipore water from the lab contained Ni and Mo (chapter 11.4.1). Hence, for setups depleted in nickel and molybdenum Ultrapure water (Rotipuran) from Roth (Karlsruhe, Germany) was used.

In all cases, the electron donor was a mixture of H_2/CO_2 (80:20), cultures were incubated at light saturation of a standard tungsten light bulb (Hegler et al., 2008). The light intensity was determined with a photometer. This setup allowed to measure the bacterial growth by measuring the optical density (OD) at 660 nm with a photospectrometer (Spekol 1300, Analytik Jena) over time. Measurements were done at least twice per week. For trace element depletion studies, the medium was filled into 15 mL test-tubes to a final volume of 7.5 mL. The inoculum was 1% (v/v) of the total medium. These experiments were conducted in independent duplicates. In studies supplementing the bacteria with additional TE, the medium was filled into 1 L Schott-bottles to a final volume of 400 mL. Again, H_2/CO_2 (80:20) was used as electron donor and cells were incubated at light saturation.

11.3.2 Data evaluation of growth experiments

Growth experiments depleted in either Co, Ni, Mo or V were evaluated. The cultures were transferred three times with each depletion type medium (no Co, Ni, V or Mo) while each time two test-tubes were inoculated. The OD in the stationary phase was determined by averaging three OD values.

The change in OD for experiments that contained additional amounts of trace metals was followed over time (n=1). The growth rate of the culture was determined according to equation 11.1 which as previously determined by correlating OD to the cell number counted in a Thoma-chamber:

$$\text{growth rate} = \ln \frac{N_2}{N_1} / \Delta t \tag{11.1}$$

N1 is the concentrations of cells at time 1 and N2 is te concentration of cells at time 2. Additionally, the trace metal content within the cell was measured by ICP-MS (see chapter 11.3.3).

The cell number needed to calculate the growth rate was determined by counting the cell number microscopically in a Thoma-chamber and correlating it to the OD_{660} (eq. 11.2).

$$\text{cell number} = 1.5E^{+9} \times \text{OD at } 660\,\text{nm} \tag{11.2}$$

11.3.3 Quantification of trace elements

Trace element concentrations were measured with a Perkin Elmer Elan6000 quadrupole ICP-MS at the University of Alberta, Edmonton, Canada. Calibration was made using certified commercial multi-element standards. Liquid samples of all solutions were analyzed in triplicates for medium depleted in one of the four TE. In order to determine the concentration of TE in the cytoplasm of cells in TE-supplemented experiments, cells were quantitatively harvested in the stationary phase by centrifugation at 8000 × g. The pellet was resuspended three times in 0.01 mol L^{-1} HCl and centrifuged at 8000 × g in order to remove adsorbed TE from the cell surface. The cells were freeze-dried.

The freeze-dried biomass was digested in concentrated trace metal grade HNO_3 at 60 °C in teflon beakers. The residues were resuspended in 8 mol L^{-1} trace metal grade nitric acid.

11.3.4 Geochemical modeling

Ferrihydrite is an nano-crystalline Fe(III) mineral (Michel et al., 2007, 2010) which is often found in nature (Jambor & Dutrizac, 1998, Cornell & Schwertmann, 2003). TE availability to cells may be limited due to adsorption to Fe(III) minerals, especially ferrihydrite is a good scavenger (Jambor & Dutrizac, 1998, Cornell & Schwertmann, 2003). Hence, geochemical modeling of the adsorption of TE to ferrihydrite yields information about a potential bio-limitation of TE to the cell due to adsorption to ferrihydrite. Geochemical modeling was performed with the SpecE8 module of Geochemists Workbench 6.05 by Rockware. The input parameters were as follows: all salts in the medium as described in Hegler et al. (2008) while the trace element concentrations were added according to the described concentrations above (chapter 11.3.1). The Minteq database for adsorption data as well as equilibrium constants was used. The concentration of ferrihydrite was set to 10 mmol L^{-1}. The constant capacitance was set to 0.9 F m^2 (Hiemstra & van Riemsdijk, 2009). The pH of the solution was varied from 6 to 8.

11.4 Results and Discussion

11.4.1 Concentrations of TE in media and stock solutions

The concentrations of most elements from Li to U were measured in all stock solutions by ICP-MS (table 11.1 and supporting information table 11.5). Some elements were excluded from the ICP-MS analysis, these were carbon, nitrogen, oxygen, fluorine, all noble gases and some elements with no biological importance. The concentration of any TE in other but the respective stock solutions did not exceed 0.4 μmol L^{-1} but usually was much lower (see supporting information tab 11.4).

Millipore water – which was normally used – contained Ni and Mo (table 11.1). Thus, in order to avoid intentioned input of Ni or Mo in depletion experiments, trace metal grade water was used (chapter 11.3.1).

Additionally, all concentrations of TE were analyzed in the medium to quantify for potential sorption to the glass and potential leaching of metals from the glass for all solutions, either containing the respective trace metal or not (background) (table 11.2). The background concentration results from impurities of

the other salts and water in the medium. Thus, the addition of any TE from the stock solution increased the concentration of that TE in the medium at least 85-fold above background level even for TE-release by the glass.

Table 11.1: Left column: Concentration of the four tested trace elements V, Ni, Co and Mo in the respective stock solutions used for preparing the medium of *"Rhodobacter ferrooxidans"* strain SW2. Stock solutions were added 1:1000 to the medium in order to supply the needed TE. Right column: Concentration of V, Ni, Co and Mo in Millipore water used to make the medium. DL - detection limit.

	TE in stock sltn. [μ**mol L**$^{-1}$]	**TE in Millipore water** [μ**mol L**$^{-1}$]
V	186	<DL
Ni	109	0.09
Co and vitamin B12	844	<DL
Mo	145	0.01

Table 11.2: Concentration of the four tested trace elements V, Ni, Co and Mo in the growth medium of *"Rhodobacter ferrooxidans"* strain SW2 either including the respective element (left column) or excluding it in the medium (middle column). In the case of the background TE concentration all other TE elements were included in the medium besides the undesired TE. The right column shows the detection limit of the ICP-MS for the four elements.

	medium incl. respective TE [**mol L**$^{-1}$]	**background of TE** [**mol L**$^{-1}$]	**detection limit ICP-MS** [**mol L**$^{-1}$]
V	1.87E^{-7}	1.37E^{-9}	9.8E^{-10}
Ni	1.10E^{-7}	1.27E^{-9}	1.0E^{-9}
Co	8.43E^{-7}	2.06E^{-11}	5.1E^{-10}
Mo	1.46E^{-7}	9.41E^{-10}	2.1E^{-10}

11.4.2 Growth of SW2 in medium lacking some TE

In order to determine if *"Rhodobacter ferrooxidans"* strain SW2 requires a certain trace metal, the concentration of either cobalt, nickel, vanadium or molybdenum was decreased as much as possible in the medium. If a certain TE was required by the cell for growth and present only in minor concentrations in the medium (chapter 11.2), the OD – as a proxy for cell number – decreased in the stationary phase after each of three consecutive transfers (figure 11.1). The concentration of the undesired TE was highest in the first transfer due to the addition of TE with the inoculum and thus likely decreased subsequently in the further transfers. No additional measurements were performed to determine the TE concentration in the first transfer.

In comparison to medium including all trace metals (c – control) the OD_{660} decreased in each transfer (T1 to T3) for setups lacking cobalt, vanadium and nickel while the OD_{660} for molybdenum did not decrease significantly in the transfer steps (fig 11.1. Thus, nickel, vanadium and cobalt are required by the cells of *"Rhodobacter ferrooxidans"* strain SW2 in concentrations higher than added in the TE depleted medium. Otherwise the cell density would not decrease in the stationary phase as shown (figure 11.1). Hence, the concentrations of Co, V and Ni are low enough to limit the cell growth. Therefore, a decrease in cell density (e.g. a decrease in OD) is a good proxy for a requirement of a certain trace metal by the cell.

Molybdenum is different to the other three TE. The OD did not decrease significantly in transfer 2 (n=8) and 3 (n=16) while the error in the first transfer (n=4) shows a high variability in the samples. Therefore, it seems likely that the cells were able to adapt to the lack of Mo, for example by replacing Mo by an other TE in the cell's enzymatic machinery. In transfer two and three, cells likely had already adapted to the low Mo-concentration, therefore a decrease in OD is not observable. Molybdenum is often associated with enzymes involved of the NO_3^- and SO_4^{2-} and N_2 turnover, species that were likley only present after the oxygenation of early earth. Williams & Fraústo da Silva (2006) state that likely tungsten predated the use of molybdenum in the cells machenery.

It was neither possible to reduce the concentration of the TE below the detection limit of the ICP-MS (chapter 11.4.1) nor below the physiological minimum needed for growth. Nonetheless, the decrease in cell number (e.g. the OD in the stationary phase) clearly showed for Co, V and Ni that the decrease of TE in the medium was sufficient to under-saturate the cells' requirements for TE. As a result, the total final cell number decreased. Cells can recycle TE efficiently and therefore will still grow with very low concentrations of TE. Therefore it is not expected that cell growth would stop entirely in the setups.

No study has so far determined the concentration of TE in phototrophic proteo-bacteria for either Co, V, Mo and Ni. Kassner & Kamen (1968) focused on other TE, nonetheless, the concentrations of TE in their experiments are in the same range as our data. For example, the concentration of iron is highest in the cells (approx. 4-8 μmol g^{-1} dry weight) while the concentrations of Mn, Cu and Zn were between 0.05 and 0.7 μmol g^{-1} dry weight in phototrophic proteo bacteria Kassner & Kamen (1968). Zerkle et al. (2005) calculated from whole genome sequences the TE-concentration in cyanobacteria. These values agree well with the values found in our case.

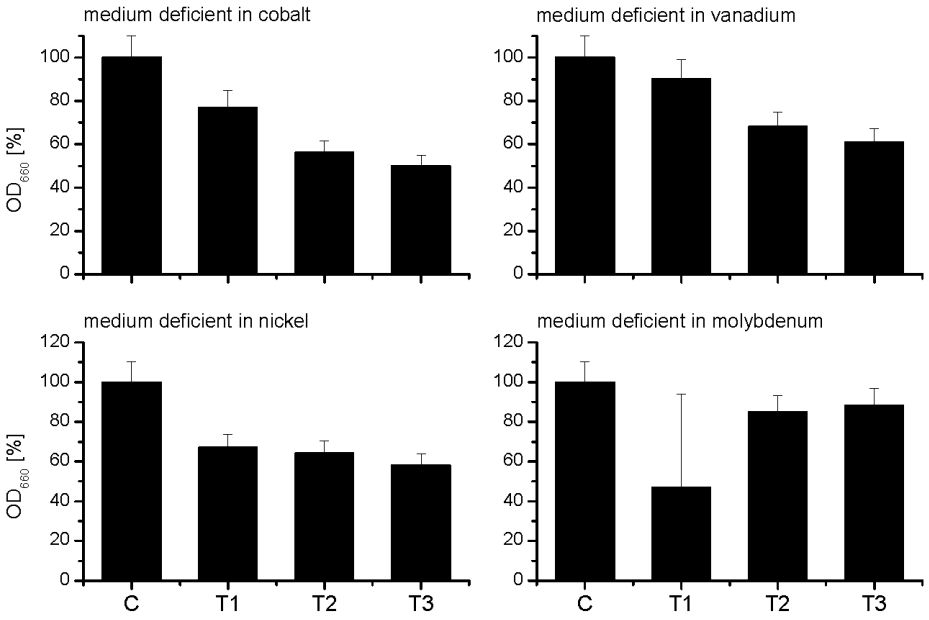

Figure 11.1: The OD_{660} was measured in medium depleted in either cobalt, vanadium, nickel or molybdenum. The culture was transferred three times (T1-T3). As comparison the OD was determined in medium containing all TE (C). (T1 – n=4; T2 – n=8; T3 – n=16). All results were normalized to the control. The error bars indicate the standard deviation.

Table 11.3: Concentration of TE in depletion study calculated per g dry weight of cells in the third transfer step. Left column: experiments including the respective TE, right column: experiments only containing the background concentration of the respective trace metal.

[mol g^{-1}] dry weight	including TE	background of TE
V	6.2×10^{-8}	4.5×10^{-10}
Ni	3.6×10^{-8}	4.2×10^{-10}
Co	2.8×10^{-7}	6.8×10^{-12}
Mo	4.8×10^{-8}	3.1×10^{-10}

11.4.3 Growth of the *"Rhodobacter ferrooxidans"* strain sp. SW2 supplemented with additional TE

In order to determine the uptake of TE by cells and the effects of high concentrations of TE to cells, we varied the amount of trace metals in the medium between 0 and 5-fold of the TE concentrations described in section 11.3.1. The growth rate and cell density in the stationary phase allowed to determine beneficial and toxic effects of TE for the cells.

Doubling or even adding five-fold the amount of TE compared to the concentrations described in section 11.3.1 yielded a 15% higher cell density in the stationary phase (figure 11.2). These results indicate a limitation of TE (1-fold addition of TE solution). The growth rate (equation 11.1) was similar in all

four setups (0.5 to 5-fold addition of TE) ranging between 0.0059 and 0.006 cell doublings per hour. Additionally, no toxic effects could be observed for the five-fold addition of trace metals, e.g. no decrease in the OD in the stationary phase (figure 11.2).

Adding 50% of the normal TE concentration (e.g. 0.5 × TE) did not result in a decrease of the OD in the stationary phase compared to the normal TE concentration (e.g. 1 × TE). The decrease in TE was not pronounced enough to substantially decrease the cell density, potentially the cells were able to compensate the lack of certain TE by using other metals or were able to recycle the TE efficiently.

The long growth phase in these experiments compared to cultures growing with Fe(II) as electron source (Hegler et al., 2008) is likely due to the limitation in hydrogen mixing with the medium as experiments were not carried out on a shaker. The growth rate was therefore slower than in a well mixed system or in smaller bottles (as published in Hegler et al., 2008). Nonetheless, experiments are comparable among each other as they were carried out under the same conditions.

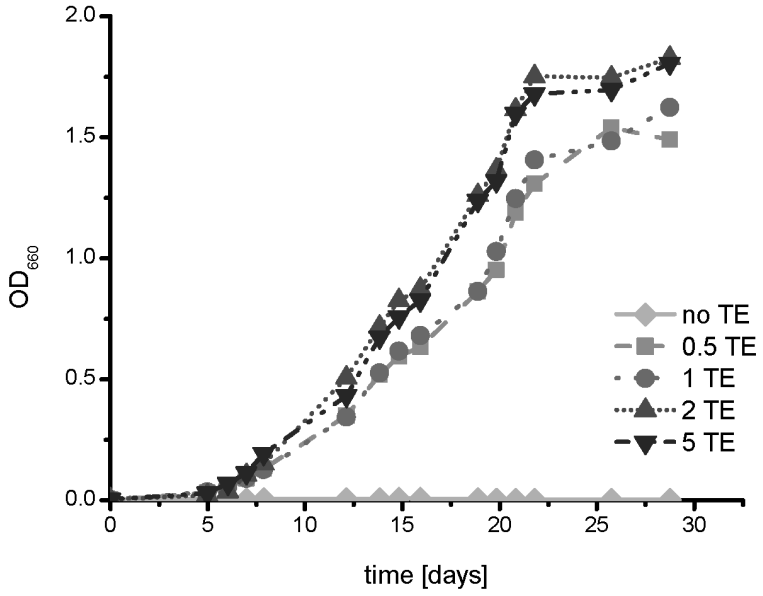

Figure 11.2: The OD_{660} plotted over time for different trace metal concentrations ranging from no addition of trace metals (no TE) to the five-fold concentration of trace metals generally used in the medium of *"Rhodobacter ferrooxidans"* strain sp. SW2.

Additionally, the TE concentration in the dry biomass was determined in the stationary phase for nickel, vanadium, molybdenum and cobalt in mol g^{-1} dry weight (figure 11.3). The results agree well with the results for cultures depleted in certain TE (chapter 11.4.2): The concentration of nickel and vanadium in the cell's biomass increases steeply from 0.5 × of the normal TE-concentration. Further addition of TE-solution doubles the concentration of vanadium and nickel in the cell's biomass (figure 11.3). Thus, both nickel and vanadium are clearly needed by the cells, especially due to the sharp increase at the lower concentration. Cobalt – in contrast to the other TE – does not seem to be saturated in the cells (figure 11.3) and its concentration increases 9-fold from the normal concentration to the 5-fold addition of TE. The concentration of molybdenum increases in the cells with higher concentration of TE in the medium up to 2-fold of the concentration of TE of the normal medium. Between the 2-fold and 5-fold

addition of Mo the concentration in the cells biomass decreases 2-fold. This is likely due to a replacement of Mo with other TE, potentially tungsten. This result agrees well with a hypothesized replacement of molybdenum with other TE by the cells if molybdenum is too scarce (section 11.4.2).

Not much data have been published for phototrophic proteobacterial cells and their TE requirements. Only Kassner & Kamen (1968) have published values for phototrophic cells for other TE but not for Co, Ni, V and Mo. Nonetheless, the TE concentrations in this study are very similar to the published values for other TE. For example the concentration of manganese in proteobacterial cell's dry weight has been evaluated for *Rhodospirillum rubrum*, *Rhodopseudomonas spheroides* and *Chromatium* by (Kassner & Kamen, 1968). In the concentration of manganese is approximately 80 pmol g^{-1} dry weight for *Rhodospirillum rubrum* (Kassner & Kamen, 1968) and *"Rhodobacter ferrooxidans"* strain SW2 (supporting information table 11.5).

Comparing these results to cyanobacteria – for which more data are available than for phototrophic proteobacteria – it is clear that cyanobacteria require Co in concentrations in the medium higher than $1E^{-12}$ mol L^{-1} for growth (Saito et al., 2003). In the case of *"Rhodobacter ferrooxidans"* strain sp. SW2 the concentration of cobalt in the medium was higher even for only 0.5 fold addition of TE (e.g. $9.4E^{-10}$ mol L^{-1} than the minimum in the case of cyanobacteria (Saito et al., 2003). Thus, likely the photoferrotroph *"Rhodobacter ferrooxidans"* strain sp. SW2 requires higher concentrations of Co than cyanobacteria.

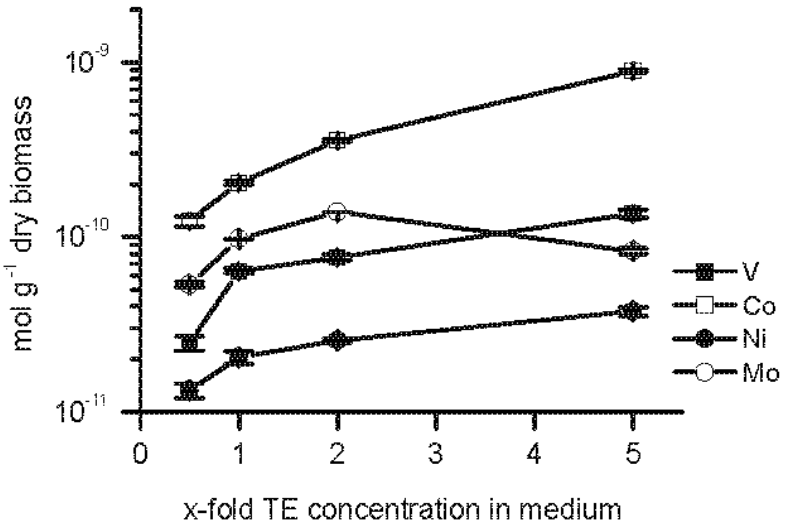

Figure 11.3: The concentration of vanadium, cobalt, nickel and molybdenum per gram dry weight of *"Rhodobacter ferrooxidans"* strain sp. SW2 for different concentrations of TE in the growth medium ranging from 0 – 5-fold of the commonly applied amount of trace metal. No growth was observed for experiments lacking all TE.

11.4.4 Geochemical modeling of the adsorption of TE to ferrihydrite

The experiments shown here were all conducted with H_2 as electron donor in order to avoid sorption of TE to Fe(III) minerals, thus causing limitation of TE for the cells due to sorption and co-precipitation.

Nonetheless, the product of the metabolism of the photoferrotroph *"Rhodobacter ferrooxidans"* strain SW2 are often Fe(III) minerals. Ferrihydrite is a good proxy for the formed Fe(III) minerals (chapter 11.3.4, Kappler & Newman (2004), Kappler & Straub (2005), Miot et al. (2009)). Thus, the adsorption of TE to ferrihydrite was modeled in mineral medium in order to determine if one of the four TE (molybdenum, nickel, vanadium and cobalt) would be less bio-available in the presence of ferrihydrite. Although differences in respect to sorption of TE probably exist between biogenic Fe(III) minerals and the abiogenic ferrihydrite, the latter was used as model basis as no systematic sorption data exists for biogenic Fe(III) minerals.

Pure ferrihydrite that was chemically precipitated in pure water, has a point of zero charge (pzc) of 7.8-7.9 (Cornell & Schwertmann, 2003). Pure ferrihydrite is positively charged at circum-neutral pH although the pzc decreases if other ions are present in the system. In nature the pzc for ferrihydrite was determined as low as 5.3 (Cornell & Schwertmann, 2003). In the model, phosphate and carbonate affected the pzc of ferrihydrite substantially and thus the sorption behavior of other ions. The pzc of ferrihydrite in the model was calculated to be negative. Biogenically precipitated Fe(III) minerals have a substantially different sorption behavior compared to chemically synthesized minerals, although further studies are needed to determine the exact properties of the minerals.

Figure 11.4 (left panel) clearly shows that molybdenum and vanadium interact only very little with ferrihydrite at any of the modeled pH-values (6-8). The model indicated a negative surface charge of the ferrihydrite under the conditions of the medium and thus vanadium and molybdenum experience electrostatic repulsion and are therefore easily bio-available for *"Rhodobacter ferrooxidans"* strain SW2.

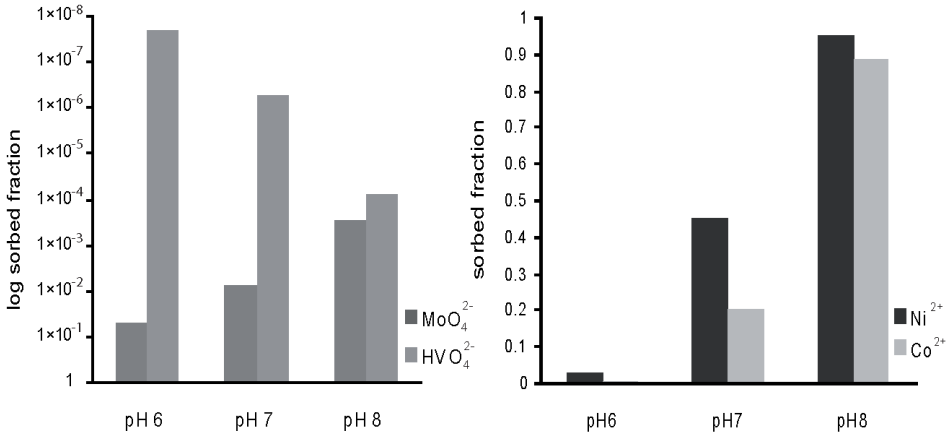

Figure 11.4: Geochemical modeling of the adsorption of TE to ferrihydrite. Modeling was performed with Geochemists Workbench. The geochemical calculations included the salts of the mineral medium of the experiments (section 11.3.1). Note the log-scale on the left panel.

In contrast, nickel and cobalt interact strongly with ferrihydrite. At pH 7 for example, already 50% of the nickel is bound to ferrihydrite while at pH 8 nearly 100% interact with the mineral (figure 11.4, right panel). The bio-availability of nickel and cobalt is thus reduced at the optimal growth pH but the bio-availability is likely not limiting. Other factors – such as other bacteria – could further limit TE-availability in an environmental setting as other strains require TE as well. Humic substances may also complex TE and thus decrease their concentration in the environment. The dominant factor influencing the pzc of the ferrihydrite in the model were HCO_3^- and $H_2PO_4^-$.

On the other side, silica may increase the fraction of bioavailable Ni (and potentially other TE) due to the competition for sorption sites on Fe(III) minerals and a change in surface properties (Konhauser et al., 2009). In todays environments, competition of humic substances for sorption sites on Fe(III) minerals may increase the bio-availability of TE due to adsorption of humic substances to ferrihydrite and the resulting change of the pzc (Cornell & Schwertmann, 2003).

The sorption of TE on biogenic minerals is dependant on may factors, likely the pzc of the minerals is negative and thus positively charged ions adsorb well at circumneutral pH while negatively charged TE will likely be easily bioavailable.

11.5 Conclusion

In order to determine if *"Rhodobacter ferrooxidans"* strain SW2 is a good model organism for understanding ancient earth environemts, one has to look at the distribution of TE in earth history and compare these with the requirements of the cells. Fraústo da Silva & Williams (2001), Zerkle et al. (2005) and Anbar (2008) state that molybdenum was likely only present at very low concentrations on ancient earth and its concentration has risen since. The concentration of molybdenum has increased from 1×10^{-9} mol L^{-1} to 1×10^{-7} mol L^{-1}. The same is true for vanadium but to a lesser extent than molybdenum (Fraústo da Silva & Williams, 2001).

Interestingly, the need of the cells for Mo is low and and it seems as if the cells are able to replace Mo with another TE. The low need of the strain for Mo would be beneficial on early earth environments as the concentration of Mo was lower than today (Zerkle et al., 2005, Anbar, 2008). Additionally, molybdenum may be replaced by other metals such as vanadium, iron or tungstate in some enzymes, like the nitrogenases (Zerkle et al., 2005, and references therein). Hence, the apparent low need of molybdenum in molybdenum-depletion experiments (chapter 11.4.2) and the drop of the OD in the first transfer (T1) may be due to an efficient replacement of molybdenum in the reactive center of enzymes by other metals. This would be beneficial for environments similar to early earth environments and thus *"Rhodobacter ferrooxidans"* strain SW2 would likely be able to live under these conditons.

Today vanadium is prominently found in enzymes relevant for dinitrogen fixation. Fraústo da Silva & Williams (2001) speculate also that vanadium may have played a role in early live photosynthesis. Although speculative, their reasons seem conclusive: high concentrations of vanadium found in oils of primitive plants and bacteria and the fact that the properties of vanadium allow a use in enzymes of nitrogen-fixation as well as CO_2 reduction point towards a more prominent use of this metal in the past (Fraústo da Silva & Williams, 2001).

Nickel and cobalt are virtually not used as TE in higher organisms while still many enzymes of bacteria and archeae require these metals. They are especially valuable to catalyze reactions with H_2, CH_4, CO and others likely present on early earth (Fraústo da Silva & Williams, 2001, Zerkle et al., 2005). The

concentration of nickel in the ocean increased slightly from 5×10^{-8} mol l^{-1} with a slight drop between 2.3 and 0.8 Ga to todays value of 1×10^{-8} mol l^{-1} (Anbar, 2008). The concentration of cobalt has decreased from the concentration 4 Ga ago of 1×10^{-8} mol l^{-1} to todays value of 1×10^{-11} mol l^{-1} (Zerkle et al., 2005, Anbar, 2008). Today, cobalt is virtually only used in cobalamin (vitamin B12) and is hardly ever used as a metal not bound to the cobalamin (Fraústo da Silva & Williams, 2001) while it has likely fulfilled additional function in the past (Zerkle et al., 2005). The use of both, nickel and cobalt by *"Rhodobacter ferrooxidans"* strain SW2 indicates that enzymes, that require these TE are relevant for the organism. Many of these enzymes are thought to have their origin on an anoxic ancient earth (Williams & Fraústo da Silva, 2006).

All the evidence presented here indicates that the photoferrotroph *"Rhodobacter ferrooxidans"* strain SW2 likely conserved trace metal use from the past. Therefore, the use of *"Rhodobacter ferrooxidans"* strain SW2 as a model organism for the formation of BIFs (Kappler et al., 2005, Posth et al., 2008) is strengthened.

Acknowledgements

We thank Sarah Köhl for her help with the measurements as well as Nicole Posth and Merle Eickhoff for discussing the data.

Bibliography

Anbar, AD: Oceans: Elements and evolution. *Science*, 322:1481–1483, 2008.

Anbar, AD; Duan, Y; Lyons, TW; Arnold, GL; Kendall, B; Creaser, RA; Kaufman, AJ; Gordon, GW; Scott, C; Garvin, J; & Buick, R: A whiff of oxygen before the great oxidation event? *Science*, 317:1903–1906, 2007.

Bekker, A; Holland, HD; Wang, PL; Rumble III, D; Stein, HJ; Hannah, JL; Coetzee, LL; & Beukes, NJ: Dating the rise of atmospheric oxygen. *Nature*, 427:117–120, 2004.

Beukes, NJ; Klein, C; Holland, HD; Kasting, JF; Kump, LR; & Lowe, DR: *Proterozoic Atmosphere and Ocean.* The Proterozoic Biosphere: a multidisciplenary study (Press Syndicate of the University of Camebridge, New York), 1992.

Cairns-Smith, AG: Precambrian solution photochemistry, inverse segregation, and banded iron formation. *Nature*, 276:808–808, 1978.

Canfield, DE: The early history of atmospheric oxygen: Homage to robert a. garrels. *Annual Review of Earth and Planetary Sciences*, 33:1–36, 2005.

Cloud, PE: Atmospheric and hydrospheric evolution on primitive earth. *Science*, 160:729–737, 1968.

Copin-Montegut, C & Copin-Montegut, G: Stoichiometry of carbon, nitrogen, and phosphorus in marine particulate matter. *Deep Sea Research Part A. Oceanographic Research Papers*, 30:31–46, 1983.

Cornell, RM & Schwertmann, U: *The iron oxides: structure, properties, reactions, occurrences and uses* (VCH, Weinheim, Cambridge), 2nd ed., 2003.

Downing, JA: Marine nitrogen: Phosphorus stoichiometry and the global N:P cycle. *Biogeochemistry*, 37:237–252, 1997.

Dzombak, DA & Morel, F: *Surface complexation modeling: hydrous ferric oxide* (Wiley, New York), 1990.

Ehrenreich, A & Widdel, F: Anaerobic oxidation of ferrous iron by purple bacteria, a new type of phototrophic metabolism. *Applied and Environmental Microbiology*, 60:4517–4526, 1994.

Ferrer, M; Golyshina, OV; Beloqui, A; Golyshin, PN; & Timmis, KN: The cellular machinery of ferroplasma acidiphilum is iron-protein-dominated. *Nature*, 445:91–94, 2007.

Fraústo da Silva, JJR & Williams, RJP: *The biological chemistry of the elements: the inorganic chemistry of life* (Oxford University Press, Oxford), 2nd ed., 2001.

Garrels, RM; Perry, EA, JR; & Mackenzie, FT: Genesis of precambrian iron-formations and the development of atmospheric oxygen. *Economic Geology*, 68:1173–1179, 1973.

Hegler, F; Posth, NR; Jiang, J; & Kappler, A: Physiology of phototrophic iron(II)-oxidizing bacteria – implications for modern and ancient environments. *FEMS Microbiology Ecology*, 66:250–260, 2008.

Hiemstra, T & van Riemsdijk, WH: A surface structural model for ferrihydrite i: Sites related to primary charge, molar mass, and mass density. *Geochimica et Cosmochimica Acta*, 73:4423 – 4436, 2009.

Jambor, JL & Dutrizac, JE: Occurrence and constitution of natural and synthetic ferrihydrite, a widespread iron oxyhydroxide. *Chemical Reviews*, 98:2549–2585, 1998.

Kappler, A & Newman, DK: Formation of Fe(III)-minerals by Fe(II)-oxidizing photoautotrophic bacteria. *Geochimica et Cosmochimica Acta*, 68:1217–1226, 2004.

Kappler, A; Pasquero, C; Konhauser, KO; & Newman, DK: Deposition of banded iron formations by anoxygenic phototrophic Fe(II)-oxidizing bacteria. *Geology*, 33:865–868, 2005.

Kappler, A & Straub, KL: Geomicrobiological cycling of iron. *Reviews in Mineralogy & Geochemistry*, 59:85–108, 2005.

Kassner, RJ & Kamen, MD: Trace metal composition of photosynthetic bacteria. *Biochimica et Biophysica Acta*, 153:270–8, 1968.

Kasting, JF: Palaeoclimatology - archaean atmosphere and climate. *Nature*, 432:–, 2004.

Kasting, JF & Siefert, JL: Life and the evolution of earth's atmosphere. *Science*, 296:1066–1068, 2002.

Konhauser, KO; Amskold, L; Lalonde, SV; Posth, NR; Kappler, A; & Anbar, A: Decoupling photochemical Fe(II) oxidation from shallow-water BIF deposition. *Earth and Planetary Science Letters*, 258:87–100, 2007.

Konhauser, KO; Hamade, T; Raiswell, R; Morris, RC; Ferris, FG; Southam, G; & Canfield, DE: Could bacteria have formed the precambrian banded iron formations? *Geology*, 30:1079–1082, 2002.

Konhauser, KO; Pecoits, E; Lalonde, SV; Papineau, D; Nisbet, EG; Barley, ME; Arndt, NT; Zahnle, K; & Kamber, BS: Oceanic nickel depletion and a methanogen famine before the great oxidation event. *Nature*, 458:750–753, 2009.

Mathur, SS & Dzombak, DA: *Surface complexation modeling: goethite*, vol. 11, chap. 16, pp. 443–468 (Elsevier), 2006.

Michel, FM; Barron, V; Torrent, J; Morales, MP; Serna, CJ; Boily, JF; Liu, QS; Ambrosini, A; Cismasu, AC; & Brown, GE: Ordered ferrimagnetic form of ferrihydrite reveals links among structure, composition, and magnetism. *Proceedings of the National Academy of Sciences of the United States of America*, 107:2787–2792, 2010.

Michel, FM; Ehm, L; Antao, SM; Lee, PL; Chupas, PJ; Liu, G; Strongin, DR; Schoonen, MAA; Phillips, BL; & Parise, JB: The structure of ferrihydrite, a nanocrystalline material. *Science*, 316:1142525–1142525, 2007.

Miot, J; Benzerara, K; Morin, G; Kappler, A; Bernard, S; Obst, M; Férard, C; Skouri-Panet, F; Guigner, JM; Posth, NR; Galvez, M; Brown, GE, JR.; & Guyot, F: Iron biomineralization by neutrophilic iron-oxidizing bacteria. *Geochimica et Cosmochimica Acta*, 73:696–711, 2009.

Posth, NR; Hegler, F; Konhauser, KO; & Kappler, A: Alternating Si and Fe deposition caused by temperature fluctuations in Precambrian oceans. *Nature Geoscience*, 1:703–708, 2008.

Redfield, A; Ketchum, B; & Richards, F: The influence of organisms on th ecomposition of seawater. In M Hill, ed., *The composition of seawater - comparitative and describitive oceanography* (Wiley, New York), 1963.

Reinhard, CT; Raiswell, R; Scott, C; Anbar, AD; & Lyons, TW: A late archean sulfidic sea stimulated by early oxidative weathering of the continents. *Science*, 326:713–6, 2009.

Saito, MA; Sigman, DM; & Morel, FMM: The bioinorganic chemistry of the ancient ocean: the co-evolution of cyanobacterial metal requirements and biogeochemical cycles at the archean proterozoic boundary? *Inorganica Chimica Acta*, 356:308–318, 2003.

Sterner, RW & Elsner, JJ: *Ecological stoichometry* (Princeton University Press), 2002.

Tschech, A & Pfennig, N: Growth yield increase linked to caffeate reduction in *Acetobacterium woodii*. *Archives of Microbiology*, 137:163–167, 1984.

Widdel, F; Schnell, S; Heising, S; Ehrenreich, A; Assmus, B; & Schink, B: Ferrous iron oxidation by anoxygenic phototrophic bacteria. *Nature*, 362:834–836, 1993.

Williams, RJP & Fraústo da Silva, JJR: *The chemistry of evolution: the development of our ecosystem* (Elsevier, Amsterdam; Boston), 1st ed., 2006.

Zerkle, AL; House, CH; & Brantley, SL: Biogeochemical signatures through time as inferred from whole microbial genomes. *American Journal of Science*, 305:467–502, 2005.

Zerkle, AL; House, CH; Cox, RP; & Canfield, DE: Metal limitation of cyanobacterial N_2 fixation and implications for the precambrian nitrogen cycle. *Geobiology*, 4:285–297, 2006.

Zhang, Y & Gladyshev, VN: General trends in trace element utilization revealed by comparative genomic analyses of Co, Cu, Mo, Ni and Se. *Journal of Biological Chemistry*, 285:3393–405, 2010.

Supporting information

Table 11.4: Concentration of V, Ni, Co, Mo, in the initial concentrated stock solutions.

	V [μ**mol L**$^{-1}$]	**Co** [μ**mol L**$^{-1}$]	**Ni** [μ**mol L**$^{-1}$]	**Mo** [μ**mol L**$^{-1}$]
detection limit	$9.82E^{-4}$	$5.09E^{-4}$	$1.02E^{-4}$	$2.08E^{-4}$
V	$1.86E^{+2}$	$2.11E^{-3}$	$1.15E^{-1}$	$7.03E^{-1}$
Ni	$3.83E^{-1}$	$3.81E^{-3}$	$1.08E^{+2}$	$1.39E^{+3}$
Co	$3.29E^{-1}$	$8.15E^{+2}$	$3.25E^{-1}$	$2.07E^{-1}$
Mo	$3.12E^{-1}$	$1.22E^{-3}$	$2.56EE^{-1}$	$1.45E^{+2}$
TE-sltn.	$3.26E^{-1}$	$1.14E^{-2}$	$3.61E^{-1}$	$1.52E^{-2}$
Vit.sltn.	$2.55E^{-2}$	$2.03E^{-3}$	$5.44E^{-2}$	$<$ DL
Cobalamin-sltn.	$<$ DL	$2.88E^{+1}$	$5.06E^{-2}$	$1.91E^{-3}$

Table 11.5: Complete ICP-MS measurement of elements in cell biomass in mol/kg dry bacterial biomass. Some elements were measured but are not included in the table due to their minor importance in biological systems. Excluded elements: Li, Be, B, Al, Ti, Cr, Ga, Ge, Rb, Sr, Y, Zr, Nb, Ru, Pd, Ag, Cd, Sb, Te, Cs, Ba, La, Ce, Pr, Nd, Sm, Eu, Gd, Tb, Dy, Ho, Er, Tm, Yb, Lu, Hf, Ta, As, Se.

	Mg	Si	P	K	Ca	V	Mn
0.5 TE	1.31E-05	2.14E-06	2.50E-04	9.97E-07	1.77E-05	2.46E-08	8.22E-08
SD	9.24E-07	3.11E-08	3.74E-05	2.13E-07	4.37E-07	2.35E-09	8.76E-09
1 TE	2.33E-05	1.93E-06	3.02E-04	1.98E-06	5.00E-05	6.37E-08	1.32E-07
SD	9.52E-07	3.25E-07	5.14E-06	1.26E-07	1.57E-06	2.11E-09	6.86E-09
2 TE	1.86E-05	2.39E-06	2.73E-04	2.07E-06	3.05E-05	7.63E-08	1.98E-07
SD	1.25E-05	1.14E-06	1.88E-04	1.65E-06	2.22E-05	5.08E-08	1.32E-07
5 TE	1.30E-05	3.13E-06	2.77E-04	3.96E-07	2.24E-05	1.36E-07	2.42E-07
SD	9.86E-07	1.60E-07	7.25E-07	3.06E-07	1.88E-06	6.99E-09	3.02E-08

	Fe	Co	Ni	Cu	Zn	Mo	W
0.5 TE	3.01E-06	1.23E-07	1.32E-08	2.28E-08	1.21E-07	5.32E-08	8.44E-09
SD	3.94E-08	8.06E-09	1.24E-09	1.44E-09	1.25E-08	1.76E-09	1.12E-09
1 TE	4.50E-06	2.04E-07	2.04E-08	2.18E-08	1.73E-07	9.75E-08	1.35E-08
SD	1.88E-07	6.44E-09	1.7E-09	7.44E-10	6.7E-09	3.41E-10	3.99E-10
2 TE	1.11E-05	3.57E-07	2.56E-08	2.76E-08	2.62E-07	1.39E-07	8.42E-09
SD	7.54E-06	2.45E-07	1.73E-08	1.98E-08	1.93E-07	9.79E-08	5.84E-09
5 TE	2.58E-05	8.93E-07	3.75E-08	4.77E-08	3.55E-07	8.28E-08	4.85E-09
SD	1.24E-06	1.33E-08	2.18E-09	2.77E-10	3.95E-08	2.98E-09	1.49E-10

12 Alternating Si and Fe deposition caused by temperature fluctuations in Precambrian oceans

Nicole R. Posth[1], Florian Hegler[1], Kurt O. Konhauser[2], Andreas Kappler[1] **Nature Geoscience, 1:703 – 708, 2008**

[1]Center for Applied Geoscience – Geomicrobiology, Eberhard Karls University Tübingen, Sigwartstrasse 10, 72076 Tübingen, Germany
[2]Department of Earth and Atmospheric Sciences, University of Alberta, Edmonton, Alberta, T6G 2E3, Canada

12.1 Abstract

Precambrian banded iron formations provide an extensive archive of pivotal environmental changes and the evolution of biological processes on early Earth. The formations are characterized by bands ranging from micrometre- to metre-scale layers of alternating iron- and silica-rich minerals. However, the nature of the mechanisms of layer formation is unknown. To properly evaluate this archive, the physical, chemical and/or biological triggers for the deposition of both the iron- and silica-rich layers, and crucially their alternate banding, must be identified. Here we use laboratory experiments and geochemical modelling to study the potential for a microbial mechanism in the formation of alternating iron-ilica bands.We find that the rate of biogenic iron(III) mineral formation by iron-oxidizing microbes reaches a maximum between 20 and 25 °C. Decreasing or increasing water temperatures slow microbial iron mineral formation while promoting abiotic silica precipitation. We suggest that natural fluctuations in the temperature of the ocean photic zone during the period when banded iron formations were deposited could have led to the primary layering observed in these formations by successive cycles of microbially catalysed iron(III) mineral deposition and abiotic silica precipitation.

12.2 Introduction

Banded iron formations (BIFs) are sedimentary rocks of alternating iron-rich (haematite, magnetite and siderite) and silicate/carbonate (chert, jasper, dolomite and ankerite) layers that were deposited between 3.6 and 2.2 billion years (Gyr) ago (Trendall, 2002, Klein, 2005). The layers vary from the microscale (micrometres in thickness) that we focus on here, to metre-thick units (Klein, 2005, Trendall, 1968). Some deposits, such as in the 2.5 Gyr old Dales Gorge Member, Hamersley Group, Western Australia, show laterally contiguous layers up to a hundred kilometres in distance (Trendall, 2002), suggesting that BIFs were formed uniformly over vast depositional areas tens of thousands of square kilometres in size (Morris & Horwitz, 1983). The layering in BIFs has been attributed to seasonal or decadal episodic hydrothermal

pulsation and/or upwelling of anoxic, Fe-rich waters (roughly 0.02-.5 mM dissolved Fe(II)) ((Holland, 1973, Morris, 1993)) into semi-restricted basins already saturated with dissolved silica (Maliva et al., 2005).

Three main models have been proposed for Fe(II) oxidation and precipitation of the Fe(III) in BIFs. The most widely accepted of these is predicated on the presence of ancient cyanobacteria (Cloud, 1968), the metabolism of which would have produced oxygen that chemically reacted with dissolved Fe(II) and thus precipitated ferric hydroxide, $Fe(OH)_3$. Although this is the likely mechanism after $\tilde{2}.5$ Gyr ago, a period named the Great Oxidation Event, abundant evidence for an anoxic Archaean era, for example, (Holland, 2002), makes it necessary to consider mechanisms of Fe(III) mineral precipitation in the absence of oxygen. One such anoxic mechanism is ultraviolet-light-driven photo-oxidation of Fe^{2+} and $Fe(OH)^+$ (Braterman et al., 1983). However, a recent study designed to test this mechanism in fluids mimicking the Archaean ocean and containing high concentrations of dissolved Fe(II), silica and HCO_3^- demonstrated that the oxidative effects of ultraviolet A or ultraviolet C were negligible (Konhauser et al., 2007a). Similarly, nitrate has been proposed as an oxidant (Weber et al., 2006); detailed studies supporting this mechanism have not yet been conducted. In contrast, another O_2-free oxidation mechanism, the direct microbial precipitation of ferric iron through anoxygenic photosynthesis (photoferrotrophy), is bolstered by the isolation of modern analogue marine and freshwater anoxygenic Fe(II)-oxidizing phototrophs (for example, *Rhodobacter ferrooxidans* sp. strain SW2 ((Widdel et al., 1993)), *Chlorobium ferrooxidans* sp. strain KoFox (Heising et al., 1999), *Rhodovulum iodosum* and *Rhodovulum robiginosum* (Straub et al., 1999)).

Models based on the Fe(II) oxidation rates of these strains under varying environmental conditions demonstrate the plausibility of photoferrotrophy as a means for primary BIF precipitation (Konhauser et al., 2002, Kappler et al., 2005, Hegler et al., 2008). Indeed, the ferric iron minerals these strains produce are consistent with the Fe(III) precipitates probably sedimented as primary BIF minerals (Widdel et al., 1993, Kappler & Newman, 2004, Konhauser et al., 2005). In particular, photoferrotrophs produce poorly crystalline ferric minerals, which carry a net positive charge (Kappler & Newman, 2004). Such biogenic minerals are expected to bind to organic carbon (cells), with the net effect being the deposition of cell-ineral aggregates to the sea floor. Once buried, metabolically driven diagenetic reactions and later-stage metamorphism would then transform the aggregates: ferric hydroxide would either dehydrate to haematite (Fe_2O_3) or be reduced to magnetite (Fe_3O_4) and/or siderite ($FeCO_3$), whereas organic carbon would be oxidized to CO_2. These reactions have been used to explain the lack of organic carbon now present in BIFs (Walker, 1984), the isotopic composition of the secondary minerals (Baur et al., 1985, Johnson et al., 2008), as well as the main Fe-mineral components of BIFs (Konhauser et al., 2005).

Critical to the argument for ancient photoferrotrophy is evidence of these bacteria in the Archaean, probably as forerunners to oxygenic photosynthesis. First, molecular phylogenetic analysis of a number of enzymes involved in (bacterio-) chlorophyll biosynthesis suggests that anoxygenic photosynthetic lineages are almost certain to be more deeply rooted than the oxygenic cyanobacterial lineages (Xiong, 2006). Second, recent studies that indicate anoxygenic phototrophs represent a considerable fraction of biomass in modern stromatolite communities25 and the construction of stromatolite-like structures with the anoxygenic phototroph Rhodopseudomonas palustris (Bosak et al., 2007) challenge the notion that stromatolites strictly mark cyanobacterial presence in the geologic record. Third, unique biomarkers for anoxygenic phototrophs, remnants of specific light-harvesting pigments, have recently been found in Palaeoproterozoic strata (Brocks et al., 2005), offering intriguing evidence for their presence on the ancient Earth. Moreover, 2-methylbacteriohopane-polyol molecules, previously interpreted as exclusive biomarkers for cyanobacteria, have also been identified in significant quantities in modern anoxygenic

phototrophic Fe(II)-oxidizers (Rashby et al., 2007), making the case for Fe(II)-oxidizing phototrophs at 2.7 Gyr ago just as plausible as that for H_2O-oxidizing cyanobacteria.

Despite the recent advances in linking ancient anoxygenic phototrophic Fe(II) oxidation to BIF precipitation, a satisfactory explanation of how primary iron and silicate mineral can precipitate independently over large areas with some regularity is still lacking in biological models. Here, we put forth the first model showing how cyclic fluctuations in photic-zone seawater temperature link the microbial deposition of Fe(III) hydroxide (through anoxygenic photo-oxidation) to abiotic silica precipitation, and explain how this interplay of biotic and abiotic processes could result in BIF layering.

12.2.1 Temperature dependence of phototrophic Fe(II) oxidation

Several extant strains of anoxygenic Fe(II)-oxidizing phototrophs use light energy to catalyse the oxidation of Fe(II) and the reduction of CO_2, which yields biomass and ferric hydroxide as shown in equation 12.1.

$$4Fe^{2+} + HCO_3^- + 10H_2O + \nu v \rightarrow 4Fe(OH)_3 + < CH_2O > +7H_2O \tag{12.1}$$

To determine the potential habitat of anoxygenic phototrophs in the Archaean ocean, we tested the eco-physiological limits of representative strains from each of the three major phylogenetic branches: the purple sulphur bacterium *Thiodictyon* sp. strain F4; the purple non-sulphur bacterium, *Rhodobacter ferrooxidans* sp. strain SW2; and the green sulphur bacterium, *Chlorobium ferrooxidans* sp. strain KoFox. We determined the Fe(II) oxidation rates of these strains under varying conditions of temperature and presence of silica (12.1 a,b; Supplementary Information, 12.2.

The optimal temperature range of phototrophic Fe(II) oxidation is typical of mesophiles: from 5 to 35 °C, with a slow decrease in rate at lower temperatures and a strict upper temperature limit (Fig. 12.1 a). The pattern shown here for strain SW2 is representative of both strains F4 and KoFox (Fig.12.3 a). The temperature dependence exhibited by our model strains suggests that ancient ocean temperature changes would have significantly affected the extent of phototrophic Fe(II) oxidation, and most importantly, the precipitation and deposition of primary ferric hydroxide.

Archaean ocean temperature is heavily debated, with estimates ranging from 10 to 85 °C. Much of the disagreement rests on the interpretation of both O and Si isotope data (Knauth & Lowe, 2003, Knauth, 2005, Robert & Chaussidon, 2006, Kasting et al., 2006, Jaffrés et al., 2007, Shields & Kasting, 2007), as well as on problems related to diagenetic overprinting of ancient rocks. The most recent interpretations, which suggest a temperate Archaean climate of 10-33 °C, view the isotope data in terms of known constraints inferred frombiological evolution (Kasting et al., 2006). Clearly, the mesophilic photoferrotrophs used in this experiment would thrive in such an ocean.

As our study with the extant photoferrotrophs indicated that temperature fluctuations in the water column could control Fe(III) precipitation, we assessed the response of the model strains to extreme temperature fluctuation stress. We tested the Fe(II) oxidation capacity of *Rhodobacter ferrooxidans* sp. strain SW2 throughout a temperature cycle (Fig. 12.3 b; Supplementary Information, Fig. 12.4). At first, all cultures of strain SW2 were incubated at the temperature optimum of 25 °C and 4 mM dissolved Fe(II). In one experiment, the cultures were transferred to 4 °C for 3 days after the commencement of Fe(II) oxidation. Thereafter, they were returned to 25 °C. At 4 °C, Fe(II) oxidation and Fe(III) mineral precipitation ceased (Fig. 12.3 b). After being returned to 25 °C, bacterially mediated Fe(III) mineral

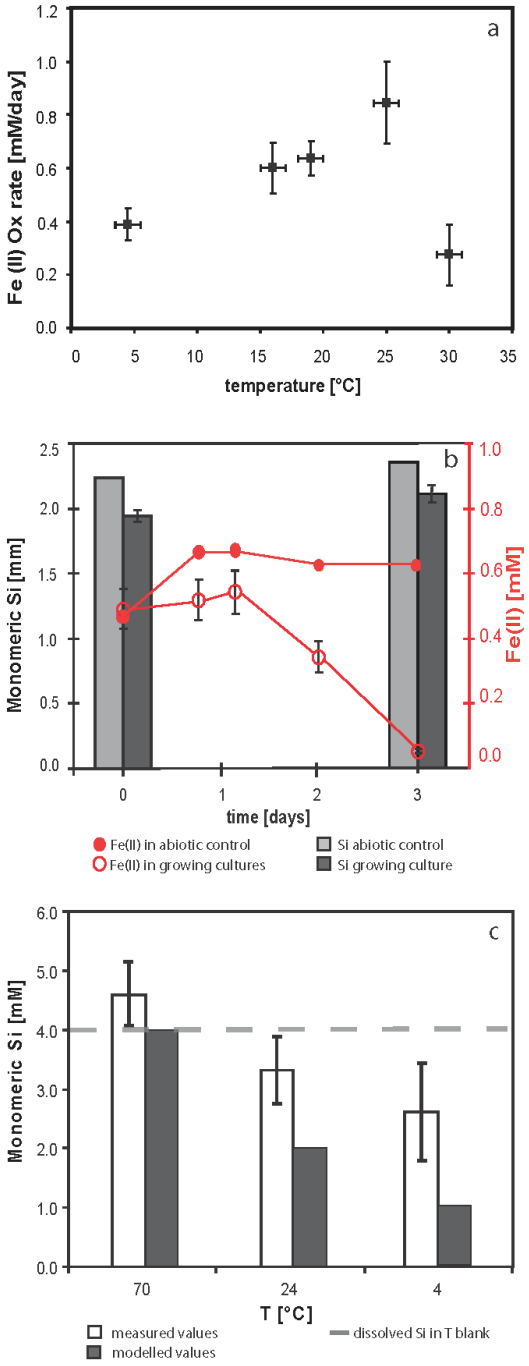

Figure 12.1: Temperature change drives both the biotic precipitation of Fe(III) minerals and the abiotic precipitation of silica. a, Dependence of *Rhodobacter ferrooxidans* sp. strain SW2 Fe(II) oxidation rates on temperature (4 mM dissolved Fe(II); 800 lux). b, Microbial oxidation of 0.5 mM Fe(II) by strain SW2 in the presence of 2.0 mM silica, at 75 lux. c, Temperature dependence of dissolved silica concentration in non-inoculated medium. Error bars depict standard deviation from the mean (triplicate experiments).

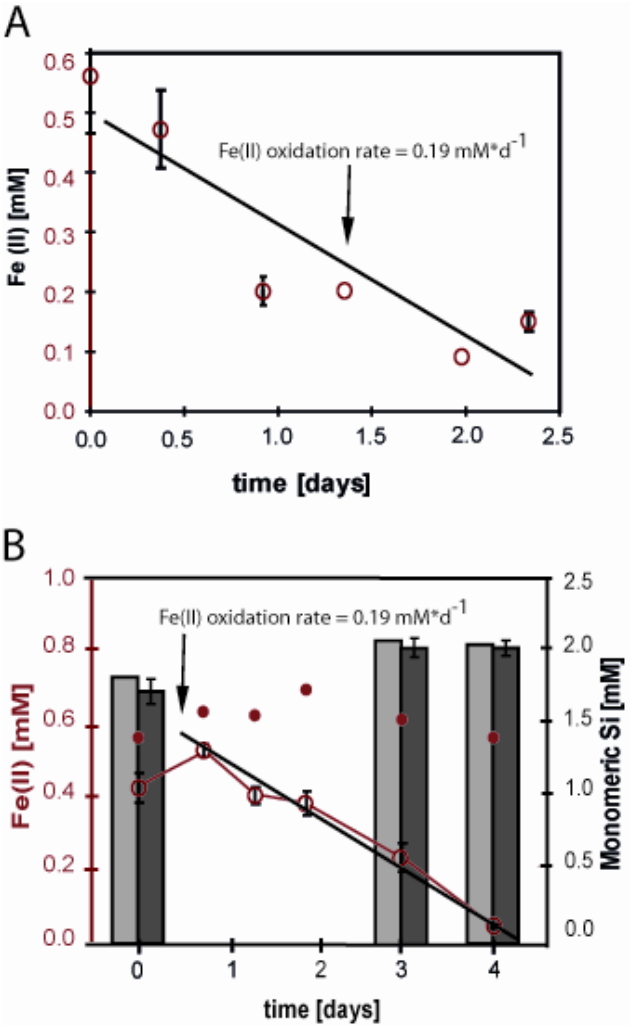

Figure 12.2: Abiotic oxidation of Fe(II) in the presence of silica. A Chemical oxidation of dissolved Fe(II) leading to a much stronger precipitation of silica in comparison to a less pronounced precipitation of silica during Fe(II) oxidation by the anoxygenic phototroph *Thiodictyon* sp. F4. Values of dissolved silica in solution shown at t = 0 (□) and t = end of Fe oxidation (■). B Solid phase Si/Fe molar ratios for ferric hydroxide precipitated during the complete oxidation of 0.18 mM (10 ppm Fe) ferrous iron ammonium sulfate solution (pH 8, 25 °C and in 0.5 M NaCl) in the presence of various amounts of dissolved silica (up to 1 mM). The co-precipitation of silica with iron appears to display typical adsorption isotherm behavior, with an approximately linear relationship between solid phase Si/Fe and dissolved Si at lower values, a plateau representing saturation at middle values, and what may represent surface precipitation of silica on the iron mineral at the highest dissolved silica concentration investigated, despite undersaturation with respect to amorphous silica in the bulk solution.

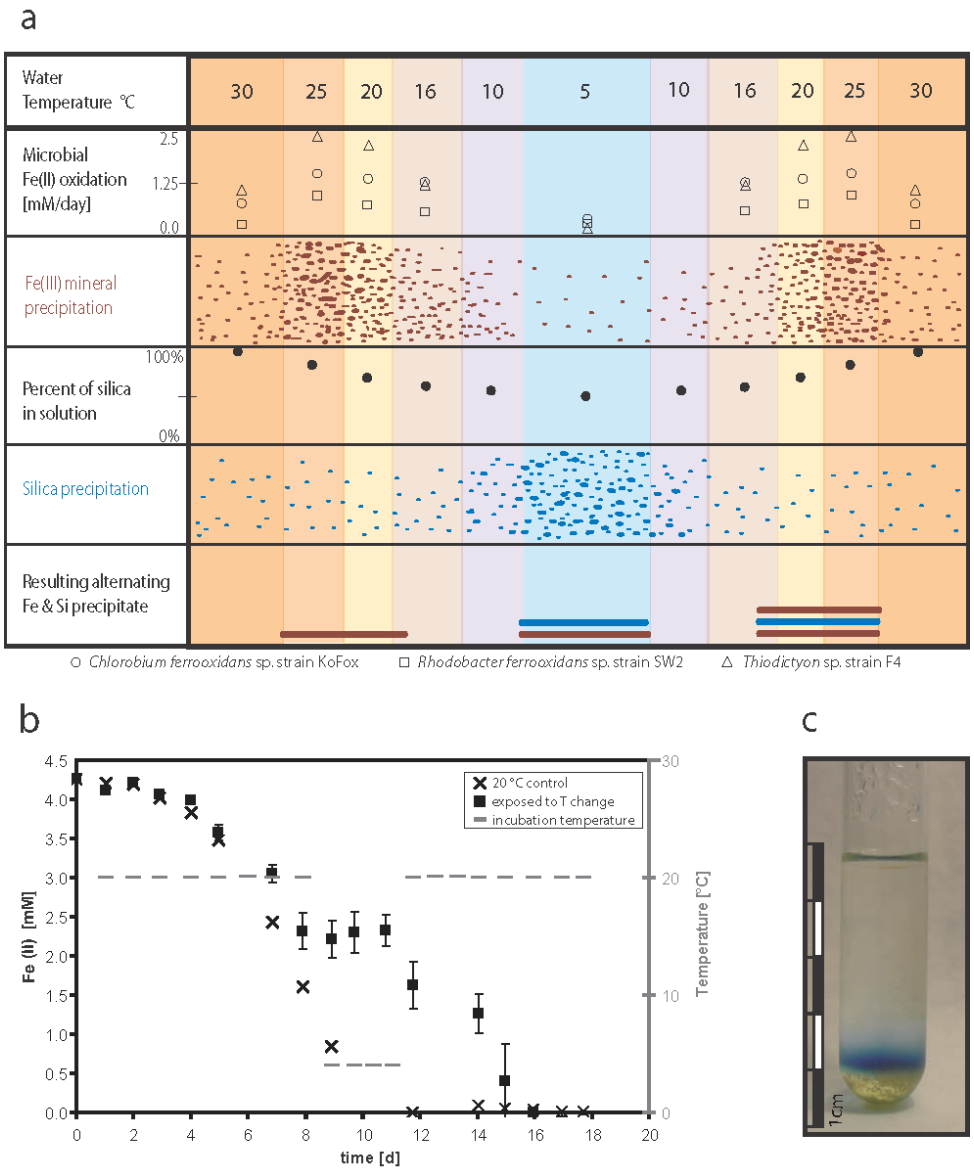

Figure 12.3: Possible deposition of alternating iron and silicate mineral layers in BIFs as triggered by temperature variations in ocean waters. a, Experimentally determined microbial Fe(II) oxidation rates at fluctuating temperature and the resulting Fe(III) mineral precipitation. The effect of temperature fluctuations between 5 and 30 °C on abiotic silica precipitation. b, Oxidation of dissolved Fe(II) by strain SW2 at changing temperatures and in a 20 °C control. Error bars depict standard deviation from the mean (triplicate experiments). c, Demonstration of microbial Fe(III) mineral precipitation in the presence of silica at 25 °C, and silica precipitation after temperature drop to 4 °C.

precipitation continued at the same Fe(II) oxidation rate as before the temperature drop. This pattern of growth effectively shows how such strains could survive a large temperature drop in ocean waters. A second experiment exposed the bacteria to a temperature increase from 24 to 55 °C to mimic what might occur if the depositional waters were subjected to input of hydrothermal fluids from shallow seamount-type systems, as recently proposed by Konhauser et al.(Konhauser et al., 2007b). In this experiment, Fe(II) oxidation continued during the temperature increase, but ceased after the bacteria were returned to 25 °C after three days (see Supplementary Information, Fig. 12.4). This confirmed the results of the temperature-dependence studies (Fig. 12.1 a); the anoxygenic phototrophic Fe(II)-oxidizers known so far cannot survive a prolonged temperature stress up to 55 °C. As no thermophilic photoferrotrophs capable of survival at higher temperatures have been isolated to date, the survival of a photoferrotroph in an Archaean ocean after a temporary large upward temperature shift would depend on its ability to move deeper into cooler parts of the water column. In fact, one of the phototrophic Fe(II)-oxidizers, *Chlorobium ferrooxidans* strain KoFox, exhibits full Fe(II) oxidation capacity even at very low-light regimes (<50 lux) (Hegler et al., 2008).

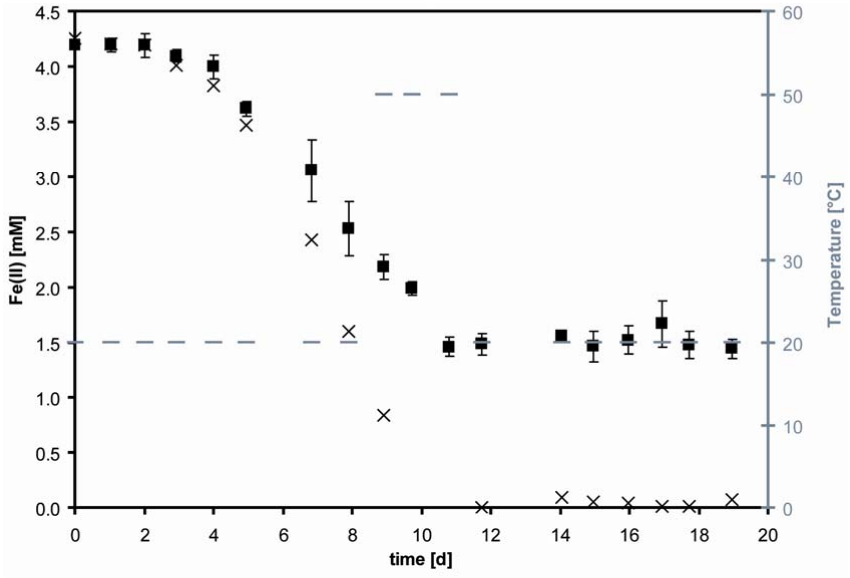

Figure 12.4: Effect of temperature increase on *"Rhodobacter ferrooxidans"* sp. strain SW2. The left y-axis displays anoxygenic phototrophic Fe(II) oxidation as a decrease in Fe(II) [mM] over time; (×) temperature control remaining at 20 °C throughout experiment, (■) mean value of experiment triplicates. The right y-axis shows the change in incubation temperature during the course of the experiment (). While microbial Fe(II) oxidation at first continues after temperature change, it is not revived 3 days after exposure to 50 °C incubation temperature.

12.2.2 Controls on Si mineral deposition

In an Archaean ocean devoid of silica-secreting eukaryotic species (for example, diatoms, radiolarians), evaporation and/or surface water temperature changes may have been the dominant processes leading to silica supersaturation and abiogenic silica precipitation (Maliva et al., 2005). Most BIF depositional models agree that amorphous silica initially precipitated from the water column and later transformed

into chert with burial (Maliva et al., 2005, Gross, 1972). Of interest to the investigation of BIFs is the behaviour of dissolved silica in cooling Archaean waters. We considered 70 °C as the maximum theoretical temperature from which cooling began (Knauth & Lowe, 2003, Robert & Chaussidon, 2006). The effect of temperature change on silica solubility both in microbial growth medium and in ocean water was modelled using Geochemist's Workbench 6.0 (Fig. 12.1c; Supplementary Information, Fig. 12.5). Abiotic laboratory experiments tested this model in cooling growth medium sampled at 70, 24 and 4 °C (Fig. 12.1c). As expected, both laboratory experiments and geochemical modelling demonstrated that a drop in temperature triggers the precipitation of silica in a salt solution from 4.6 mM monomeric silica measured in solution at 70 °C to 3.3 mM at 24 °C and 2.6 mM at 4 °C . Regardless of whether decreasing temperature from 70 to 4 °C or from 24 to 4 °C , silica precipitates from solution (see Supplementary Information, Fig. 12.5).

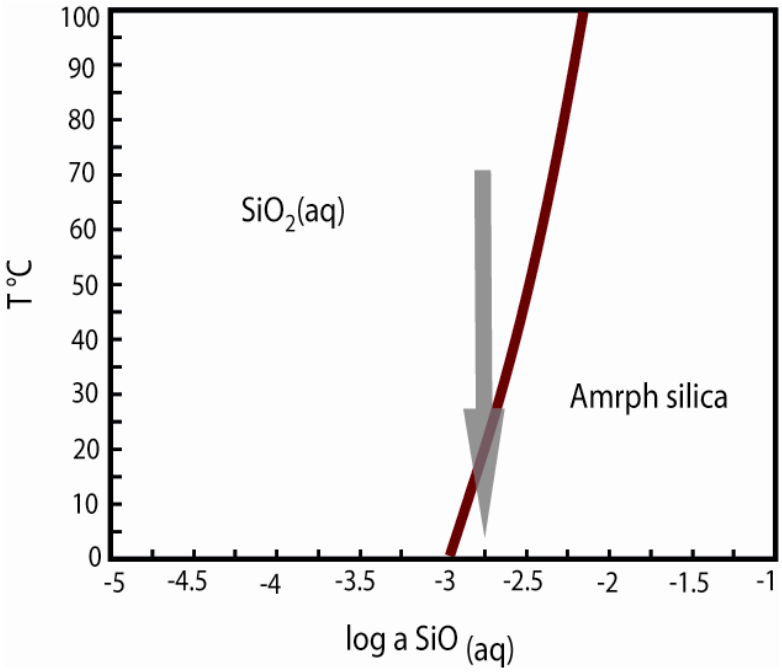

Figure 12.5: Geochemical model (Geochemists Workbench Standard 6.0) of silica solubility in a solution of microbial mineral medium at circumneutral pH composed of 0.6 g/L potassium phosphate (KH_2PO_4); 0.3 g/L ammonium chloride (NH_4Cl); 0.5 g/L magnesium sulphate ($Mg_SO_4 \times 7H_2O$); and 0.1 g/L calcium carbonate ($CaCl_2 \times 2H_2O$); and 22 mM carbonate buffer. This model was designed to estimate the precipitation of silica due to temperature decrease in abiotic batch cultures. The batch culture data is presented in the manuscript. The red line separates the two silica phases amorphous silica (precipitate) and dissolved $SiO_2(aq)$, while the grey arrow marks the change in phase as temperature decreases at the 2 mM silica estimated for the Archean ocean. According to this model, as temperature drops, silica will precipitate as an amorphous silica phase.

12.2.3 Layering model of iron and silica mineral precipitation

On the basis of previous studies of Fe-silica mineral interactions (Konhauser et al., 2007b), it would be assumed that ferric hydroxide-ell aggregates produced by photoferrotrophs would bind any dissolved silica present and remove it from solution. However, experiments carried out in the presence of dissolved silica concentrations relevant for the Archaean ocean (2.0 mM) ((Siever, 1992)) showed that biological Fe(II) oxidation rates were unaffected by the presence of silica. Fe(III) minerals even seemed to precipitate separately from silica: *Rhodobacter ferrooxidans* strain SW2 oxidized 0.5 mM dissolved Fe(II) at rates of 0.19 mM Fe(II) day^{-1}, both in the absence and presence of 2.0 mM silica, respectively, but the silica remained largely in solution whereas the Fe(II) was oxidized and Fe(III) minerals precipitated (see fig. 12.1b, and fig 12.2, 12.6). Furthermore, the concentration of dissolved silica in solution at the end of Fe(II) oxidation was significantly lower in batch cultures containing abiotically formed minerals compared with biogenic Fe(III) minerals (see Supplementary Information, Fig. 12.7A).

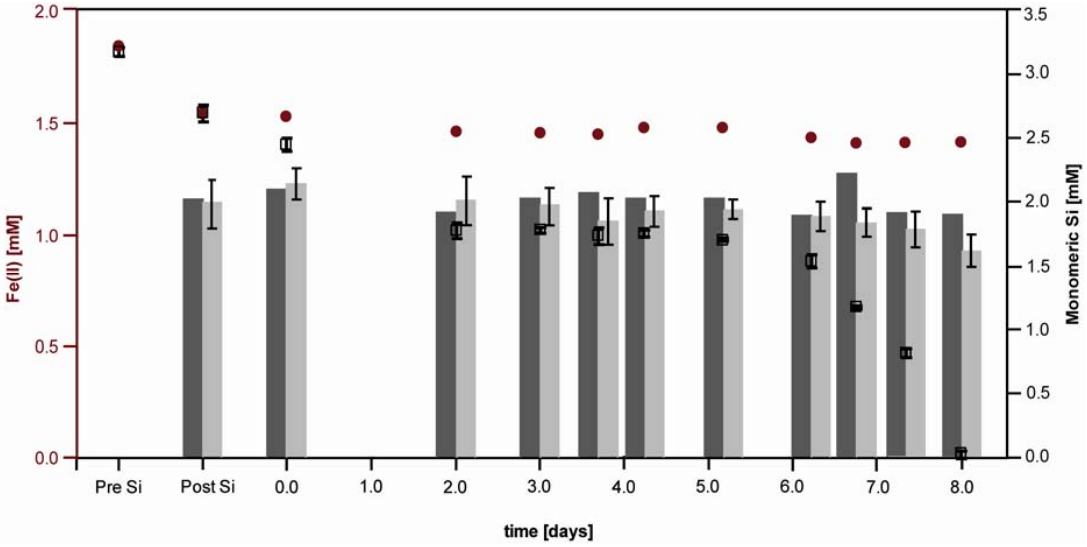

Figure 12.6: Fe(II) oxidation and silica in solution over time for anoxygenic Fe(II)-oxidizing phototroph *Thiodictyon* sp. strain F4. All experiments were conducted in triplicate and with an abiotic (uninoculated) control. The left y-axis (labelled in red) shows the concentration of Fe(II) in solution at various time points; abiotic control, experimental triplicates. The right y-axis in depicts the concentration of monomeric silica in the culture solution, represented by dark (abiotic control) and light grey bars (experimental triplicates).

Unlike abiotic oxidation experiments of SiO_2-containing solutions of dissolved Fe(II) that confirm the effect of silica sorption to ferric hydroxide in the absence of microbes (see Supplementary Information, Fig. 12.7B), it is possible that microbially formed ferric hydroxides carry a layer of cell-derived organic matter sorbed to their surfaces that hinders silica binding. Indeed, synchrotron-based X-ray spectroscopy and tomographic imaging of anoxygenic phototroph cultures, which oxidized Fe(II) in the absence and presence of 2.0 mM silica, shows the presence of cell-mineral aggregates at a distance from the amorphous silica (see Supplementary Information, Fig. 12.8A,B, respectively). Although the mechanism behind this phenomenon is not yet fully understood, it implies that biogenic ferric hydroxide produced by anoxygenic phototrophs is largely decoupled from silica in these systems. This decoupling is important because it

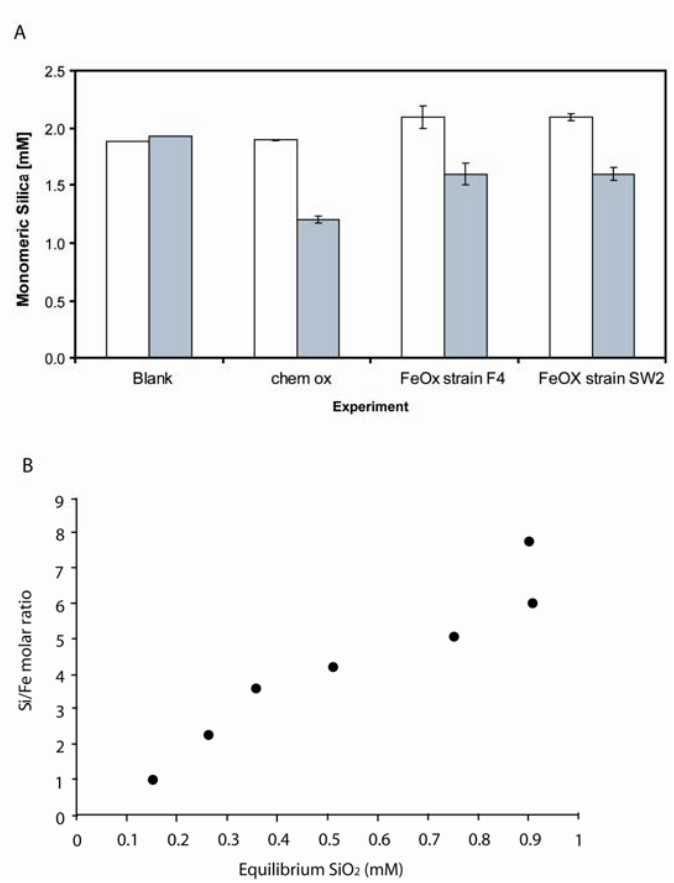

Figure 12.7: Abiotic oxidation of Fe(II) in the presence of silica. (a) Chemical oxidation of dissolved Fe(II) leading to a much stronger precipitation of silica in comparison to a less pronounced precipitation of silica during Fe(II) oxidation by the anoxygenic phototroph *Thiodictyon* sp. F4. Values of dissolved silica in solution shown at t = 0 (□) and t = end of Fe oxidation ■. (b) Solid phase Si/Fe molar ratios for ferric hydroxide precipitated during the complete oxidation of 0.18 mM (10 ppm Fe) ferrous iron ammonium sulfate solution (pH 8, 25 °C and in 0.5 M NaCl) in the presence of various amounts of dissolved silica (up to 1 mM). The coprecipitation of silica with iron appears to display typical adsorption isotherm behavior, with an approximately linear relationship between solid phase Si/Fe and dissolved Si at lower values, a plateau representing saturation at middle values, and what may represent surface precipitation of silica on the iron mineral at the highest dissolved silica concentration investigated, despite undersaturation with respect to amorphous silica in the bulk solution.

suggests a mechanism by which the Fe-rich and silica-rich layers in BIFs were deposited separately, yet triggered by a uniting parameter.

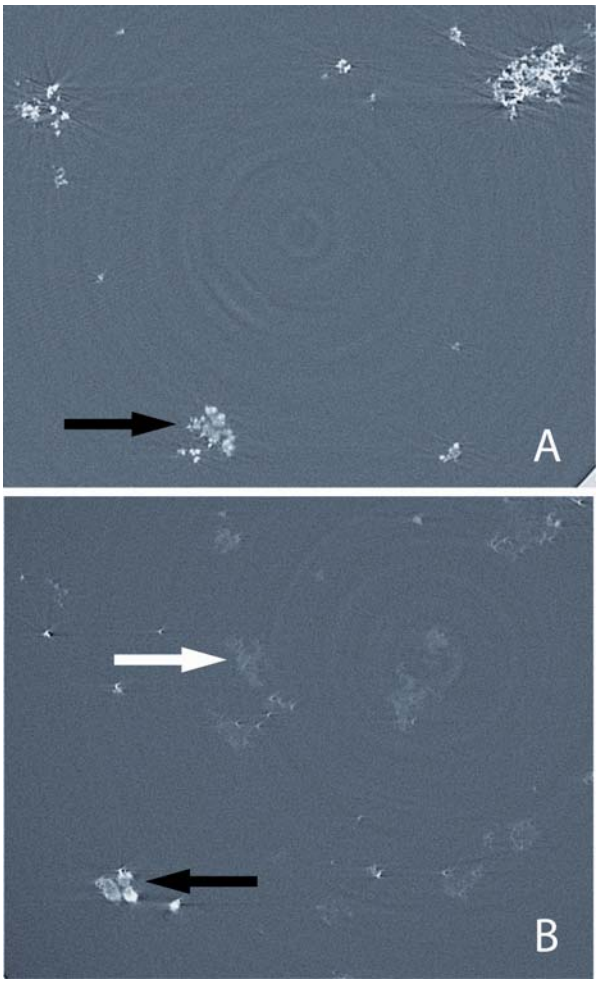

Figure 12.8: Synchrotron-based computer tomography slice images of *Thiodictyon* sp. strain F4 cell-mineral aggregates precipitated at the end of 0.5 mM Fe(II) oxidation in the absence (a) and in the presence of 2 mM silica (b). Various elements, including Si and Fe, can be distinguished based on the element specific absorption of the synchrotron X-rays. This leads to a marked difference in brightness and contrast of particles that contain either silica or iron. The distinct particles can be seen in Fig. a and b: Silica shown with the white arrow, cell-mineral aggregates with black arrows. Cell-mineral aggregates were taken up with warm 5% low melt agarose solution into 0.5 μm diameter glass capillaries The agarose solidifies with cooling to room temperature, preserving the orientation and structure of the precipitates. These images show larger aggregates forming in the absence of silica but also the separation of the cell-Fe(III) mineral aggregates from the amorphous silica precipitate. Image dimensions are approximately 200 $\times$ 200 μm.

We tested the effects of temperature changes as the uniting parameter of silica and Fe mineral precipitation in Archaean oceans using a combined experimental and modelling approach. Although reconstruction of Precambrian ocean temperature cycles from the BIF rock record is problematic, two

lines of evidence suggest that ocean water temperatures fluctuated in the Precambrian period. First, in modern oceans, temperature fluctuations occur with incoming currents, as well as with seasonal variation (see Supplementary Information, Fig. 12.9). Second, models of the Earth obliquity through time suggest even a minimal tilt of the Earth axis could cause ocean temperature fluctuations(Laskar & Robutel, 1993). Given both these calculations of obliquity-driven temperature variations and modern oceans as an analogue, the photic zone of the Archaean BIF basins probably experienced temperature fluctuations of at least ±15 °C due to seasonal/climatic changes or incoming cooler currents (Emery et al., 2006).

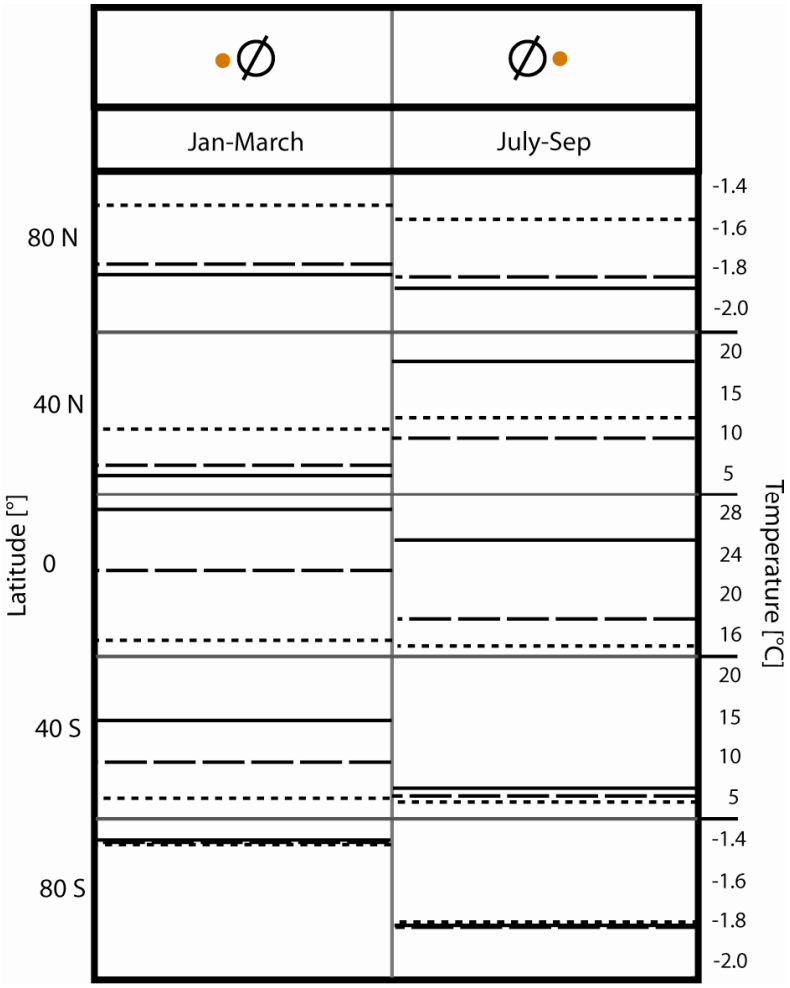

Figure 12.9: Seasonal temperature variations in the modern ocean at 80°N, 40°N, 0°N, 40°S and 80°S. Temperatures compiled from World Ocean Atlas 2005 profiling depths of 10, 50 and 100 m for Northern Hemisphere winter (January - March) and summer (July - September). Full lines represent temperatures at 10 m, broad dashed lines represent temperatures at 50 m, and dotted line represent temperatures at 100 m. Symbols in the top row indicate positions of Earth's axis and sun.

Even if just the upper 50 m of the ocean experienced temperature fluctuations, phototrophic Fe(II) oxidation rates, and ferric hydroxide precipitation, would be highest at water temperatures optimal for the growth of the phototrophs (25-30 °C for the model strains) (Figs 12.1A, 12.3A). At temperatures above and below this range, precipitation of biogenic aggregates would decrease, and cease completely

beyond the metabolic range (Fig. 12.3a). Owing to the decoupled precipitation of silica and biogenic ferric iron, silica would remain in solution in warm (25-30 °C) waters, whereas microbial Fe(II) oxidation would precipitate Fe(III) minerals. A drop in temperature, however, would trigger the precipitation of amorphous silica, whereas microbial populations would be incapable of oxidizing Fe(II) to Fe(III) to a significant extent (Fig. 12.3a). The significance of this mechanism is supported by the lack of psychrophilic, anoxygenic Fe(II)-oxidizing isolates so far. The diminished microbial Fe(II) oxidation rates sustained at low temperatures by the known strains could still result in silicate layers containing trace amounts of Fe(III) minerals. In fact, transitions between Fe mineral and silica layering (as described by (Garrels, 1987)) could also be explained by this microbial mechanism.

As temperatures gradually drop from the optimum for microbial Fe(II) oxidation, a broader transition would be formed as rates slowly decrease. We attempted to verify this model by laboratory experiments in which dissolved Fe(II) was oxidized by *Rhodobacter ferrooxidans* sp. strain SW2 in the presence of silica at 25 °C. After the completion of Fe(II) oxidation, the culture was placed at 4 °C for three days and subsequently stained with the silica stain, Molybdenum Blue (Fig. 12.3c), verifying the production of a silica layer above a Fe(III) mineral layer due to temperature drop. In contrast, as temperatures increase above 35 °C, the transition from the Fe mineral layer formed by microbial Fe(II) oxidation to the silica layer would be abrupt, owing to the strict upper temperature limit of the strains.

As described above, the model strains used in this study do not oxidize Fe(II) at high temperature. However, mesophiles in an Archaean ocean warming to temperatures higher than 35 °C would also produce alternating silica and Fe mineral layering through evaporation within a shallow-water depositional basin (Garrels, 1987) when photoferrotrophic mineral precipitation has stopped.

The present study was done with freshwater Fe(II)-oxidizing strains, yet similar oxidation rates observed for marine strains (Straub et al., 1999) imply that these results are also representative for marine environments. In addition, the present study was carried out with pure strains, and cannot model natural community dynamics. A microbial community of Fe(II)-oxidizing phototrophs would potentially have members that oxidize over a broad temperature range with specific optimal temperatures from each strain. When the ocean temperature deviates from optimum, the microbes will either decrease their rates of Fe(II) oxidation, or move to a more desirable location in the water column. This dynamic could result in mixed precipitation of Fe/Si, potentially even explaining the fine-scaled variation observed in BIFs.

Although a microbial role in the primary deposition of BIFs has been suggested in past models, we have for the first time described how climatic changes or incoming cooler currents in an Archaean basin inhabited by anoxygenic Fe(II)-oxidizing phototrophs is a uniform trigger that links the initial precipitation of iron and silica minerals, and offers a plausible explanation for the alternating nature of BIF deposits.

12.2.4 Methods

The model organism *Rhodobacter ferrooxidans* sp. strain SW2 was isolated from a pond in Schaumburger Wald, Hannover region, Germany (Ehrenreich & Widdel, 1994). Bacterial strains were cultivated in anoxic microbial mineral medium modified from Ehrenreich and Widdel (Ehrenreich & Widdel, 1994), composed of 0.6 g L^{-1} potassium phosphate (KH_2PO_4), 0.3 g L^{-1} ammonium chloride (NH_4Cl), 0.5 g L^{-1}magnesium sulphate ($MgSO_4\times 7H_2O$) and 0.1 g L^{-1} calcium carbonate ($CaCl_2\times 2H_2O$). To ensure that no Fe minerals were transferred to the experimental cultures with the inoculum, either hydrogen (as H_2/CO_2 90:10 v/v) or 4 mM acetate was used as an electron donor for pre-experimental cultures. Experimental cultures were supplied with 0.5-4 mM dissolved Fe(II), added as $FeCl_2$, filtered and buffered

at pH 6.8-.0 following the procedure described previously (Widdel et al., 1993, Kappler & Newman, 2004). Silica was added to the medium already containing dissolved Fe(II) in the form of sodium metasilicate nonahydrate ($Na_2O_3Si \times 9H_2O$) to a final concentration of 2 mM monomeric Si (dissolved silica). The inoculum was then immediately added to an initial density of 107 cells ml^{-1}.

Cultures were incubated in triplicate with an abiotic control at 20 °C with a 40 W incandescent light bulb (Philips) light source at light saturation for these strains (Hegler et al., 2008) (800 lux). The cultures were incubated in 25 mL serum bottles, upside down, so that the stopper was at the bottom of the experimental vial. As particular care was taken not to shake the cultures during incubation and sampling, it was possible to sample just from the solution and quantify silica or Fe that had not precipitated.

The rate of Fe(II) oxidation was determined over time using the ferrozine assay (Stookey, 1970), a spectrophotometric test that enables quantification of Fe(II) and total iron in solution. Oxidation rates were determined from the maximum slope of the line plotted as Fe(II) concentration measured over time. A comparison of this simplified zero-order-rate approach with first-order-rate data analysis shows that the zero-order analysis represents a reasonable approximation with only 10-20% lower values than oxidation rates determined by the first-order approach. Therefore, the simpler zero-order approach was used in this study for all further data analysis. The concentration of monomeric silica (dissolved silica) in solution was measured spectrophotometrically based on the molybdosilicate method (Eaton et al., 2005).

The abiotic precipitation of silica due to temperature change was first modelled with Geochemist's Workbench Standard 6.0. Using TACT in a simplified approach, the activity coefficient was set to one, which rendered the activity equal to the concentration. The microbial mineral medium solution described above was the solvent considered for these calculations. pH and carbonate buffer was accordingly added to the model calculation. Extra calculations for Archaean ocean water composition yielded qualitatively and quantitatively similar results as calculations for the freshwater medium (see Supplementary Information, Fig. 12.5). For batch experiments testing the abiotic precipitation of silica due to temperature change, 4 mM silica was added to anoxic microbial mineral medium, prepared as described above (Eaton et al., 2005), and placed at 70 °C. At 70 °C, the solubility of silica is approximately 4 mM, as shown by the geochemical model described above (Geochemist's Workbench). After 24 h, silica remaining in the water column was sampled and monomeric (dissolved) silica quantified with the molybdosilicate method as described above. The procedure was carried out at 24 and 4 °C with 24 h intervals until equilibrium was reached.

To determine whether the strains revive after exposure to temperature changes, cultures were prepared in anoxic microbial mineral medium with dissolved Fe(II) and silica as described above. Fe(II) oxidation was followed throughout the experiment with the ferrozine assay. After the microbial oxidation of Fe(II) was observed for a number of days, the cultures were moved from 20 to 4 °C for a number of days. These cultures were afterwards returned to 20 °C.

Bibliography

Baur, ME; Hayes, JM; Studley, SA; & Walter, MR: Millimeter-scale variations of stable isotope abundances in carbonates from banded iron-formations in the hamersley group of western australia. *Economic Geology*, 80:270–282, 1985.

Bosak, T; Greene, SE; & Newman, DK: A likely role for anoxygenic photosynthetic microbes in the formation of ancient stromatolites. *Geobiology*, 5:119–126, 2007.

Braterman, PS; Cairns-Smith, AG; & Sloper, RW: Photo-oxidation of hydrated Fe^{2+} – significance for banded iron formations. *Nature*, 303:163–164, 1983.

Brocks, JJ; Love, GD; Summons, RE; Knoll, AH; Logan, GA; & Bowden, SA: Biomarker evidence for green and purple sulphur bacteria in a stratified palaeoproterozoic sea. *Nature*, 437:866–870, 2005.

Cloud, PE: Atmospheric and hydrospheric evolution on primitive earth. *Science*, 160:729–737, 1968.

Eaton, A; Clesceri, L; Rice, E; & Greenberg, A: *Standard methods for the Examination of Water and Wastewater* (American Public Health Association, Maryland), 21st ed., 2005.

Ehrenreich, A & Widdel, F: Anaerobic oxidation of ferrous iron by purple bacteria, a new type of phototrophic metabolism. *Applied and Environmental Microbiology*, 60:4517–4526, 1994.

Emery, WJ; Talley, LD; & Pickard, GL: *Descriptive Physical Oceanography*, vol. 1 (Elsevier), unpublished 6th ed. ed., 2006.

Garrels, RM: A model for the deposition of the microbanded precambrian iron formations. *American Journal of Science*, 287:81–106, 1987.

Gross, GA: Primary features in cherty iron-formations. *Sedimentary Geology*, 7:241–261, 1972.

Hegler, F; Posth, NR; Jiang, J; & Kappler, A: Physiology of phototrophic iron(II)-oxidizing bacteria – implications for modern and ancient environments. *FEMS Microbiology Ecology*, 66:250–260, 2008.

Heising, S; Richter, L; Ludwig, W; & Schink, B: *Chlorobium ferrooxidans* sp nov., a phototrophic green sulfur bacterium that oxidizes ferrous iron in coculture with a *"Geospirillum"* sp strain. *Archives of Microbiology*, 172:116–124, 1999.

Holland, HD: The oceans; a possible source of iron in iron-formations. *Economic Geology*, 68:1169–1172, 1973.

Holland, HD: Volcanic gases, black smokers, and the great oxidation event. *Geochimica et Cosmochimica Acta*, 66:3811–3826, 2002.

Jaffrés, JBD; Shields, GA; & Wallmann, K: The oxygen isotope evolution of seawater: A critical review of a long-standing controversy and an improved geological water cycle model for the past 3.4 billion years. *Earth-Science Reviews*, 83:83–122, 2007.

Johnson, CM; Beard, BL; Klein, C; Beukes, NJ; & Roden, EE: Iron isotopes constrain biologic and abiologic processes in banded iron formation genesis. *Geochimica et Cosmochimica Acta*, 72:151–169, 2008.

Kappler, A & Newman, DK: Formation of Fe(III)-minerals by Fe(II)-oxidizing photoautotrophic bacteria. *Geochimica et Cosmochimica Acta*, 68:1217–1226, 2004.

Kappler, A; Pasquero, C; Konhauser, KO; & Newman, DK: Deposition of banded iron formations by anoxygenic phototrophic Fe(II)-oxidizing bacteria. *Geology*, 33:865–868, 2005.

Kasting, JF; Howard, MT; Wallmann, K; Veizer, J; Shields, G; & Jaffrés, J: Paleoclimates, ocean depth, and the oxygen isotopic composition of seawater. *Earth and Planetary Science Letters*, 252:82–93, 2006.

Klein, C: Some precambrian banded iron-formations (bifs) from around the world: Their age, geologic setting, mineralogy, metamorphism, geochemistry, and origin. *American Mineralogist*, 90:1473–1499, 2005.

Knauth, LP: Temperature and salinity history of the precambrian ocean: implications for the course of microbial evolution. *Palaeogeography Palaeoclimatology Palaeoecology*, 219:53–69, 2005.

Knauth, LP & Lowe, DR: High archean climatic temperature inferred from oxygen isotope geochemistry of cherts in the 3.5 ga swaziland supergroup, south africa. *Geological Society of America Bulletin*, 115:566–580, 2003.

Konhauser, KO; Amskold, L; Lalonde, SV; Posth, NR; Kappler, A; & Anbar, A: Decoupling photochemical Fe(II) oxidation from shallow-water BIF deposition. *Earth and Planetary Science Letters*, 258:87–100, 2007a.

Konhauser, KO; Hamade, T; Raiswell, R; Morris, RC; Ferris, FG; Southam, G; & Canfield, DE: Could bacteria have formed the precambrian banded iron formations? *Geology*, 30:1079–1082, 2002.

Konhauser, KO; Lalonde, SV; Amskold, L; & Holland, HD: Was there really an archean phosphate crisis? *Science*, 315:1234–, 2007b.

Konhauser, KO; Newman, DK; & Kappler, A: The potential significance of microbial Fe(III) reduction during deposition of precambrian banded iron formations. *Geobiology*, 3:167–177, 2005.

Laskar, J & Robutel, P: The chaotic obliquity of the planets. *Nature*, 361:608–612, 1993.

Maliva, RG; Knoll, AH; & Simonson, BM: Secular change in the precambrian silica cycle: Insights from chert petrology. *Geological Society of America Bulletin*, 117:835–845, 2005.

Morris, RC: Genetic modelling for baded iron formation of the hamersly group, pilbara craton, western australia. *Precambrian Research*, 60:243–280, 1993.

Morris, RC & Horwitz, RC: The origin of the iron-formation-rich hamersley group of western australia – deposition on a platform. *Precambrian Research*, 21:273–297, 1983.

Rashby, SE; Sessions, AL; Summons, RE; & Newman, DK: Biosynthesis of 2-methylbacteriohopanepolyols by an anoxygenic phototroph. *Proceedings of the National Academy of Sciences*, 104:15099–15104, 2007.

Robert, F & Chaussidon, M: A palaeotemperature curve for the precambrian oceans based on silicon isotopes in cherts. *Nature*, 443:969–72, 2006.

Shields, GA & Kasting, JF: Palaeoclimatology: Evidence for hot early oceans? *Nature*, 447:E1, 2007.

Siever, R: The silica cycle in the precambrian. *Geochimica et Cosmochimica Acta*, 56:3265–3272, 1992.

Stookey, LL: Ferrozine – a new spectrophotometric reagent for iron. *Analytical Chemistry*, 42:779–781, 1970.

Straub, KL; Rainey, FA; & Widdel, F: *Rhodovulum iodosum* sp. nov. and *Rhodovulum robiginosum* sp. nov., two new marine phototrophic ferrous-iron-oxidizing purple bacteria. *International Journal of Systematic Bacteriology*, 49:729–735, 1999.

Trendall, AF: Three great basins of precambrian banded iron formation deposition: A systematic comparison. *Geological Society of America Bulletin*, 79:1527–1544, 1968.

Trendall, AF: The significance of iron-formation in the precambrian stratigraphic record. In W Altermann & PL Corcoran, eds., *Precambrian sedimentary environments: a modern approach to ancient depositional systems*, vol. 33, pp. 33–66 (Blackwell Science Ltd.), 2002.

Walker, JCG: Suboxic diagenesis in banded iron formations. *Nature*, 309:340–342, 1984.

Weber, KA; Achenbach, LA; & Coates, JD: Microorganisms pumping iron: anaerobic microbial iron oxidation and reduction. *Nature Reviews: Microbiology*, 4:752–764, 2006.

Widdel, F; Schnell, S; Heising, S; Ehrenreich, A; Assmus, B; & Schink, B: Ferrous iron oxidation by anoxygenic phototrophic bacteria. *Nature*, 362:834–836, 1993.

Xiong, J: Photosynthesis: what color was its origin. *Genome Biology*, 7:245–245, 2006.

13 Cryopreservation of anoxygenic phototrophic Fe(II)-oxidizing bacteria

Florian Hegler[1], Andreas Kappler[1] **Cryobiology, 61:158 – 160, 2010**

[1]Center for Applied Geoscience – Geomicrobiology, Eberhard Karls University Tübingen, Sigwartstrasse 10, 72076 Tübingen, Germany

13.1 Abstract

Preservation and storage of microbial stock cultures is desirable since the risk of contamination or loss of living cultures is immanent while over long periods mutations accumulate. Generally, it is rather difficult to preserve photosynthetic bacteria due to their sensitive photosynthetic membranes (Malik, 1984). Phototrophic Fe(II)-oxidizing bacteria face an additional challenge; since they are exposed to light and Fe(II) during growth, they have to cope with radicals from Fenton-reactions of Fe(II)-species, light and water. Therefore, phototrophic Fe(II)-oxidizing strains are thought to be especially susceptible to genetic modifications. Here we provide a simple and fast protocol using glycerol as cryo-protectant to cryopreserve three strains of anoxygenic phototrophic Fe(II)-oxidizing bacteria from different taxa: α-proteobacteria, γ-proteobacteria and chloroflexi. All three strains investigated could be revived after 17 months at -72 °C. This suggests that a long term-storage of phototrophic Fe(II)-oxidizing strains is possible.

13.2 Methods, Results and Discussion

Iron is the fourth most abundant element in the earth crust and can be used by microorganisms either as electron donor or electron acceptor for energy generation and growth (Kappler & Straub, 2005). Phototrophic Fe(II)-oxidizing microorganisms were discovered about 15 years ago and since then have been found in various environments (Kappler & Straub, 2005). Originally the strains were isolated from Fe(II)-rich surface-near freshwater environments. These organisms are especially prone to mutations due to impairments of the cells through hydroxyl radicals produced by Fenton reactions (van der Zee et al., 1993) according to the following equation:

$$Fe^{2+} + H_2O \rightarrow Fe^{3+} + OH^- + {}^{\bullet}OH \tag{13.1}$$

Such radicals are known to cause stress and undesired mutations in the bacteria (Drake et al., 1998). Therefore, in order to preserve the isolated strains with their original genetic systems, it is desirable to have a robust and easy to use method for long-term storage of phototrophic Fe(II)-oxidizing bacteria minimizing the risk of mutations.

Generally, all methods for storage of bacterial strains have advantages as well as disadvantages. When living subcultures are kept as stock, they have to be transferred to fresh growth medium in regular time intervals. Contamination and accumulation of mutations that could potentially lead to a loss of function are a constant risk. In contrast, cryo-preservation of stock culture makes regular transfer of stock cultures unnecessary and therefore provides a solution to avoid potential risks when transferring stock cultures (Snell, 1991). When freezing and thawing the cultures, ice-crystal formation has to be minimized as it can destroy cell and photosynthetic membranes. Often, chemicals such as glycerol are used to protect these membranes during freezing. In the case of phototrophic Fe(II)-oxidizing bacteria, not only the protection of the membranes during freezing is of paramount importance but in addition anoxic conditions must be maintained due to oxygen sensitivity of some of the cells. This is potentially necessary to ensure that the cells could be revived using Fe(II) as electron donor for their anaerobic metabolism.

The following cryopreservation methods have been applied in previous studies for long term storage of bacteria: I) freezing in liquid N_2 (Malik, 1984), II) freezing at -72 °C (Feltham et al., 1978), III) freezing the cultures on glass-beads at -72 °C (Nagel & Kunz, 1972), or IV) lyophilisation (Antheunisse, 1973). Each preservation method has its own requirements with respect to technical equipment and culture preparation.

The goal of this study was to develop a method that makes preservation of phototrophic Fe(II)-oxidizing bacteria easily accessible without sophisticated equipment and thus be generally applicable. Therefore permanent storage in liquid nitrogen was not considered a method of choice because such storage tanks are not ubiquitously available to many microbiology laboratories. The fact that cultures of anoxygenic phototrophic Fe(II)-oxidizing bacteria preferably are kept anoxic further limits the choice of available methods for cryopreservation. Therefore lyophilisation and storage on glass-beads were also excluded because these techniques cannot be applied under anoxic conditions without significant methodological and/or technical efforts. Given these limitations, freezing at -72 °C seemed to be the most promising option with the lowest requirements for long-term storage of anoxygenic phototrophic Fe(II)-oxidizing bacteria. Various concentrations of glycerol as a cryo-protectant were tested based on a previous study by Feltham et al Feltham et al. (1978). Other cryo-protectants were not tested since glycerol showed promising results in initial experiments.

In order to test whether phototrophic Fe(II)-oxidizing bacteria from different taxa can be frozen at -72 °C, we grew cultures of the α-proteobacterium *Rhodobacter* sp. strain SW2, the γ-proteobacterium *Thiodictyon* sp. strain F4 and *Chlorobium ferrooxidans* strain KoFox of the chloroflexi in 22 mM bicarbonate buffered mineral medium according to Hegler et al. (2008) with 10 mM Fe(II) as electron donor. Cell counts and Fe(II) quantification over time (Hegler et al., 2008) were used for determination of the growth phase.

Glycerol (87% p.a. quality, Fluka, Steinheim, Germany) was sterile filtered (0.22
*mu*m, cellulose ester, Fisher Brand, Germany) and deoxygenated by alternating cycles of vacuum and flushing the headspace of the bottle with N_2 for 3 × 20 min and 3 × 2 min, respectively. The anoxic glycerol was added to a sterile and anoxic 6 mL N_2/CO_2-flushed glass-vial (BGB-Analytik, Boeckten, Switzerland) closed with a butyl-rubber-stopper.

Samples from the cultures were taken at the late exponential or early stationary growth phase when all Fe(II) was visibly oxidized and transferred anoxically with a N_2/CO_2-flushed (90:10) sterile syringe into the anoxic glass vial containing glycerol. After complete oxidation of the Fe(II), a culture of *Rhodobacter* sp. strain SW2 contained 1.9E+8 ± 1.4E+7 cells mL^{-1}, *Chlorobium ferrooxidans* sp. KoFox cultures contained 1.1E+8 ± 1.9E+7 cells mL^{-1} and *Thiodictyon* sp. strain F4 cultures contained 1.5E+7 ± 1.3E+6 cells mL^{-1}. The final volume of glycerol-cell-culture suspension was 1 mL containing between 10

to 20% (v/v) glycerol. The concentrations of glycerol were chosen according to (Feltham et al., 1978). After 20 s of careful shaking, the vial was shock-frozen in liquid nitrogen and immediately transferred to a -72 °C freezer. Our results showed that *Rhodobacter* sp. strain SW2 and *Chlorobium ferrooxidans* sp. KoFox could be revived well using 20% glycerol while *Thiodictyon* sp. strain F4 required only 10% glycerol.

In order to revive the strains, we allowed the vials to slowly thaw at room temperature. The cell survival rate of a freeze/thaw cycle was determined by counting dead and live cells after staining cells according to the LIVE/DEAD BacLight Bacterial Viability and Counting Kit (Molecular Probes: (L34856)). The number of dead cells in a stationary phase culture and in an autoclaved control sample was compared to the cell numbers of a culture that underwent freezing and thawing in an anoxic glycerol-containing vial.

We also determined the extent of Fe(II) oxidation after 17 months of storage at -72 °C. In order to do so, we anoxically transferred the total volume of the thawed culture-glycerol-mixture (1 mL) to a 60 mL serum bottle containing 25 mL medium amended with 10 mM Fe(II) buffered with 22 mM bicarbonate (Hegler et al., 2008). The liquid culture first established after thawing was again transferred to fresh growth medium after about 3 weeks (1% v/v inoculum). This procedure reduced the glycerol concentration from initially 20% during freezing to 0.004% (v/v) in the second culture after thawing. Glycerol is a potential substrate for the Fe(II)-oxidizing cells that could be used during photoorganotrophic growth. More importantly, however, organic compounds such as glycerol are potential reductants for the Fe(III) minerals formed by microbial Fe(II) oxidation. During this process glycerol is degraded and toxic intermediates are formed (Feng & Nansheng, 2000). Therefore, by transferring the revived culture a second time before determining the extent of Fe(II) oxidation, potential artifacts could be prevented: either microbial glycerol oxidation (or oxidation of its products resulting from the abiotic reduction of Fe(III)) or more importantly, the alteration of the amount of Fe(II) oxidation in the medium due to the abiotic reduction of Fe(III) coupled to the oxidation of glycerol.

In the second transfer after thawing, we quantified the amount of Fe(II) oxidizable by the thawed, revived cells. Using a spectrophotometric assay with ferrozine, we determined the Fe(II) concentration directly after inoculation and when Fe(II) oxidation halted (Hegler et al., 2008). We found that all cultures oxidized Fe(II) phototrophically to Fe(III) oxy-hydroxides after the second transfer (figure 13.1) to an extent of $> 99\%$ within 21 days, demonstrating the successful revival of the cultures after freezing. Estimation of oxidation rates of >0.5 mM/day based on the concentrations of Fe(II) used (10 mM) and the time after which complete oxidation was observed (in maximum 21 days) we conclude that the oxidation rates of all cultures after freezing are comparable to the oxidation rates before freezing where maximum Fe(II) oxidation rates of 0.5-1.0 mM Fe(II) per day for strain SW2, 1.0-1.5 mM per day for KoFox and 2.0-2.5 mM per day for strain F4 were described (Hegler et al., 2008).

Cell viability analysis in experiments with *Rhodobacter* sp. strain SW2 cells harvested at late exponential stage using the dead-live staining kit showed that freezing killed about 5-10% of the cells (figure 13.2). For cells harvested at early stationary growth phase similar survival rates were observed. *Chlorobium ferrooxidans* sp. KoFox and *Thiodictyon* sp. strain F4 survival rates could not be determined using the dead-live stain because the staining kit did not allow a clear distinction between dead and living cells, probably due to the membrane properties of the strains KoFox and F4. Since these two cultures represent mixed cultures and consist of more than one strain, a dilution series to determine the viable number is not possible without ambiguity since the role of the individual strains in the Fe(II) oxidation process is unknown.

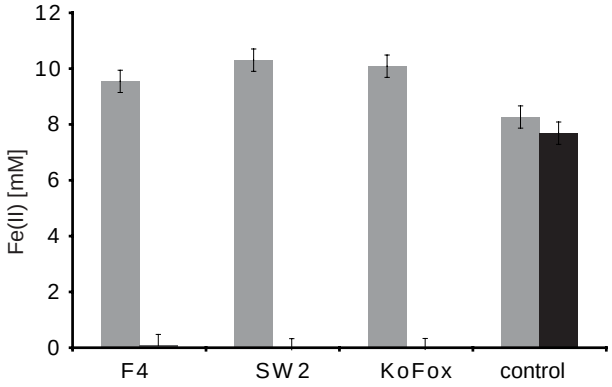

Figure 13.1: Fe(II) oxidation by three phototrophic Fe(II)-oxidizing strains *Thiodictyon* sp. strain F4, *Rhodobacter* sp. strain SW2 and *Chlorobium ferrooxidans* sp. KoFox after freezing and thawing. The graph shows the Fe(II) concentration at the beginning (0 hours, grey bars) and after complete Fe(II) oxidation (21 days, black bars) (n=2). The control shows the Fe(II) concentrations in a non-inoculated culture bottle.

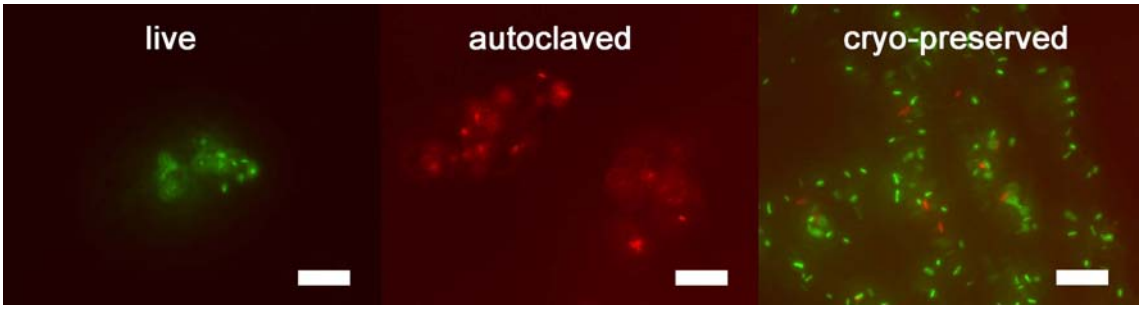

Figure 13.2: Dead-live staining of *Rhodobacter* sp. strain SW2. Live cells were stained from a growing culture at late exponential stage (left), as control cells were autoclaved (middle), and cryo-preserved cells were analyzed directly after thawing (right). Scale-bar = 10 μm.

Nonetheless, the results presented in this study clearly demonstrate that the cryopreservation method developed for phototrophic Fe(II)-oxidizing bacteria is easy to perform, robust and suitable for storage of these bacteria for at least 17 months, potentially even longer, offering a simple and inexpensive method to laboratories not specialized in permanent cryo-preservation of microorganisms in liquid nitrogen.

Acknowledgements

We would like to thank Dr. Sebastian Behrens and Emily-Denise Melton for their help in improving the quality of the manuscript. This work was supported by the Graduate Program ("Promotionsverbund") Cell-Material-Interactions funded by the University of Tuebingen.

Bibliography

Antheunisse, J: Viability of lyophilized microorganisms after storage. *Antonie Van Leeuwenhoek*, 39:243–248, 1973.

Drake, JW; Charlesworth, B; Charlesworth, D; & Crow, JF: Rates of spontaneous mutation. *Genetics*, 148:1667–1686, 1998.

Feltham, RK; Power, AK; Pell, PA; & Sneath, PA: A simple method for storage of bacteria at -76 degrees c. *J Appl Bacteriol*, 44:313–316, 1978.

Feng, W & Nansheng, D: Photochemistry of hydrolytic iron (iii) species and photoinduced degradation of organic compounds. a minireview. *Chemosphere*, 41:1137–47, 2000.

Hegler, F; Posth, NR; Jiang, J; & Kappler, A: Physiology of phototrophic iron(II)-oxidizing bacteria – implications for modern and ancient environments. *FEMS Microbiology Ecology*, 66:250–260, 2008.

Kappler, A & Straub, KL: Geomicrobiological cycling of iron. *Reviews in Mineralogy & Geochemistry*, 59:85–108, 2005.

Malik, KA: A new method for liquid nitrogen storage of phototrophic bacteria under anaerobic conditions. *Journal of Microbiological Methods*, 2:41–47, 1984.

Nagel, JG & Kunz, LJ: Simplified storage and retrival of stock cultures. *Applied Microbiology*, 23:837–838, 1972.

Snell, JJS: General introduction to maintainance methods. In BE Kirsop & A Doyle, eds., *Maintenance of microorganisms and cultured cells: a manual of laboratory methods*, pp. 21–30 (Academic Press, London), 1991.

van der Zee, J; Krootjes, BBH; Chignell, CF; Dubbelman, TMAR; & van Steveninck, J: Hydroxyl radical generation by light-dependent fenton reactions. *Free Radical Biology & Medicine*, 14:105–113, 1993.

14 Conclusion and Outlook

The work presented in this thesis encompasses several aspects of microbial Fe(II) oxidation from cell-mineral interactions, physiology, and habitat to the role of Fe(II)-oxidizers in the Precambrian.

The interaction of iron-oxidizing bacteria with Fe(III) minerals they produce is complex and can be influenced by various factors, e.g. cell-surface pH, organic fibers that localize precipitation, and an adaptation of the cell surface functional groups changing the overall cell surface charge. Scanning electron microscopy already shows that cells are either encrusted with minerals or they are loosely associated with the minerals (chapter 8). It is known that the solubility of Fe(III) increases with decreasing pH (Cornell & Schwertmann, 2003). One of the strategies to avoid encrustation by Fe(III) minerals is to lower the pH at the cell surface. In this thesis, I visualized a low cell surface pH of the photoferrotroph *Thiodyction* sp. strain F4 by confocal laser scanning microscopy (chapter 4). Modeling suggests that the difference between cell surface pH and bulk pH is sufficient to direct mineral precipitation away from the cell surface.

In this study we used *Thiodyction* sp. strain F4 since it is larger than other Fe(II)-oxidizers (approx. 5 µm long). This made microscopic analysis of the cell surface pH feasible. Overcoming the size limitation in confocal laser scanning microscopy and determining the cell surface pH of other iron-oxidizing bacteria would broaden the basis of this study. Furthermore, I speculate the mixotrophic nitrate-reducing Fe(II)-oxidizing strain *Acidovorax* sp. strain BoFeN1 (Kappler et al., 2005b) does not have such a low cell surface pH at all growth phases (chapter 6). *Acidovorax* sp. strain BoFeN1 is much smaller than the previously studied *Thiodyction* sp. strain F4. The smaller size did not allow for an easy use of confocal laser scanning microscopy. These limitations could potentially be overcome with a different setup of the microscope coupled to careful statistical analysis of of multiple images. A determination of the cell surface pH over the growth phase of *Acidovorax* sp. strain would allow to determine how strongly the pH at the cell surface fluctuates with growth. Furthermore, a careful evaluation of cell-mineral interaction depending on the cell's carbon source (e.g. autotrophy or mixotrophy) could help to reveal hints on why cells encrust. For example the mixotrophic Fe(II)-oxidizing phototrophic *Rhodomicrobium vannielii* strain is coated with Fe(III) minerals (Heising & Schink, 1998), similarly to the micotrophic *Acidovorax* sp. BoFeN1 (Kappler et al., 2005c, Miot et al., 2009, Schaedler et al., 2009). In contrast, none of the autotrophic strains known so far encrusts with Fe(III) minerals (Widdel et al., 1993, Heising et al., 1999, Straub et al., 1999, Kappler & Newman, 2004) and chapter 4.

We showed that cell surface encrustation can be avoided by the cell by having a lower cell surface pH (chapter 4). In this thesis we determined if an overall lower pH in the medium has a similar influence on the encrustation of the nitrate-reducing Fe(II)-oxidizer *Acidovorax* sp. strain BoFeN1 as the lower cell surface pH for the photoferrotrophs (chapter 6). The pH in the medium was varied between pH 6.2 and 7.4. We did not find that an overall lower pH in the medium has detectable influence on encrustation of cells with Fe(III) minerals. Furthermore, mineral identity and crystallinity of microbially mediated mineral precipitation depended on the same factors as in the chemical synthesis of minerals (Larese-Casanova et al., 2010). Ions, such as phosphate and carbonate, influence mineral properties stronger than a change in pH does. Thus, small pH-changes – which are common in nature – do not affect mineral properties

and encrustation significantly.

Therefore, the identity and crystallinity of minerals forming at pH 6.2 to 7.4 as well as cell-mineral interaction was determined. We found no evidence that a lower overall pH decreased the encrustation of bacteria. Additionally, we found that other factors, such as the high carbonate and phosphate concentration in the growth medium, likely influenced mineral phase identity more than the pH.

Differences between chemically and microbially formed minerals are known (Châtellier et al., 2001, 2004). The differences of geochemistry on biologically produced minerals need to be carefully determined, not only for the nitrate-reducing Fe(II)-oxidizers (Larese-Casanova et al., 2010) but also for the photoferrotrophs. For example we showed that the photoferrotroph *"Rhodobacter ferrooxidans"* strain SW2 produces fibers onto which the Fe(III) minerals can precipitate (chapter 7). These fibers can influence mineral formation. Especially the crystallinity of the Fe(III) minerals could be influenced by the fibers because the fibers disturb mineral formation (Cornell & Schwertmann, 2003). Determining the factors that influence crystallinity and mineral phase identity of microbially produced Fe(III)(hydr)oxides could allow predictions on reactivity of minerals with contaminants or sorption behavior of other ions on these minerals. A careful determination of sorption constants (similar to Dzombak & Morel (1990), Mathur & Dzombak (2006)) depending on the precipitation conditions could allow to predict the availability of trace metals for microorganisms as well as the transport of contaminants in soils, for example arsenic. Predicting the availability of trace metals based on the sorption behavior of biogenic minerals could also allow to predict the availability of trace metals in the Precambrian oceans (Zerkle et al., 2005, Anbar, 2008, and references therein).

The properties of the microbially produced Fe(III) minerals are additionally important to understand the cell-mineral interaction. The surface charge of the biogenic minerals was shown to be negative at circumneutral pH (chapter 5). We determined the pK_a and concentration of the cell surfaces functional groups of *"Rhodobacter ferrooxidans"* strain SW2 and *Acidovorax* sp. strain BoFeN1 with acid-base titrations (chapter 5). The functional groups of the bacterial cells are directly interacting with the environment and thus determine also the surface charge of the cells (Beveridge, 1988, Madigan et al., 2006, Turner & Fein, 2006). We showed that the surface charge of the encrusting bacteria is less negative. The negatively charged cell surfaces and the negatively charged Fe(III) minerals repulse each other electrostatically. In contrast, chemically synthesized minerals have a positive cell surface charge which would lead to electrostatic attraction.

The effect of the background ions in the mineral medium on the iep of the minerals will need to be determined carefully in order to allow predictions of the surface charge of the Fe(III) minerals, e.g., sorption of trace metals and contaminants. Furthermore, a careful determination of the iep of cells and minerals can allow to predict the behavior of cell-mineral aggregates (Posth et al., 2010). Cell-mineral aggregate formation is likely also influenced by fibers produced by *"Rhodobacter ferrooxidans"* strain SW2 onto which the minerals can precipitate onto (chapter 7). These fibers are similar to the stalks produced by microaerophilic Fe(II)-oxidizers (Hanert, 2006). Cell-mineral aggregates may influence the sedimentation rate of Fe(III) minerals in water which is important to understand the formation and sedimentation scenario of BIFs in the Precambrian.

Multiple individual factors were found that can influence cell-mineral interaction. Therefore, the interplay between the factors (e.g. organic fibers, low pH micro-environment around cells, iep of Fe(III) minerals and the cell surface properties) as well as the contribution of each of these individual factors needs to be determined in further studies. Determining the processes involved and especially separating the contribution of each process can help to predict cell-Fe(III) mineral interaction. The processes described

here are not exclusive for avoiding the interaction with Fe(III) minerals but are also relevant for the sorption mechanisms of heavy metals to bacterial cells (Beveridge & Fyfe, 1985, Johnson et al., 2006).

The mechanisms of the interaction of cells and materials are not exclusive to the system cell-mineral interaction. For example, in medical research cell adhesive or antimicrobially coated materials are still under development (Mermel, 2001). The results of our studies on the cell surface properties and mode of interaction may be beneficial to other areas of research, such as the medical field.

Iron-metabolizing bacteria are not exclusive for the laboratory but can also be found in the environment. In chapter 9 I showed that seasonal changes influence the microbial communities at a chalybeate spring stronger than the geochemical gradients do. Due to the presence of Fe(III)-reducers and O_2 as well as microaerophilic Fe(II)-oxidizers and some phototrophic and nitrate-reducing Fe(II)-oxidizers, iron-cycling is very likely at the field site. The microbial mats at the field site are likely layered as other microbial mats (Revsbech et al., 1983, Canfield & Des Marais, 1993). Microelectrode studies at the microbial mats determining the concentrations of major metabolites, such as iron and oxygen, can reveal the anoxic zones in the cyanobacterial mat and thus localize Fe(III)-reducing microorganisms. Small scale pH determination with confocal laser scanning microscopy was used to study pH differences in microbial mats (Hunter & Beveridge, 2005) as well as iron redox-speciation in microbial mats (Hunter et al., 2008). The described technique of confocal laser scanning microscopy can similarly be applied to determining the iron-cycling in the cyanobacterial mats described in chapter 9.

I showed that the crystallinity of the Fe(III) minerals increases with distance from the source while microaerophilic Fe(II)-oxidizers have been shown to be present. The stalks these bacteria form to avoid precipitation of Fe(III) mineral onto their cell surfaces (Hanert, 2006, Chan et al., 2009) could influence the crystallinity of the precipitating Fe(III) minerals. Microscopic analysis of the cell-mineral aggregates forming in the flow path of the water at the spring as well as quantifying and correlating the number of microaerophilic Fe(II)-oxidizers to the crystallinity of the Fe(III) minerals can answer this question.

Additionally, at the field site cyanobacteria and microaerophilic Fe(II)-oxidizers are spatially closely associated. Emerson et al. (2010) suggested that microaerophilic Fe(II)-oxidizers could have been already present on early earth using the µmolar concentrations of O_2 present after 2.3 Ga (Kasting & Siefert, 2002, Bekker et al., 2004). Emerson et al. (2010) suggested that microaerophilic Fe(II)-oxidizers were actively involved in the oxidation of the Fe(II) on early earth leading to the precipitation of the BIFs. The involvement of microaerophilic Fe(II)-oxidizers would lead to an association of cells and minerals similar to the cell-mineral aggregates for photoferrotrophs (Posth et al., 2010). In any case, the biomass associated with the Fe(III) minerals could form the basis for Fe(III)-reducing microorganisms (Kappler et al., 2005a). This field site can thus be used as a modern analogue for the formation of younger BIFs.

How the banded iron formations formed in the Precambrian helps us to elucidate the conditions prevailing on early earth (Beukes et al., 1992). The exact mechanisms for the oxidation of the Fe(III) are heavily debated (Garrels et al., 1973, Cloud, 1968, Braterman et al., 1983, Konhauser et al., 2002, Kappler et al., 2005b, Posth et al., 2008). Potentially, photoferrotrophs were involved in the oxidation of Fe(II) in the older BIFs (Kappler et al., 2005b). In this thesis, I determined the rates of Fe(II) oxidation for photoferrotrophs under various conditions (chapter 10). These oxidation rates agree well with the rates calculated for the BIF-deposition (Kappler et al., 2005b). We suggest an explanation of the peculiar banding pattern in BIFs of alternating silica and iron bands. We modeled silicate precipitation depending on temperature and a coupled that to the known Fe(II) oxidation rates by photoferrotrophs and found that a temperature difference may explain the preferential precipitation of either silica or iron-minerals (chapter 12).

The physiological constraints, e.g., the Fe(II) oxidation rates, of the photoferrotrophs showed that these bacteria have to be considered for explaining the Fe(II) oxidation in the early Precambrian (Kappler et al. (2005b) and chapter 10). The need of bacteria for certain trace metals is encoded in the genome (Madigan et al., 2006). Enzymes that evolved very early on earth may have metals in their reactive centers that reflect the abundance of trace metals on early earth and not the availability of the trace metals today (Fraústo da Silva & Williams, 2001, Williams & Frausto Da Silva, 2003, Williams & Fraústo da Silva, 2006). In this thesis I showed that the trace metals cobalt, vanadium, nickel and molybdenum utilized by *"Rhodobacter ferrooxidans"* strain SW2 reflect the bioavailability of these metals on early earth (chapter 11).

The sorption and co-precipitation of trace metals with Fe(III) minerals will need to be evaluated before the availability of vanadium, cobalt, nickel and molybdenum in the Precambrian ocean is clear. Synchrotron-based techniques, modeling and sorption experiments may help to tackle this question. Comparing the need of trace metals of *"Rhodobacter ferrooxidans"* strain SW2 to the need of other photoferrotrophs may reveal the robustness of this study. Genome-based studies, such as the one by Zerkle et al. (2005) for cyanobacteria, may also be done for photoferrotrophs once the full genome is available for several strains. These results are then directly comparable to the data compiled for cyanobacteria (Zerkle et al., 2005).

Finally, photoferrotrophic bacteria are exposed to high radical concentrations because iron in the presence of light leads to radical formation via the Fenton reaction (van der Zee et al., 1993). In order to assure that mutations of photoferrotrophs are minimized I developed a glycerol-based freezing protocol which allows to preserve the bacteria anoxically.

Overall, in this thesis I investigated cell-mineral interaction of Fe(II)-oxidizing bacteria, I described the natural habitat of an iron-metabolizing community and found evidence for an active role of photoferrotrophs on early earth.

Bibliography

Anbar, AD: Oceans: Elements and evolution. *Science*, 322:1481–1483, 2008.

Bekker, A; Holland, HD; Wang, PL; Rumble III, D; Stein, HJ; Hannah, JL; Coetzee, LL; & Beukes, NJ: Dating the rise of atmospheric oxygen. *Nature*, 427:117–120, 2004.

Beukes, NJ; Klein, C; Holland, HD; Kasting, JF; Kump, LR; & Lowe, DR: *Proterozoic Atmosphere and Ocean.* The Proterozoic Biosphere: a multidisciplenary study (Press Syndicate of the University of Camebridge, New York), 1992.

Beveridge, TJ: The bacterial surface: general considerations towards design and function. *Canadian Journal of Microbiology*, 34:363–372, 1988.

Beveridge, TJ & Fyfe, WS: Metal fixation by bacterial-cell walls. *Canadian Journal of Earth Sciences*, 22:1893–1898, 1985.

Braterman, PS; Cairns-Smith, AG; & Sloper, RW: Photo-oxidation of hydrated Fe^{2+} – significance for banded iron formations. *Nature*, 303:163–164, 1983.

Canfield, DE & Des Marais, DJ: Biogeochemical cycles of carbon, sulfur, and free oxygen in a microbial mat. *Geochimica et Cosmochimica Acta*, 57:3971–3984, 1993.

Chan, CS; Fakra, SC; Edwards, DC; Emerson, D; & Banfield, JF: Iron oxyhydroxide mineralization on microbial extracellular polysaccharides. *Geochimica et Cosmochimica Acta*, 73:3807–3818, 2009.

Châtellier, X; Fortin, D; West, MM; Leppard, GG; & Ferris, FG: Effect of the presence of bacterial surfaces during the synthesis of Fe oxides by oxidation of ferrous ions. *European Journal of Mineralogy*, 13:705–714, 2001.

Châtellier, X; West, MM; Rose, J; Fortin, D; Leppard, GG; & Ferris, FG: Characterization of iron-oxides formed by oxidation of ferrous ions in the presence of various bacterial species and inorganic ligands. *Geomicrobiology Journal*, 21:99–112, 2004.

Cloud, PE: Atmospheric and hydrospheric evolution on primitive earth. *Science*, 160:729–737, 1968.

Cornell, RM & Schwertmann, U: *The iron oxides: structure, properties, reactions, occurrences and uses* (VCH, Weinheim, Cambridge), 2nd ed., 2003.

Dzombak, DA & Morel, F: *Surface complexation modeling: hydrous ferric oxide* (Wiley, New York), 1990.

Emerson, D; Fleming, EJ; & McBeth, JM: Iron-oxidizing bacteria: an environmental and genomic perspective. *Annual Review of Microbiology*, 64:561–83, 2010.

Fraústo da Silva, JJR & Williams, RJP: *The biological chemistry of the elements: the inorganic chemistry of life* (Oxford University Press, Oxford), 2nd ed., 2001.

Garrels, RM; Perry, EA, JR; & Mackenzie, FT: Genesis of precambrian iron-formations and the development of atmospheric oxygen. *Economic Geology*, 68:1173–1179, 1973.

Hanert, H: *The Genus Gallionella*, vol. Proteobacteria: Delta, Epsilon subclass, pp. 996–997 (Springer), 2006.

Heising, S; Richter, L; Ludwig, W; & Schink, B: *Chlorobium ferrooxidans* sp nov., a phototrophic green sulfur bacterium that oxidizes ferrous iron in coculture with a *"Geospirillum"* sp strain. *Archives of Microbiology*, 172:116–124, 1999.

Heising, S & Schink, B: Phototrophic oxidation of ferrous iron by a *Rhodomicrobium vannielii* strain. *Microbiology*, 144:2263–2269, 1998.

Hunter, RC & Beveridge, TJ: Application of a pH-sensitive fluoroprobe (c-snarf-4) for pH microenvironment analysis in pseudomonas aeruginosa biofilms. *Applied and Environmental Microbiology*, 71:2501–2510, 2005.

Hunter, RC; Hitchcock, AP; Dynes, JJ; Obst, M; & Beveridge, TJ: Mapping the speciation of iron in *Pseudomonas aeruginosa* biofilms using scanning transmission X-ray microscopy. *Environmental Science & Technology*, 42:8766–8772, 2008.

Johnson, KJ; Cygan, RT; & Fein, JB: Molecular simulations of metal adsorption to bacterial surfaces. *Geochimica Et Cosmochimica Acta*, 70:5075–5088, 2006.

Kappler, A; Konhauser, KO; & Newman, DK: The potential significance of microbial Fe(III) reduction during deposition of precambrian banded iron formations. *Geobiology*, 3:167–177, 2005a.

Kappler, A & Newman, DK: Formation of Fe(III)-minerals by Fe(II)-oxidizing photoautotrophic bacteria. *Geochimica et Cosmochimica Acta*, 68:1217–1226, 2004.

Kappler, A; Pasquero, C; Konhauser, KO; & Newman, DK: Deposition of banded iron formations by anoxygenic phototrophic Fe(II)-oxidizing bacteria. *Geology*, 33:865–868, 2005b.

Kappler, A; Schink, B; & Newman, DK: Fe(III) mineral formation and cell encrustation by the nitrate-dependent Fe(II)-oxidizer strain BoFeN 1. *Geobiology*, 3:235–245, 2005c.

Kasting, JF & Siefert, JL: Life and the evolution of earth's atmosphere. *Science*, 296:1066–1068, 2002.

Konhauser, KO; Hamade, T; Raiswell, R; Morris, RC; Ferris, FG; Southam, G; & Canfield, DE: Could bacteria have formed the precambrian banded iron formations? *Geology*, 30:1079–1082, 2002.

Larese-Casanova, P; Haderlein, S; & Kappler, A: Biomineralization of lepidocrocite and goethite by nitrate-reducing Fe(II)-oxidizing bacteria: Effect of pH, bicarbonate, phosphate and humic acids. *Geochimica Et Cosmochimica Acta*, 74:3721–3734, 2010.

Madigan, MT; Martinko, JM; & Brock, TD: *Brock biology of microorganisms* (Pearson Prentice Hall, Upper Saddle River, NJ), 11th ed., 2006.

Mathur, SS & Dzombak, DA: *Surface complexation modeling: goethite*, vol. 11, chap. 16, pp. 443–468 (Elsevier), 2006.

Mermel, LA: New technologies to prevent intravascular catheter-related bloodstream infections. *Emerging Infections Deseases*, 7:197–199, 2001.

Miot, J; Benzerara, K; Morin, G; Kappler, A; Bernard, S; Obst, M; Férard, C; Skouri-Panet, F; Guigner, JM; Posth, NR; Galvez, M; Brown, GE, JR.; & Guyot, F: Iron biomineralization by neutrophilic iron-oxidizing bacteria. *Geochimica et Cosmochimica Acta*, 73:696–711, 2009.

Posth, NR; Hegler, F; Konhauser, KO; & Kappler, A: Alternating Si and Fe deposition caused by temperature fluctuations in Precambrian oceans. *Nature Geoscience*, 1:703–708, 2008.

Posth, NR; Huelin, S; Konhauser, K; & Kappler, A: Size, density and composition of cell-mineral aggregates formed during anoxigenic phototrophic Fe(II) oxidation: Impact on modern and ancient environments. *Geochimica Et Cosmochimica Acta*, 74:3476–3493, 2010.

Revsbech, NP; Jørgensen, BB; & Blackburn, TH: Microelectrode studies of the photosynthesis and O_2, H_2S and pH profiles of a microbial mat. *Limnology and Oceanography*, 28:1062–1074, 1983.

Schaedler, S; Burkhardt, C; Hegler, F; Straub, KL; Miot, J; Benzerara, K; & Kappler, A: Formation of cell-iron-mineral aggregates by phototrophic and nitrate reducing anaerobic Fe(II)-oxidizing bacteria. *Geomicrobiology Journal*, 26:93–103, 2009.

Straub, KL; Rainey, FA; & Widdel, F: *Rhodovulum iodosum* sp. nov. and *Rhodovulum robiginosum* sp. nov., two new marine phototrophic ferrous-iron-oxidizing purple bacteria. *International Journal of Systematic Bacteriology*, 49:729–735, 1999.

Turner, BF & Fein, JB: Protofit: A program for determining surface protonation constants from titration data. *Computers & Geosciences*, 32:1344–1356, 2006.

van der Zee, J; Krootjes, BBH; Chignell, CF; Dubbelman, TMAR; & van Steveninck, J: Hydroxyl radical generation by light-dependent fenton reactions. *Free Radical Biology & Medicine*, 14:105–113, 1993.

Widdel, F; Schnell, S; Heising, S; Ehrenreich, A; Assmus, B; & Schink, B: Ferrous iron oxidation by anoxygenic phototrophic bacteria. *Nature*, 362:834–836, 1993.

Williams, RJ & Frausto Da Silva, JJ: Evolution was chemically constrained. *Journal of Theoretical Biology*, 220:323–43, 2003.

Williams, RJP & Fraústo da Silva, JJR: *The chemistry of evolution: the development of our ecosystem* (Elsevier, Amsterdam; Boston), 1st ed., 2006.

Zerkle, AL; House, CH; & Brantley, SL: Biogeochemical signatures through time as inferred from whole microbial genomes. *American Journal of Science*, 305:467–502, 2005.

Acknowledgments

The work presented herein was carried out from February 2007 until December 2010 in the Geomicrobiology Research Group of Prof. Andreas Kappler at the the Center for Applied Geosciences (ZAG) of the Eberhard Karls University of Tübingen. It is most likely much harder to finish a PhD without ideas, discussions, coffee, sport and fun beyond the lab shared with others. Therefore, I would like to thank many colleges and friends:

Andreas Kappler for his continuous support throughout my work from being a HiWi to the end of my PhD. Interesting discussions and ideas as well as challenges and opportunities were a great environment for working on such a diverse topic. The possibility to go to conferences, meetings, discussions and going abroad was not only scientifically interesting but broadened my horizon.

Karim Benzerara for his support throughout as well as discussions and helpful comments and the invitation to Paris. Within this framework , I would like to acknowledge my examiners Prof. Andreas Kappler, Prof. Karim Benzerara and additionally at the defense Prof. Andreas Peschel and Dr. Sebastian Behrens.

Kristina Straub for helpful questions and support, I learned a lot of microbiology from her. Thank you for the invitation to Vienna.

Kurt Hanselmann, for numerous visits to the Engadin, discussions, challenges and catching interest in microbiology and also Kurt Hanselmann and his wife for the hospitality in Zürich.

Thomas Neu for help in the challenge of LPS and CLSM.

The two HiWis, Steffanie Lutz and Sarah Köhl.

I also thank my actual and former colleagues from Tübingen and abroad. I especially thank Nicole Posth, Sebastian Behrens, Jennyfer Miot, Caroline Schmidt, Tina Lösekann, Katja Amstätter, Karin Stögerer, Urs Dippon, Ellen Struve, Heinz Schwarz, Jürgen Berger, Katharina Porsch, Martin Obst, Petra Kühner, Sebastian Schädler, Claudia Pantke, Phil Larese-Casanova, Jie Jiang, Eva Winkler, Sarah Richter, Marie Mühe, Emily Melton, Iris Bauer, Christian Schröder, Sonia Huelin, Johanna Gloël, Florian Latteyer, Nadine Göring, Raul Martinez, Stephan Lalonde, Merle Eickhoff, Kurt Konhauser. Others contributed non-scientifically: the various eat & drink teams over the years, the running team and all those, who were there at the right moments – I think you know who I mean.

Schließlich möchte ich mich auch bei meinen Freunden und meiner Familie für Geduld, gemeinsam verbrachte Zeit und Unterstützung bedanken.

Janika – vielen Dank! Außerdem sind nicht zu vergessen: Mareike, Tina, Erich, Judith, Verena, Oli, Sebastian, Anja-Maria, Dirk, Silke, Clemens, Caro, Hanna, Steffi, Nicole, Seb, Urs, Katja, Marie & the climbing people.

Last but not least I thank the Promotionsverbund “Bakterien-Material-Wechselwirkungen” of the Eberhard Karls University of Tübingen for my stipend and DFG for travel support.

14.1 Curriculum vitæ

Florian Hegler

3^{rd} September 1979 in Tübingen

Education

2007-2011 Ph.D. at the Eberhard Karls Universität Tübingen, supervisor: Prof. Andreas Kappler

2004-2006 M.Sc. Applied environmental Geoscience, Eberhard Karls Universität Tübingen Thesis: *"Anoxygenic photosynthetic Fe(II)-oxidizers – physiological and mineral studies"* including a research period at the Californian Institute of Technology, supervisor: Dr. Andreas Kappler

June 2000 Abitur

Publications

2008 Hegler, F., Posth, N., Jiang, J., and Kappler, A.: *"Physiology of phototrophic iron(II)-oxidizing bacteria – implications for modern and ancient environments"* **FEMS Microbiology Ecology**, v. 66, p. 250-260

2009 Miot, J., Benzerara, K., Obst, M., Kappler, A., Hegler, F., Schaedler, S., Bouchez, C., Guyot, F., and Morin, G.: *"Extracellular iron biomineralization by photoautotrophic iron-oxidizing bacteria"* **Applied and Environmental Microbiology** v. 75, p. 5586-5591

2008 Posth, N., Hegler, F., Konhauser, K.O., and Kappler, A. *"Alternating Si and Fe deposition caused by temperature fluctuations in Precambrian oceans"* **Nature Geoscience** v. 1, p. 703-708

2009 Schaedler, S., Burkhardt, C., Hegler, F., Straub, K.L., Miot, J., Benzerara, K., and Kappler, A. *"Formation of cell-iron-mineral aggregates by phototrophic and nitrate reducing anaerobic Fe(II)-oxidizing bacteria"* **Geomicrobiology Journal** v. 26, p. 93-103.

2010 Hegler, F., Kappler, A. *"Cryopreservation of anoxygenic phototrophic Fe(II)-oxidizing bacteria"* **Cryobiology** v. 61, p. 158-160

2010 Hegler, F., Schmidt, C., Schwarz, H., Kappler, A. *"Does a low pH-microenvironment around phototrophic Fe(II)-oxidizing bacteria prevent cell encrustation by Fe(III) minerals?"* **FEMS Microbiology Ecology** v. 74, p. 592-600

Presentations and posters, first author only

2009	Jahreskonferenz der Geologischen Vereinigung Deutschlands, presentation: *"How carbonate precipitation and dissolution is regulated during the formation of ferronous banded microbialites – Observations on geochemical iron and carbon cycling in a cold, iron-rich mineral spring"*
2009	Goldschmidt conference, presentation: *"Phototrophic Fe(II) oxidizing bacteria – strategies to avoid encrustation by Fe(III) minerals"* poster: *"Microbially mediated geochemical iron and carbon cycling in a cold mineral spring"*
2009	Universität Wien, Center for Earth Sciences - Environmental Geosciences, Earth Science Kolloquium, presentation: *Hard rock – heavy metal and microbiology Fe(II)-oxidizing bacteria: encrustation by Fe(III) minerals"*
2009	Goldschmidt conference, presentation: *"Phototrophic Fe(II) oxidizing bacteria – to encrust or not to encrust"*
2008	Netzwerk für Elektronenmikroskopie Tübingen (NET), presentation: *"Scanning and transmission electron microscopy of Fe(II)-oxidizing bacteria"*
2008	Congrès des Doctorants am Institut de Physique du Globe de Paris (IPGP), presentation: *"Cell-mineral-interactions – to encrust or not to encrust"*
2007	StEVE (Students in Evolution & Ecology Forum), Universität Tübingen, presentation: *"Cell mineral interaction"*
2007	Institut de Physique du Globe de Paris (IPGP), presentation: *"Physiology, mineral formation and encrustation of iron(II)-oxidizing bacteria"*
2007	Jahreskonferenz der Vereinigung für Allgemeine und Angewandte Mikrobiologie, poster *"Membrane properties, pH-, temperature and light-dependence of anoxygenic phototautotrophic Fe(II)-oxidizing bateria"*

Complete list of references

Amstaetter, K; Borch, T; Larese-Casanova, P; & Kappler, A: Redox transformation of arsenic by Fe(II)-activated goethite (α-FeOOH). *Environmental Science & Technology*, 44:102–8, 2010.

Anagnostidis, K & Komárek, J: Modern approach to the classification system of cyanophytes. 3-oscillatoriales. *Archiv für Hydrobiologie*, 80:327–472, 1988.

Anbar, AD: Oceans: Elements and evolution. *Science*, 322:1481–1483, 2008.

Anbar, AD; Duan, Y; Lyons, TW; Arnold, GL; Kendall, B; Creaser, RA; Kaufman, AJ; Gordon, GW; Scott, C; Garvin, J; & Buick, R: A whiff of oxygen before the great oxidation event? *Science*, 317:1903–1906, 2007.

Antheunisse, J: Viability of lyophilized microorganisms after storage. *Antonie Van Leeuwenhoek*, 39:243–248, 1973.

Archibald, DD & Mann, S: Template mineralization of self-assembled anisotropic lipid microstructures. *Nature*, 364:430–433, 1993.

Auffan, M; Achouak, W; Rose, J; Roncato, MA; Chaneac, C; Waite, DT; Masion, A; Woicik, JC; Wiesner, MR; & Bottero, JY: Relation between the redox state of iron-based nanoparticles and their cytotoxicity toward escherichia coli. *Environmental Science & Technology*, 42:6730–6735, 2008.

Baer, ML; Ravel, J; Chun, J; Hill, RT; & Williams, HN: A proposal for the reclassification of *Bdellovibrio stolpii* and *Bdellovibrio starrii* into a new genus, *Bacteriovorax* gen. nov. as *Bacteriovorax stolpii* comb. nov. and *Bacteriovorax starrii* comb. nov., respectively. *International Journal of Systematic and Evolutionary Microbiology*, 50:219–24, 2000.

Baker, BJ & Banfield, JF: Microbial communities in acid mine drainage. *FEMS Microbiology Ecology*, 44:139–152, 2003.

Balashova, VV & Zavarzin, GA: Anaerobic reduction of ferric iron by hydrogen bacteria. *Mikrobiologiia*, 48:773–78, 1979.

Banfield, JF & Nealson, KH: *Geomicrobiology: Interactions between microbes and minerals*, vol. 35 of *Reviews in Mineralogy* (Mineralogical Society of America, Washington D.C.), 1st ed., 1997.

Barbeau, K; Rue, EL; Bruland, KW; & Butler, A: Photochemical cycling of iron in the surface ocean mediated by microbial iron(III)-binding ligands. *Nature*, 413:409–13, 2001.

Baur, ME; Hayes, JM; Studley, SA; & Walter, MR: Millimeter-scale variations of stable isotope abundances in carbonates from banded iron-formations in the hamersley group of western australia. *Economic Geology*, 80:270–282, 1985.

Bekker, A; Holland, HD; Wang, PL; Rumble III, D; Stein, HJ; Hannah, JL; Coetzee, LL; & Beukes, NJ: Dating the rise of atmospheric oxygen. *Nature*, 427:117–120, 2004.

Benz, M; Brune, A; & Schink, B: Anaerobic and aerobic oxidation of ferrous iron at neutral pH by chemoheterotrophic nitrate-reducing bacteria. *Archives of Microbiology*, 169:159–165, 1998.

Benzerara, K; Menguy, N; Guyot, F; Skouri-Panet, F; de Lucca, G; & Huelin, T: Bacteria-controlled precipitation of calcium phosphate by ramlibacter tataouinensis. *Earth and Planetary Science Letters*, 228:439–449, 2004a.

Benzerara, K; Yoon, T; Tyliszczak, T; Constanz, B; Spormann, AM; & Brown, G: Scanning transmission x-ray microscopy study of microbial calcification. *Geobiology*, 2:249–259, 2004b.

Bernard, S; Benzerara, K; Beyssac, O; Menguy, N; Guyot, F; Brown, G; & Goffé, B: Exceptional preservation of fossil plant spores in high-pressure metamorphic rocks. *Earth and Planetary Science Letters*, 262:257–272, 2007.

Beukes, NJ; Klein, C; Holland, HD; Kasting, JF; Kump, LR; & Lowe, DR: *Proterozoic Atmosphere and Ocean*. The Proterozoic Biosphere: a multidisciplenary study (Press Syndicate of the University of Camebridge, New York), 1992.

Beveridge, TJ: Mechanisms of the binding of metallic ions to bacterial walls and the possible impact on the microbial ecology. In CA Reddy & MJ Klug, eds., *Current perspectives in microbial ecology proceedings of the 3. International Symposium on Microbial Ecology, Michigan State University, 7 - 12 August 1983*, pp. 601–607 (Michigan State University, Washington), 1983.

Beveridge, TJ: The bacterial surface: general considerations towards design and function. *Canadian Journal of Microbiology*, 34:363–372, 1988.

Beveridge, TJ: Role of cellular design in bacterial metal accumulation and mineralization. *Annual Review of Microbiology*, 43:147–171, 1989.

Beveridge, TJ & Fyfe, WS: Metal fixation by bacterial-cell walls. *Canadian Journal of Earth Sciences*, 22:1893–1898, 1985.

Beveridge, TJ & Murray, RG: Uptake and retention of metals by cell walls of *Bacillus subtilis*. *Journal of Bacteriology*, 127:1502–1518, 1976.

Beveridge, TJ & Murray, RG: Sites of metal deposition in the cell wall of *Bacillus subtilis*. *Journal of Bacteriology*, 141:876–887, 1980.

Bissig, P: Die CO_2-reichen Mineralquellen von Scuol-Tarasp (Unterengadin, Kt. GR). *Bulletin für angewandte Geologie*, 9:39–47, 2004.

Bissig, P; Goldscheider, N; Mayoraz, J; Surbeck, H; & Vuataz, FD: Carbogaseous spring waters, coldwater geysers and dry co_2 exhalations in the tectonic window of the Lower Engadine Valley, Switzerland. *Eclogae Geologicae Helvetiae*, 99:143–155, 2006.

Blake, RC; Shute, EA; Greenwood, MM; Spencer, GH; & Ingledew, WJ: Enzymes of aerobic respiration on iron. *FEMS Microbiology Reviews*, 11:9–18, 1993.

Borch, T; Kretzschmar, R; Kappler, A; Cappellen, PV; Ginder-Vogel, M; Voegelin, A; & Campbell, K: Biogeochemical redox processes and their impact on contaminant dynamics. *Environmental Science and Technology*, 44:15–23, 2010.

Borrok, D; Fein, JB; Tischler, M; O'Loughlin, E; Meyer, H; Liss, M; & Kemner, KM: The effect of acidic solutions and growth conditions on the adsorptive properties of bacterial surfaces. *Chemical Geology*, 209:107–119, 2004.

Borrok, D; Turner, BF; & Fein, JB: A universal surface complexation framework for modeling proton binding onto bacterial surfaces in geologic settings. *American Journal of Science*, 305:826–853, 2005.

Bosak, T; Greene, SE; & Newman, DK: A likely role for anoxygenic photosynthetic microbes in the formation of ancient stromatolites. *Geobiology*, 5:119–126, 2007.

Braterman, PS; Cairns-Smith, AG; & Sloper, RW: Photo-oxidation of hydrated Fe^{2+} – significance for banded iron formations. *Nature*, 303:163–164, 1983.

Britton, G: Structure and properties of carotenoids in relation to function. *FASEB Journal*, 9:1551–1558, 1995a.

Britton, G: *UV/Visible Spectroscopy.* Carotenoids (Birkhäuser, Basel), 1995b.

Brocks, JJ; Love, GD; Summons, RE; Knoll, AH; Logan, GA; & Bowden, SA: Biomarker evidence for green and purple sulphur bacteria in a stratified palaeoproterozoic sea. *Nature*, 437:866–870, 2005.

Brown, I; Bryant, DA; Casamatta, D; Thomas-Keprta, KL; Sarkisova, SA; Shen, G; Graham, JE; Boyd, ES; Peters, JW; Garrison, DH; & McKay, DS: Polyphasic characterization of a thermotolerant siderophilic filamentous cyanobacterium that produces intracellular iron deposits. *Applied and Environmental Microbiology*, 2010.

Bruun, AM; Finster, K; Gunnlaugsson, HP; Nornberg, P; & Friedrich, MW: A comprehensive investigation on iron cycling in a freshwater seep including microscopy, cultivation and molecular community analysis. *Geomicrobiology Journal*, 27:15–34, 2010.

Buresh, R & Moraghan, J: Chemical reduction of nitrate by ferrous iron. *Journal of Environmental Quality*, 5:320, 1976.

Caiazza, NC; Lies, DP; & Newman, DK: Phototrophic Fe(II) oxidation promotes organic carbon acquisition by *Rhodobacter capsulatus* SB1003. *Applied Environmental Microbiology*, 73:6150–6158, 2007.

Cairns-Smith, AG: Precambrian solution photochemistry, inverse segregation, and banded iron formation. *Nature*, 276:808–808, 1978.

Canfield, DE: Reactive iron in marine sediments. *Geochimica et Cosmochimica Acta*, 53:619–632, 1989.

Canfield, DE: The early history of atmospheric oxygen: Homage to robert a. garrels. *Annual Review of Earth and Planetary Sciences*, 33:1–36, 2005.

Canfield, DE & Des Marais, DJ: Biogeochemical cycles of carbon, sulfur, and free oxygen in a microbial mat. *Geochimica et Cosmochimica Acta*, 57:3971–3984, 1993.

Canfield, DE; Thamdrup, B; & Hansen, JW: The anaerobic degradation of organic matter in danish coastal sediments: Iron reduction, manganese reduction, and sulfate reduction. *Geochimica et Cosmochimica Acta*, 57:3867–3883, 1993.

Canfield, DE; Thamdrup, B; & Kristensen, E: *Aquatic Geomicrobiology*, vol. 48 of *Advances in Marine Biology* (Elsevier Academic Press, San Diego, California), 1st ed., 2005.

Carlé, W: *Die Mineral- und Thermalwässer von Mitteleuropa* (Wissenschaftliche Verlagsgesellschaft, Stuttgart), 1975.

Chan, CS; de Stasio, G; Welch, SA; Girasole, M; Frazer, BH; Nesterova, MV; Fakra, S; & Banfield, JF: Microbial polysaccharides template assembly of nanocrystal fibers. *Science*, 303:1656–1658, 2004.

Chan, CS; Fakra, SC; Edwards, DC; Emerson, D; & Banfield, JF: Iron oxyhydroxide mineralization on microbial extracellular polysaccharides. *Geochimica et Cosmochimica Acta*, 73:3807–3818, 2009.

Châtellier, X & Fortin, D: Adsorption of ferrous ions onto *Bacillus subtilis* cells. *Chemical Geology*, 212:209–228, 2004.

Châtellier, X; Fortin, D; West, MM; Leppard, GG; & Ferris, FG: Effect of the presence of bacterial surfaces during the synthesis of Fe oxides by oxidation of ferrous ions. *European Journal of Mineralogy*, 13:705–714, 2001.

Châtellier, X; West, MM; Rose, J; Fortin, D; Leppard, GG; & Ferris, FG: Characterization of iron-oxides formed by oxidation of ferrous ions in the presence of various bacterial species and inorganic ligands. *Geomicrobiology Journal*, 21:99–112, 2004.

Chaudhuri, SK; Lack, JG; & Coates, JD: Biogenic magnetite formation through anaerobic biooxidation of Fe(II). *Applied and Environmental Microbiology*, 67:2844–2848, 2001.

Cloud, PE: Atmospheric and hydrospheric evolution on primitive earth. *Science*, 160:729–737, 1968.

Cochran, WG: Estimation of bacterial densities by means of the "most probable number". *Biometrics*, 6:105–16, 1950.

Copin-Montegut, C & Copin-Montegut, G: Stoichiometry of carbon, nitrogen, and phosphorus in marine particulate matter. *Deep Sea Research Part A. Oceanographic Research Papers*, 30:31–46, 1983.

Cornell, RM & Schwertmann, U: *The iron oxides: structure, properties, reactions, occurrences and uses* (VCH, Weinheim, Cambridge), 2nd ed., 2003.

Croal, LR; Gralnick, JA; Malasarn, D; & Newman, DK: The genetics of geochemistry. *Annual Review of Genetics*, 38:175–202, 2004a.

Croal, LR; Jiao, Y; & Newman, DK: The fox operon from *Rhodobacter* strain SW2 promotes phototrophic fe(II) oxidation in *Rhodobacter capsulatus* sb1003. *Journal of Bacteriology*, 189:1774–1782, 2007.

Croal, LR; Johnson, CM; Beard, BL; & Newman, DK: Iron isotope fractionation by Fe(II)-oxidizing photoautotrophic bacteria. *Geochimica et Cosmochimica Acta*, 68:1227–1242, 2004b.

Curl, J, Herbert; Hardy, JT; & Ellermeier, R: Spectral absorption of solar radiation in alpine snowfields. *Ecology*, 53:1189–1194, 1972.

Davison, W & Seed, G: The kinetics of the oxidation of ferrous iron in synthetic and natural waters. *Geochimica et Cosmochimica Acta*, 47:67–79, 1983.

Deo, N; Natarajan, KA; & Somasundaran, P: Mechanisms of adhesion of *Paenibacillus polymyxa* onto hematite, corundum and quartz. *International Journal of Mineral Processing*, 62:27–39, 2001.

Downing, JA: Marine nitrogen: Phosphorus stoichiometry and the global N:P cycle. *Biogeochemistry*, 37:237–252, 1997.

Drake, JW; Charlesworth, B; Charlesworth, D; & Crow, JF: Rates of spontaneous mutation. *Genetics*, 148:1667–1686, 1998.

Druschel, GK; Emerson, D; Sutka, R; Suchecki, P; & Luther, GW: Low oxygen and chemical kinetic constraints on the geochemical niche of neutrophilic iron(ii) oxidizing microorganisms. *Geochimica et Cosmochimica Acta*, 72:3358–3370, 2008.

Duckworth, OW; Holmstrom, SJM; Pena, J; & Sposito, G: Biogeochemistry of iron oxidation in a circumneutral freshwater habitat. *Chemical Geology*, 260:149–158, 2009.

Dynes, JJ; Lawrence, JR; Korber, DR; Swerhone, GDW; Leppard, GG; & Hitchcock, AP: Quantitative mapping of chlorhexidine in natural river biofilms. *Science of the Total Environment*, 369:369–383, 2006.

Dzombak, DA & Morel, F: *Surface complexation modeling: hydrous ferric oxide* (Wiley, New York), 1990.

Eaton, A; Clesceri, L; Rice, E; & Greenberg, A: *Standard methods for the Examination of Water and Wastewater* (American Public Health Association, Maryland), 21st ed., 2005.

Edwards, KJ; McCollom, TM; Konishi, H; & Buseck, PR: Seafloor bioalteration of sulfide minerals: Results from in situ incubation studies. *Geochimica et Cosmochimica Acta*, 67:2843–2856, 2003.

Ehrenberg, CG: Vorläufige Mitteilungen über das wirkliche Vorkommen fossiler Infusorien und ihre grosse Verbreitung. *Poggendorfs Annalen der Physik und Chemie*, 38:213–227, 1836.

Ehrenreich, A & Widdel, F: Anaerobic oxidation of ferrous iron by purple bacteria, a new type of phototrophic metabolism. *Applied and Environmental Microbiology*, 60:4517–4526, 1994.

Ehrlich, HL & Newman, DK: *Geomicrobiology* (CRC Press, New York), 5th ed., 2009.

Emerson, D: Microbial oxidation of Fe(II) and mn(ii) at circumentural pH. In *Environmental Microbe-Metal Interactions*, Environmental Microbe-Metal Inteactions (Wiley-VCH), 2000.

Emerson, D; Fleming, EJ; & McBeth, JM: Iron-oxidizing bacteria: an environmental and genomic perspective. *Annual Review of Microbiology*, 64:561–83, 2010.

Emerson, D & Moyer, C: Isolation and characterization of novel iron-oxidizing bacteria that grow at circumneutral pH. *Applied and Environmental Microbiology*, 63:4784–4792, 1997.

Emerson, D & Revsbech, NP: Investigation of an iron-oxidizing microbial mat community located near Aarhus, Denmark: Field studies. *Applied and Environmental Microbiology*, 60:4022–4031, 1994.

Emerson, D & Weiss, J: Bacterial iron oxidation in circumneutral freshwater habitats: Findings from the field and the laboratory. *Geomicrobiology Journal*, 21:405–414, 2004.

Emery, WJ; Talley, LD; & Pickard, GL: *Descriptive Physical Oceanography*, vol. 1 (Elsevier), unpublished 6th ed. ed., 2006.

Evans, U; Leal, J; & Arnold, P: The interfacial electrochemistry of goethite (α-FeOOH) especially the effect of CO_2 contamination. *Journal of Electroanalytical Chemistry*, 105:161–167, 1979.

Farquhar, J; Bao, H; & Thiemens, M: Atmospheric influence of earth's earliest sulfur cycle. *Science*, 289:756–758, 2000.

Fein, JB; Daughney, CJ; Yee, N; & Davis, TA: A chemical equilibrium model for metal adsorption onto bacterial surfaces. *Geochimica et Cosmochimica Acta*, 61:3319–3328, 1997.

Fein, JB; Martin, AM; & Wightman, PG: Metal adsorption onto bacterial surfaces: Development of a predictive approach. *Geochimica et Cosmochimica Acta*, 65:4267–4273, 2001.

Feltham, RK; Power, AK; Pell, PA; & Sneath, PA: A simple method for storage of bacteria at -76 degrees c. *J Appl Bacteriol*, 44:313–316, 1978.

Feng, W & Nansheng, D: Photochemistry of hydrolytic iron (iii) species and photoinduced degradation of organic compounds. a minireview. *Chemosphere*, 41:1137–47, 2000.

Ferrer, M; Golyshina, OV; Beloqui, A; Golyshin, PN; & Timmis, KN: The cellular machinery of ferroplasma acidiphilum is iron-protein-dominated. *Nature*, 445:91–94, 2007.

Ferris, FG; Beveridge, TJ; & Fyfe, WS: Iron-silica crystallite nucleation by bacteria in a geothermal sediment. *Nature*, 320:609–611, 1986.

Finneran, KT; Housewright, ME; & Lovley, DR: Multiple influences of nitrate on uranium solubility during bioremediation of uranium-contaminated subsurface sediments. *Environmental Microbiology*, 4:510–6, 2002.

Folk, R & Lynch, F: The possible role of nanobacteria (dwarf bacteria) in clay-mineral diagenesis and the importance of careful sample preparation in high-magnification sem study. *Journal of Sediment Research*, 67:583–589, 1997.

Fortin, D: What biogenic minerals tell us. *Science*, 303:1618–1619, 2004.

Fortin, D; Ferris, FG; & Beveridge, TJ: Surface-mediated mineral development by bacteria. *Reviews in Mineralogy and Geochemistry*, 35:161–180, 1997.

Fortin, D; Ferris, FG; & Scott, SD: Formation of Fe-silicates and Fe-oxides on bacterial surfaces in samples collected near hydrothermal vents on the Southern Explorer Ridge in the northeast Pacific Ocean. *American Mineralogist*, 83:1399–1408, 1998.

Fortin, D & Langley, S: Formation and occurrence of biogenic iron-rich minerals. *Earth-Science Reviews*, 72:1–19, 2005.

Fraústo da Silva, JJR & Williams, RJP: *The biological chemistry of the elements: the inorganic chemistry of life* (Oxford University Press, Oxford), 2nd ed., 2001.

Fredrickson, JK & Zachara, JM: Electron transfer at the microbe-mineral interface: a grand challenge in biogeochemistry. *Geobiology*, 6:245–253, 2008.

Gadd, GM: Metals, minerals and microbes: geomicrobiology and bioremediation. *Microbiology*, 156:609–643, 2010.

Garrels, RM: A model for the deposition of the microbanded precambrian iron formations. *American Journal of Science*, 287:81–106, 1987.

Garrels, RM; Perry, EA, JR; & Mackenzie, FT: Genesis of precambrian iron-formations and the development of atmospheric oxygen. *Economic Geology*, 68:1173–1179, 1973.

Gault, AG; Ibrahim, A; Langley, S; Renaud, R; Takahashi, Y; Boothman, C; Lloyd, JR; Clark, ID; Ferris, FG; & Fortin, D: Microbial and geochemical features suggest iron redox cycling within bacteriogenic iron oxide-rich sediments. *Chemical Geology*, 281:41–51, 2011.

Gerhardt, S; Brune, A; & Schink, B: Dynamics of redox changes of iron caused by light-dark variations in littoral sediment of a freshwater lake. *Biogeochemistry*, 74:323–339, 2005.

Ghiorse, WC: Biology of iron- and manganese-depositing bacteria. *Annual Review of Microbiology*, 38:515–550, 1984.

Gold, T: The deep, hot biosphere. *Proceedings of the National Academy of Sciences of the United States of America*, 89:6045–9, 1992.

Good, NE; Winget, GD; Winter, W; Connolly, TN; Izawa, S; & Singh, RMM: Hydrogen ion buffers for biological research. *Biochemistry*, 5:467–477, 1966.

Gorby, YA; Yanina, S; McLean, JS; Rosso, KM; Moyles, D; Dohnalkova, A; Beveridge, TJ; Chang, IS; Kim, BH; Kim, KS; Culley, DE; Reed, SB; Romine, MF; Saffarini, DA; Hill, EA; Shi, L; Elias, DA; Kennedy, DW; Pinchuk, G; Watanabe, K; Ishii, S; Logan, B; Nealson, KH; & Fredrickson, JK: Electrically conductive bacterial nanowires produced by shewanella oneidensis strain mr-1 and other microorganisms. *Proceedings of the National Academy of Sciences*, 103:11358–11363, 2006.

Green, S; Leigh, M; & Neufeld, J: Denaturing gradient gel electrophoresis (dgge) for microbial community analysis. In K Timmis, ed., *Handbook of Hydrocarbon and Lipid Microbiology.*, pp. 4137–4158 (Springer, Heidelberg, Germany), 2009.

Gross, GA: Primary features in cherty iron-formations. *Sedimentary Geology*, 7:241–261, 1972.

Grotzinger, JP & Kasting, JF: New constraints on precambrian ocean composition. *Journal of Geology*, 101:235–243, 1993.

Grundl, T & Delwiche, J: Kinetics of ferric oxyhydroxide precipitation. *Journal of Contaminant Hydrology*, 14:71–97, 1993.

Haaijer, SC; Harhangi, HR; Meijerink, BB; Strous, M; Pol, A; Smolders, AJ; Verwegen, K; Jetten, MS; & Op den Camp, HJ: Bacteria associated with iron seeps in a sulfur-rich, neutral pH, freshwater ecosystem. *ISME Journal*, 2:1231–42, 2008.

Hafenbradl, D; Keller, M; Dirmeier, R; Rachel, R; Rossnagel, P; Burggraf, S; Huber, H; & Stetter, KO: *Ferroglobus placidus* gen. nov., sp. nov., a novel hyperthermophilic archaeum that oxidizes Fe^{2+} at neutral pH under anoxic conditions. *Archives of Microbiology*, 166:308–314, 1996.

Hallbeck, L & Pedersen, K: Benefits associated with the stalk of *Gallionella ferruginea*, evaluated by comparison of a stalk-forming and a non-stalk-forming strain and biofilm studies in-situ. *Microbial Ecology*, 30:257–268, 1995.

Hallberg, R & Ferris, F: Biomineralization by *Gallionella*. *Geomicrobiology Journal*, 21:325–330, 2004.

Hanert, H: *The Genus Gallionella*, vol. Proteobacteria: Delta, Epsilon subclass, pp. 996–997 (Springer), 2006.

Hansel, CM; Benner, SG; & Fendorf, S: Competing fe (ii)-induced mineralization pathways of ferrihydrite. *Environmental Science & Technology*, 39:7147–53, 2005.

Harold, FM: Conservation and transformation of energy by bacterial membranes. *Bacteriological Reviews*, 36:172–230, 1972.

Harris, DC: *Quantitative chemical analysis* (Freeman), 5th ed., 1995.

Hartmann, H: The evolution of photosynthesis and microbial mats: a speculation on banded iron formations. In Y Cohen; RW Castenholz; HO Halvorson; & CW Boylen, eds., *Microbial Mats - Stromatolites*, pp. 451–453 (Liss, A. R., New York), 1984.

Hegler, F; Posth, NR; Jiang, J; & Kappler, A: Physiology of phototrophic iron(II)-oxidizing bacteria – implications for modern and ancient environments. *FEMS Microbiology Ecology*, 66:250–260, 2008.

Hegler, F; Schmidt, C; Schwarz, H; & Kappler, A: Does a low pH-microenvironment around phototrophic Fe(II)-oxidizing bacteria prevent cell encrustation by Fe(III) minerals? *FEMS Microbiology Ecology*, accepted:accepted, 2010.

Heinzel, E; Janneck, E; Glombitza, F; Schlomann, M; & Seifert, J: Population dynamics of iron-oxidizing communities in pilot plants for the treatment of acid mine waters. *Environmental Science and Technology*, 43:6138–44, 2009.

Heising, S; Richter, L; Ludwig, W; & Schink, B: *Chlorobium ferrooxidans* sp nov., a phototrophic green sulfur bacterium that oxidizes ferrous iron in coculture with a *"Geospirillum"* sp strain. *Archives of Microbiology*, 172:116–124, 1999.

Heising, S & Schink, B: Phototrophic oxidation of ferrous iron by a *Rhodomicrobium vannielii* strain. *Microbiology*, 144:2263–2269, 1998.

Henke, BL; Gullikson, EM; & Davis, JC: X-ray interactions - photoabsorption, scattering, transmission, and reflection at e=50-30,000 ev, z=1-92. *Atomic Data and Nuclear Data Tables*, 54:181–342, 1993.

Hiemstra, T & van Riemsdijk, WH: A surface structural model for ferrihydrite i: Sites related to primary charge, molar mass, and mass density. *Geochimica et Cosmochimica Acta*, 73:4423 – 4436, 2009.

Hitchcock, AP: axis2000 - analysis of x-ray images and spectra. 2008.

Hitchcock, AP; Li, J; Reijerkerk, S; Foley, P; Stover, HDH; & Shirley, I: X-ray absorption spectroscopy of polyureas and polyurethanes and their use in characterizing chemical gradients in thin-walled polyurea capsules. *Journal of Electron Spectroscopy and Related Phenomena*, 156:Ciii–Civ, 2007.

Hohmann, C; Morin, G; Ona-Nguema, G; Guigner, JM; Brown, GEJ; & Kappler, A: Molecular-level modes of As binding to iron (oxy)hydroxides precipitated by the anaerobic nitrate-reducing iron(II)-oxidizing *Acidovorax* sp. strain BoFeN1, 2010. Submitted.

Holland, HD: The oceans; a possible source of iron in iron-formations. *Economic Geology*, 68:1169–1172, 1973.

Holland, HD: Volcanic gases, black smokers, and the great oxidation event. *Geochimica et Cosmochimica Acta*, 66:3811–3826, 2002.

Hong, SH; Bunge, J; Jeon, SO; & Epstein, SS: Predicting microbial species richness. *Proceedings of the National Academy of Sciences*, 103:117–22, 2006.

Hunter, RC & Beveridge, TJ: Application of a pH-sensitive fluoroprobe (c-snarf-4) for pH microenvironment analysis in pseudomonas aeruginosa biofilms. *Applied and Environmental Microbiology*, 71:2501–2510, 2005.

Hunter, RC; Hitchcock, AP; Dynes, JJ; Obst, M; & Beveridge, TJ: Mapping the speciation of iron in *Pseudomonas aeruginosa* biofilms using scanning transmission X-ray microscopy. *Environmental Science & Technology*, 42:8766–8772, 2008.

Invitrogen: SNARF pH indicators: user manual. 2003.

Ivarsson, M; Lindblom, S; Broman, C; & Holm, N: Fossilized microorganisms associated with zeolite-carbonate interfaces in sub-seafloor hydrothermal environments. *Geobiology*, 6:155–170, 2008.

Jaffrés, JBD; Shields, GA; & Wallmann, K: The oxygen isotope evolution of seawater: A critical review of a long-standing controversy and an improved geological water cycle model for the past 3.4 billion years. *Earth-Science Reviews*, 83:83–122, 2007.

Jambor, JL & Dutrizac, JE: Occurrence and constitution of natural and synthetic ferrihydrite, a widespread iron oxyhydroxide. *Chemical Reviews*, 98:2549–2585, 1998.

James, RE & Ferris, FG: Evidence for microbial-mediated iron oxidation at a neutrophilic groundwater spring. *Chemical Geology*, 212:301–311, 2004.

Jeon, B; Dempsey, B; Burgos, W; Royer, R; & Roden, E: Modeling the sorption kinetics of divalent metal ions to hematite. *Water Research*, 38:2499–2504, 2004.

Jiao, Y; Kappler, A; Croal, LR; & Newman, DK: Isolation and characterization of a genetically traceable photoautotrophic Fe(II)-oxidizing bacterium, *Rhodopseudomonas palustris* strain tie-1. *Applied and Environmental Microbiology*, 71:4487–4496, 2005.

Jiao, Y & Newman, DK: The pio operon is essential for phototrophic Fe(II) oxidation in rhodopseudomonas palustris tie-1. *Journal of Bacteriology*, 189:1765–1773, 2007.

Johnson, CM; Beard, BL; Beukes, NJ; Klein, C; & O'Leary, JM: Ancient geochemical cycling in the earth as inferred from fe isotope studies of banded iron formations from the transvaal craton. *Contributions to Mineralogy and Petrology*, 144:523–547, 2003.

Johnson, CM; Beard, BL; Klein, C; Beukes, NJ; & Roden, EE: Iron isotopes constrain biologic and abiologic processes in banded iron formation genesis. *Geochimica et Cosmochimica Acta*, 72:151–169, 2008.

Johnson, KJ; Ams, DA; Wedel, AN; Szymanowski, JES; Weber, DL; Schneegurt, MA; & Fein, JB: The impact of metabolic state on Cd adsorption onto bacterial cells. *Geobiology*, 5:211–218, 2007.

Johnson, KJ; Cygan, RT; & Fein, JB: Molecular simulations of metal adsorption to bacterial surfaces. *Geochimica Et Cosmochimica Acta*, 70:5075–5088, 2006.

Kappler, A; Konhauser, KO; & Newman, DK: The potential significance of microbial Fe(III) reduction during deposition of precambrian banded iron formations. *Geobiology*, 3:167–177, 2005a.

Kappler, A & Newman, DK: Formation of Fe(III)-minerals by Fe(II)-oxidizing photoautotrophic bacteria. *Geochimica et Cosmochimica Acta*, 68:1217–1226, 2004.

Kappler, A; Pasquero, C; Konhauser, KO; & Newman, DK: Deposition of banded iron formations by anoxygenic phototrophic Fe(II)-oxidizing bacteria. *Geology*, 33:865–868, 2005b.

Kappler, A; Schink, B; & Newman, DK: Fe(III) mineral formation and cell encrustation by the nitrate-dependent Fe(II)-oxidizer strain BoFeN 1. *Geobiology*, 3:235–245, 2005c.

Kappler, A & Straub, KL: Geomicrobiological cycling of iron. *Reviews in Mineralogy & Geochemistry*, 59:85–108, 2005.

Kassner, RJ & Kamen, MD: Trace metal composition of photosynthetic bacteria. *Biochimica et Biophysica Acta*, 153:270–8, 1968.

Kasting, JF: Earth's early athmosphere. *Science*, 259:920–926, 1993.

Kasting, JF: Earth history. the rise of atmospheric oxygen. *Science*, 293:819–20, 2001.

Kasting, JF: Palaeoclimatology - archaean atmosphere and climate. *Nature*, 432:–, 2004.

Kasting, JF; Howard, MT; Wallmann, K; Veizer, J; Shields, G; & Jaffrés, J: Paleoclimates, ocean depth, and the oxygen isotopic composition of seawater. *Earth and Planetary Science Letters*, 252:82–93, 2006.

Kasting, JF & Siefert, JL: Life and the evolution of earth's atmosphere. *Science*, 296:1066–1068, 2002.

Kiernan, JA: Formaldehyde, formalin, paraformaldehyde and glutaraldehyde: What they are and what they do. *Microscopy today*, 8:8–12, 2000.

Klausen, J; Trober, SP; Haderlein, SB; & Schwarzenbach, RP: Reduction of substituted nitrobenzenes by Fe(II) in aqueous mineral suspensions. *Environmental Science & Technology*, 29:2396–2404, 1995.

Klee, AJ: A computer program for the determination of most probable number and its confidence limits. *Journal of Microbiological Methods*, 18:91–98, 1993.

Klein, C: Some precambrian banded iron-formations (bifs) from around the world: Their age, geologic setting, mineralogy, metamorphism, geochemistry, and origin. *American Mineralogist*, 90:1473–1499, 2005.

Knauth, LP: Temperature and salinity history of the precambrian ocean: implications for the course of microbial evolution. *Palaeogeography Palaeoclimatology Palaeoecology*, 219:53–69, 2005.

Knauth, LP & Lowe, DR: High archean climatic temperature inferred from oxygen isotope geochemistry of cherts in the 3.5 ga swaziland supergroup, south africa. *Geological Society of America Bulletin*, 115:566–580, 2003.

Konhauser, K: *Introduction to Geomicrobiology* (Blackwell Publishing, Malden, MA, USA), 1st ed., 2007.

Konhauser, KO: Bacterial iron biomineralization in nature. *FEMS Microbiology Reviews*, 20:315–326, 1997.

Konhauser, KO; Amskold, L; Lalonde, SV; Posth, NR; Kappler, A; & Anbar, A: Decoupling photochemical Fe(II) oxidation from shallow-water BIF deposition. *Earth and Planetary Science Letters*, 258:87–100, 2007a.

Konhauser, KO; Fyfe, WS; Schultze-Lam, S; Ferris, F; & Beveridge, TJ: Iron phosphate precipitation by epilithic microbial biofilms in arctic canada. *Canadian Journal of Earth Science*, 31:1320–1324, 1994.

Konhauser, KO; Hamade, T; Raiswell, R; Morris, RC; Ferris, FG; Southam, G; & Canfield, DE: Could bacteria have formed the precambrian banded iron formations? *Geology*, 30:1079–1082, 2002.

Konhauser, KO; Jones, B; Phoenix, V; Ferris, G; & Renaut, R: The microbial role in hot spring silicification. *Ambio*, 33:552–558, 2004.

Konhauser, KO; Lalonde, SV; Amskold, L; & Holland, HD: Was there really an archean phosphate crisis? *Science*, 315:1234–, 2007b.

Konhauser, KO; Newman, DK; & Kappler, A: The potential significance of microbial Fe(III) reduction during deposition of precambrian banded iron formations. *Geobiology*, 3:167–177, 2005.

Konhauser, KO; Pecoits, E; Lalonde, SV; Papineau, D; Nisbet, EG; Barley, ME; Arndt, NT; Zahnle, K; & Kamber, BS: Oceanic nickel depletion and a methanogen famine before the great oxidation event. *Nature*, 458:750–753, 2009.

Lack, JG; Chaudhuri, SK; Chakraborty, R; Achenbach, LA; & Coates, JD: Anaerobic biooxidation of Fe(II) by *Dechlorosoma suillum*. *Microbial Ecology*, 43:424–431, 2002.

Lane, DJ; Harrison, AP; Stahl, D; Pace, B; Giovannoni, SJ; Olsen, GJ; & Pace, NR: Evolutionary relationships among sulfur-oxidizing and iron-oxidizing eubacteria. *Journal of Bacteriology*, 174:269–278, 1992.

Larese-Casanova, P; Haderlein, S; & Kappler, A: Biomineralization of lepidocrocite and goethite by nitrate-reducing Fe(II)-oxidizing bacteria: Effect of pH, bicarbonate, phosphate and humic acids. *Geochimica Et Cosmochimica Acta*, 74:3721–3734, 2010.

Laskar, J & Robutel, P: The chaotic obliquity of the planets. *Nature*, 361:608–612, 1993.

Ley, RE; Harris, JK; Wilcox, J; Spear, JR; Miller, SR; Bebout, BM; Maresca, JA; Bryant, DA; Sogin, ML; & Pace, NR: Unexpected diversity and complexity of the guerrero negro hypersaline microbial mat. *Applied Environmental Microbiology*, 72:3685–95, 2006.

Li, D; Li, Z; Yu, J; Cao, N; Liu, R; & Yang, M: Characterization of bacterial community structure in a drinking water distribution system during an occurrence of red water. *Applied and Environmental Microbiology*, 76:7171–7180, 2010.

Little, C; Glynn, S; & Mills, R: Four-hundred-and-ninety-million-year record of bacteriogenic iron oxide precipitation at sea-floor hydrothermal vents. *Geomicrobiology Journal*, 21:415–429, 2004.

Lovley, DR: Dissimilatory Fe(III) and Mn(IV) reduction. *Microbiology and Molecular Biology Reviews*, 55:259–287, 1991.

Lovley, DR & Phillips, EJ: Novel mode of microbial energy metabolism: organic carbon oxidation coupled to dissimilatory reduction of iron or manganese. *Applied and Environmental Microbiology*, 54:1472–80, 1988.

Ludwig, W; Strunk, O; Westram, R; Richter, L; Meier, H; Yadhukumar; Buchner, A; Lai, T; Steppi, S; Jobb, G; Forster, W; Brettske, I; Gerber, S; Ginhart, AW; Gross, O; Grumann, S; Hermann, S; Jost, R; Konig, A; Liss, T; Lussmann, R; May, M; Nonhoff, B; Reichel, B; Strehlow, R; Stamatakis, A; Stuckmann, N; Vilbig, A; Lenke, M; Ludwig, T; Bode, A; & Schleifer, KH: ARB: a software environment for sequence data. *Nucleic Acids Research*, 32:1363–71, 2004.

Madigan, MT; Martinko, JM; & Brock, TD: *Brock biology of microorganisms* (Pearson Prentice Hall, Upper Saddle River, NJ), 11th ed., 2006.

Malik, KA: A new method for liquid nitrogen storage of phototrophic bacteria under anaerobic conditions. *Journal of Microbiological Methods*, 2:41–47, 1984.

Maliva, RG; Knoll, AH; & Simonson, BM: Secular change in the precambrian silica cycle: Insights from chert petrology. *Geological Society of America Bulletin*, 117:835–845, 2005.

Marcotte, N & Brouwer, AM: Carboxy SNARF-4F as a fluorescent pH probe for ensemble and fluorescence correlation spectroscopies. *The Journal of Physical Chemistry B*, 109:11819–11828, 2005.

Martinez, RE; Gardés, E; Pokrovsky, OS; Schott, J; & Oelkers, EH: Do photosynthetic bacteria have a protective mechanism against carbonate precipitation at their surfaces? *Geochimica et Cosmochimica Acta*, 74:1329–1337, 2010.

Martinez, RE; Smith, DS; Kulczycki, E; & Ferris, FG: Determination of intrinsic bacterial surface acidity constants using a donnan shell model and a continuous pK_a distribution method. *Journal of Colloid and Interface Science*, 253:130–9, 2002.

Mathur, SS & Dzombak, DA: *Surface complexation modeling: goethite*, vol. 11, chap. 16, pp. 443–468 (Elsevier), 2006.

McConnaughey, TA & Whelan, JF: Calcification generates protons for nutrient and bicarbonate uptake. *Earth-Science Reviews*, 42:95–117, 1997.

Mermel, LA: New technologies to prevent intravascular catheter-related bloodstream infections. *Emerging Infections Deseases*, 7:197–199, 2001.

Michel, FM; Barron, V; Torrent, J; Morales, MP; Serna, CJ; Boily, JF; Liu, QS; Ambrosini, A; Cismasu, AC; & Brown, GE: Ordered ferrimagnetic form of ferrihydrite reveals links among structure, composition, and magnetism. *Proceedings of the National Academy of Sciences of the United States of America*, 107:2787–2792, 2010.

Michel, FM; Ehm, L; Antao, SM; Lee, PL; Chupas, PJ; Liu, G; Strongin, DR; Schoonen, MAA; Phillips, BL; & Parise, JB: The structure of ferrihydrite, a nanocrystalline material. *Science*, 316:1142525–1142525, 2007.

Millero, FJ; Sotolongo, S; & Izaguirre, M: The oxidation kinetics of Fe(II) in seawater. *Geochimica et Cosmochimica Acta*, 51:793–801, 1986.

Miot, J; Benzerara, K; Morin, G; Bernard, S; Larquet, E; Ona-Nguema, G; Kappler, A; & Guyot, F: Transformation of vivianite by anaerobic nitrate-reducing iron-oxidizing bacteria. *Geobiology*, 7:373–384, 2009a.

Miot, J; Benzerara, K; Morin, G; Kappler, A; Bernard, S; Obst, M; Férard, C; Skouri-Panet, F; Guigner, JM; Posth, NR; Galvez, M; Brown, GE, JR.; & Guyot, F: Iron biomineralization by neutrophilic iron-oxidizing bacteria. *Geochimica et Cosmochimica Acta*, 73:696–711, 2009b.

Miot, J; Benzerara, K; Obst, M; Kappler, A; Hegler, F; Schaedler, S; Bouchez, C; Guyot, F; & Morin, G: Extracellular iron biomineralization by photoautotrophic iron-oxidizing bacteria. *Applied and Environmental Microbiology*, 75:5586–5591, 2009c.

Mitchell, P: Keilin's respiratory chain concept and its chemiosmotic consequences. *Science*, 206:1148–1159, 1979.

Morris, RC: Genetic modelling for baded iron formation of the hamersly group, pilbara craton, western australia. *Precambrian Research*, 60:243–280, 1993.

Morris, RC & Horwitz, RC: The origin of the iron-formation-rich hamersley group of western australia – deposition on a platform. *Precambrian Research*, 21:273–297, 1983.

Muehe, EM; Gerhardt, S; Schink, B; & Kappler, A: Physiology of mixotrophic ferrous iron oxidation by a nitrate-reducing *Acidovorax* strain isolated from a freshwater lake sediment. *FEMS Microbiology Ecology*, 70:335–343, 2009.

Müller, HE; Brenner, DJ; Fanning, GR; Grimont, PAD; & Kämpfer, P: Emended description of *Buttiauxella agrestis* with recognition of six new species of *Buttiauxella* and two new species of *Kluyvera*: *Buttiauxella ferragutiae* sp. nov., *Buttiauxella gaviniae* sp. nov., *Buttiauxella brennerae* sp. nov., *Buttiauxella izardii* sp. nov., *Buttiauxella noackiae* sp. nov., *Buttiauxella warmboldiae* sp. nov., *Kluyvera cochleae* sp. nov., and *Kluyvera georgiana* sp. nov. *International Journal of Systematic Bacteriology*, 46:50–63, 1996.

Muyzer, G; Teske, A; Wirsen, CO; & Jannasch, HW: Phylogenetic-relationships of *Thiomicrospira* species and their identification in deep-sea hydrothermal vent samples by denaturing gradient gel-electrophoresis of 16S RDNA fragments. *Archives of Microbiology*, 164:165–172, 1995.

Myers, CR & Nealson, KH: Bacterial manganese reduction and growth with manganese oxide as the sole electron-acceptor. *Science*, 240:1319–1321, 1988.

Nadkarni, MA; Martin, FE; Jacques, NA; & Hunter, N: Determination of bacterial load by real-time PCR using a broad-range (universal) probe and primers set. *Microbiology*, 148:257–266, 2002.

Nagel, JG & Kunz, LJ: Simplified storage and retrival of stock cultures. *Applied Microbiology*, 23:837–838, 1972.

Nealson, K & Scott, J: *Ecophysiology of the Genus Shewanella*, vol. Volume 6: Proteobacteria: Gamma Subclass, chap. Section 3.3, pp. 1133–1151 (Springer, New York), 2006.

Nesterova, M; Moreau, J; & Banfield, JF: Model biomimetic studies of templated growth and assembly of nanocrystalline feooh. *Geochimica et Cosmochimica Acta*, 67:1177–1187, 2003.

Neubauer, SC; Toledo-Durán, GE; Emerson, D; & Megonigal, JP: Returning to their roots: Iron-oxidizing bacteria enhance short-term plaque formation in the wetland-plant rhizosphere. *Geomicrobiology Journal*, 24:65–73, 2007.

Nicholls, DG & Ferguson, SJ: *Bioenergetics 3* (Academic Press, Amsterdam, London), 3rd ed., 2002.

Nubel, U; Garcia-Pichel, F; & Muyzer, G: Pcr primers to amplify 16s rrna genes from cyanobacteria. *Applied and Environmental Microbiology*, 63:3327–32, 1997.

Overmann, J & Schubert, K: Phototrophic consortia: model systems for symbiotic interrelations between prokaryotes. *Archives of Microbiology*, 177:201–208, 2002.

Padan, E; Zilberstein, D; & Schuldiner, S: pH homeostasis in bacteria. *Biochimica et biophysica acta*, 650:151–166, 1981.

Pham, AN; Rose, AL; Feitz, AJ; & Waite, TD: Kinetics of Fe(III) precipitation in aqueous solutions at pH 6.0-9.5 and 25 degrees C. *Geochimica Et Cosmochimica Acta*, 70:640–650, 2006.

Phoenix, VR; Adams, DG; & Konhauser, KO: Cyanobacterial viability during hydrothermal biomineralisation. *Chemical Geology*, 169:329–338, 2000.

Phoenix, VR & Konhauser, KO: Benefits of bacterial biomineralization. *Geobiology*, 6:303–308, 2008.

Pierson, BK; Parenteau, MN; & Griffin, BM: Phototrophs in high-iron-concentration microbial mats: Physiological ecology of phototrophs in an iron-depositing hot spring. *Applied and Environmental Microbiology*, 65:5474–5483, 1999.

Planavsky, N; Rouxel, O; Bekker, A; Shapiro, R; Fralick, P; & Knudsen, A: Iron-oxidizing microbial ecosystems thrived in late paleoproterozoic redox-stratified oceans. *Earth and Planetary Science Letters*, 286:230–242, 2009.

Popoff, M & Veron, M: A taxonomic study of the *Aeromonas hydrophila- Aeromonas punctata* group. *Journal of General Microbiology*, 94:11–22, 1976.

Posth, NR; Hegler, F; Konhauser, KO; & Kappler, A: Alternating Si and Fe deposition caused by temperature fluctuations in Precambrian oceans. *Nature Geoscience*, 1:703–708, 2008.

Posth, NR; Huelin, S; Konhauser, K; & Kappler, A: Size, density and composition of cell-mineral aggregates formed during anoxigenic phototrophic Fe(II) oxidation: Impact on modern and ancient environments. *Geochimica Et Cosmochimica Acta*, 74:3476–3493, 2010.

Pringsheim, EG: Iron bacteria. *Biological Reviews of the Cambridge Philosophical Society*, 24:200–45, 1949.

Pruesse, E; Quast, C; Knittel, K; Fuchs, BM; Ludwig, WG; Peplies, J; & Glockner, FO: Silva: a comprehensive online resource for quality checked and aligned ribosomal rna sequence data compatible with arb. *Nucleic Acids Research*, 35:7188–7196, 2007.

Rakshit, S; Matocha, CJ; & Coyne, MS: Nitrite reduction by siderite. *Soil Science of America Journal*, 72:1070–1077, 2008.

Rashby, SE; Sessions, AL; Summons, RE; & Newman, DK: Biosynthesis of 2-methylbacteriohopanepolyols by an anoxygenic phototroph. *Proceedings of the National Academy of Sciences*, 104:15099–15104, 2007.

Ratering, S & Schnell, S: Nitrate-dependent iron(II) oxidation in paddy soil. *Environmental Microbiology*, 3:100–109, 2001.

Raven, KP; Jain, A; & Loeppert, RH: Arsenite and arsenate adsorption on ferrihydrite: Kinetics, equilibrium, and adsorption envelopes. *Environmental Science & Technology*, 32:344–349, 1998.

Redfield, A; Ketchum, B; & Richards, F: The influence of organisms on th ecomposition of seawater. In M Hill, ed., *The composition of seawater - comparitative and describitive oceanography* (Wiley, New York), 1963.

Reguera, G; McCarthy, KD; Mehta, T; Nicoll, JS; Tuominen, MT; & Lovley, DR: Extracellular electron transfer via microbial nanowires. *Nature*, 435:1099–1101, 2005.

Reinhard, CT; Raiswell, R; Scott, C; Anbar, AD; & Lyons, TW: A late archean sulfidic sea stimulated by early oxidative weathering of the continents. *Science*, 326:713–6, 2009.

Revsbech, NP; Jørgensen, BB; & Blackburn, TH: Microelectrode studies of the photosynthesis and O_2, H_2S and pH profiles of a microbial mat. *Limnology and Oceanography*, 28:1062–1074, 1983.

Robert, F & Chaussidon, M: A palaeotemperature curve for the precambrian oceans based on silicon isotopes in cherts. *Nature*, 443:969–972, 2006a.

Robert, F & Chaussidon, M: A palaeotemperature curve for the precambrian oceans based on silicon isotopes in cherts. *Nature*, 443:969–72, 2006b.

Roden, EE; Sobolev, D; Glazer, B; & Luther, GW: Potential for microscale bacterial fe redox cycling at the aerobic-anaerobic interface. *Geomicrobiology Journal*, 21:379–391, 2004.

Rose, AL & Waite, TD: Kinetics of hydrolysis and precipitation of ferric iron in seawater. *Environmental Science and Technology*, 37:3897–3903, 2003.

Rose, AL & Waite, TD: Reconciling kinetic and equilibrium observations of iron(III) solubility in aqueous solutions with a polymer-based model. *Geochimica et Cosmochimica Acta*, 71:5605–5619, 2007.

Rosso, L; Lobry, JR; Bajard, S; & Flandrois, JP: Convenient model to describe the combined effects of temperature and pH on microbial-growth. *Applied and Environmental Microbiology*, 61:610–616, 1995.

Saito, MA; Sigman, DM; & Morel, FMM: The bioinorganic chemistry of the ancient ocean: the co-evolution of cyanobacterial metal requirements and biogeochemical cycles at the archean proterozoic boundary? *Inorganica Chimica Acta*, 356:308–318, 2003.

Schaedler, S; Burkhardt, C; Hegler, F; Straub, KL; Miot, J; Benzerara, K; & Kappler, A: Formation of cell-iron-mineral aggregates by phototrophic and nitrate reducing anaerobic Fe(II)-oxidizing bacteria. *Geomicrobiology Journal*, 26:93–103, 2009.

Schaedler, S; Burkhardt, C; & Kappler, A: Evaluation of electron microscopic sample preparation methods and imaging techniques for characterization of cell-mineral aggregates. *Geomicrobiology Journal*, 25:228–239, 2008.

Schloss, PD; Westcott, SL; Ryabin, T; Hall, JR; Hartmann, M; Hollister, EB; Lesniewski, RA; Oakley, BB; Parks, DH; Robinson, CJ; Sahl, JW; Stres, B; Thallinger, GG; Van Horn, DJ; & Weber, CF: Introducing mothur: Open-source, platform-independent, community-supported software for describing and comparing microbial communities. *Applied and Environmental Microbiology*, 75:7537–7541, 2009.

Schönhuber, W; Zarda, B; Eix, S; Rippka, R; Herdman, M; Ludwig, W; & Amann, R: In situ identification of cyanobacteria with horseradish peroxidase-labeled, rRNA-targeted oligonucleotide probes. *Applied and Environmental Microbiology*, 65:1259–67, 1999.

Schotterer, U; Siegenthaler, U; Oeschger, H; Riesen, T; MÃ¼ller, I; & Kelts, K: Isotopic geochemistry of the engadine mineral springs of scuol-tarasp, switzerland. In *Isotope Techniques in Water Resources Development (Vienna, 30 March - 3 April 1987)*, pp. 277–286. 1987.

Schultze-Lam, S; Fortin, D; Davis, BS; & Beveridge, TJ: Mineralization of bacterial surfaces. *Chemical Geology*, 132:171–181, 1996.

Schwertmann, U & Cornell, RM: *Iron oxides in the laboratory : preparation and characterization* (Wiley-VCH, Weinheim), 2nd ed., 2000.

Senko, JM; Dewers, TA; & Krumholz, LR: Effect of oxidation rate and Fe(II) state on microbial nitrate-dependent Fe(III) mineral formation. *Applied and Environmental Microbiology*, 71:7172–7177, 2005.

Shapiro, L; McAdams, HH; & Losick, R: Generating and exploiting polarity in bacteria. *Science*, 298:1942–1946, 2002.

Shields, GA & Kasting, JF: Palaeoclimatology: Evidence for hot early oceans? *Nature*, 447:E1, 2007.

Siever, R: The silica cycle in the precambrian. *Geochimica et Cosmochimica Acta*, 56:3265–3272, 1992.

Smith, DS & Ferris, FG: Proton binding by hydrous ferric oxide and aluminum oxide surfaces interpreted using fully optimized continuous pk_a spectra. *Environmental Science & Technology*, 35:4637–4642, 2001.

Smith, DS & Ferris, FG: Specific surface chemical interactions between hydrous ferric oxide and iron-reducing bacteria determined using pk_a spectra. *Journal of Colloid and Interface Science*, 266:60–67, 2003.

Snell, JJS: General introduction to maintainance methods. In BE Kirsop & A Doyle, eds., *Maintenance of microorganisms and cultured cells: a manual of laboratory methods*, pp. 21–30 (Academic Press, London), 1991.

Sobolev, D & Roden, EE: Suboxic deposition of ferric iron by bacteria in opposing gradients of Fe(II) and oxygen at circumneutral pH. *Applied and Environmental Microbiology*, 67:1328–1334, 2001.

Sterner, RW & Elsner, JJ: *Ecological stoichometry* (Princeton University Press), 2002.

Stolzberg, RJ & Hume, DN: Rapid formation of iminodiacetate from photochemical degradation of iron(III) nitrilotriacetate solutions. *Environmental Science & Technology*, 9:654–656, 1975.

Stookey, LL: Ferrozine – a new spectrophotometric reagent for iron. *Analytical Chemistry*, 42:779–781, 1970.

Straub, KL; Benz, M; & Schink, B: Iron metabolism in anoxic environments at near neutral pH. *FEMS Microbiology Ecology*, 34:181–186, 2001.

Straub, KL; Benz, M; Schink, B; & Widdel, F: Anaerobic, nitrate-dependent microbial oxidation of ferrous iron. *Applied and Environmental Microbiology*, 62:1458–1460, 1996.

Straub, KL & Buchholz-Cleven, BEE: Enumeration and detection of anaerobic ferrous iron-oxidizing, nitrate-reducing bacteria from diverse european sediments. *Applied and Environmental Microbiology*, 64:4846–4856, 1998.

Straub, KL; Rainey, FA; & Widdel, F: *Rhodovulum iodosum* sp. nov. and *Rhodovulum robiginosum* sp. nov., two new marine phototrophic ferrous-iron-oxidizing purple bacteria. *International Journal of Systematic Bacteriology*, 49:729–735, 1999.

Straub, KL; Schonhuber, WA; Buchholz-Cleven, BEE; & Schink, B: Diversity of ferrous iron-oxidizing, nitrate-reducing bacteria and their involvement in oxygen-independent iron cycling. *Geomicrobiology Journal*, 21:371–378, 2004.

Stumm, W & Morgan, JJ: *Aquatic chemistry: chemical equilibria and rates in natural waters* (Wiley-Interscience, New York), 3rd ed., 1995.

Stumm, W & Sulzberger, B: The cycling of iron in natural environments: Considerations based on laboratory studies of heterogeneous redox processes. *Geochimica et Cosmochimica Acta*, 56:3233–3257, 1992.

Suda, S; Watanabe, MM; Otsuka, S; Mahakahant, A; Yongmanitchai, W; Nopartnaraporn, N; Liu, Y; & Day, JG: Taxonomic revision of water-bloom-forming species of oscillatorioid cyanobacteria. *International Journal of Systematic and Evolutionary Microbiology*, 52:1577–1595, 2002.

Svenson, A; Kaj, L; & Björndal, H: Aqueous photolysis of the iron (III) complexes of NTA, EDTA and DTPA. *Chemosphere*, 18:1805–1808, 1989.

Tebo, B; Bargar, J; Clement, B; Dick, G; Murray, K; Parker, D; & SM., RVW: Biogenic manganese oxides: Properties and mechanisms of formation. *Annual Reviews of Earth and Planetary Sciences*, 32:287–328, 2004.

Thamdrup, B: Bacterial manganese and iron reduction in aquatic sediments. *Advances in Microbial Ecology, Vol 16*, 16:41–84, 2000.

Thompson, JB & Ferris, FG: Cyanobacterial precipitation of gypsum, calcite and magnesite from natural alkaline lake water. *Geology*, 18:995–998, 1990.

Tipping, E: The adsorption of aquatic humic substances by iron oxides. *Geochimica et Cosmochimica Acta*, 45:191–199, 1981.

Torrent, J & Barron, V: Key role of phosphorus in the formation of the iron oxides in Mars soils? *Icarus*, 145:645–647, 2000.

Touati, D: Iron and oxidative stress in bacteria. *Archives of Biochemistry and Biophysics*, 373:1–6, 2000.

Trendall, AF: Three great basins of precambrian banded iron formation deposition: A systematic comparison. *Geological Society of America Bulletin*, 79:1527–1544, 1968.

Trendall, AF: The significance of iron-formation in the precambrian stratigraphic record. In W Altermann & PL Corcoran, eds., *Precambrian sedimentary environments: a modern approach to ancient depositional systems*, vol. 33, pp. 33–66 (Blackwell Science Ltd.), 2002.

Tschech, A & Pfennig, N: Growth yield increase linked to caffeate reduction in *Acetobacterium woodii*. *Archives of Microbiology*, 137:163–167, 1984.

Tufano, KJ & Fendorf, S: Confounding impacts of iron reduction on arsenic retention. *Environmental Science and Technology*, 42:4777–4783, 2008.

Turner, BF & Fein, JB: Protofit: A program for determining surface protonation constants from titration data. *Computers & Geosciences*, 32:1344–1356, 2006.

Urrutia Mera, M; Kemper, M; Doyle, R; & Beveridge, TJ: The membrane-induced proton motive force influences the metal binding ability of *Bacillus subtilis* cell walls. *Applied Environmental Microbiology*, 58:3837–3844, 1992.

van der Zee, J; Krootjes, BBH; Chignell, CF; Dubbelman, TMAR; & van Steveninck, J: Hydroxyl radical generation by light-dependent fenton reactions. *Free Radical Biology & Medicine*, 14:105–113, 1993.

Viollier, E; Inglett, PW; Hunter, K; Roychoudhury, AN; & Van Cappellen, P: The ferrozine method revisited: Fe(II)/Fe(iii) determination in natural waters. *Applied Geochemistry*, 15:785–790, 2000.

Wächtershäuser, G: Evolution of the first metabolic cycles. *Proceedings of the National Academy of Sciences of the United States of America*, 87:200–204, 1990.

Wächtershäuser, G: Origin of life: Life as we don't know it. *Science*, 289:1307–1308, 2000.

Wagner, C; Mau, M; Schlömann, M; Heinicke, J; & Koch, U: Characterization of the bacterial flora in mineral waters in upstreaming fluids of deep igneous rock aquifers. *Journal of Geophysical Research*, 112:1–8, 2007.

Waite, TD; Sompongchaiyakul, P; & Pham, AN: Kinetics of Fe(II) removal from seawater in the absence and presence of organic matter. *Abstracts of Papers of the American Chemical Society*, 220:U337–U337, 2000.

Walker, JCG: Suboxic diagenesis in banded iron formations. *Nature*, 309:340–342, 1984.

Wan, J; Tyliszczak, T; & Tokunaga, TK: Organic carbon distribution, speciation, and elemental correlations within soil micro aggregates: Applications of stxm and nexafs spectroscopy. *Geochimica et Cosmochimica Acta*, 71:5439–5449, 2007.

Warren, LA & Ferris, FG: Continuum between sorption and precipitation of Fe(III) on microbial surfaces. *Environmental Science & Technology*, 32:2331–2337, 1998.

Weber, KA; Achenbach, LA; & Coates, JD: Microorganisms pumping iron: anaerobic microbial iron oxidation and reduction. *Nature Reviews: Microbiology*, 4:752–764, 2006a.

Weber, KA; Urrutia, MM; Churchill, PF; Kukkadapu, RK; & Roden, EE: Anaerobic redox cycling of iron by freshwater sediment microorganisms. *Environmental Microbiology*, 8:100–113, 2006b.

Wexsteen, P; Jaffé, FC; & Mazor, E: Geochemistry of cold co2-rich springs of the scuol-tarasp region, lower engadine, swiss alps. *Journal of Hydrogeology*, 104:77–92, 1988.

Widdel, F: *Anaerober Abbau von Fettsäuren und Benzoesäure durch neu isolierte Arten.* Ph.D. thesis, Universität Göttingen, Göttingen, 1980.

Widdel, F & Pfennig, N: Studies on dissimilatory sulfate-reducing bacteria that decompose fatty acids. i. isolation of a new sulfate-reducer enriched with acetate from saline environments. description of desulfobacter postgatei gen. nov. sp. nov. *Archives of Microbiology*, 129:395–400, 1981.

Widdel, F; Schnell, S; Heising, S; Ehrenreich, A; Assmus, B; & Schink, B: Ferrous iron oxidation by anoxygenic phototrophic bacteria. *Nature*, 362:834–836, 1993.

Williams, RJ & Frausto Da Silva, JJ: Evolution was chemically constrained. *Journal of Theoretical Biology*, 220:323–43, 2003.

Williams, RJP & Fraústo da Silva, JJR: *The chemistry of evolution: the development of our ecosystem* (Elsevier, Amsterdam; Boston), 1st ed., 2006.

Winogradsky, S: Über Eisenbacterien. *Botanische Zeitung*, 17:261–270, 1888.

Xiong, J: Photosynthesis: what color was its origin. *Genome Biology*, 7:245–245, 2006.

Yee, N & Fein, JB: Quantifying metal adsorption onto bacteria mixtures: A test and application of the surface complexation model. *Geomicrobiology Journal*, 20:43–60, 2003.

Yu, Q; Kandegedara, A; Xu, Y; & Rorabacher, DB: Avoiding interferences from good's buffers: A contiguous series of noncomplexing tertiary amine buffers covering the entire range of pH 3-11. *Analytical biochemistry*, 253:50–56, 1997.

Zegeye, A; Mustin, C; & Jorand, F: Bacterial and iron oxide aggregates mediate secondary iron mineral formation: green rust versus magnetite. *Geobiology*, 8:209–222, 2010.

Zerkle, AL; House, CH; & Brantley, SL: Biogeochemical signatures through time as inferred from whole microbial genomes. *American Journal of Science*, 305:467–502, 2005.

Zerkle, AL; House, CH; Cox, RP; & Canfield, DE: Metal limitation of cyanobacterial N_2 fixation and implications for the precambrian nitrogen cycle. *Geobiology*, 4:285–297, 2006.

Zhang, Y & Gladyshev, VN: General trends in trace element utilization revealed by comparative genomic analyses of Co, Cu, Mo, Ni and Se. *Journal of Biological Chemistry*, 285:3393–405, 2010.

Zhou, J; Bruns, MA; & Tiedje, JM: DNA recovery from soils of diverse composition. *Applied and Environmental Microbiology*, 62:316–22, 1996.

Züllig, H & Rheineck, SG: Pigmente phototropher bakterien in seesedimenten und ihre bedeutung für die seenforschung. *Aquatic Sciences - Research Across Boundaries*, 47:87–126, 1985.